Characterization of Aluminum Silicon/Short Carbon Fiber Composites Fabricated by Novel Thixomixing Method

Ebrahim AKBARZADEH

UNIVERSITAT POLITÈCNICA DE CATALUNYA

DOCTORAL THESIS

Characterization of Aluminum Silicon/Short Carbon Fiber Composites Fabricated by Novel Thixomixing Method

Author:
Ebrahim AKBARZADEH

Directors:

Dr. Josep A. PICAS BARRACHINA
Dra. *M^a^*. Teresa BAILE PUIG

Thesis submitted to obtain the qualification of Doctor from the Universitat Politècnica de Catalunya

in the

Light Alloys and Surface Treatments Design Center (CDAL)
Departamento de Ciencia de los Materiales e Ingeniería Metalúrgica
Escola Politècnica Superior d'Enginyeria de Vilanova i la Geltrú

September 2016

UNIVERSITAT POLITÈCNICA DE CATALUNYA
BARCELONATECH
Escola de Doctorat

Acta de calificación de tesis doctoral

Curso académico: 2015/2016

Nombre y apellidos
Ebrahim Akbarzadeh

Programa de doctorado
Materials Science and Metallurgical Engineering

Unidad estructural responsable del programa
Departament de Ciència del Materials i Enginyeria Metal·lúrgica

Resolución del Tribunal

Reunido el Tribunal designado a tal efecto, el doctorando / la doctoranda expone el tema de la su tesis doctoral titulada “Characterization of Aluminum Silicon/Short Carbon Fiber Composites Fabricated by Novel Thixomixing Method”.

Acabada la lectura y después de dar respuesta a las cuestiones formuladas por los miembros titulares del tribunal, éste otorga la calificación:

☐ NO APTO ☐ APROBADO ☐ NOTABLE ☐ SOBRESALIENTE

(Nombre, apellidos y firma) Presidente/a	(Nombre, apellidos y firma) Secretario/a	
(Nombre, apellidos y firma) Vocal	(Nombre, apellidos y firma) Vocal	(Nombre, apellidos y firma) Vocal

_____, _____ de _____ de _____

El resultado del escrutinio de los votos emitidos por los miembros titulares del tribunal, efectuado por la Escuela de Doctorado, a instancia de la Comisión de Doctorado de la UPC, otorga la MENCIÓN CUM LAUDE:

☐ SÍ ☐ NO

(Nombre, apellidos y firma) Presidente de la Comisión Permanente de la Escuela de Doctorado	(Nombre, apellidos y firma) Secretario de la Comisión Permanente de la Escuela de Doctorado

Barcelona a _____ de _____ de _____

به پایان آمد این دفتر حکایت همچنان باقی

به صد دفتر نشاید گفت شرح حال مشتاقی

سعدی

Abstract

The metal matrix composites (MMC) are widely used in different applications and offer high strength-to-weight ratio. In this thesis, it was developed a novel method to fabricate composite material in semi-solid state of aluminum with short carbon fibers (C_{sf}). The semi-solid slurry of aluminum silicon alloys represent thixotropic feature when sheared. The intensive shear stress created by high viscosity at mushy zone impacts on uniform distribution and effective dispersion of C_{sf} into the eutectic without serious physical or chemical damages.

For this process, called thixomixing, a prototype mixer was designed to study on A356, A357 and hypereutectic 4047 alloys. The homogenous distribution of C_{sf} were obtained under optimum conditions: around 48% of solid fraction in slurry and 100 rpm mixing speed. The C_{sf} was wetted in the molten of eutectic when the primary α-phase was formed. Deposition of silicon or intermetallic compounds on the fiber surface improves wettability aluminum and provides relatively good adherence.

The extruded and T6 heat treated Al composites had around 24% improvement of mechanical strength. The fractography analysis illustrated the ductile fracture with some plastic deformation as the results of dimples and some fiber pullout in the fractured surface. Ultra-micro hardness evaluation showed relatively good interfacial bonding after heat treatment.

Hypereutectic aluminum alloy (4047)/C_{sf} composite was used to evaluate the tribological properties. This composite showed low coefficient of friction, when the C_{sf} acts self-lubricant material. Taguchi method was employed to design the experiments to analyze the effects of the sliding speed, applied load and the volume fraction of C_{sf} on the tribological properties of thixomixed Al/C_{sf} composite. The contribution percentage for each parameter was determined by the analysis of variance. The results were indicated that Al/C_{sf} composite had better tribological properties than matrix alloy due to the carbon as solid-lubricant. The interfacial adherence of matrix/C_{sf} was shown with no fibers pull out in the tracking area. The presence of coherent and adherent graphite-rich layer on the worn surface was detected.

Electrochemical tests were conducted over three alloys, Al/C_{sf} composites with and without T6 heat treatment. The exposure surfaces were evaluated by SEM in order to find out the localized corrosion and the interfacial adherence. The C_{sf}, Si particles and iron-intermetallics play as cathode and the matrix as anode to form a galvanic couples.

The corrosion current density was decreased for un-reinforced alloys in compare to the composite samples.

Resumen

Los compuestos de matriz metálica (MMC) son ampliamente utilizados en diferentes aplicaciones y ofrecen una alta relación resistencia-peso. En esta tesis se ha desarrollado un nuevo método de conformación en estado semisólido de materiales compuestos en base aluminio con fibras cortas de carbono (C_{sf}). Las aleaciones de aluminio en estado semisólido presentan características tixotrópicas cuando son agitadas. La tensión de cizalla provocada por la alta viscosidad repercute en la distribución uniforme y eficaz de las fibras en el constituyente eutéctico, sin daños físicos o químicos graves.

Para este proceso, denominado thixomixing, se ha diseñado un prototipo mezclador, con el cual se han estudiado las aleaciones A356, A357 y la aleación hipereutéctica 4047. La óptima distribución del C_{sf} se ha obtenido en las siguientes condiciones: en torno al 48% de fracción sólida y 100 rpm de velocidad de mezclado. La deposición de silicio o de compuestos intermetálicos en la superficie de la fibra mejora su mojabilidad en el aluminio y proporciona relativamente buena adherencia.

Los materiales compuestos base alumino extruidos y sometidos a tratamiento térmico T6 tuvieron una mejoría en torno al 24% de su resistencia mecánica. El análisis fractográfico indica una fractura de carácter dúctil, dando como resultado la presencia en la superficie fracturada de hoyuelos y el desprendimiento de algunas fibras. La evaluación mediante ensayos de ultramicrodureza mostró una relativamente buena adherencia fibra-matriz después del tratamiento térmico.

Para evaluar las características tribológicas se utilizó como matriz la aleación de aluminio hipereutéctica (4047) reforzada con fibras de carbono. Este material compuesto mostró un bajo coeficiente de fricción debido al carácter lubricante del C_{sf}. Se ha realizado un diseño de experimentos utilizando el método Taguchi para analizar el efecto de la velocidad de deslizamiento, la carga aplicada y la fracción de volumen de los C_{sf} en las propiedades tribológicas del material compuesto Al/C_{sf}. El porcentaje de contribución de cada parámetro se determinó mediante análisis de varianza. Los resultados han indicado que el material compuesto presenta mejores propiedades tribológicas que la matriz debido al carácter lubricante del C_{sf}. La ausencia de fibras en el canal de desgaste demuestra la buena adherencia entre fibras y matriz. En la superficie del canal de desgaste se observó la presencia de una capa coherente y adherente rica en grafito.

Los ensayos electroquímicos se realizaron en las tres aleaciones y en los tres materiales compuestos Al/C_{sf}, con y sin tratamiento térmico T6. El C_{sf}, las partículas de Si y

los compuestos intermetálicos de hierro actúan como cátodo en una matriz de aluminio anódica, formando pares galvánicos. La densidad de corriente de corrosión es menor en las aleaciones sin reforzar en comparación con los materiales compuestos.

Acknowledgements

Big dreams are the strong motivations for progress, and I have a lot of them through my life so far and a lot since now. Now, at finishing my scholar in doctoral, I am so thankful from merciful God for bestowing of my dreams and life to be able to more progress and hardworking. The great experience of living in Spain and Barcelona was not only worthwhile to approach higher degree in doctoral of materials science and metallurgical engineering but also a way to taste different cultures, foods, art, living style and the best is friendship with nice peoples in that region.

I can remember clearly, the first day in Light Alloys and Surface Treatments Design Center (CDAL) when Professor Forn introduced me to my kind future colleagues and give me the explanations of labs and facilities in CDAL.

Besides, it is undeniable to consider my family's support, both financially and morally. I sincerely thank my parents, my parents in law and all my family members and gratitude especially from my dear and lovely wife, Elham Kheiroddin, for her unassuming encouragements and her patient companion during these years.

Nice chance to work with contributory and responsible supervisors, so I would like to express my sincere gratitude to Prof. Antonio Forn Alonso, Prof. Josep A. Picas Barrachina, Prof. Maite Baile Puig. I am indebted to all my nice colleagues, Dr. Enric Martín Fuentes, Dr. Sergi Menargues Muñoz, Eulàlia Nogués, Manel Campillo Betbesé in CDAL for their immeasurable companions and to share all their joys and happiness with me.

I also want to appreciate, Helena Querol and Yolanda Collado who are so helpful and kind during my working in Tecnològic centre de Vilanova i la Geltrú (CTVG). I would grateful all my Spanish friends, to teach me the lovely language, Spanish. As the least, I can pray for them all to be healthy and successfully. I will never forget them and hope this relationship will continue constantly in future. This work was supported by internal research funds of the CDAL for the doctoral program.

Apart from the CDAL members, I would like to thank: Dr. Lluís Gil Espert and his colleagues in the laboratory of Technological Innovation of Structures and Materials (LITEM) in Terrasa, the kind staff of Electron Microscopy Center, the kind persons in the different laboratories of the Department of Materials Science and Metallurgical Engineering (CMEM) of the Escola Tècnica Superior d'Enginyeria Industrial de Barcelona

and Prof. Jose Maria Cabrera, the staff of doctoral school of Polytechnic University of Catalunya. I wish to express my gratitude to Mr. Erik van Lennep to helping me in grammatical double checking through my articles.

Here is my warm gratitude to all my friends, Mohammadreza Zolfaghari, Hamed Ahmadloo, Vahid Joroughi for being supportive throughout the time when passed together and perennial friends and having happy times during my stay in Barcelona.

Barcelona-June, 2016
Ebrahim Akbarzadeh

Contents

List of Figures

List of Tables

Abbreviations

AMC	**A**luminum **M**etal **C**omposite
ANOVA	**AN**alysis **o**f **VA**riance
ASTM	**A**merican **S**tandard **T**esting **M**aterials
AN	**A**acrylo **N**itrile
BH	**B**rinell **H**ardness
C_{sf}	**C**arbon **s**hort **f**iber
CMC	**C**eramic **M**atrix **C**omposite
CPE	**C**onstant **P**hase **E**lement
CNT	**C**arbon **N**ano **T**ube
CNC	**C**omputer **N**umerical **C**ontrol
CVD	**C**hemical **V**apor **D**eposition
DoE	**D**esign **o**f **E**xperiment
DCP	**D**endrite **C**oherent **P**oint
DRC	**D**ynamic **R**e **C**rystalization
ECAP	**E**qual **C**hannel **A**ngular **P**ressing
ESCA	**E**lectron **S**pectroscopy **C**hemical **A**nalysis
EIS	**E**lectrochemical **I**mpedance **S**pectroscopy
EMS	**E**lectro **M**agnetic **S**tirring
EDX	**E**nergy **D**ispersive **X**-ray
FFC	**F**ace **C**enter **C**ubic
GP	**G**uinier **P**reston
HEC	**H**ydroxy **E**thyl **C**ellulose
HPDC	**H**igh **P**ressure **D**ie **C**asting
MMC	**M**etal **M**atrix **C**omposite

MH	**M**artense **H**ardness
MP	**M**esophase **P**itch
OCP	**O**pen **C**ircuit **P**otential
PAN	**P**oly **A**crylo **N**itrile
PDF	**P**ower **D**iffraction **F**ile
PVD	**P**hysical **V**apor **D**eposition
PMC	**P**olymer **M**atrix **C**omposite
PM	**P**owder **M**etallurgy
SEM	**S**canning **E**lectron **M**icroscopy
SLS	**S**urface **L**iquid **S**egregation
SPD	**S**ever **P**lastic **D**eformation
SSM	**S**emi **S**olid **M**etal
SSR	**S**emi **S**olid **R**heocasting
SSS	**S**upersaturated **S**olid **S**olution
TEM	**T**ransmission **E**lectron **M**icroscopy
UTS	**U**ltimate **T**ensile **S**trength
XRD	**X**- **R**ay **D**iffraction

Symbols

a	Distance	m
h	Gap between two parallel plates	m
f_s	Solid fraction	%
T_m	Melting point of solvent	Celsius
D	Sliding distance	m
T_L	Liquidus temperature of the alloy	Celsius
E_f	Property of reinforcement	
E_m	Property of matrix	
E_c	Property of composite	
f	Volume fraction	%
W	Weight of mass	g
l_{cr}	Critical fiber length	m
d_f	Diameter of fiber	m
W	Wear rate	$m^3.m^{-1}$
HV	Vickers hardness	
HB	Brinell hardness	
HM	Martens hardness	
F	Load	N
h_{total}	Total depth of penetration	m
h_r	Depth of footprint	m
$h\acute{r}$	Average penetration depth	m
W_e	elastic Energy or elastic recovery	J
W_r	plastic Energy or permanent deformation	J

W_{total}	Total energy of load	J
E_{corr}	Corrosion potential	mV
E_{ocp}	Open circuit potential	mV
L	Inductive capacitance	H
C	Capacitor capacitance	F
V	Velocity of momentum	$g.m.s-1$
ω	angular frequency	rads^{-1}
v	Velocity of moving plates	$m.s^{-1}$
$\dot{\gamma}$	Shear rate	
τ	Shear Stress	MPa
τ_0	yield stress	MPa
η	Viscosity	Pa.s
η_a	Apparent Viscosity	Pa.s
ρ	Density	$g.cm^{-3}$
λ	Structural parameter	

Publications

1. Akbarzadeh, Ebrahim, Picas, Josep A., & Baile, M. Teresa. (2015). Microstructure and properties of aluminum silicon/short fibre carbon composites fabricated by semi-solid thixomixing. Materials and Design, 88, 683–692

2. Akbarzadeh, Ebrahim, Picas, Josep A., & Baile, M. Teresa. (2015). Orthogonal experimental design applied for wear characterization of aluminum/C_{sf} metal composite fabricated by the thixomixing method. International Journal of Material Forming, 1-12

3. Akbarzadeh, Ebrahim, Picas, Josep A., & Baile, M. Teresa. (2015) Thixomixing as novel method for fabrication aluminum composite with carbon and alumina fibers, World Academy of Science, Engineering and Technology (WASET), ICCM 2015: 17^{th} International Conference on Composite Materials Vol:9, No:8

Dedicated to my love; *Elham* and my parents

Objectives

In this study, a novel method was developed on compo-casting to fabricate composite of aluminum silicon reinforced with short carbon fibers. This process was named thixomixing and its objective was to produce optimal dispersion and distribution of carbon fibers by intensive shearing force at mushy zone of semi-solid slurry. The new technique was investigated on the following different aspects in this study:

General objective

- The main objective is to contribute to knowledge of the processes of production of composite materials.

Specifics objectives

- To design an initial thixomixer and calculate the operational parameters to achieve a homogenous distribution of reinforcement in matrix.
- To investigate shearing force and viscosity for the dispersion of fibers and optimize the temperature and mixing speed.
- To improve the wettability and adherence between reinforcement and matrix avoiding the undesirable intermetallic compounds formation.
- To evaluate the effect of heat treatment on microstructure and quality of compounds.
- To relate the microstructure of the AMC with the mechanical and tribological properties and with the electrochemical and corrosion behaviour.
- To analyse the effect of severe plastic deformation (ECAP) in the microstructure and mechanical strength of the composite fabricated by thixomixing.

Chapter 1

INTRODUCTION

1.1 Composite Materials

Composite is a type of materials which contains two or more fundamental materials like metals, ceramics or polymers which has significant and different physical and chemical properties that are insoluble in each other [Mallick, 2007*a*]. Reinforcing phase is an element which has minor fraction and embedded in the matrix phase with major fraction. The composite materials can be divided into three categories based on the matrix and give us unlimited variation:

- Polymeric Matrix Composite (PMC) is common, relatively cheap and easy to fabricate. The PMCs are designed to provide high strength and stiffness supported by reinforcement when the loads applied and the matrix bonded the reinforcements to each other and transferred the loads between them. The main advantages of PMCs are their lightness joined with high strength and stiffness and corrosion resistance whereas their drawback is their low service temperature around < 200 $^{\circ}$C.

- Ceramic Matrix Composite (CMC) is developed to improve the ductility and fracture toughness for high temperature applications differ from other composite. The

mechanism by which these materials are toughened is that the reinforcing particles interfere with crack propagation in the brittle ceramic matrix. This can happen by crack deflection, crack bridging, or fiber pull out.

- Metal Matrix Composite (MMC) is fabricated to get high strength to weight ratio at high temperatures and better electrical and thermal conductivities. MMCs are more complicated for fabrication and expensive than PMC and CMC but are non-flammable and resistant to the organic agents with good load bearing capabilities.

Different types of composite materials can be classified based on the shape and orientation of reinforcement in matrix or structural form of composite components as illustrated in Figure 1.1. Different components in composite have specific mechanical properties. In general, composite materials have high strength-weight ratio, good fatigue

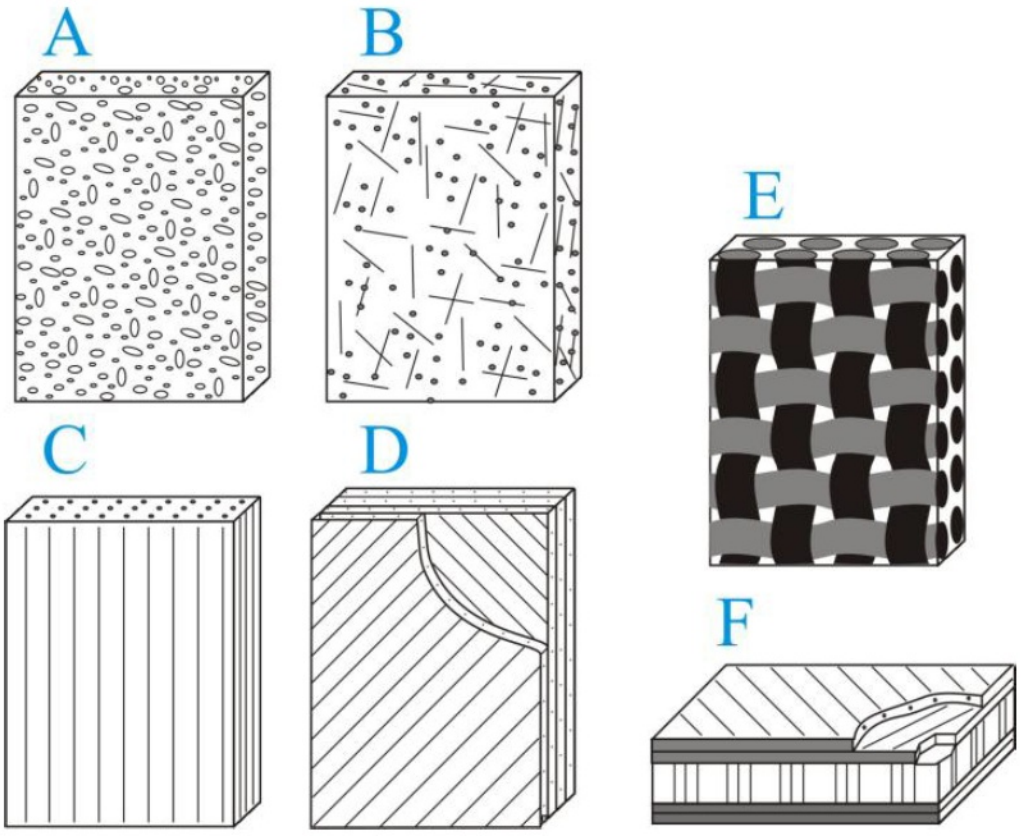

FIGURE 1.1: Schematic illustration of composite materials A) reinforced by particles B) reinforced by chopped fibers or whiskers C) unidirectional and continuous fibers D) laminated composite E) woven fabrics F) honeycomb composite (sandwich panel) [Kokcharov and Burov, 2013]

resistance, high tolerance of impact and corrosion resistance, which introduce them as

main competitor for conventional materials for different applications. The engineers are focusing to improve their properties and reduce the production costs with right selection of reinforcement and matrix properties. Although the composite materials show anisotropy and heterogenous, their applications can be introduced for various sectors.

1.2 Metal Matrix Composite

Metal Matrix Composites (MMCs) have various applications in several industrial sectors, such in aerospace, automobile, electrical, military and sport. The MMCs are made by homogenous dispersing of reinforcement material into a metal matrix. The most important point regarding MMC is fabrication of light weight material with homogenous dispersed reinforcement with good interfacial bonding to the metal matrix. Mallick et al. has been divided MMCs to three common categories based on the size and geometry of reinforcement [Mallick, 2007*a*]:

- Strengthened MMC with particles size $< 0.1\mu m$ in diameter, such as carbon nanotube.
- Reinforced with continuous or discontinuous fiber which is in the form of whiskers with aspect ratio (length-to-diameter) up to 200 and approximately 0.1-10 μm in diameter.
- MMC reinforced with particles or platelets in the range size of 0.5 to 100 μm and higher volume fraction, such as silicon carbide whisker (SiC_W).

In Figure 1.2, three form of reinforcement categorised on the shape was shown, which can be used mainly for fabrication of MMCs. The suitable reinforced particles must be cheap with good adhesion and good wettability to the matrix, prohibited chemical reaction and no thermodynamic equilibrium in fabrication process or in service [Baker, 1975, Islam and Wallace, 1988, Nie, 2012].

The most used and common reinforcement to produce MMC are alumina (Al_2O_{3p}), alumino-silicate (Al_2SiO_5) and silicon carbide. Later on the carbon fiber has also been

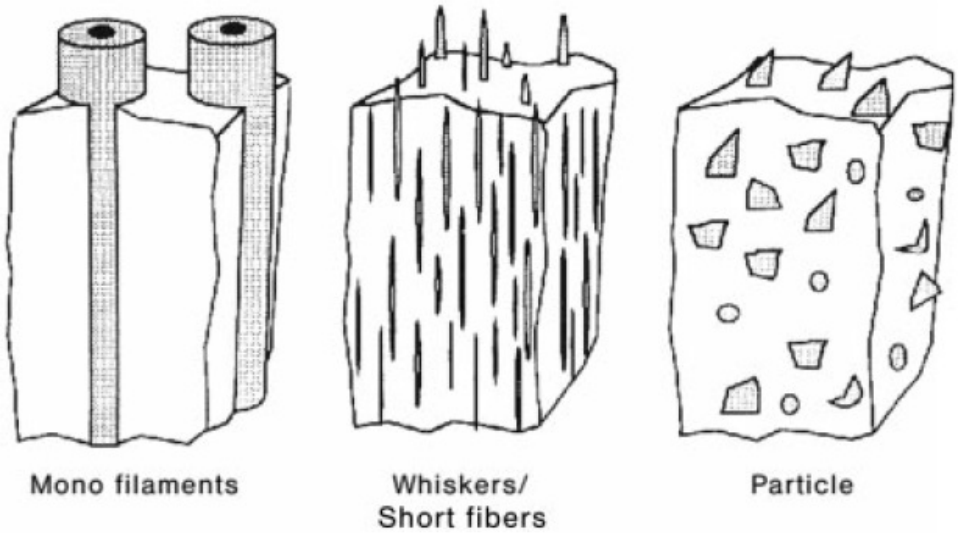

FIGURE 1.2: Schematic illustration of three main metal matrix composites based on the shape of reinforcement [Clyne and Withers, 1993]

considered as a reinforcement material for making the metal matrix composites [Cheng et al., 1993]. Aluminum, magnesium and titanium are commonly using as matrix due to their low cost, density and availability in variety forms of alloy. Metal matrix has some advantages in applications versus of other type of composite materials:

- High strength and stiffness relative to low weight
- Good resistance at relative high temperature
- Good thermal and electrical conductivity
- The yield strength and elastic modulus of most metals are higher than polymers
- Plastically can be deformed and strengthened

Some of the disadvantages of MMCs applications relative to the other composite materials are:

- Higher densities
- Some of metal matrix has undesirable chemical reaction with reinforcement
- Corrosion affinity at the interface

Some of the different applications of MMC such as high voltage electrical cable or satellite's structure illustrated in Figure 1.3.

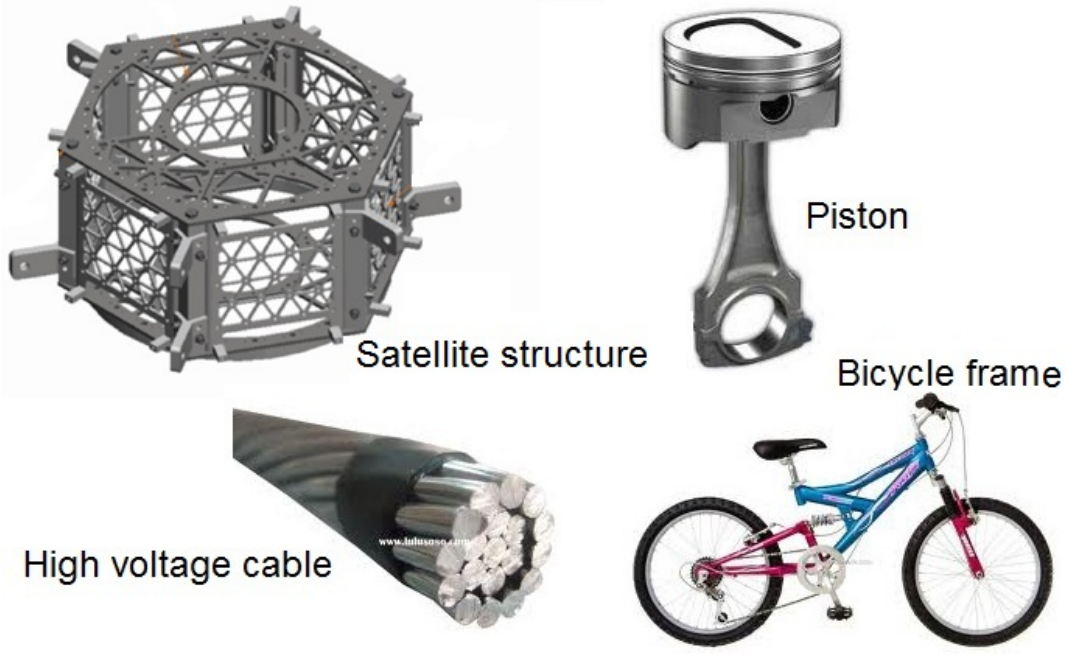

FIGURE 1.3: Some the applications of metal matrix composite (MMC) in different industrial sectors

1.3 Aluminum/Carbon Fiber Composite

Aluminum and its alloys have attracted the most attention as matrix in metal composites regarding to the weight-strength ratio, cost, availability and corrosion stability. Different alloys have been selected due to their specific characteristics for fabrication of aluminum matrix composite (AMC). If the AMC is designed and fabricated correctly, it combines the strength of the reinforcement with the toughness of the matrix to achieve a combination of desirable properties. The main reinforcement materials are fibers and/or particles of alumina, SiC, graphite, etc.

There are different advantages for using carbon fiber in AMC [Ogawa et al., 2010, Park et al., 2005]:

- At current time carbon fibers are produced relatively cheap and easy

- They are suitable for many applications because their outstanding and widespread properties
- These fibers have a very low density which are proper for the designed composite which need weight reduction
- The electrical conductivity is high for using as electrical conductor applications
- The ratio of weight to strength is good and is suitable for utilizing in transportation systems

The aluminum alloy/carbon fiber composites are a very promising advanced materials but the main problem regarding their usage is the production based on their theoretical properties. The pure aluminum and different type of aluminum alloys such as casting alloys (i.e. 3xx or 4xx) or wrought alloys (i.e. 6061 or 7075) can be used as matrix for fabrication of AMC in order to achieve the final properties and application of the material. Some of the application of AMC can be mentioned as transmission high voltage cable which now using alumina fibers by a American company, structural body of satellites and the frame of sport bicycles or other sporting instruments. Aluminum reinforced carbon fiber composite are used also to make golf club shafts, bicycle frames, automotive springs, sailboat masts, and many other components where light weight and high strength are needed.

Thermal expansion is reduced substantially by silicon and much less pronouncedly by all other additions except magnesium, which tends to increase it slightly. The high specific tensile strength of aluminum alloys is very strongly influenced by their composed poly-phase microstructure. Alloys prepared from powders exhibit somewhat higher strengths, especially at elevated temperatures. Increasing silicon content increases strength at the expense of ductility, but this effect is not very marked. Impact resistance is improved by spheroidizing the silicon.

1.3.1 Carbon Fiber

Carbon fibers are developing and high-performance materials with continuous long fibers manufactured by controlled pyrolysis process on suitable polymeric fibers containing at least 90% carbon. Manufacture of carbon fibers of high strength in the 1960s and 1970s made them the first choice for the manufacture of advanced composites for use in rocket nozzle exit cones, missile nose tips, re-entry heat shields, packaging and thermal management.

Different types of precursors provide various properties and must be easily conversion to carbon fiber, high carbon yield, and cost-effective processing. Carbon fibers are manufactured from two types of precursors, namely as textile (such polyacrylonitrile, PAN) and pitch precursor (a schematic illustration shown in Figure 1.4).

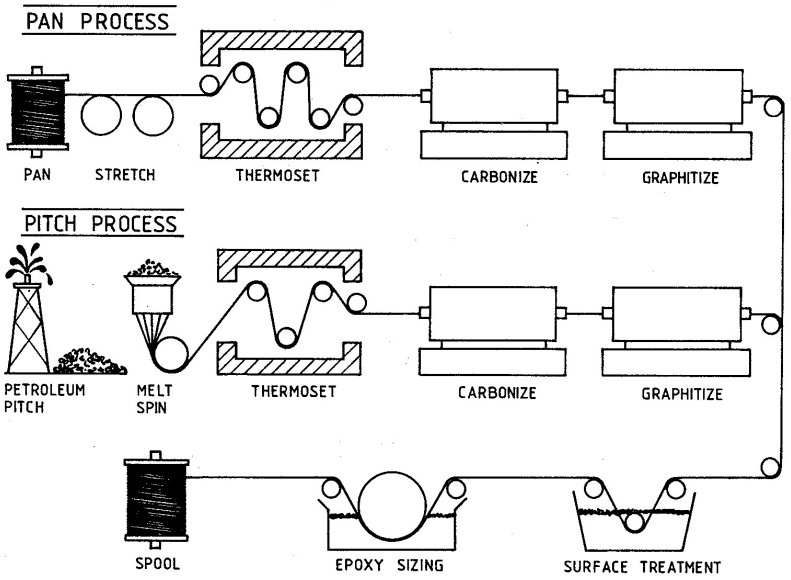

FIGURE 1.4: Schematic production line of carbon fibers [Diefendorf, 1987]

The potential precursors for manufacturing of carbon fibers are [Aykut et al., 2013, Hammel et al., 2004]:

- The most common and important precursor is acrylic based materials which contains $> 85\%$ acrylonitrile (AN) monomer. It is originated from commercial scale producers of textile-grade of acrylic fibers. In particular, polyacrylonitrile (PAN)

is the most popular acrylic precursor, which is used widely to produce the carbon fibers. (Figure 1.5)

FIGURE 1.5: Bulk and micrograph of PAN-based carbon fiber

- Pitch-based precursors are the second important raw material for carbon fiber such as mesophase pitch (MP). The carbon fiber yields from these materials have 85% carbon and show a high modulus owing to the more graphitic nature. On the other hand, the pitch-based carbon fibers have poorer compression and transverse properties compared to the PAN-based carbon fibers.

- Cellulosic precursors contain 44.4 % carbon. However, in practice, the reaction is more complicated than mere dehydration, and the carbon yield is only approximately 25-30 %.

- The vinylidene chloride and phenolic resins are the other forms of precursors proposed for the manufacturing of carbon fibers, but were not found to be commercially viable.

Production of carbon fiber from pitch is a lower cost process than PAN and the carbon atoms are arranged in low molecular weight aromatic ring patterns. The PAN type carbon fibers have lower thermal conductivity rather than pitch carbon fibers. Since 1960, the production of carbon fibers in large scale is being developed by subsequent researches by carbonization of Rayon, polyacrilonitrile (PAN) [Hiramatsu and Nishimura, 1989, Johnson, 1969, Otani and Yokoyama, 1969, Watt and Johnson, 1969]. Two important commercial surface treatments for carbon fibers are suggested [Agarwal et al., 2006, Chawla, 2012]:

- Oxidative: by producing acidic functional groups such as carboxylic, phenolic and hydroxylic on the carbon fiber surface in an oxygen-containing gas at 250 °C and above (air, oxygen or carbon dioxide) or in a liquid (nitric acid or sodium hypochloride). Oxidation at very high temperatures provides excessive pitting and reduces the strength of fibers. The effectiveness of surface treatment by nitric acid depends on concentration of acid, time and temperature of treating (Figure 1.6).

- Non-oxidative: the common method for non-oxidative treatment of carbon fiber is coating with an appropriate materials which provide the linkage by reacting with the matrix. The improved results can be achieved where the strong bonding provided between fiber surface and the coating which is suggested to oxidize the surface of carbon before coating process.

The carbon fibers have high tensile strength-weight ratio as well as tensile modulus-weight ratio, low densities, very low coefficient of linear thermal expansion and dimensional stability (suitable for space structure applications), high fatigue strengths, high electrical conductivity, high thermal and chemical stabilities in the absence of oxidizing agents, high thermal conductivity, excellent creep resistance and almost free-defect structure. The disadvantages are their high cost, low strain to failure, and low impact

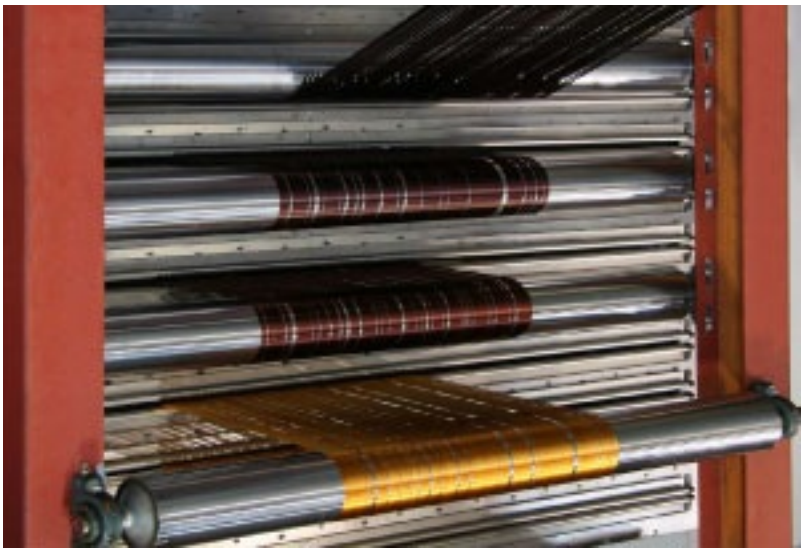

FIGURE 1.6: Oxidation process in the specific aerated oven and the color of continuous fibers changed from light to gold and brownish to black [zoltek.com, has been surfed in May, 2016]

resistance. Carbon fibers are available in different range of tensile modulus from 207 GPa to 1035 GPa [Yu and Yao, 2006].

Some of the properties (e.g. electrical conductivity and tensile strength) will be improved during the fabrication processes by the amount of crystallinity and eliminating of defects in carbon filaments. The carbon fiber microstructure depends on the precursors and processing conditions.

The favorite properties of fibers made them the first choice for the manufacture of metal reinforced composites [Anon, 1969] have been employed in a wide array of applications such as automobile parts, airspace structures, electrical instruments and military applications [Pearce, 1969].

The commercial carbon fibers have been coated by an organic material as sizing to prevent damaging or oxidation which is necessary to remove it before employment into metal matrix and also achieving a proper roughness on the fiber surface. The sizing agent on carbon fibers can improves in easy handling of fiber yarn and protect the surface of fibers from probable damages [Guigon and Klinklin, 1994, Yumitori et al., 1994].

It was suggested, in order to achieve a proper roughness and improve the interfacial strength and the dispersion, on the fiber surface, and to eliminate possible rests of sizing, fibers were also subjected to an oxidation treatment in a mixture of nitric acid and sulfuric acid then dried at an air furnace at 500 °C for 10 min [Feng et al., 2005, Urena et al., 2005]. Some coatings such as titanium boride (TiB_2) or sodium has been used on carbon fibers to reduce the problem of fiber degradation as well as to improve their wetting with aluminum alloy matrix [Mallick, 2007*b*].

The technological difficulty of fabricating carbon fiber metal composites are how to disentangle the fiber bundles for better infiltration and disperse them homogeneously in a matrix [Tanaka et al., 2009]. A closely packed fiber is main reason of poor infiltration and creates defects in the composite.

1.4 Fabrication Methods Used for Aluminum Alloy/Carbon Fiber Composite

Since 1960, various methods have been used to fabricate AMC reinforced with carbon fibers [Bakshi et al., 2010, Matsunaga, Matsuda, Hatayama, Shinozaki and Yoshida, 2007]. All technologies used for manufacturing of particulate reinforced metal matrix composites can be divided into three main category, solid state (powder metallurgy) [Esawi and Morsi, 2007] semi-solid state [Wu and Kim, 2011] and liquid state process [Shalu et al., 2009]. Conventional liquid stir casting and powder metallurgy are the main methods, but they are more costly and less effective for direct fabrication of aluminum alloy/carbon fiber composites.

Carbon fiber reinforced aluminum alloy matrix composites are provided through a wide range of processing techniques. As with carbon fiber-reinforced metal-matrix composites, the performance of the fibers is largely controlled by the interface between the fibers and the matrix, with the dispersion of them into the matrix. Generally, in order to fabrication of aluminum alloy/carbon fiber composites need to pay some attentions for following important points:

1. Complete infiltration
2. Strong adhesion and good wettability
3. Homogenous distribution of reinforcement
4. Avoid chemical reactions (intermetallics formation)
5. Good mechanical properties (high strength and stiffness)

Good adhesion at the fiber/matrix interface and homogeneous distribution of reinforcement are the main technical problems, which remained unsolved [Bakshi et al., 2010, Botelho et al., 2006]. There are some possibilities to produce carbon fiber/Al alloy composite will be discussed on their feasibility and characterization in the following steps:

1.4.1 Powder Metallurgy Method

All fabrication processes used aluminum alloy metal powder as main constituent, must be mixed with the reinforcement homogeneously and can be classified as solid state. The basic steps consist of mixing of reinforcement particles with aluminum alloy powder by mechanical millings such as SPEX milling (Figure 1.7) or planetary high speed milling which followed consolidation by compaction and sintering to form a rigid part. Mechanical alloying, spark plasma sintering, mixing-hot pressing are some of the methods which utilized for solid state fabrication of aluminum alloy matrix composite by powder metallurgy technique. Baker et al. have been reported a lot of broken fibres in carbon-aluminium composites produced by powder metallurgy and it was revealed a relatively weak interfaces bonding [Baker, Braddick and Jackson, 1972]. The weak interfacial adherence acts as easy rout which has been demonstrated the propagation of fatigue cracks.

Undesirable fibers cracking occurs under high load pressure in the powder metallurgy process [Even et al., 2010]. High compression load is necessary to produce a compact mixture of metal powder and short carbon fiber which made undesirable fiber crack

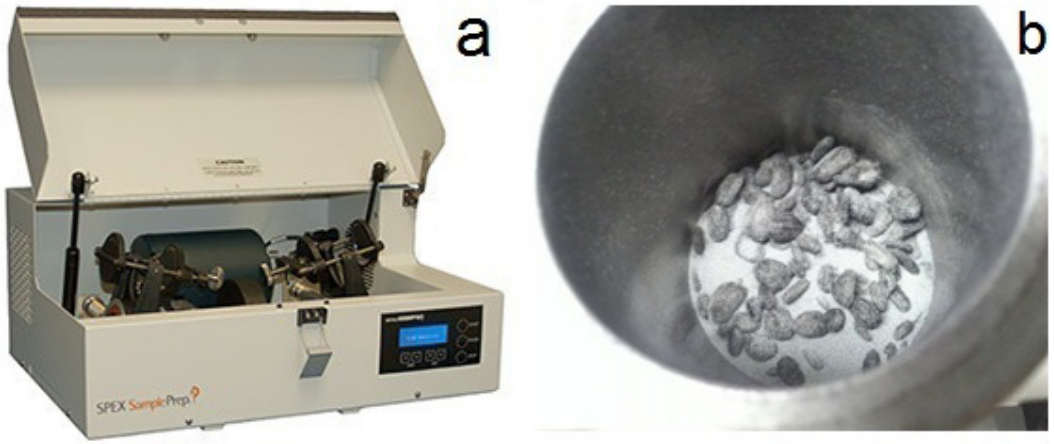

FIGURE 1.7: a) SPEX machine b) unsuccessful dispersion of C_{sf} and aluminum alloy powder after 60 min shaking in SPEX

leads to the strength of the composite significantly influenced by interfacial bonding and fiber length. The grains of metal powder punch the fiber filaments at very small different size generally depends on powder grain size whereas some studies have been employed hot extrusion or very hot pressing to avoid cracking [Jahedi et al., 2012, Kwon et al., 2009]. Figure 1.8 is shown the cracked carbon fibers by aluminum alloy powder after cold pressing which has been done by author to verifying this phenomenon.

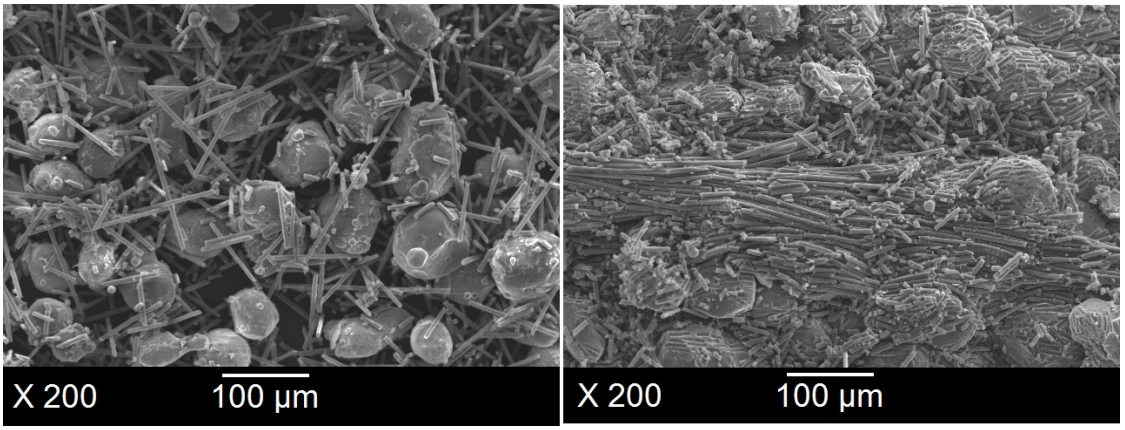

FIGURE 1.8: SEM images of cracked fibers at different sizes by aluminum alloy powder under pressing in powder metallurgy

Simancik and his colleague have been reported small or no interfacial interaction by hot extrusion to fabricate aluminum alloy/C_{sf} [Simancik and Jangg, 1994]. Interfacial fiber/matrix bonding strength and fiber length are effective on average axial stress even fibers are long enough, the strength is suitable whereas no bonding occurs due to the frictional stress along to length of the matrix-fiber interface [Nie, 2012]. Rams et al.

has been utilized the nickel coated short carbon fiber with Al 6061 powder to avoid aluminum carbide formation and improving of wettability [Rams et al., 2007]. Other methods such as mechanical alloying and sintering and deformation processing of powder compact are not effective to manufacture metal matrix composite with carbon fiber or other type of fibers [Adamiak, 2008, Peng and Chang, 2014, Ruiz-Navasa et al., 2006].

Hot extrusion of aluminum alloy powder pre-mixed with short carbon fibers fabricated unidirectional fiber composite in 1994 is expected higher strength at low cost compared to the continuous fibers [Simancik and Jangg, 1994, Varshavskij, 1995]. Effective processing parameters can be outlined as extrusion temperature, ram speed, fiber length and chemical interfacial reaction between fibers and matrix.

Another challenge regarding metal powder and C_{sf} is dispersion of fiber tows and distribution into powder grains. The previous attempts have been utilized the dispersant materials such Hydroxyethyl cellulose (HEC), cellulose sodium (CMC) or Polyvinylpyrrolidone (PVP) for dispersion of fibers by by rotary stirring [Che et al., 2011, Hao et al., n.d.]. The effects of dispersant agent concentration, stirring speed and stirring time on C_{sf} are important for instance if the concentration of HEC is too high or too low, the dispersion of C_{sf} in water is not obvious. This kind of materials provides the electrostatic charges on carbon filaments in water and repulsion force between them. Figure 1.9 illustrates a suspension sample of C_{sf} in distilled water and 5 g.l^{-1} HEC.

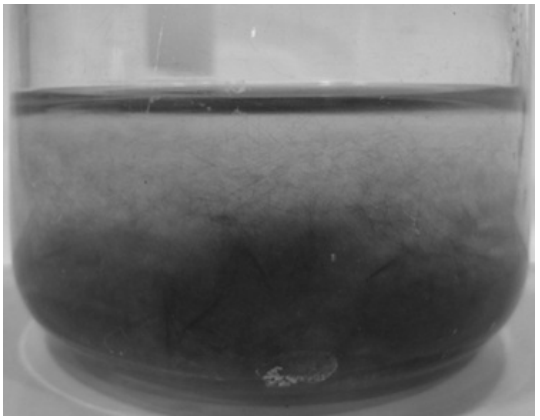

FIGURE 1.9: Dispersion of short fiber bundles in a 5 $g.l^{-1}$ HEC solution in distilled water powered by ultrasonic agitator

The carbon fiber is fragile but it could be good solution for fabrication of metal composite with reinforcement such as CNT, Al_2O_3, SiC, SiO_2 and TiO_2 which bear against crashing. Most of studies on Al/nanoparticles composite have been carried out using powder metallurgy [Nie, 2012, Wu and Kim, 2011]. Aluminum alloy powder is being used for fabrication CNT/aluminum composite in different applications for good distribution and easily production. But the former studies which have been utilized short carbon fiber to produce aluminum metal composite were unsuccessful [Kohara and Muto, 1988].

1.4.2 Liquid State Processing

The most conventional rout for processing of MMCs is mixing in fully liquid molten metal especially for those which have low melting point. By this method, aluminum alloy must be melted firstly at over melting point then mixing the reinforcement particles under mechanical stirring or infiltration of molten into the prepreg. The process may limit due to low wettability, undesirable chemical reaction, cluster formation is occurred under surface tension and float the fibers at top of the molten alloy, regardless of the speed of stirring. The stir casting (schematically shown in Figure 1.10) [Bhav Singh and Balasubramanian, 2009, Shi et al., 2012], pressured or vacuum pressure infiltration technique (Figure 1.11) [Wang et al., 2012], diffusion bonding [Nayeb-Hashemi and Seyyedi, 1989], infiltration technique [Mortensen and Cornie, 1987], squeeze casting [Hajjari and Divandari, 2008] and spray forming [Zambon et al., 2004] are the methods have been conducted to fabricate aluminum alloy/C_f matrix composite. Direct pressure or vacuum pressure infiltration is effective and general routs regarding liquid state fabrication of MMC. The MMCs are also prepared with prepreg methods using liquid metal routes such as squeeze casting or vacuum pressure infiltration, which leads to poor wettability and weak adherence at the interface (Figure 1.11) [Hari Babu et al., 2008]. Low interfacial adherence and non-homogeneous distribution are the main challenges for the liquid metal composite manufacturing process [Hashim et al., 2002]. The infiltration was carried out by high pressure of liquid metal or vacuum pressure-less infiltration.

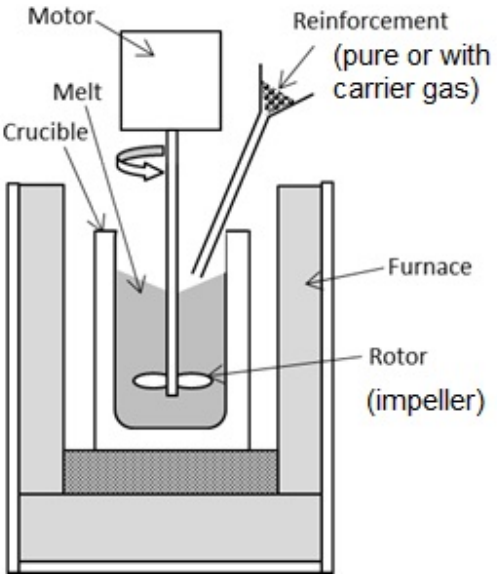

FIGURE 1.10: Schematic operational sequence during melt stirring [Tzamtzis et al., 2009]

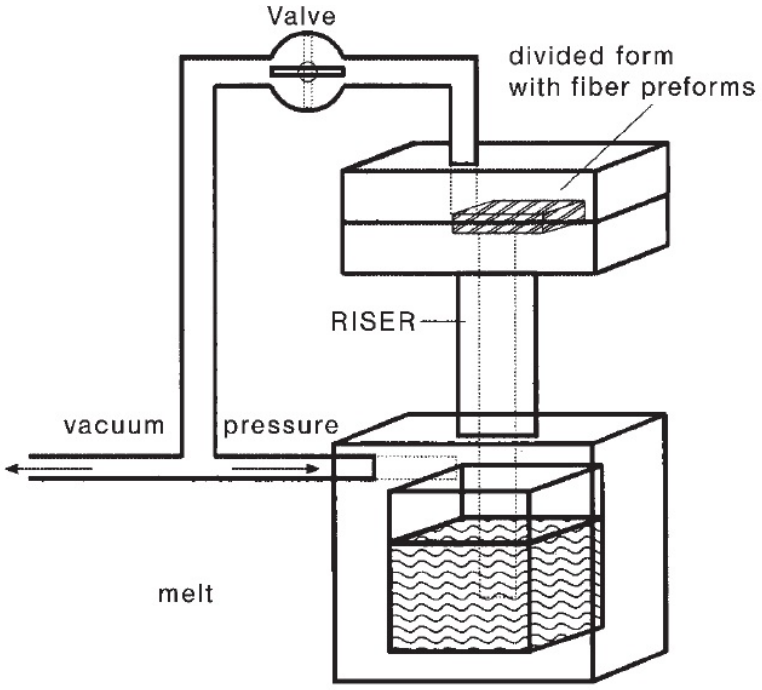

FIGURE 1.11: Vacuum pressure infiltration technique [Karl, 2003]

A common and cheaper technique is infiltrating of aluminum liquid into fiber (ceramic or graphitic) tows by high pressure. The high pressure is needed to compensate the non-wetting condition and provide the driving force to flow liquid between filaments [Pippel et al., 2000]. The high temperature which in needed for this process caused to form brittle aluminum carbide [Wang et al., 1997].

Baumli et al. proposed the a new method for fabrication pure aluminum/carbon fiber composite using aluminum liquid and a special flux containing K_2TiF_6 dissolved in salt mixture flux NaCl, KCl [Baumli et al., 2013, Juhasz et al., 2012]. The salt flux removes the oxides at the interfaces and facilitates the formation of a TiC layer coated on C_f with good wettability so this composite can be fabricated spontaneously without applying any external pressure or mixing (In Figure 1.12 shows the TiC layer over fibers). The thin film layer of Ti was clearly investigated along the C_{sf}/Al interfaces especially at high salt:Al ratio and higher content of the molten salt. However, the titanium is presented in the molten by the spontaneous exchange reaction between the salt and aluminum and reacted by the C_{sf} in the form of thin titanium carbide layer along the fibers which shows the perfect wettability of C_{sf} by liquid aluminum.

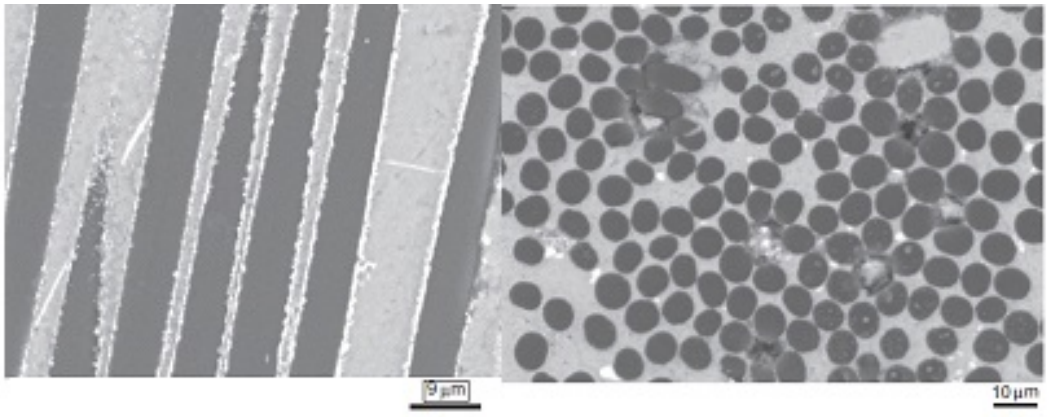

FIGURE 1.12: SEM of the a) longitudinal and b) cross section of C_{sf} in Al-matrix (white: Ti deposited at the Al/C_{sf} interface by 20 wt.% K_2TiF_6, gray: Al-matrix) [Baumli et al., 2013]

Incorporation of the reinforcement component to be homogenous mixing and solidification control are the main important steps regarding liquid casting composite production. The microstructure of matrix was influenced by alloy elements, cooling rate and viscosity of the melt. In addition, the size, shape and volume fraction of reinforcement have impacts on the microstructure of casted composite [Qin et al., 2004].

Squeeze casting is able to fabricate fiber reinforced metal composite under at high temperature and short time. Some of the conventional compo-casting methods such as squeeze casting (Figure 1.13) are limited by the component geometry, process cost due to long time and the additional fiber coatings. Another challenge evolving of squeeze

casting is entrapment of air which arrested between tows and cannot be released by high pressure. The pores may act as crack initiation site and decrease strength. Direct squeeze infiltration method needs a die and piston which powered by high pressure pressing machine then high temperature molten metal infiltrates along the fiber filaments.

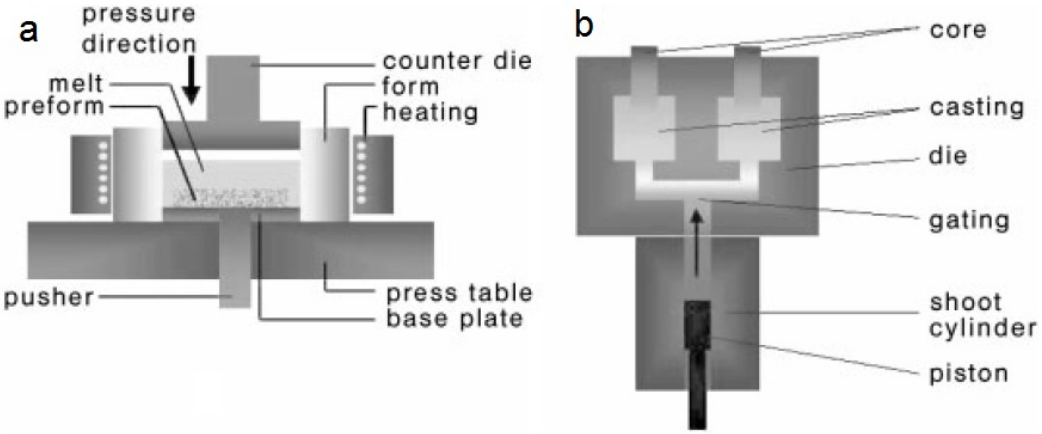

FIGURE 1.13: Direct and indirect squeeze casting [Karl, 2003]

The following attempt to fabricate aluminum/carbon fiber with squeeze casting has been performed by Li et al. using PAN based C_{sf} with 14 vol.% and aluminum liquid at 500 and 800 °C [Li and Chao, 2004]. The interface structure of composite has been investigated and shown in Figure 1.14 by high resolution TEM and electron spectroscopy for chemical analysis (ESCA). In some previous studies in order to reach good wettability or hindering of carbide formation, an extra coating has been applied on carbon fiber but the coating was delaminated or broken under high pressure [Hajjari et al., 2010, Rams et al., 2007, Urena et al., 2007].

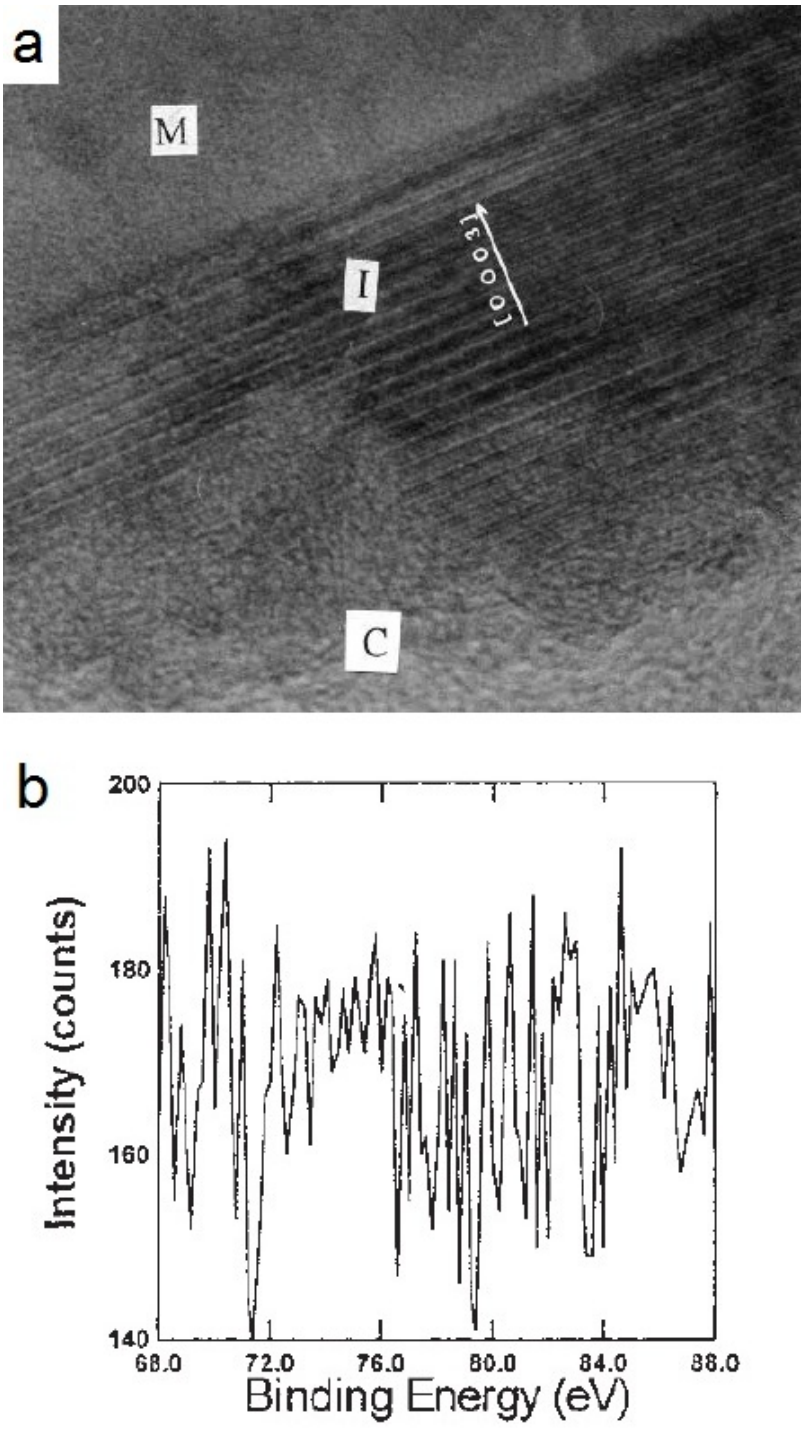

FIGURE 1.14: (a) High-resolution TEM analysis of Al_4C_3 and at the upper side of the lath like carbide reveals several plates (M: matrix, I: intermetallic, C: carbon fiber) (b) ESCA spectra of Al 2p [Li and Chao, 2004]

1.4.3 Semi-Solid State Processing

Semisolid metal (SSM) processing has been developed initially by Flemings M. C. et al. since early 70s as new industrial processes to overcome the main disadvantages of conventional casting alloys [Mehrabian et al., 1974*a*,*b*]. This process involves slurry of non-dendritic and produces homogenous globular microstructure of alpha phase as solid particles which dispersed in the molten liquid (Figure 1.15).

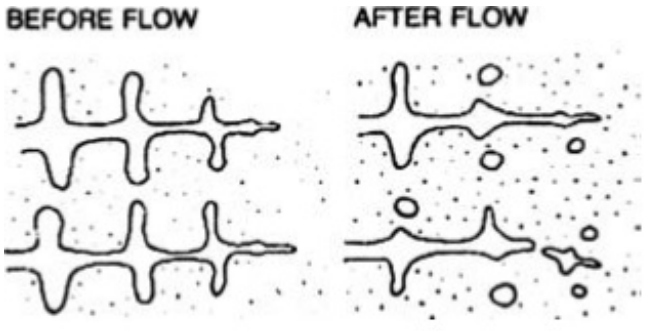

FIGURE 1.15: The schematic mechanism for fragment of dendrite

A metal in semi-solid is in a thixotropic state, with a globular microstructure. The final chemical and mechanical properties are quite different from those obtained by dendritic alloys of conventional forming technologies which use either solid or liquid metals as starting materials [Fan, 2002]. The following attempts have been carried out based on semi-solid techniques to develop the methods using slurry and die casting [Girot et al., 1987, Mehrabian et al., 1974*b*, Pai et al., 1994]. All semi-solid techniques are being used for composite fabrication have a big advantage which is using temperature within freezing range between liquidus and solidus. This lower processing temperature eliminate the superheat and reduce the chemical reaction at fiber-matrix interface. There are two techniques to produce metal slurries namely, thixocasting and rheocasting which result a globular structure at an appropriate temperature of casting (Figure 1.16).

In the thixocasting process, the billets or bars are produce over direct chilled casting while stirring in order to shear off the dendrites in the mushy zone. A mushy zone referred to a condition which the solids and liquids are existed simultaneously. A stirring device is used to produce non-dendritic microstructure over continuous casting operation then casted into billets or rods after that the globular structured billets or rods cut

and reheated to the optional semi-solid temperature for final casting into mold. This process has a big disadvantage, which is the scrap that cannot be recycled at the workshop site.

In the rheocasting, the molten metal treated by controlled stirring/cooling from fully liquid state to semi-solid temperature in one-step in order to produce a globular structured of solid particles in the slurry followed by direct casting into a mold. Rheocasting prepares the slurry on demand at site which is a big benefit compared to the thixomixing process [Ivanchev et al., 2008].

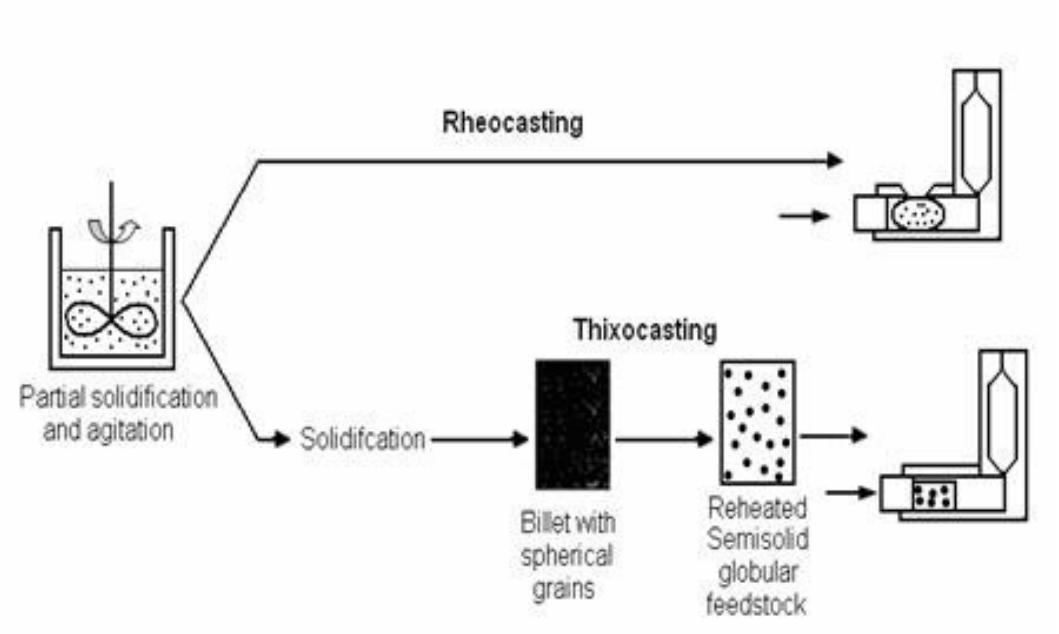

FIGURE 1.16: A schematic of both semi-solid process thixocasting and rheocasting [Kirkwood et al., 2010*b*]

Mechanical and electromagnetic stirring are typical methods for slurry preparing which are used beside a die-casting machine. In all die-casting operation a non-adhesive material used to easy final part removal from dies and protect die from damaging. There are two common tool protector coatings were employed, ceraspray and graphite powder. Ceraspray which contains ceramic powder reduces heat exchanges between the semi-solid material and the tool, which have a higher thermal conductivity. Graphite powder has high thermal conductivity and is conventional material for non-adhesion action.

The mechanical properties of semisolid cast parts are improved considerably in against of fully liquid cast parts with the same alloys. Published literature reveals that there is around 25% increase in elongation, 30% increase in impact and 7-10% increase in fatigue strength [Yan and Fan, 2001].

In conventional fully liquid casting, solidification shrinkage is one of the major problem and leading to macro-porosity formation in final part. Turbulent flow of molten liquid into the die result to the air entrapment and porosity formation. But, most of these problems can be overcome through the semi-solid casting for instance, partial solidification before casting may reveal very little shrinkage during casting in SSM.

The gas entrapment into the work piece is reduced in SSM methods over conventional casting process due to a linear flow of slurry into the mold. In this method, the slurry moves very easily into the mould with excellent consistency and integrity. When the viscosity of semi-solid slurry is high, the velocity of filling can be high so the metal will be flow easily even at low Reynolds number for casting thin-walled parts.

The semi-solid processes is expected from an economic point of view, because the short duration of production cycles, longer life of molds, lower machining requirements and the use of less expensive heat treatments [Arrabal et al., 2013]. There are several advantages of semisolid processing over conventional alloy casting processes. The semi-solid castings offer the following characteristics [Forn et al., 2007, Mehrabian et al., 1974*a*][Forn et al., 2010]:

- Few defects (Less shrinkage, porosity and oxide film)
- High resistance to mechanical stresses (yeild strength, ultimate tensile strength, fatigue behavior)
- High resistance to high pressures (hydraulic and pneumatic)
- Minimum amount of air entrapment in final product due to laminar flow of slurry into the mold
- Can be heat treated

Processing semi-solid aluminum alloy also yields cost reductions through:

- High production rate
- Extended mould life because of low working temperature
- Cast at near net shape
- The shrinkage is minimum
- Lower temperature and less thermal chock and longer tool life

1.4.3.1 Electro-Magnetic Stirring (EMS)

A typical electro-magnetic stirring for semi-solid casting process is illustrated schematically in Figure 1.17 that a stack of coils around it generates magnetic field and circulations along the longitudinal direction. This is a continuous process with an inlet velocity, u_{in} of molten metal through the top of mould and solidified billet drawn away at bottom with constant casting speed, u_{cast}. The EMS provides strong linear stirring and flows which will shear off the dendritic structures from the solidification front so the fragmented dendrites transported along the fluid into the melt that act as nuclei for a globular microstructure and produce semi-solid slurry.

The EMS process control the electromagnetic circulation and shearing action with the rate of heat removal, hence provide the desired microstructure [Barman and Dutta, 2008]. The billet made after stirring and the microstructure has been modified called "raw material" and for further process must be reheated to a temperature in the mushy zone and injected into the die by die-casting machine [Kirkwood et al., 2010*b*].

1.4.3.2 Mechanical Stirring

Mechanical stirring is a conventional rout to create globular microstructure of solid particles in liquid for semi-solid slurry production. Depends on the semi-solid processing, different slurry preparation method conducted. In SSR, the molten aluminum alloy

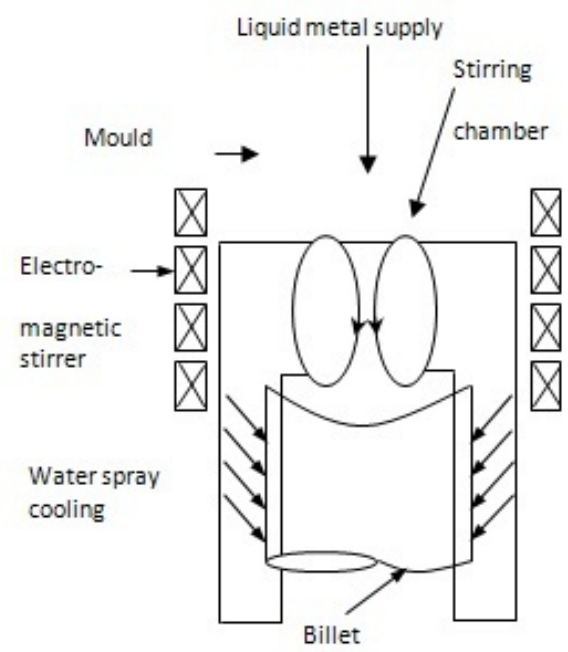

FIGURE 1.17: Schematic of Electro-magnetic stirring (EMS) and the circulation [Niedermainer et al., 1998]

cooled by a rotating device as cold finger generally made from graphite and acts as heat sink (Figure 1.18 and 1.19). The nucleation occurs while molten temperature reduced and the nuclei grow to form particles by the shearing force to fragment the dendrite arms [Kirkwood et al., 2010*a*].

The size of fine-grained microstructure is obtained with this method, is 30 μm approximately. The heat transfer through the mold wall is controlled by a water cooling system circulate around it. Some previous attempts have been carried out based on semi-solid compo-casting for aluminum alloy and carbon fiber. Pai et al. have been used C_{sf} (3-5 mm) to embedded into the aluminum alloy at 25-30 % primary solid fraction in slurry for 10-20 min stirring by paddle stirrer, but the fibers has been cracked undesirably and there were no more information available regarding mechanical properties [Pai et al., 1994]. The very old attempts for semi-solid rheocasting process have been conducted the aluminum alloy slurry and short fibers or whiskers to fabricate aluminum matrix composite by paddle stirrer [Girot et al., 1987, Mehrabian et al., 1974*b*]. In 2008, Hari Babu et al. have been utilized a twin screw machine for fabricate aluminum alloy composite reinforced with SiC particles under intensive shearing load [Hari Babu et al.,

2008]. Two step processes have been used, first stirring by impeller at fully liquid condition and shearing followed by a twin crew machine under rheo-process to disperse and distribute particles into the metal matrix.

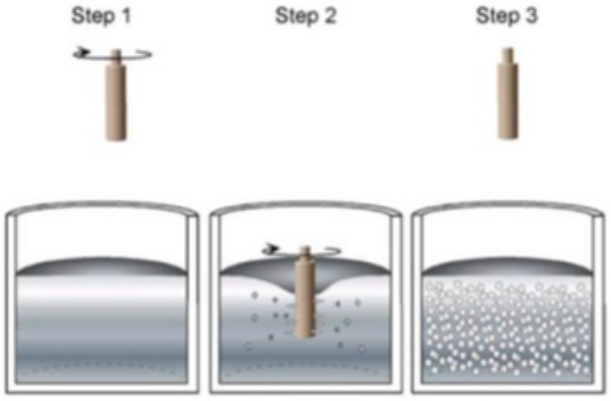

FIGURE 1.18: Schematic of semi-solid rheocasting (SSR)[Flemings, 1991]

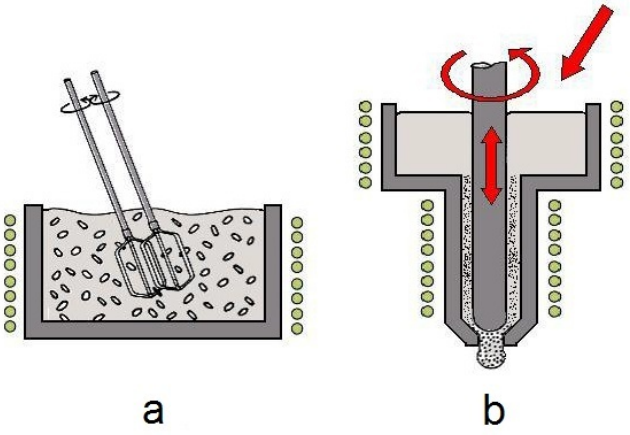

FIGURE 1.19: Mechanical slurry production a) mechanical agitation of the liquid, b) mechanical agitation and continuous process [Kirkwood et al., 2010*b*]

1.5 Properties of Aluminum Alloy/Carbon Fiber Composites

The theoretical calculations for all properties such as strength, modulus and other properties of a fiber-reinforced composite are based on the fiber volume fraction in the material. A general rule of mixtures is a weighted mean used to predict various properties of

a composite material made up of continuous and unidirectional fibers. The theoretical values of mechanical parameters such as UTS, Young's modulus and also density of samples can be calculated by the rule of mixtures.

1.5.1 Mechanical Properties

Pure aluminum is not a suitable choice for the matrix in the composite, for instance, the tensile strength or hardness increased 13% and 8%, respectively when Mg content is 0.9 wt.% by stir casting of copper coated short carbon fibers [Shi et al., 2012]. For 8 wt.% graphite particulates addition, the composite becomes brittle, and the wear rate increase [Lin et al., 1998]. In the longitudinal tensile strength, two most important parameters could be affected; first, the surface quality of carbon fiber due on the individual fiber strength, and Second, interface strength leads to better load transfer in the composite [Ivens et al., 1994]. Moreover, in the case of short fiber reinforcement the strength of composite influenced by the length of short fibers.

Poor infiltration, low interfacial adherence of matrix reinforcement, undesirable intermetallic formation, good dispersion and homogeneous distribution and weak tensile strength are common problems in aluminum composite fabrication. The interfacial adherence plays very important role in all composite materials so the good adherence provides the mechanical properties near to ideal or theoretical values (Figure 1.20). Wang et al. have been reported good mechanical property of bulk composite achieved when SiC coating was conducted on carbon fiber by Sol-gel method [Wang et al., 1997].

Different amounts of pressure impressed tensile strength so high pressure may separate coating from the fiber and reduce the strength. The silica coating did not improve the quality of carbon fiber/aluminum interface and Al_4C_3 particles have been seen occasionally at the interface due to cracking of coating under high pressure [Brown et al., 2002]. Then, it is possible that Al_4C_3 nucleates and grows heterogeneously from C_f to the matrix as an interfacial reaction.

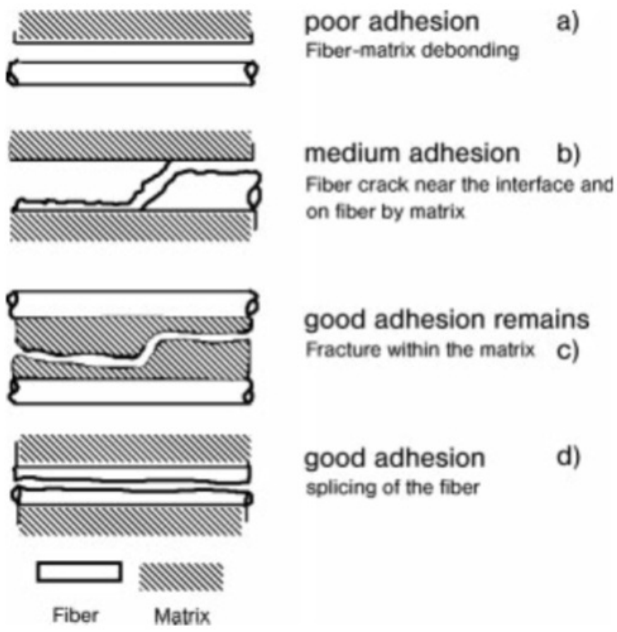

FIGURE 1.20: Schematic illustration of interfacial fiber/matrix adherence quality [Karl, 2003]

Another challenge may occur in fully liquid or thixomixing process is entrapment of air arrested in the matrix as bubbles so act as crack initiation sites in the composite under loading.

The influence of alloying elements such as Si, Mg and Ca have been investigated on interfacial properties and mechanical strength in aluminum alloy matrix composite reinforced by carbon fiber [Towata et al., 1985]. The primary α-Al was nucleated on the carbon fiber surface and undesirable carbide and spinels formed which it was at minimum can improve the interfacial bonding. The interfacial effects of Al/C on the strength of composite and fracture morphology showed that the growth of Al_4C_3 was anisotropic and increasing amount of brittle phase of carbide after heat treatment weakened the strength and elongation of composite. A large amount of brittle phase in composite may produce notches and degrade mechanical properties of fibers that play as crack initiated and embrittlement of aluminum alloy matrix.

The challenged mechanical property in order to composite materials is the tensile strength can be attributed strongly to the interfacial bonding and uniform distribution and dispersion of carbon fibers into the matrix. Different mechanisms and scenario have been interpreted regarding fracture surface of aluminum alloy/carbon fiber composite [Blucher

et al., 2001, Vidal-Setif et al., 1999]. For example, the flat fractured surface with no fiber pulls out is related to the brittle characteristic and presence of Al_4C_3, after testing. If this brittle phase cracked before fiber while loading, a crack initiation site created and the crack propagate in the fiber and the matrix surrounded it, finally resulting in low stress fracture [Wang, Chen, Li, Wu and Jiang, 2009].

1.5.2 Wear and Tribological Properties

The moving parts in all application such as automobile pistons are needed to protect against wearing and erosion by lubrication. On the other hand, the graphite particles on the surface can act as self-lubrication for those particles which are sliding on each other. High-silicon aluminum alloys (hypereutectic alloys with 20-25% Si) are 10 times more wear resistance than plain steel and low friction coefficients however, they are not successful unless contain substantial tin [Mondolfo, 2013].

The C_{sf} embedded in hypereutectic alloys, making this composite an ideal material choice where good wear and high strength properties are required in light weight components. Addition of carbon fiber improves the machinability and wear resistance similarly with graphite particulates which provide the good tribological properties with an excellent lubricity and lower coefficient of friction [Ramesh et al., 2013]. Liu et al. have been reported a good wear resistance of aluminum composite reinforced with short carbon fiber and with increasing of volume fraction of carbon fiber the wear rate and friction coefficients decreased [Liu et al., 2009]. A graphite rich layer was covered over wear track area and demonstrated carbon mixture with aluminum during wearing (Figure 1.21). The results of previous attempts on C_f/2014 Al alloy composites shown the improvement of wear resistance by forming a graphite film formed on the worn surface [Daoud, 2004]. Song et al. [Song and Han, 1997] has been indicated the wear resistance of Al/Al_2O_3/C hybrid composites was improved remarkably by addition of C_f over wear track as solid lubrication film.

The good mechanical strength and high wear resistance are not only essential for aluminum matrix composites while self-lubrication properties are also desirable [Suresha

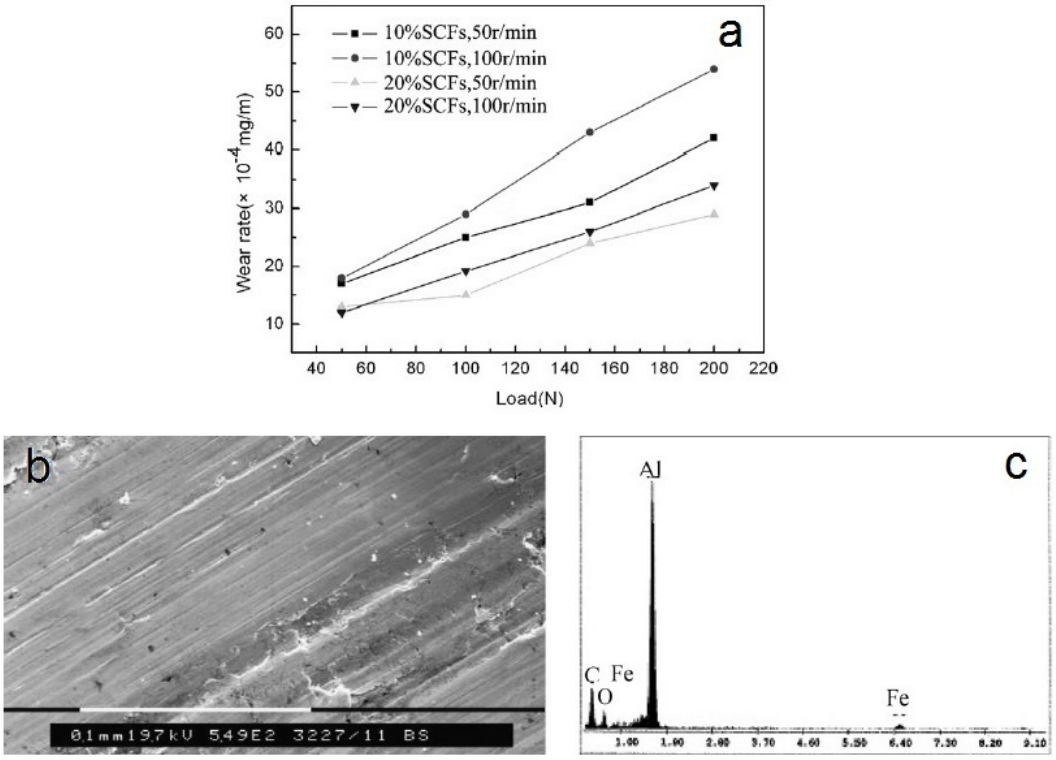

FIGURE 1.21: (a) Wear rate of SCFs/Al composites at different loads and rotating rates (b) , (c) SEM of worn surfaces tested under 100 N with 100 rpm,10% C_{sf}/Al [Liu et al., 2009]

and Sridhara, 2010]. In wearing of metal-to-metal contact, the carbon fiber plays a role as solid lubricant based on its graphite microcrystalline composition. The surface of Al/C_{sf} deformed plastically and the C_{sf} milled on the metal surface as small particles and reduced the friction. The results of tribological study on the effect of fiber-orientation of Al_2O_3 and C_{sf} in aluminum alloy matrix were revealed that average value of wear rate was higher when the fiber in parallel-oriented wear surface than that in normal-oriented wear surface [Du et al., 2003].

The specific wear rate was calculated using the transverse area of the worn channel, which was measured by a profile-roughness measuring unit. Generally, the wear rate (W) m^3/m was calculated by using the Eq. 1.1

$$W = \Delta V / D \tag{1.1}$$

where ΔV is the volume loss (m^3) and D is the sliding distance (m). The following equation was used to calculate the specific wear rate of the specimen affected by the

chemical composition of the exposed material and the environment of the exposure.

$$k = \Delta V / (F.\Delta s) \tag{1.2}$$

where k is wear factor or specific wear rate, $m^3.(N.m)^{-1}$, ΔV is volume loss, m^3, Δs is sliding distance, m and F is load, N. It must be mentioned that the Eqs. 1.1 and 1.2 were deviations of Archard equation for sliding wear.

1.5.3 Corrosion Behaviour of Aluminum Metal Composite

Metal composite which is made by aluminum silicon alloy and carbon fiber can be utilized in various applications, so the corrosion behavior of matrix, matrix/fiber interface and the reaction of intermetallics are interesting [Wielage and Dorner, 1999*a*]. Aluminum-silicon alloys without copper have good corrosion resistance in most reagents; only in alkaline solutions which attack silicon as well as aluminum. Aluminum is susceptible to the pitting corrosion, particularly in the media containing halide ions, for example the chloride ions breakdown the passive film and initiate the pits. Copper and iron reduce the corrosion resistance appreciably, unless corrected with manganese or chromium. Tin and calcium also have a deleterious effect on corrosion resistance. The aluminum is so sensitive to pH of corrosive environment and corrosion rate was increasing with increasing of pH. The corrosion rate is lower in room temperature than the high temperature as reported for different samples [Payan et al., 2001].

Porosity in the matrix decreases corrosion resistance. Corrosion may lead to weakening fiber/matrix interface and reduce load transferring from matrix to fiber and potential site for crack initiation under tension [Lu et al., 2005]. Contact corrosion is especially poor in aluminum-silicon-copper alloys, but even copper-free alloys are worse in this respect than aluminum 99.8%. Aluminum composite reinforced with carbon fibers have specific mechanical properties but are also poor resistance to corrosion in the solutions contain chloride.

From the electrochemical point of view, both silicon and carbon fiber play a cathodic role resulting in galvanic couples with aluminum as anode in electrolyte solution and

lead to a localized destructive galvanic corrosion at aluminum/carbon fiber interface. The lower surface ratio of anodic in against of cathodic may result an accelerated corrosion attack [Peng and Nie, 2013].

Carbon fiber is a good electrical conductor and very noble than most of metals, which cause the galvanic corrosion, so acts as cathode and more positive corrosion potential $\sim$1 V than aluminum [Tahamtan and Fadavi Boostani, 2010, Wang, Chen and Wu, 2009]. Payan et al. have been investigated the galvanic corrosion (Figure 1.22) progressive in aluminum matrix composites reinforced with graphite fiber using in situ long focal Video Microscopy (ISVM) for evaluation of pitting corrosion and Atomic Force Microscopy (ISAFM) to investigate localized corrosion [Payan et al., 2001].

It has been revealed that the interfacial galvanic corrosion was increased by the precipitation of silicon crystals over carbon fibers.

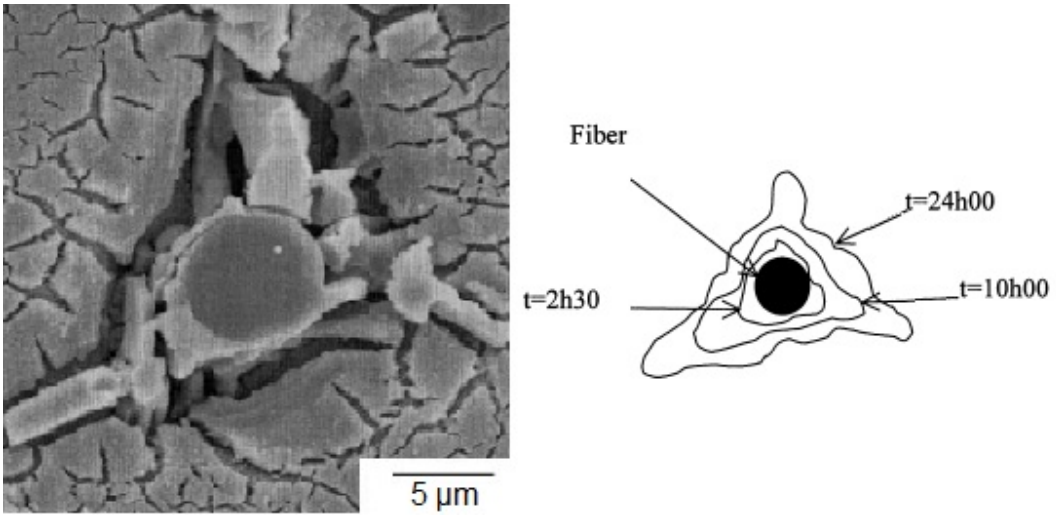

FIGURE 1.22: Micrograph of the single fiber and the interface for sample after 24 h of corrosion with the evolution of the cavity over time [Payan et al., 2001]

Wang et al. have been reported the improved corrosion resistance electroless plating nickel-phosphor (Ni-P) coatings on the carbon fiber in aluminum matrix composite [Wang et al., 2003]. There are few studies have been conducted on the corrosion and electrochemical behavior of aluminum matrix composite reinforced with carbon fibers.

Chapter 2

THIXOMIXING

2.1 Thixomixing

As it mentioned, the conventional liquid stir casting and powder metallurgy are less effective and costly methods for fabrication of aluminum/carbon fiber composite because of low interfacial adherence, unwanted fragile intermetallics and non-homogeneous distribution. In this study, a novel thixo-process was developed for the dispersion of carbon fiber filaments and mixing them in semi-solid slurry of aluminum under high shear stress.

This process is named thixomixing due to embedding of reinforcement fibers in a thixotropic fluid. Thixomixing can be classified as a method of compo-casting. Generally, the compo-casting method is a process that, the reinforcement particles are added to a fully liquid metal under vigorously mixing when the solid particles are added to solidifying melt [Abbasipour et al., 2010]. It has been revealed that the primary formed solid particles in semi-solid slurry can infiltrate into the particles or fibers tow to eliminate agglomeration, reduce gravity segregation and improve wettability.

Semi-solid slurry techniques are carried out at temperature range between liquidus and solidus so it eliminates the superheat and reduce chemical reaction between reinforcement and matrix and also the higher viscosity of matrix alloy the gravity segregation during mixing and solidification. Thixotropic nature of slurry helps to smooth die filling

without turbulence under pressure. The long processing methods at high temperature are not economic and cause deleterious chemical reaction such as brittle phases at the interfacial bonding [Pelleg et al., 2000].

Basically, it is an application of high shear stress (τ) on agglomerated solid particles embedded in semi-solid slurry to overcome the internal force between the particles and the strength of dendrite microstructure. In the case of aluminum, the dendrite microstructure of solidification front was improved and becomes globular under shearing load. Some problems associated with the reinforced MMCs, such as weak interfacial bonding, non-distributive microstructure, and deleterious interfacial reactions can be solved by this method.

A load can be transfer easily through a good interfacial mechanical bonding or strong adherence. Adherence and well dispersed and distributed reinforcement are essential to increase mechanical strength and load transferring.

To the best of our knowledge, the thixomixing method was not being utilized for distribution of C_{sf} into the aluminum matrix before this study [Akbarzadeh et al., 2015*a*,*b*]. Siegert et al. have been utilized tailor-made carbon fiber to embed in aluminum silicon alloy by thixoforging of laminates [Siegert et al., 2006]. It has been reported, the stirring while the slurry is solidifying improves incorporation of the fibers into the matrix alloy [Abbasipour et al., 2010].

Some of the advantages of this method are:

- improved interfacial adherence
- less damage to the fibers
- no flotation
- low cost
- good distribution and dispersion of fibers.

This method is suitable for compo-casting of alloys having wide range of solidification particularly with dendrite growth.

2.1.1 Principles of Thixomixing

Fluids are categorized in two types, Newtonian (which the viscosity that is independent of the stress like water) and non-Newtonian. The non-Newtonian fluids are deviated in different types based on Newton's law (all types shown in Figure 2.1) [Panton, 2013]. For example:

- Shear thickening liquids which the viscosity increases with the rate of shear strain.
- Shear thinning liquids which the viscosity decreases with the rate of shear strain.
- Bingham plastics that behave as a solid at low stresses or flow as a viscous fluid at high stresses.
- Rheopectic liquids become more viscous when stress applied over time.
- Thixotropic liquids become less viscous when stress applied over time.

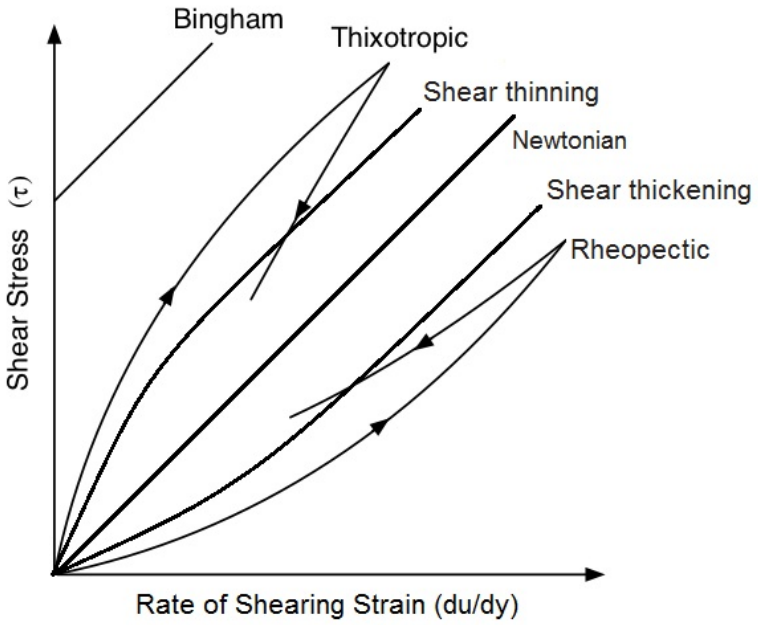

FIGURE 2.1: A diagram of non-Newtonian fluids [Panton, 2013]

Semi-solid slurry contains a fraction of solid particles which solidified initially in the molten metal. The internal solid-to-solid bonding in absence of external load put them in the stable condition but when a load applied becomes flow. Theoretically, it can be

interpreted that the semisolid aluminum slurry shows non-Newtonian or viscoplastic behavior which depends on the yield strength and the shear rate. This non-Newtonian specification has been applied for dispersion and distribution of reinforcement particles in aluminum matrix. Shear rate is physical parameter which a shearing deformation is applied to a fluid flowing between two parallel plates, when one is moving at a constant speed the other is stationary (Couette flow). Shear rate is measured in reciprocal seconds can be calculated by equation 2.1.

$$\dot{\gamma} = \frac{\upsilon}{h} \tag{2.1}$$

where, υ is the velocity of moving plates in meters per second and h is the gap between two parallel plates in meters. The semi-solid slurry of metals is thixotropic fluids that temporarily becomes liquid under stress and shearing and reverts back when static. Commonly, the shearing begins when the shear stress reaches to yield strength and it is mainly depends on the solid faction which proportionally related to temperature of alloy [Alexandrou, 2008]. Laminar flow, induced in the liquid by the rotating of rotor, is associated normally with high viscosity fluids. The agglomerates of fibers break-up within the high shearing, which can lead to deagglomeration and homogenization. The Herschel–Bulkley model can be considered for shear stress (τ) (equation 2.1):

$$\tau = [\frac{\tau_0(\lambda)}{\dot{\gamma}} + K\dot{\gamma}^{n-1}]\dot{\gamma} \tag{2.2}$$

where, (τ_0) is yield stress, $\dot{\gamma}$ is shear rate, λ is structural parameter, K is the consistency index and n is the power law index or structural parameter which is the rate of agglomeration and deagglomeration [Atkinson, 2005]. Burgos et al. represent the K as time dependent factor in semisolid behavior, when all the solid particles are connected, K=1 and none of the particles are connected, K=0 [Burgos et al., 2001]. Based on the predicted temperature, the yield stress (τ_0) for A356 alloy is calculated as:

$$\tau_0 = 4 \times 10^{49} \times exp(-0.181 \times T) \tag{2.3}$$

which is corresponding variation of (τ_0) with temperature. Viscosity is a very important parameter in rheology and plays an important role in the case of semi-solid alloys as well as fluidity concept in fully liquid alloys or strength in solids. Viscosity can be defined

by Newton's first law, which is a constant to introduce the capability of momentum diffusion through the body of fluid and it shows visco-plastic behavior of materials, Eq. 2.4

$$\tau = \eta(\frac{\delta V}{\delta y}) = \eta\dot{\gamma} \tag{2.4}$$

where, τ is the shear stress, V is the velocity of momentum; η is the viscosity and $\dot{\gamma}$ is the shear rate.

The values of viscosity in rheological behavior of a semi-solid slurry is represented in Eq. 2.5

$$\tau = \eta_a\dot{\gamma} \tag{2.5}$$

where, η_a is apparent viscosity that can be calculated (Eq. 2.6)

$$\eta_a = [\frac{\tau_0(\lambda)}{\dot{\gamma}} + K\dot{\gamma}^{n-1}] \tag{2.6}$$

As the apparent viscosity increases sharply with a small increase in fraction of solid and is a function of shear and cooling rates.

Viscosity increases with increasing of solid fraction till the dendrite coherent point (DCP). The DCP could be different for various alloys whereas after it the viscosity of semi-solid slurry increases sharply as is shown schematically in Figure 2.2. Generally, in non-Newtonian fluids, viscosity is a function of physical properties of fluid and testing condition such as temperature, shear rate, particle size and distribution.

Aluminum silicon alloy shows different solid fraction of initial alpha phase versus temperature. Different values of solid fraction leads to various amount of viscosity of slurry. Solid fraction can be measured by analyzing the resulted images of microstructure or investigation of solidification regime from cooling curve. It can be calculated also by Scheil's equation (Eq. 2.7): [Flemings, 1974]

$$f_s = 1 - (\frac{T_m - T_L}{T_m - T})^{\frac{1}{1-k}} \tag{2.7}$$

where, f_s, T_m, T_L and k are fraction of solid, melting point of solvent (in Al/Si alloy is the melting point of Al), liquidus temperature of the alloy and equilibrium partition

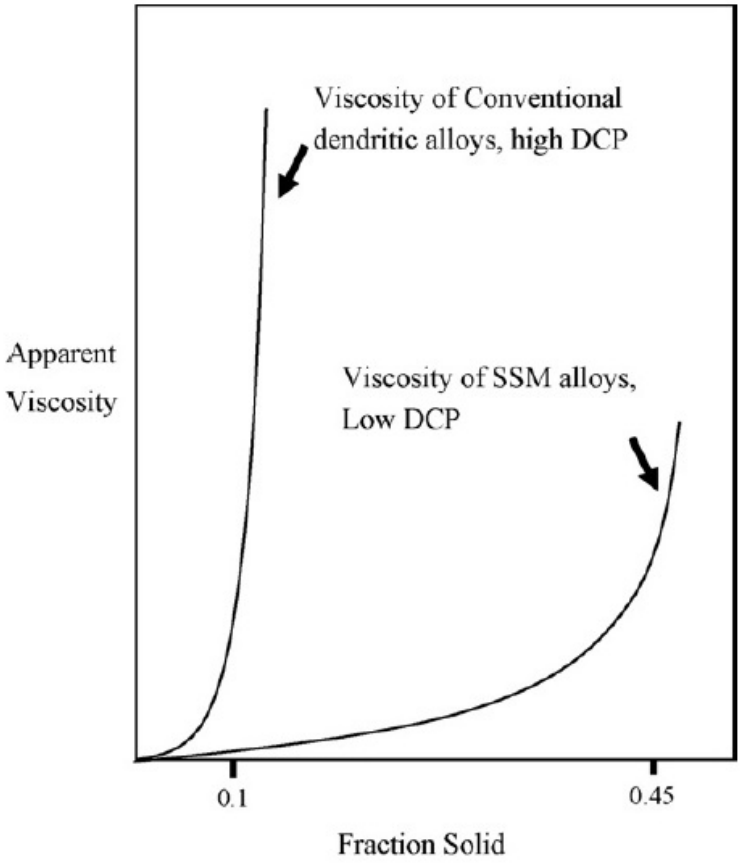

FIGURE 2.2: Schematic relationship between solid fraction and apparent viscosity [Lashkari and Ghomashchi, 2007]

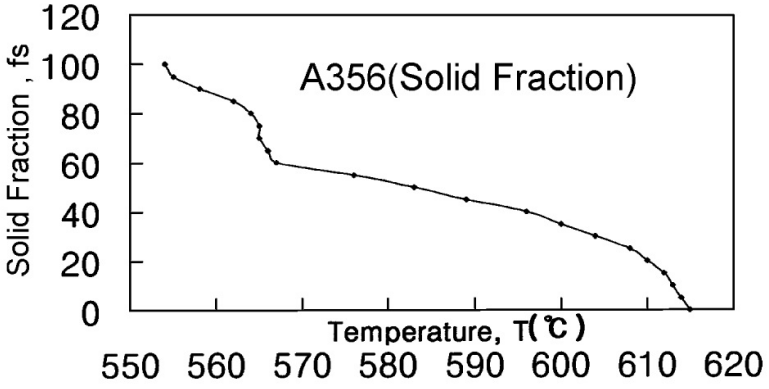

FIGURE 2.3: Temperature vs. solid fraction for A356 [Jung, 2000]

ratio, respectively. A relationship between temperature and solid fraction for A356 is shown in Figure 2.3.

2.2 Wettability and Adherence of Carbon Fibers

Wettability refers to the interfacial bonding at unreacted interface between a liquid and solid surface due to the van der Waals interactions, or the ability of liquid to make a contact with solid surface. Wetting is usually characterized by the contact angle, θ, related with the interfacial energies of the solid:liquid:vapor system by the classical Young–Dupré equation 2.8:

$$\cos(\theta) = (\frac{W_a}{\sigma_{LV}}) - 1 \tag{2.8}$$

in which W_a is the work of adhesion of the liquid on the solid, and σ_{LV} is the liquid:vapor surface tension. W_a quantifies the strength of the interactions between the metal and the ceramic at the interface [Landry et al., 1998]. If θ >90° the liquid does not wet the solid surface and if θ <90° the liquid wet the surface (the contact angle shows in Figure 2.4).

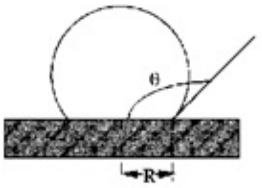

FIGURE 2.4: The contact angle θ and drop base radius, R

Wettability of the carbon fibers by molten aluminum at the convectional casting temperatures (700-800 °C) is limited, even for long time exposures. It has been proved that the molten aluminum alloys ($T < 1000$ °C) and carbon fibers; whatever the microstructure of graphite, do not wet each other. Moreover, temperatures above 900-1000 °C increase the wettability by molten aluminum due to the interfacial reaction between aluminum and carbon fibers to form the brittle aluminum carbide (Al_4C_3). However, the poor wettability and chemical reaction between fibers and molten aluminum are the main obstacles for this fabrication. One way has been suggested, the contact time between the reinforcement and the molten metal at high temperature has to be shorted [Hajjari et al., 2010, Pippel et al., 2000].

The addition of Si in Al causes to formation of SiC if x_{Si} is high enough as suitable adhesive intermetallic instead of Al_4C_3 formation. 0.5-0.75% Mg was added to the melt to enhance wettability of the Al_2O_3 particulates in the liquid of aluminum because magnesium is a powerful surfactant [Venkata Siva et al., 2011]. The addition of magnesium to an aluminum melt improves wettability because of the lower surface tension of magnesium [Hashim et al., 2002].

Stirring at a fully liquid condition does not help to incorporate fibers into the matrix. In this condition, fibers tend to float to the top of the molten alloy, regardless of the speed of stirring. Stirring while the slurry is solidifying improves incorporation of the fibers into the matrix alloy [Abbasipour et al., 2010].

It is well known that the wettability between C_f and Al is poor, but this problem can be solved by controlling chemical composition and temperature of alloy, also suggested to be solved by the vacuum pressure infiltration technique [Liu et al., 2009]. In the thixomixing process, wettability between the aluminum slurry and carbon fiber was improved effectively due to the deposition of Si on the fibers and formation of useful intermetallics.

2.3 Aluminum Carbide Formations

It is well-known that carbon fiber and aluminum are chemically incompatible. At higher temperatures, brittle rhombohedral lath-like crystals of aluminum carbide (Al_4C_3) arise at the fiber-matrix interface [Simancik and Jangg, 1994]. The Al_4C_3 grows on the prism plane of the carbon fiber. This reaction takes place above 500 °C that the reaction is possible even below this temperature [Baker, Shipman, Cripwell and Jackson, 1972]. At temperature (700-800 °C) uses for fully liquid casting of aluminum composite, the wettability between all types of carbon fibers and molten aluminum alloy, even for long time of exposures is low. Long time of exposure leads to the formation of aluminum carbide and a segregation of the reinforcement particles into the matrix and causing final heterogeneous composites. The basal planes of graphite structure are stacked along the

carbon fibers with the reactive bonds at the ends of them causing reactivity of fibers with aluminum [Yang and Scott, 1991].

Poor wettability is one of the major problems during the fabrication of carbon fiber reinforced aluminum matrix composites [Matsunaga, Ogata, Hatayama, Shinozaki and Yoshida, 2007]. At lower temperatures using for aluminum casting (under 700 °C), the wettability of carbon fibers by molten aluminum is limited, whereas the higher temperatures (up to 1000 °C) provide the better wettability following by aluminum carbide formation [Amateau, 1976, Kozera et al., 2011]. A 4 pm thickness aluminum carbide layer was formed by Khan [Khan, 1976] via thermal treating of specimen at 500 °C for 24 hours.

The aluminum carbide formation is serious due to a sharp notch (Figure 2.5) on the fiber by attack of growing Al_4C_3 needles results in a drastic decrease in the composite strength and deteriorate the mechanical properties of composites [Pai et al., 2008]. In addition, preferential precipitation of Al_4C_3 was found to take place as 1-2 nm crystalline grains at fiber interfaces possessing an amorphous carbon layer. The carbon surface reacts with aluminum to generate a brittle and water-soluble Al_4C_3 compound on it. When the C_f content in the composite is high, carbon atoms can diffuse into the reaction interface effectively, which is good for the growth, and the matrix in adjacent fibers is filled with Al_4C_3 phase. The Al_4C_3 phase connects each other and form "bridge", which is unfavorable to the performance of composites [Tang et al., 2009].

The reinforcement surface can be coated to prevent a chemical reaction with the matrix. For example, carbon fibers are commonly used in aluminum matrix to synthesize composites showing low density and high strength.

The aluminum carbide was investigated to nucleate heterogeneously from carbon fibers and to grow into the aluminum matrix in the form of lath-like crystals and its nucleation is associated with defect sits on carbon fiber surface [Yang and Scott, 1991]. Yang and Scott have been stated that a chemical reaction of Al_4O_3 will be formed during liquid metal infiltration at temperatures 540 °C with 20 nm thickness after 48 hours. Brittle aluminum carbide expands in humid environments stressing and breaks the composite

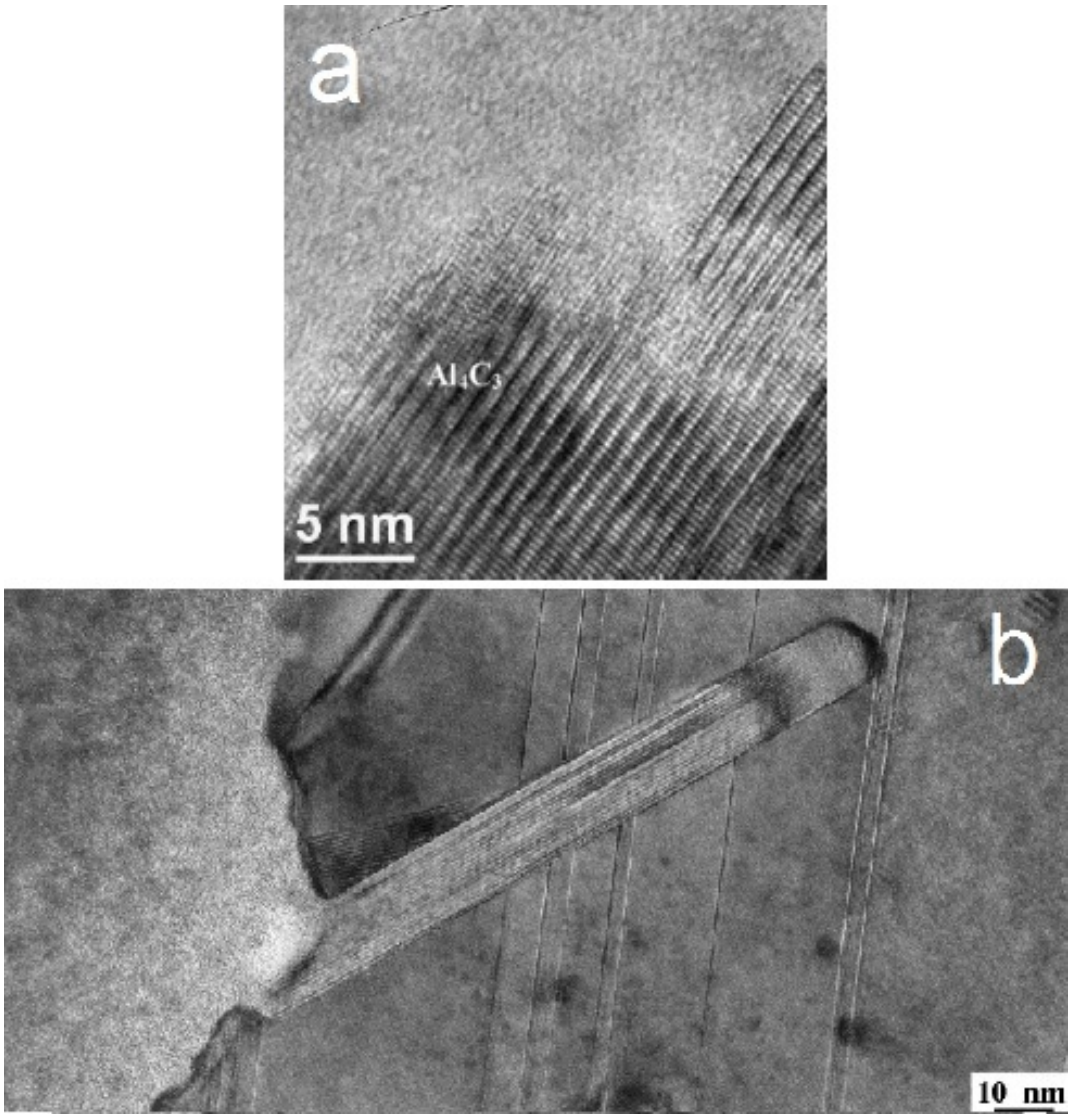

FIGURE 2.5: HRTEM image of Al_4C_3 needle-like grain at the interface of aluminum carbon fiber (a) [Seong et al., 2008] (b) [Lancin and Marhic, 2000]

surface [Urena et al., 2007]. Commonly, the reaction between the fibers and the aluminum seems to deteriorate the interface, furthermore; lowering the mechanical properties.

The polyacrylonitrile (PAN)-based carbon fibers has been reported more reactive than graphitized (pitch based) carbon fibers [Amateau, 1976], indicated also the formation of different morphology of aluminum carbide at interface of PAN-based carbon fiber with aluminum matrix [Kohara and Muto, 1988]. It has been investigated that holding temperature increased, the quantity of Al_4C_3 increased and tensile strength will be decreased due to corroding of Al_4C_3 on carbon fibers especially at higher temperatures

[Yamaguchi et al., 2009]. The reaction rate of aluminum carbide formation can be reduced by prohibiting of fibers solution in the matrix. Addition of an appropriate element to aluminum can decrease the solubility. Increasing of Mg content in the Al composite would increase the Gibbs free energy and the formation of Al_4C_3 is less possible.

Consequently, high-purity aluminum cannot be suggested as matrix for Al composite which carbon base reinforcement. Formation of the harmful aluminum carbide at the interface acts as the crack initiators, cause tensile strength to be reduced significantly. The Al_4C_3 is a brittle phase and may break during loading as crack initiation point and earlier than fiber; subsequently crack may propagate in the fiber and the surrounding aluminum matrix and finally cause to fracture of composites at low stress. The brittle fracture with no fiber pull-out due to strong interface bonding, was investigated fracture after tensile and bending tests [Wang, Chen and Wu, 2009]. But, some controlled chemical reaction between carbon fiber and aluminum as matrix can be suggested to provide stronger bonding due to low wettability of Al on C_f.

One of the proposed methods for measuring the amount of aluminum carbide is being described which it reacts with hydrochloric acid (HCl) and produces methane (CH_4) as follows:

$$Al_4C_3 + 2Al + Al_2O_3 + 24HCl \rightarrow 8AlC_13 + 3CH_4 + 3H_2O + 3H_2 \qquad (2.9)$$

specimens were immersed in a HCl (6N) aqueous solution produce gases such, CH_4 and H_2, which were injected into a gas chromatograph. The present volume of CH_4 and H_2 were determined by a hydrogen-flame ionization detector and thermal conductivity detector, respectively [Padilla et al., 1975]. Obviously, an amount of pure Al_4C_3 powder was used to calibrate its weight fraction.

2.4 Carbon Fiber Coatings

A fiber coating is a solution to overcome the problem of aluminum carbide formation and improve the wettability and prohibit in excessive time or temperature of process

[Amateau, 1976]. In 1970s, Galasso, et al. [Galasso and Pinto, 1970] started to using coatings on fibers and were compared properties of bare fibers and different type of coatings on carbon fibers. Some of the other coating such as titanium carbide [Himbeault et al., 1989, Roy et al., 2012], titanium boride (TiB_2), silicon carbide [Wang et al., 1997], silica [Brown et al., 2002], copper [Bhav Singh and Balasubramanian, 2009, Urena et al., 2007], potassium halide salts [Juhasz et al., 2012, 2013]and nickel [Hajjari et al., 2010, Rams et al., 2007] have been coated on carbon fibers to fabrication of aluminum composites.

The methods of CVD, PVD as well as sol–gel were used to obtain non-metal coatings such as SiC, TiN, TiO_2 and SiO_2 on C_{sf} surface as diffusion barrier that improved the interface of C_f/Al. In some cases, the coatings were not affected due to its failure throughout the fabrication like applying high pressures will lead to the separation of the nickel layer on the carbon fibers and may damage and change the distribution of the fibers then decreases the strength of the composite [Hajjari et al., 2010]. The brittle coatings such as titanium carbide or silica reduce the strength of the carbon fibers, therefore; a thin enough layer of coating is required for protection of fiber which has less impact on mechanical strength.

In some cases, the application of coatings cannot improve the adherence and mechanical strength of final composite. For example, one of most important benefit of aluminum composites is the strength to weight ratio, so the coating on the fibers may increase their density and insufficient effect on strength. Although the coating reduce chemical reaction, the bonding between C_f and any materials as coating may not be suitable for stress transferring along the fibers. In the case of nickel or copper, the thin film deposition can be conducted through electrodeposition with current or electroless with 2-16% phosphorus content [Rams et al., 2007]

2.5 Rule of Mixture

The rule of mixtures states theoretical calculation for a material property such as (A) in composite by simple Eq. 2.10:

$$E_c = fE_f + (1-f)E_m \tag{2.10}$$

where the volume fraction of the fiber is $f = \frac{V_f}{V_f+V_m}$, E_f is the material property of the reinforcement, E_m is the material property of the matrix. The overall properties of each type of composite materials are depended on:

- Physical and chemical properties of the constituents
- Volume fraction or relative amount of each constituent
- Interfacial quality and geometrical properties of reinforcement (i.e. shape, size, orientation and distribution)

Similarly, In terms of volume fractions, the composite density ρ_c can be written as:

$$\rho_c = \rho_f V_f + \rho_m V_m \tag{2.11}$$

where V_f is the fiber volume fraction and V_m is the matrix volume fraction and is equal to (1-V_f). The fiber volume fraction V_f and composite density ρ_c can be calculated:

$$V_f = \frac{(W_f \rho_f)}{((W_f \rho_f) + (W_m \rho_m)} \tag{2.12}$$

Or, the fiber volume fraction can be calculated by:

$$V_f = \frac{\rho_m W_f}{\rho_f W_m + \rho_m W_f} \tag{2.13}$$

where, W_f , W_m weight of fiber and matrix, ρ_f , ρ_m density of fiber and matrix, respectively. Different methods have been conducted to measure V_f in composite material for

instance, in 1989, Himbeault et al. proposed counting the fibers observed on a composite cross section and using the relation

$$V_f = (N \times A_f)/A_t \tag{2.14}$$

where, N is the number of fibers, A_f is the average cross sectional area of a single fiber and A_t is the total cross sectional area [Himbeault et al., 1989]. Another method calculates V_f by extraction of embedded short carbon fibers from samples by dissolution of matrix in diluted hydrochloric acid (1 M). The sample firstly weighted with an accurate digital balance, and then dissolved in the solution at room temperature. The residual fibers has been filtered, dried and weighted by an accurate digital balance. The last method was utilized in this study as mentioned in Chapter III.

2.5.1 Critical Fiber Length in Composite Materials

The specific strength and stiffness are expected throughout a low cost method, but the quality of interfacial bonding highly pertained to critical fiber length and interfacial chemical reactions. The reinforcement of metals with discontinuous brittle fibers is likely to result in greater strengthening, compared to continuous reinforcement. The critical fiber length, l_{cr} is

$$l_{cr} = \frac{(\frac{\bar{\sigma}_f(l_1)(l_1)^{1/\beta} d_f}{2\tau})\beta}{1+\beta} \tag{2.15}$$

where $\bar{\sigma}_f(l_1)$ is the average strength of l_1 based fibers (m); d_f is the fiber diameter. The increase in the average length of the fibers pulled out of the matrix is inversely proportional to the interface bond density and proportional to the critical fiber length in logarithmic coordinates [Ustinov and Verkhovsky, 1992]. The efficiency of reinforced particles in the composite are related to the fiber length, interfacial bonding and coefficient of friction are the most important in the process of preparation of composite [Simancik and Jangg, 1994]. The length L of short fiber in composite is:

$$\bar{\sigma}_f = \frac{1}{L}\int_0^L \sigma(x)dx \tag{2.16}$$

where, $\bar{\sigma}_f$ average axial stress in fibers.

$$\sigma(x) = \frac{4}{d_f} \int_0^x \tau(x) dx \tag{2.17}$$

where, $\sigma(x)$ and $\tau(x)$ are the fiber axial tensile stress and interfacial shear stress at a distance x from the fiber end, while d_f is the fiber diameter. The optimum fiber length is very important for fiber strengthening even when fiber is sufficiently long without any bonding due to frictional stress τ_f along the interfacial matrix/fiber. Fiber diameter, coefficient of friction between fiber and matrix and interfacial bonding τ_B are the most important parameter for controlling of efficiency of fiber reinforcement in composite.

Chapter 3

EXPERIMENTAL METHODS

3.1 Materials

3.1.1 Aluminum Silicon Alloys

Three different aluminum silicon alloys were used for fabrication of aluminum/short carbon fiber (C_{sf}) composites. These alloys contain various amounts of silicon (6.5-21%) and magnesium (0.25-0.7%) which is the main aspect for their differences. Both of the alloying elements (Si and Mg) have good effects on the wettability onto carbon fiber surface, although the magnesium excess improve the corrosion resistance and lower the strength and formability; high content of silicon provides higher strength but may cause the intergranular corrosion [Park et al., 2005]. Si and Mg allows to improve the mechanical properties by heat treatments.

The A356, A357 and hypereutectic alloy (4047) are three aluminum alloys were used in this study to fabricate aluminum matrix composite. The A356 and A357 are most commonly high consuming alloys utilized in thixoforming process for industrial casting. The chemical analyses were illustrated in Table 3.1. It has been reported, Mg (0.5-0.75%) can provide the uniform distribution of reinforcement into the matrix and no agglomeration by increase the wettability of carbon fibers in composite and it helps to improve the mechanical properties of composite [Liu et al., 2010, Scharhoff et al.,

TABLE 3.1: Chemical composition of the A356, A357 and 4047 alloys (wt. %)

Element	Si	Mg	Cu	Mn	Fe	Zn	Ti	Al
A356	7.12	0.335	0.0025	0.0049	0.21	0.1	0.104	Balance
A357	6.76	0.513	0.0011	0.0056	0.14	0.1	0.123	Balance
4047	11.2	0.7	0.13	0.665	2.4	0.1	0.2	Balance

2004, Shi et al., 2012]. The proper ratio, Mg/Si = 1.73 is possible to achieve Mg_2Si but it is not possible to form in the composites studied in this project in fact due to quick quenching in water after thixomixing process Totten and MacKenz [2003]. In the present thixomixing process, The Mg_2Si cannot be detected probably as consequence of the quick quenching in water, and magnesium dissolved in α-phase.

Aluminum Association classification proposed series 3xx.x for aluminum-silicon contain silicon between 5 to 22 wt.% which alloyed by copper and/or magnesium and series 4xx.x contain silicon in the range of 6 to 23 wt.% were standardized for commercial applications and mainly control properties by silicon amount and structure. The structure of the alloys can be hypoeutectic, hypereutectic, or eutectic, as can be seen on the equilibrium phase diagram Figure 3.1.

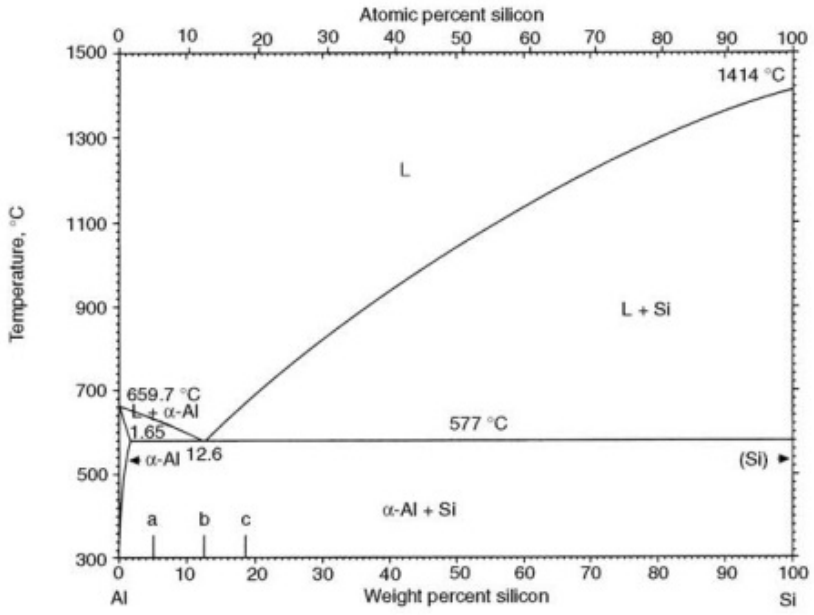

FIGURE 3.1: Equilibrium binary diagram of aluminum-silicon [Murray and McAlister, n.d.]

Aluminum-silicon alloys are mainly used for casting. Silicon exposes high fluidity and low shrinkage which are important for casting and welding. The properties of a

specific alloy can be attributed to the individual physical properties of its main phase components and to the volume fraction and morphology of these components.

Mechanical properties of the commercial alloys depend on content of alloying elements such as Mg, Si, Cu and the heat treatment process. High copper or nickel contents, decreases ductility and resistance to corrosion. Copper also improve fatigue resistance without loss of castability. High iron contents decreases strength and ductility and is the main impurity which must be keep it as low as economically possible.

3.1.2 Poly-acrylonitrile (PAN)-based Carbon Fibers

The carbon fibers are composed mostly of carbon atoms, and coated with a resin to protect them during handling and easier fabricating. The structure of carbon fibers contains graphite basal planes, parallel oriented to the axis of the fiber, which make the carbon fiber incredibly strong for its size. The carbon atoms are arranged in a crystallographic structure of parallel planes like graphene layer which stacked on each other in graphitic structure to provide high tensile modulus.

Carbon fibers are chemically inactive and the fibers surface area must be treated by increasing number of micro-pores or pits which provides a larger number of contact points for better bonding between fibers and matrix. Highly anisotropic physical and mechanical properties for the carbon fiber resulted from strong covalent bonds between the adjacent atoms in graphitic planes which are aligned in the fiber axis and bonded to each other by weaker van der Waals bonding. This carbon-carbon atomic bond in the graphite layer of carbon fibers is one of the strongest which leads to outstanding mechanical properties. The chemical structure of fiber is similar to the graphite [Seong et al., 2008], consisting of graphene layers stacked parallel on each other [Huang, 2009]. The carbon fiber has high chemical resistance at high temperature, but the fibers are fragile [Burkanudeen et al., 2013].

The carbon fibers produce continuously in the form of long and thin strand of fibers about 5-10 μm diameter and several thousands of them are twisted together to form a yarn, which may be used by itself or woven into a fabric. The carbon fibers used in all

parts of this project is polyacrylonitrile (PAN)-based, M40JB, made by Japan Toray Co. Ltd.

The short carbon fibers were chopped into 5±1 mm length from long strand (Refer to Figure 3.2). After that, the pyrolytical sizing agent on the fibers must be removed. All commercial carbon fibers have been coated by an organic material as sizing to prevent damaging or oxidation which is necessary to remove it before employment into metal matrix and also achieving a proper roughness on the fiber surface. The sizing agent on carbon fibers can improves in easy handling of fiber yarn and protect the surface of fibers from probable damages [Guigon and Klinklin, 1994, Yumitori et al., 1994].

FIGURE 3.2: The chopped PAN-based Carbon fiber

The organic sizing was removed by heating the fibers up to 500 °C furnace for 10 min, under the air, so was cleaned and washed with distilled water and activation under ultrasonic agitation for 10 min in order to get catalytic surfaces [Galasso and Pinto, 1970, Hajjari et al., 2010, Liu et al., 2009, Rams et al., 2007, Urena et al., 2005]. Some previous studies used the acetone to removing sizing agent [Patankar et al., 1990]. The necessity of removing of sizing agent is resulted from adsorption of moisture in the air by hydrophilic groups in its molecules [Kozera et al., 2011]. Finally, the C_{sf} is ready for using in compo-casting process. The physical properties are mentioned in Table 3.2.

TABLE 3.2: Physical properties of carbon fiber

Type	Diameter μm	Tensile Strength MPa	Tensile Modulus GPa	Elongation %	Mass per Unit length tex $mg.m^{-1}$	Density g.cm^{-3}
M40JB	6	4400	377	1.2	454.5	1.75

3.2 Thixomixing Process

3.2.1 Design and Fabrication of the Thixomixer

As it was mentioned, a novel specific mixer was designed and developed to embed C_{sf} into slurry of aluminum at semi-solid state in this study. It is based on thixotropic property and different values of viscosity which can produce shearing force to disperse fibers and distribute them homogenously in the matrix. This mixer equipment was named thixomixer and the process thixomixing.

In the initial design of thixomixer, it consists of two main parts. The stationary part called as a die and the rotary part called rotor, and both made of H13 steel alloy. The schematic illustration of thixomixer is shown in Figure 3.3 and the Appendix A. A 2 mm gap provided between die and rotor. This space among two walls provides high shear rate ($\dot{\gamma}$) and shear stress (τ) by semi-solid slurry at the appropriate temperature and rotating speed which are needed for dispersion of fibers.

For better hardness and toughness both die and rotor were heat treated. Both die and rotor were heated up to 1050 °C for 20 minutes in electrical furnace under air atmosphere and quickly quenched in the oil to the room temperature. Die was subjected vertically on heat isolated basement and clamped on it, and the rotor joined to the head of electrical motor of a CNC machine to provide various rotating speed and for precision vertical movement. The induction furnace and a set of thermocouples supplied for heating and control the temperatures. To avoid convection heat transfer during mixing, die was covered by thermal isolating materials. In Figure 3.4, different parts of thixomixer and its configuration are shown.

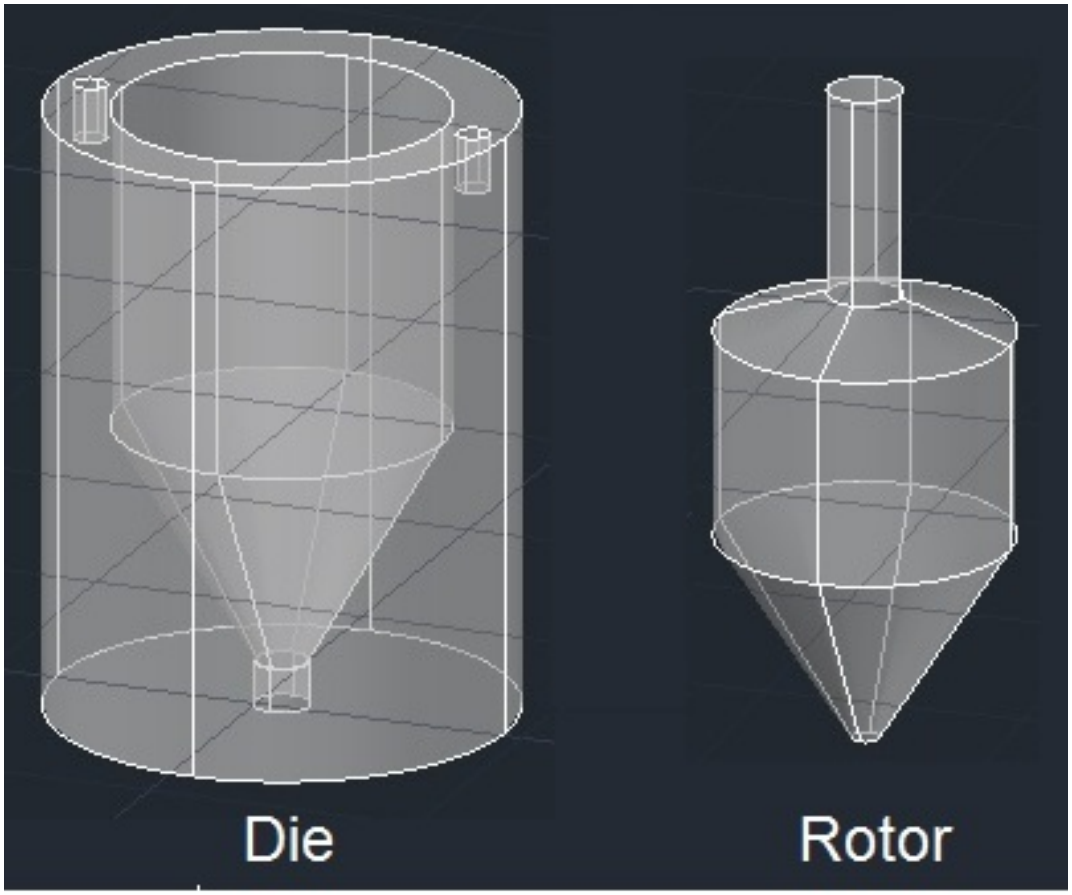

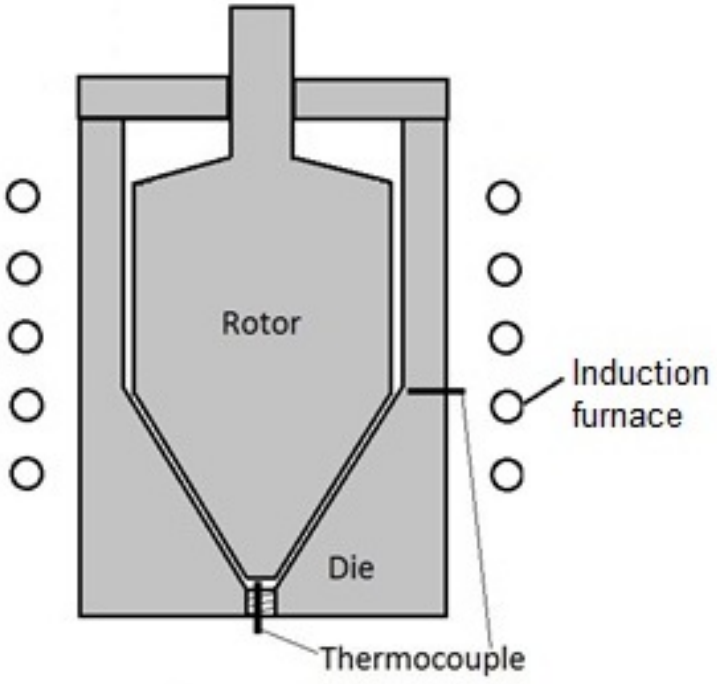

FIGURE 3.3: A 3D design and schematic illustration of thixomixer, the inner part (Rotor) is rotating and the outer cylinder (Die) is stationary

FIGURE 3.4: Real image of thixomixer which stands on a CNC machine

3.2.2 Mixing and Preparation of Samples

The compo-casting process for fabrication of metal matrix composite at semi-solid state for dispersion and distribution of reinforcement by intensive shear stress was named thixomixing. The short carbon fibers were embedded in aluminum matrix by thixomixing in this study. A continues shearing must be maintained by specific mixing speed at the appropriate temperature and solid fraction for a successful process.

Prior of mixing, die and rotor were preheated to 600 °C then the molten alloy poured into the die, so the temperature of system must be maintained for thermal stabilization to form semi-solid slurry at desired solid fraction. At first, to optimize appropriate solid fraction for thixomixing, the slurry keep at the suitable temperature for a short time (Figure 3.5 shows the process of thixomixing based on temperature and time). Three levels of solid fractions have been selected as 10%, 48%, and 90% based on the susceptibility of solid fraction from temperature as shown in Figure 3.6 and studying the effect of the maximum and the minimum levels of solid fraction in the slurry while thixomixing. The values of solid fraction can be extracted from the diagram of temperature versus solid fraction for each alloy (i.e. diagram of solid fraction versus temperature for A357

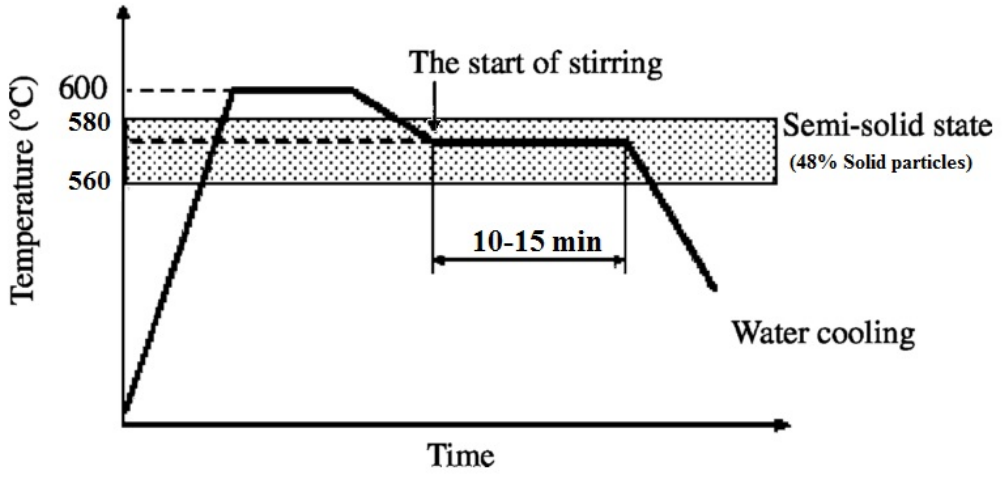

FIGURE 3.5: The process of thixomixing was used for aluminum silicon alloys and C_{sf}

was shown in Figure 3.6). The rotating speed of mixer is another parameter is needed to

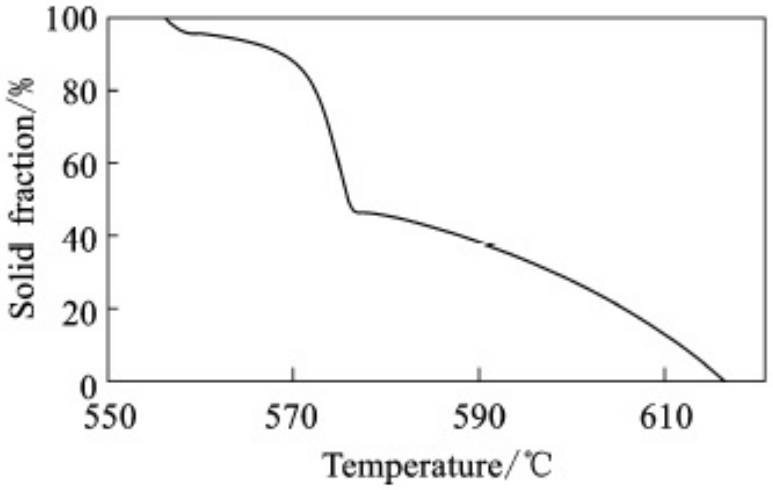

FIGURE 3.6: Diagram of solid fraction versus temperature for A357 [Calcom, 1997]

be optimized, because higher speed may segregate C_{sf} from the liquid and at the lower speed may do not provide sufficient shear stress. The rotating speed was varied at two levels, 100 and 300 rpm. The 100 rpm for speed of mixing has been chosen by calculation and optimization on this factor. The 300 rpm has been selected just to compare and show the deleterious effect of high speeds on fibers and mixing.

When the temperature of the die, rotor, and aluminum was maintained at the suitable

temperature, the chopped carbon fibers were added gradually to the mixer under continuous mixing for around 10 min. The chopped carbon fiber was added by a metal tweezers gradually into the mixer to prevent agglomeration when the slurry of aluminum was sheared continuously. The samples were prepared between a 4.2 and 8.1% volume fraction of the carbon fiber for all tests and characterizations. These amount of volume fraction have been calculated and analyzed after batch fabrication by thixomixing. All dendritic structures were degraded into fine and small grain sizes and converted into spherical shapes due to high shearing load produced by the mixer. Finally, after mixing process was completed the rotor removed out from the die and the composite was cooled to the solid form and then quenched in water to reaches room temperature. The cold sample (Figure 3.7) can be extracted easily from mixer, and it is ready for post-processing and characterization.

FIGURE 3.7: The thixomixed aluminum/C_{sf} composite which has the shape of the internal form of the die

3.3 Flowchart of Experimental Procedures Through the Study

All processes include fabrication and post-fabrication on aluminum matrix composite reinforced with C_{sf} and the corresponded characterizations which have been conducted are illustrated in Figure 3.8.

3.4 Sample Preparation and Hot Extrusion of A356 and A357 Metal Composite Reinforced with C_{sf}

As shown in Figure 3.7, the final shape and geometric condition of thixomixed samples are not suitable for tensile test or further characterization. So, the ax-mixed samples were melted and re-shaped into the bar, so the term "ax-mixed" was used to refer the remelted thixomixed Al/C_{sf} composite sample. So, this process is included in thixomixing process in current study. Before extrusion we have to melting samples at mushy zone ($\sim$ 540 °C) and casted into the bar quickly before the segregation and the flotation of fibers. The modified microstructure of as-mixed matrix was changed after this process, and it was inevitable.

In order to extrusion process, a steel die was made of H13 steel alloy as illustrated in Figure 3.9a and Appendix A with the following specification. The die body consists of twin parts were bolted to each other. The tool used to perform the extrusion has the extrusion ratio 9 (18/6) which has a convergent length of 6 mm. The slugs have a length of 20 mm and a diameter of 18 mm. A pressing machine was utilized for hot extrusion vertically.

The extrusion temperature was conducted at 490 °C; to avoid fibers cracking during the extrusion and also reduce fir-tree cracking on the extruded composite sample as shown in Figure 3.10. The final surface of extruded sample may contain fir-tree if the surface temperature is so high. The final dimension of extrusion parts is 6 mm in diameter and 45-55 mm in length.

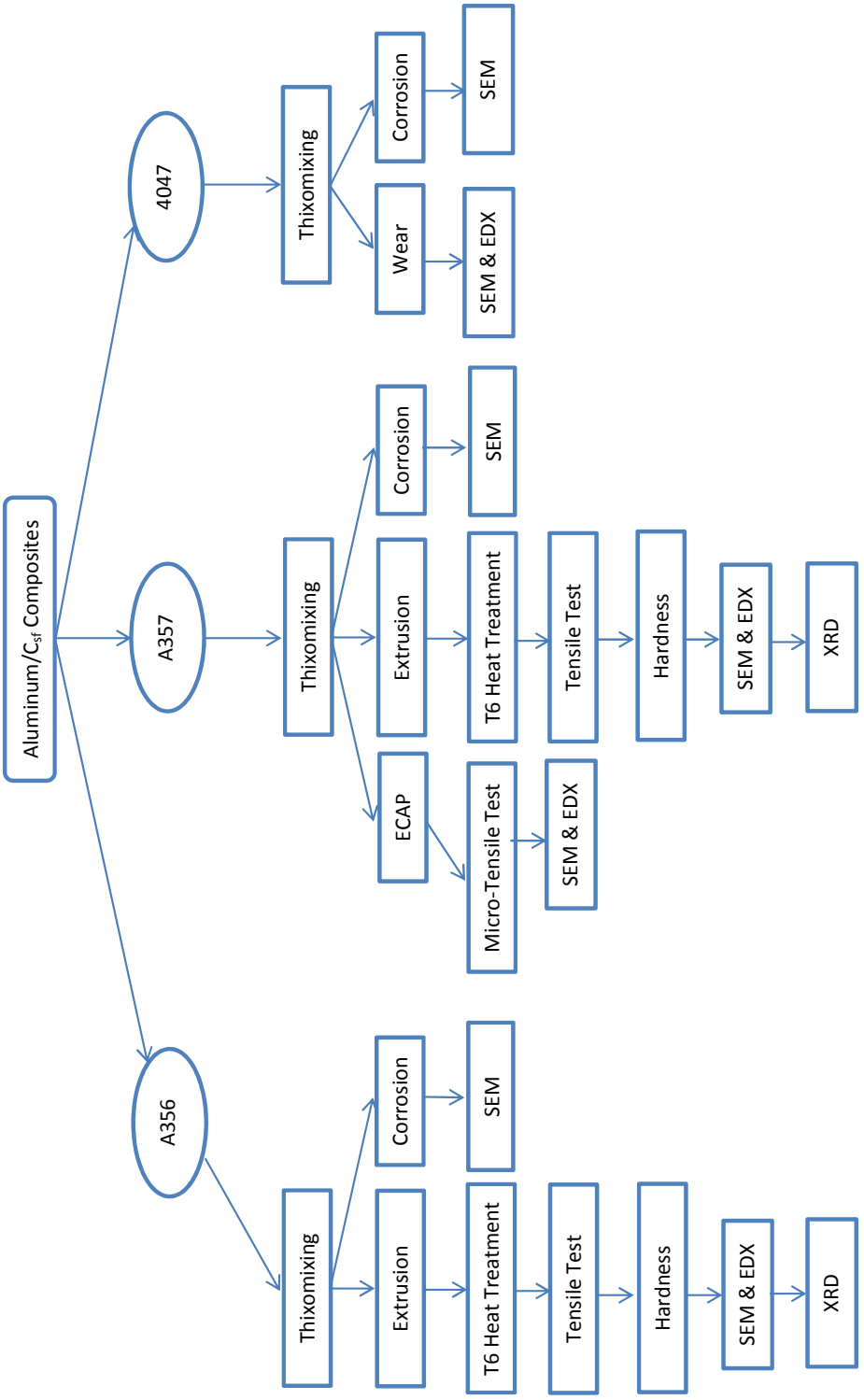

FIGURE 3.8: The flowchart of fabrication and post-fabrication and their related characterization on aluminum silicon/C_{sf} composite

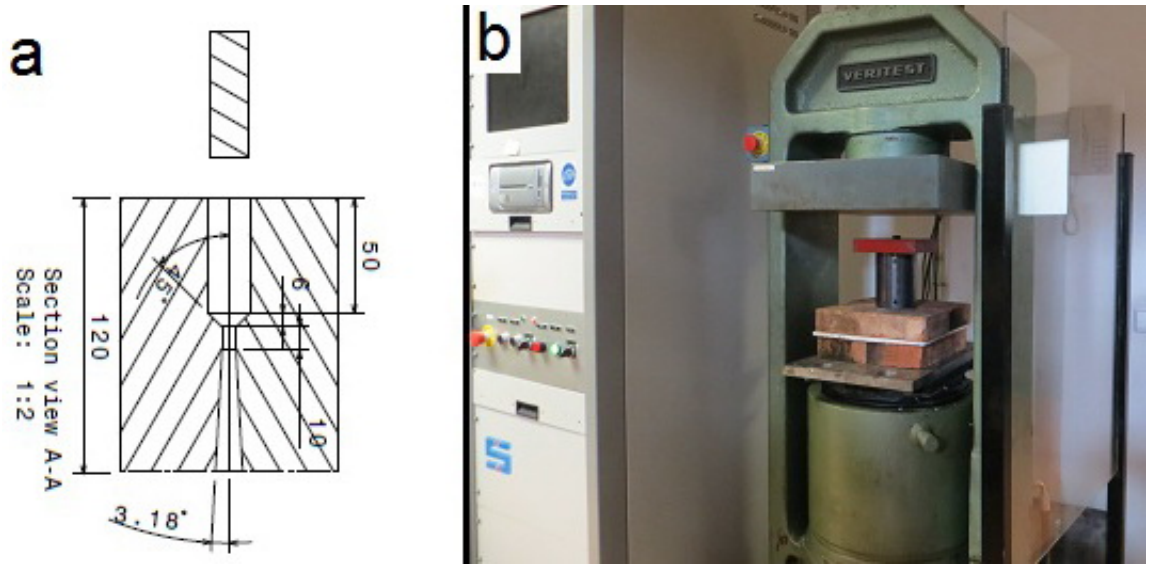

FIGURE 3.9: (a) Schematic illustration of extrusion die (b) pressing machine and the die subjected for pressing load

FIGURE 3.10: The extruded sample after hot extrusion at 490 °C

Extrusion speed was at 0.5 mm.s^{-1} and a lubricant materials (ceraspray) used for lubricating for better finish surface. For extrusion, the die, piston and samples were heated up to 520 °C (to compensate heat removal before starting), after it first put the sample into the extrusion channel and then piston into the extrusion rout. To perform process, the tools were adjusted between two gages of pressing machine and start operation. The extruded samples were removed out easily by opening two sections of the die which is illustrated in Figure 3.9.

Extrusion has been selected due to the following advantageous: (1) simplicity, (2) better homogeneity of fiber distribution in matrix, (3) high productivity rate at lower cost, (4) improvement of mechanical properties and microstructure [Jahedi et al., 2012].

3.5 T6 Heat Treatment Process on Extruded A356 and A357 Metal Composite Reinforced with C_{sf}

The T6 heat treatment consists of three main steps, solutionizing at high temperature, quenching and artificial aging. The balance between strength and ductility obtained after this heat treatment can be attributed to changes in Si particles characteristics resulted after solution action and formation of non-equilibrium $\beta'(Mg_2Si)$ after aging. The effect of solution treatment on casting are: 1) dissolves Mg_2Si particles 2) homogenize the microstructure 3) changes in morphology of Si particles and iron intermetallic compounds [Es-Said et al., 2002].

The unique globular microstructure of SSM processed components shows a shorter diffusion path and promotes enhanced dissolution of solutes before heat treatment. The optimum temperature for solution treatment provide the best compromise between time savings, lower risk of distortion, energy consumption and maximum dissolution of alloying elements. The aging is a precipitation of solute atoms either at room temperature (natural aging) or elevated temperature (artificial aging or precipitation heat treatment)

To achieve precipitation strengthening of supersaturated solid solution (SSS) in aluminum alloys needs a finely dispersed precipitates among the aging heat treatment which is accomplished below a metastable miscibility gap called Guinier-Preston (GP) zone. The sequences of Mg_2Si phase formation for un-reinforced samples submitted to the heat treatment are: initial solid solution $\rightarrow$ GP zones $\rightarrow$ coherent needle shaped β" phases $\rightarrow$ semicoherent needle and rod shaped β' phases $\rightarrow$ semicoherent platelets β phases (Mg_2Si) [Vidal-Setif et al., 1999]. Aluminum alloys submitted to the T6 tempers generally show the highest strengths without sacrifice of the minimum levels of other properties and characteristics which are useful for engineering applications. The T6 heat treatment can significantly improve the mechanical properties of aluminum silicon alloys such as hardness, tensile strength and ductility of A356 and A357.

To study the effect of heat treatment on microstructural and mechanical properties of fabricated composites, two groups of samples which made of Al matrix as A356 and A357 were examined. The T6 heat treatment was carried out on the successful extruded

samples. The mechanical properties are expected to be improved by an adequate heat treatment process. Through T6 heat treatment the precipitation hardening will precipitate the alloying elements in the form of fine coherent particles inside the grains during the aging stage to promote the mechanical properties of alloy [Pio, 2011].

Homogenization, annealing and precipitation hardening (T6 heat treatment) are the main heat treatment procedures. The T6 heat treatment is a common process for the components made of Al-Si-Mg alloys to achieve good mechanical properties. Generally, the T6 heat treatment gives maximum strength (hardness) to the some of the aluminum alloys (A356, A357 and 4047) and the process consists of two main parts, first solutionizing and then aging (Figure 3.11).

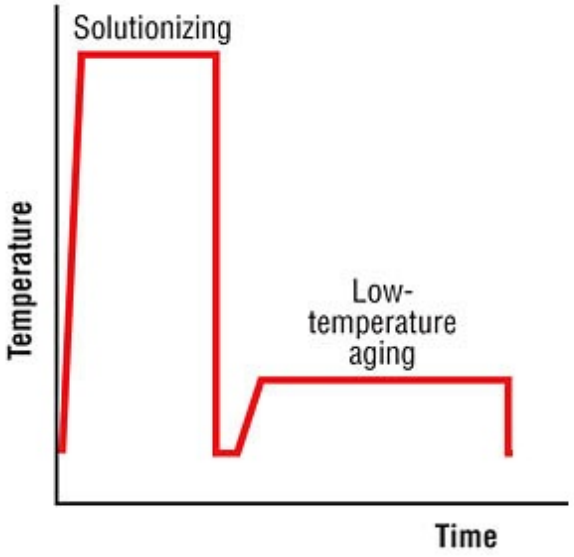

FIGURE 3.11: T6 heat treatment cycle

The solutionizing is to keep the samples at an elevated temperature, but below the melting, in which the alloying elements are dissolved in the aluminum matrix. This process usually involves the dissolution of intermetallic compounds and other phases formed during solidification. The artificial aging is a precipitation of solute atoms at slightly high (∼170 °C) temperature for longer time.

In order to perform T6 heat treatment, the samples were put on a flat horizontal ceramic crucible and introduced into the a Hobersal tubular electric furnace as shown in Figure 3.12 with tube oven model ST-11 PAD-OF and heating elements Kanthal wire, 220 V,

2.2 kW and heating zone of 200 mm which can provide a maximum temperature of 1150 °C. The furnace was equipped by a P.I.D control temperature with ±1 °C under air atmosphere.

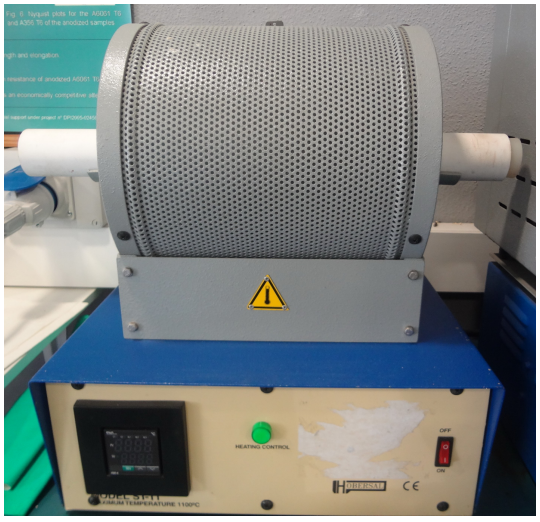

FIGURE 3.12: Hobersal tubular electric furnace

Heat treatment conditions depend on casting method, there are many works have been done for optimization temperature cycles for semi-solid casted components [Menargues et al., 2015, Moller et al., 2008]. Some authors claim that, one hour is the shortest possible time for solution treatment at 540 °C of rheocasted parts made of A356 [Rosso and Actis Grande, 2006]. In the most of cases, T6 heat treatment leads to air bubble accumulation to become big pores in sample and cause the stress concentration and crack initiation. There is no agreement for optimum heat treatment conditions for rheocast parts but an optimum solution temperature has influence on energy and time savings, minimum risk of blistering and distortion and maximum dissolution of alloying elements for the components.

The T6 heat treatment was performed based on the information and conditions of process has been studied by the previous authors. The solutionizing was carried out at 540 °C for 30 min and following quenched up to 25 °C in water and then artificially aged at 170 °C for 3 h finally, cooled under flow of air [Menargues et al., 2015, Vencl et al., 2008]. The samples after removal from the oven and let them cool air.

3.6 Measurement of Density and Calculation of Porosity in the Composites

The Archimedes' principle has been used to measure the density by the difference between measured values and the theoretical densities of thixomixed Al/C_{sf} composite. The theoretical density can be calculated by rule of mixture that was defined in section 2-5. The bulk density of the fabricated sample can be measured by the water displacement approach according to ASTM B962-08. The sample must weighted accurately by digital balance then soaked into the water in the graduated cylinder. The amount of displaced water measured and used for calculation to approach the density.

The volume fraction was measured by chemical dissolution method or extraction of embedded short carbon fibers from samples by dissolution of matrix. Diluted hydrochloric acid was used for dissolution. Three pieces of each sample were cut from different portions, then firstly weighted with an accurate digital balance having an accuracy of 0.1 mg. They were dissolved in diluted hydrochloric acid (1 M) at room temperature (27 °C) under evacuation system. Aluminum was dissolved in HCl and short carbon particles were settled at the bottom of the beaker as a residue. The residual fibers has been filtered, dried and weighted by an accurate digital balance. The volume fraction of these three samples calculated by equation 3.1 and got average.

$$\%V_f = \frac{\rho_m W_f}{\rho_f W_m + \rho_m W_f} \tag{3.1}$$

where, W_f , $W_m = (W_c - W_f)$ weight of fiber, composite and matrix, ρ_f , ρ_m density of fiber and matrix, respectively. The density of A357 = 2.67 g.cm^{-3}, A357 = 2.68 g.cm^{-3} and 4047 = 2.60 g.cm^{-3}.

3.7 Analysis of Microstructure and Metallographic Characterization

3.7.1 Preparation of Metallographic Specimens

Metallographic characterization is necessary for all samples after thixomixing to investigate matrix microstructure, shape and size of intermetallic compounds, dispersion and distribution of reinforcement and defects. Samples were cut off from initial samples (as-mixed or re-melted bar) by precision wheel cutting machine (Struers Accutom-5) and mounted in a conductive thermosetting resin by metallographic press.

Next, specimens surface were ground with abrasive emery paper of 180, 600, 1200, 4000 grades sequentially, in an automatic disk polisher. Finally, two stages of polishing were performed using diamond polishing and then polished by colloidal silica (SiO_2) suspension on chem-dur cloth of Struers for 15 minutes.

Following the polishing, a chemical etchant to attack the surface and dissolving the grain boundaries to reveal the grains by the preferential attack. Those samples which need an etchant so were subjected to the chosen reagent with 0.5 vol.% hydrofluoric acid for 15 seconds (ASTM E3-95) this etchant is widely used for most aluminum silicon alloys.

3.8 Qualitative Metallographic Analysis

3.8.1 Optical Microscopy

The microstructural characterization were performed using optical microscopy (Leica MEF4M and QWin program) is shown in Figure 3.13. It used Leica optical microscope for qualifying dispersion and distribution of fibers in the matrix and extruded samples with studying the presence of micro constituents and the shape or size of the α-phase.

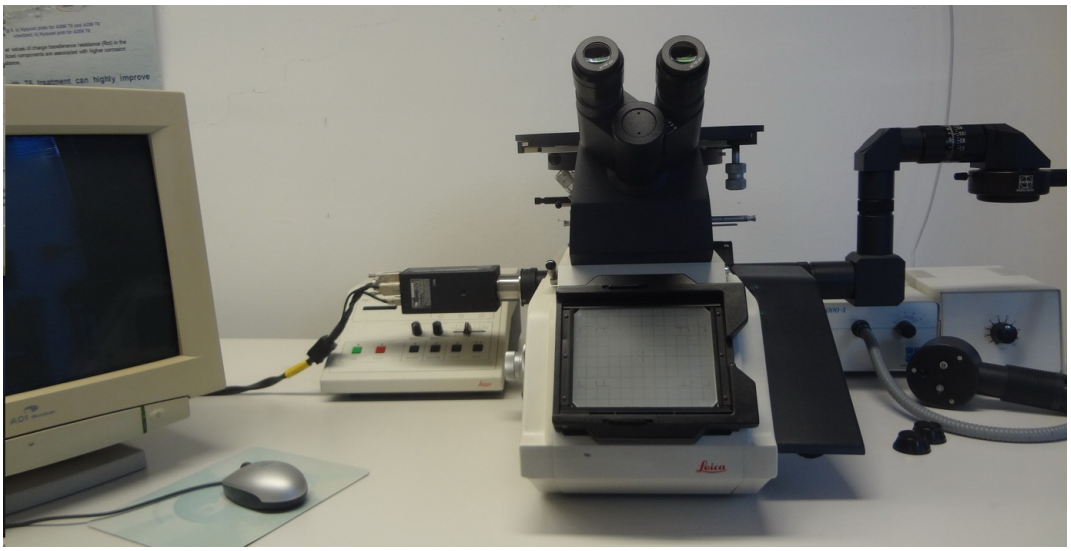

FIGURE 3.13: Optical microscopy (Leica MEF4M)

3.8.2 Scanning Electron Microscopy (SEM)

The SEM was used for analyzing the microstructure of the different phases that presents in the matrix and its shape and distribution. The quality of the fractured surface of tensile specimens and the adherence of fibers to the matrix can be examined under high resolution images of SEM.

Chemical analyzes were performed by EDS (energy dispersive spectrometry X-rays). The equipment allows knowing the approximate composition of the sample elements with atomic number $Z > 6$, although the accuracy of the given composition by this method is limited (1500-2000 ppm detection limit) and scanning electron microscopy (JSM-5600 JEOL) powered by EDX analysis (Oxford ISIS L300) are figured in Figure 3.14.

3.9 Mechanical Characterizations

The mechanical characterization includes the tensile testing, micro-tensile test and hardness tests (such as Brinell , micro-hardness and ultramicro-hardness) for different composite which were heat treated which contain different amount of reinforcement or deformed under sever plastic deformation (ECAP processing). Each characterization and

FIGURE 3.14: Scanning Electron Microscopy-SEM (JSM-5600 JEOL)

the methods is described in the following sections with the parameters belong to each one.

3.10 Tensile Tests

3.10.1 Preparation of Tensile Specimens

For preparation of cylindrical specimens of tensile test, the dimension and tolerances of finishes samples was according standard ASTM E8/E8M as well as the procedure for running characterization. M4 specimens are machined according to dimensions specified in Figure 3.15, with the gage length of 15 mm. The specimens were taken from the mass part of as-extruded or as-mixed (after mixing and re-melting into the bar shape for more information refer to 3.4) as shown in Figure 3.10. The machining was carried out from the cylinders by diamond tools and cubic boron nitride.

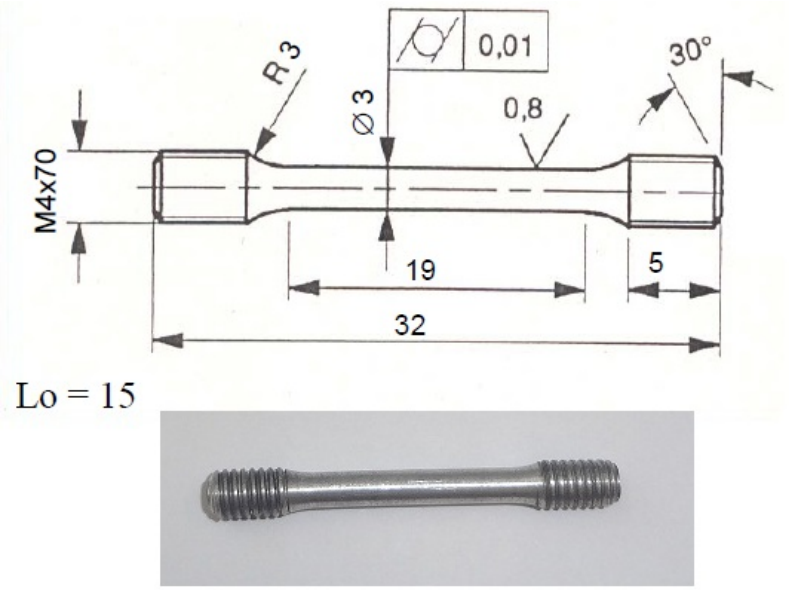

FIGURE 3.15: Schematic and real sample prepared for tensile test

3.10.2 Procedure for the Tensile Tests

To perform tensile test a ZWICK Z100 / TL3S machine 10 kN equipped with extensometer Zwick 066550.02 was employed for this study (as shown in Figure 3.16). All tests were carried out at room temperature with the at the crosshead speed of 1 $mm.s^{-1}$ according ASTM E8 / E8M standard. The successful thixomixed extruded specimens with and without T6 heat treatment were used for the tensile test at parallel path of the extrusion. The gauge length of the specimen was 19 mm and a diameter of 3 mm. The fractured surfaces of specimens were examined by SEM.

After testing, the results auto-saved in a file and can be interpreted in the form of engineering stress-strain diagram by software of tensile machine and the other specific parameters can be extracted. When we assume the initial section area and the length for plotting, so we have engineering stress-strain curve, on the other hand the true stress-strain curve plotted when the momentary section area and the length assumed.

FIGURE 3.16: ZWICK Z100/TL3S tensile testing machine

3.11 Hardness Evaluations

3.11.1 Brinell Hardness Test (BH)

To do the test a predetermined load (F) was applied by tungsten carbide ball with fixed diameter (D) for a time which is determined in the test procedure and then removed it from surface. The average of at least three points of ball's impression measured and calculated so a chart helps to convert averaged diameter to the Brinell hardness values.

The Brinnell hardness measurements were performed by a universal durometer Metrocom, model RC-MP according to ASTM E10 standard. A set of 6 points at different regions on both aluminum alloy and the composite samples were tested using a load of 60 kg and a spherical indenter WC of 2.5 mm diameter for duration of 30 s and then got averaged. In this study, our equipment for Brinell hardness implemented and calculated automatically with the predetermined testing parameters (Figure 3.17a).

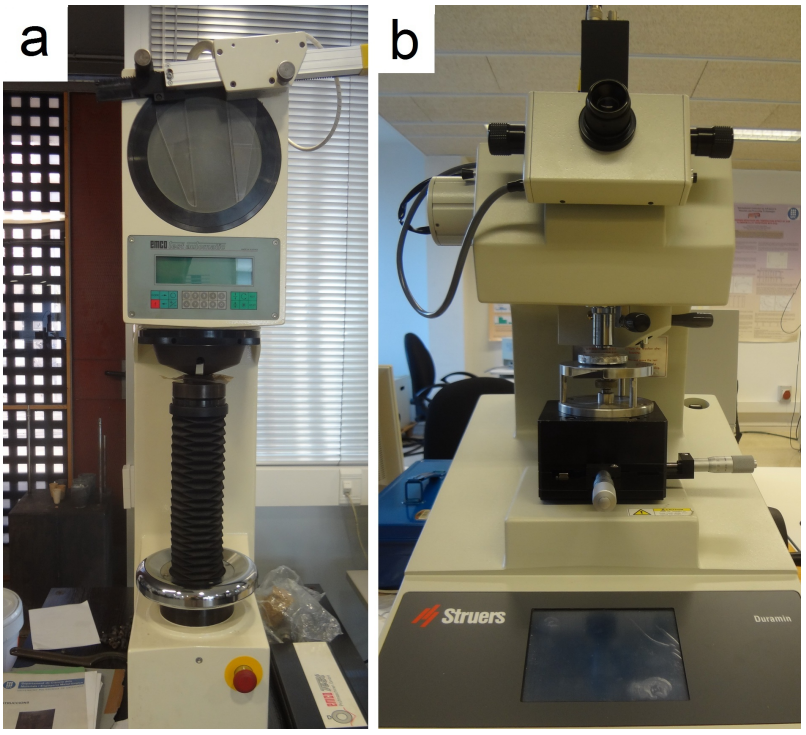

FIGURE 3.17: (a) a universal durometer, Metrocom (RC-MP) (b) micro-hardness tester, Struers- Duramin 20

3.11.2 Micro-Hardness Tests

To evaluate the intermetallic compounds and their hardness, a micro-hardness characterization was employed by using a light loads on a diamond indenter. A specifies rang of lighter loads (start from few grams to one or several kilograms) make the indentation points on the surface utilized for a hardness value for different types of materials, almost for all samples is more commonly used. The indenter in this method is a square base pyramid shape from diamond categorized as Vickers testing.

A micro-hardness tester (Struers- Duramin 20) was utilized based on standard ASTM E-384 using 100 g loads at 10 s time for all the test specimens (Figure 3.17b). Microhardness measurements were carried out at regions around the carbon rod fiber to ascertain the above phenomenon. A load of 100 g for duration of 10 s was adopted for all the microhardness tests.

3.11.3 Ultra Micro-Hardness Tests

Ultra Micro-hardness Test was conducted to study the interfacial micro-mechanical properties of manufactured composite. The strength of interfacial bonding can be measured by application of a small-size Vickers indenter to determine hardness Martens and the depth of penetration. The indenter penetrates into the samples and the depth of penetration is measured by a computer equipped with the software. The applied load can change from 0.4 mN to 1000 mN, with the speed penetration 1 μm.s^{-1} of indenter. All tests are conducted in accordance with standard ASTM E384-99. The ultra micro-hardness equipment (FISCHERSCOPE H100) is shown in Figure 3.18.

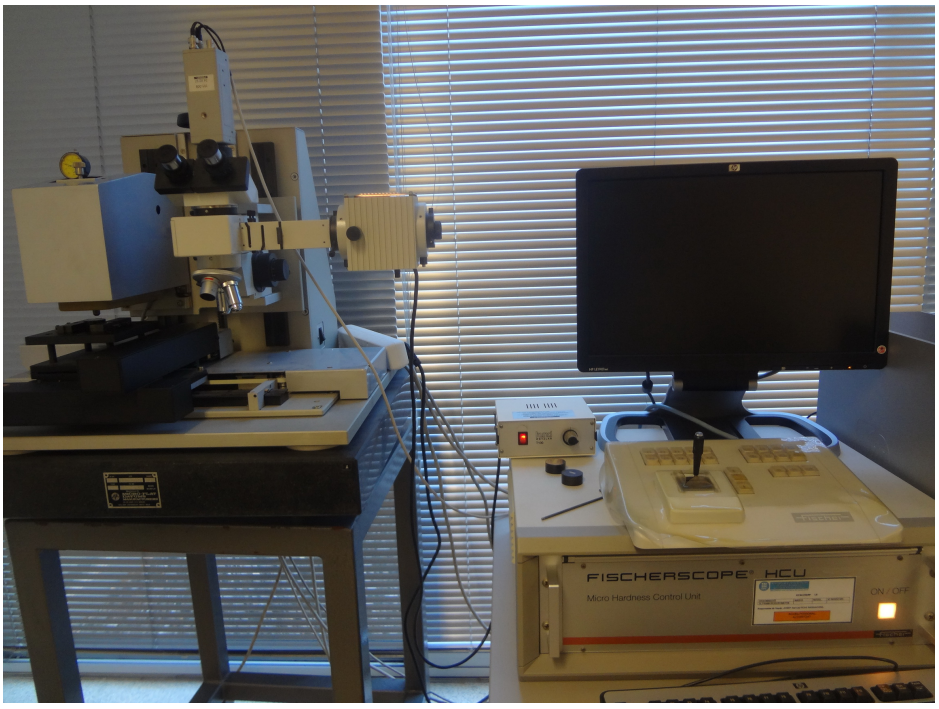

FIGURE 3.18: The ultra-microhardness equipment, FISCHERSCOPE H100

The measuring process of machine contain two steps: first approaches to the surface of the sample at the determined rate for initial contact time, then the intensity of applied force increased by impression of Vickers indenter into the sample surface. The depth of penetration can measure with the machine then gradually withdraws the load and plotted the recovery load versus the displacement which produced in the material. In this technique, a range of very low load values compared the conventional micro-hardness

is utilized. A shallow penetration made by this technique allows studying the properties of interfacial adherence and given phases present in a multi-phase material.

This technique has been performed on A357 composite before and after T6 heat treatment were subjected to ultra micro-hardness machine which the indentation points were following the lines across fibers under 0.5 mN load with 3 μm distances between marks. This evaluation has been repeated three times for different fiber and position and got average, finally the hardness values have been plotted at fiber/matrix interface and evolution properties throughout the matrix region near to the fiber. This method has been used by Ureña et al. to investigate the interfacial properties between matrix and reinforcement particle [Urena et al., 2005].

3.11.3.1 Martens Hardness (HM)

The word Martens hardness HM or universal hardness or HVL (Vickers Hardness under Load) is a relatively new method for the study of elasto-plastic material properties. It is based on the hardness determination from the relationship between the applied load and the surface area which is under active loading and contains both plastic and the elastic deformation. In another word, the hardness can be measured in a condition where the applied load and the material resistance reach to a steady state.

To determine Universal hardness or Martens hardness uses Vickers indenter pyramid, given the geometry of the pyramid with square section area is created from the penetration with the depth (h), under the active load (F). The hardness expressed in $N.mm^{-2}$ to distinguish it from Vickers hardness the numerical values can be calculated according the equation 3.2:

$$MH = \frac{F}{A} = \frac{F}{26.43h^2} \tag{3.2}$$

where, A is the area that was formed by indentor over surface.

The main difference between conventional Vickers hardness (HV) and Martens hardness is the magnitude of the elastic deformation of the total deformation depends on the

elastic modulus of elasticity of tested material. Regarding very small size of indenter, so a very small volume of material corresponds to hardness and related to the surface tension, roughness and homogeneity of present phases.

To calculate the contact area under active load deduced the elastic deformation components or by consideration of shape deformation of sample. Martens hardness reveals plastic deformation components of indentation hardness. A graphical output is demonstrated as result of this technique which plotted the applied load versus displacement of indenter as shown in Figure 3.19 which provides additional information on the elastic-plastic behavior. The parameters of this graph are:

h_{total} total depth of penetration

h_r depth of footprint

$h\acute{r}$, average penetration depth

W_e elastic energy or elastic recovery

W_r plastic energy or permanent deformation

W_{total} total energy of load.

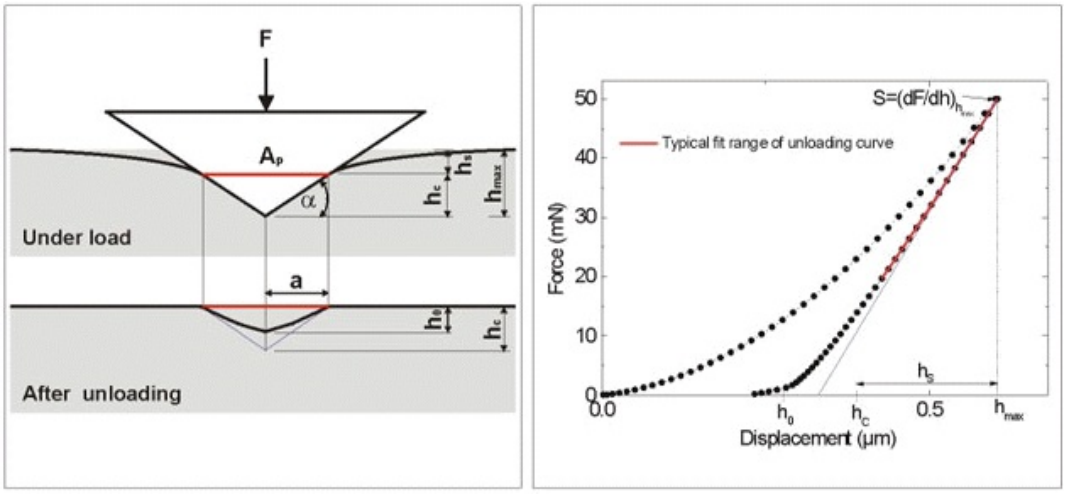

FIGURE 3.19: (a) presentation of contact area during loading and after unloading (b) the force/displacement curve [Rafaja et al., 2012]

As shown in Figure 3.20, the loading started from point A to B and then unloading in the rout B to C which reveals the mechanical work was done for plastic deformation and the purple area represents the permanent energy remained in the material as plastic deformation (W_r). The light blue area shows the energy released in the elastic recovery

during load reduction or unloading. In general, the ratio W_r/W_t is a constant characteristic of each material. The curvature form of the rout $A-B-C'$ is determined by plastic and elastic properties of the material and the contact area on the sample is not constant during load reduction as shown in Figure 3.19. The loading part of curve depth/load for the most of material is linear up to the maximum test load, so in this case the contact area is constant.

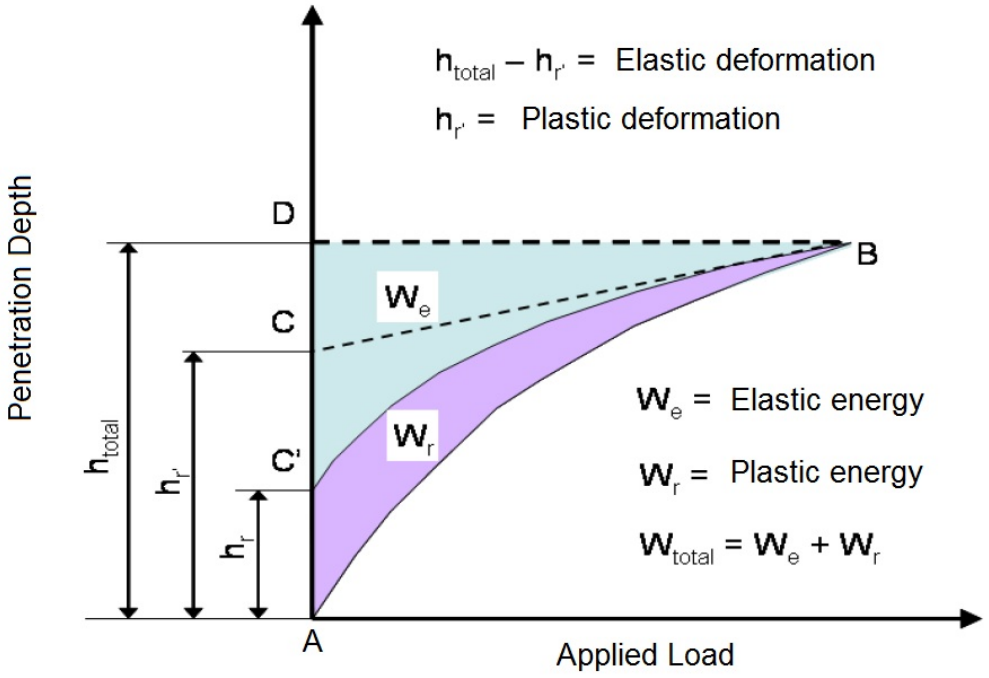

FIGURE 3.20: The applied load/penetration depth curve for ultra microhardness characterization [Picas, 2000]

3.12 Wear and Tribological Tests on 4047 Aluminum Alloy

The wear means erosion or interactions between abrasive and surface with deformation and removing of materials due to mechanical action. The wear is a part of tribology and consists of different types as followed:

- Adhesive wear
- Abrasive wear
- Surface fatigue
- Erosive wear
- Corrosion and oxidation wear

The pin-on-disc is a common device to determine the tribological parameters such as coefficient of friction and wear rate. The machine is illustrated in Figure 3.21a, involves a rotating disc with variable angular speed that the sample is placed on it.

A spherical counterpart made of WC-6% Co held by vertical pin is pressed continuously by predetermined load onto the sample which run according to standard ASTM G-99-05 of testing. The tangential force impressed a tracking area and the frictional coefficient can be measured by instruments on the machine. Finally, a profilometer utilized to measure the depth of semi-circular footprint of counterpart and calculate the track area and wear rate for each experiment. The coupons were cut at an appropriate size from the product of the mixer, directly. The three different samples were prepared at three volume fraction 0, 4.2 and 8.1% of the C_{sf} for wear tests.

The coupons were cut and their surfaces were polished with the sequence grades of emery papers as 500, 800 and 1000. After the polishing the Brinnell hardness values were measured at 5 different points at various regions on each sample with the mentioned procedure. An average of 5 points achieved and presented for the hardness of each sample.

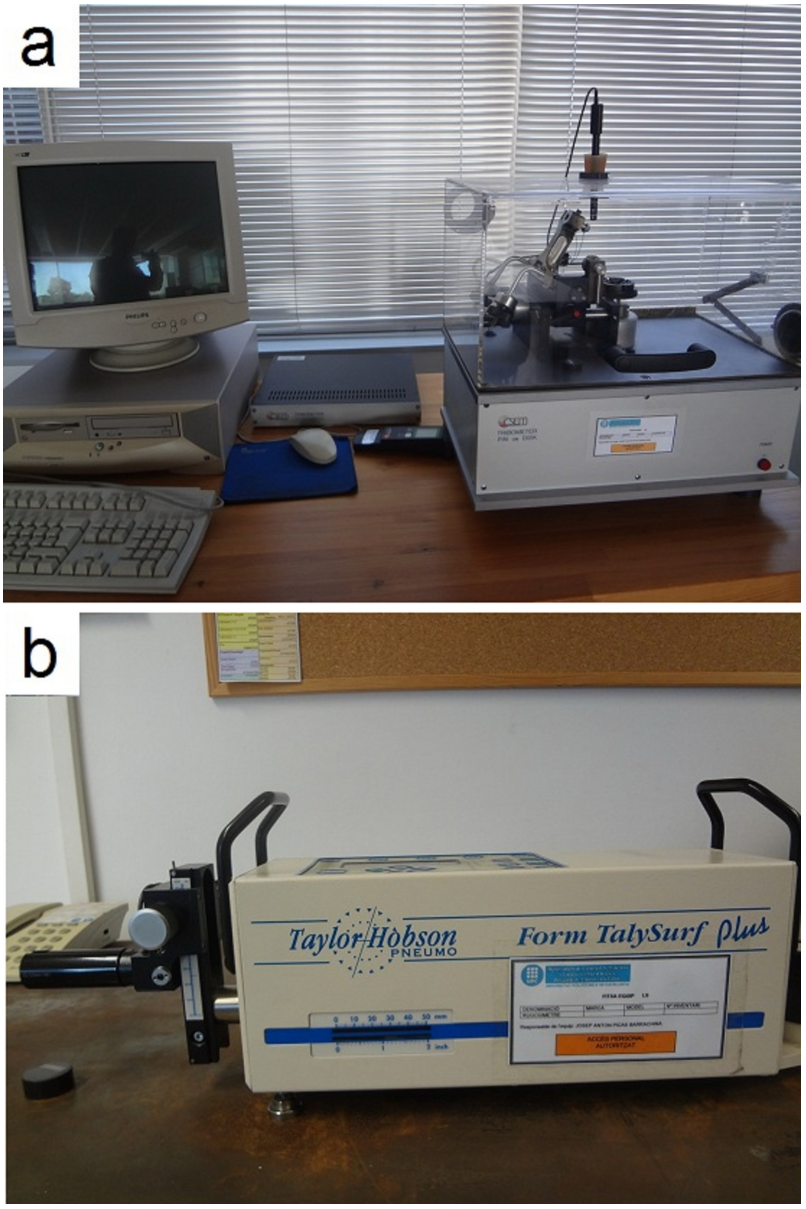

FIGURE 3.21: (a) pin-on-disk machine CSEM Tribometer and (b) profile-roughness measuring machine (Profilometer)

The density measurements were carried out to estimate the porosity content that is presence in the thixomixed composite samples with and without C_{sf} by a precision digital balance and the standard Archimedes principle. Finally, the values of hardness and density were tabulated and reported. All dendritic structures were degraded into fine and small primary α-phase size and converted into spherical shapes due to high shearing load produced by the mixer.

The spherical pin with counterpart made of WC-6 % Co with diameter of 6 mm (CSEM Tribometer) was utilized during the study. All nine tests (were design by L9 orthogonal

array of Taguchi method specified in Table 3.3) were carried out in dry conditions without liquid lubrication under 24% relative humidity rate, at 0.05, 0.1 and 0.2 cm.s^{-1}, the loads of 5, 10 and 20 N with three levels of carbon fiber content, until 10^4 laps completed according to standard ASTM G-99 of testing. Each composite sample had a rectangular shape of 2×2 cm and the wear track was a circle with 12 mm diameter.

The profilometer as shown in Figure 3.21b was used to measure the transverse area of tracking which created after wearing process. The probe of profilometer was passed along the radial and perpendicular line correspond to the circular shape of wear track, to measure the penetration depth of wear track into the sample. This process was repeated 5 times at different radial lines and the semi-circular area of wear penetration measured by the software and got average. The specific wear rate can be calculated using the transverse area of the wear track as measured by a profile-roughness measuring unit. Generally, the wear rate (W) ($m^3.(N.m)^{-1}$) was calculated by using the equation 3.3

$$W = \frac{\Delta V}{D} \tag{3.3}$$

where ΔV is the volume loss (m^3) and D is the sliding distance (m). The following equation was used to calculate the specific wear rate of the specimen.

$$k = \frac{\Delta V}{F.\Delta S} \tag{3.4}$$

where k is wear factor or specific wear rate, ΔV is volume loss, m^3, ΔS is sliding distance (m) and F is load (N) [Khoddamzadeh et al., 2012]. It must be mentioned that the eqs. 3.3 and 3.4 were derivations of Archard equation for sliding wear.

3.12.1 Design of Experiment (DOE)

In this study, Design of experiments (DOE) was used to reduce the number of experiments and analysis the effect of wearing parameters on the tribological properties. The DOE, is a powerful tool of six sigma methods, to develop experimentation by maximizing the achievements using minimum of running trials and reduction of cost and

time. The DOE is widely used by engineers and scientist to improve of production process and cost reduction to obtain maximum achievements and decrease variability. In the concept of DOE, the dependent variables called responses and the independent variables are called factors whiles the experiments are run at different factor values as levels. Each run of experiments is called trials and involves a combination of investigated factors at different levels. The number of trials depends on the number of factors and levels, basically. For instance, if the number of factors is n and the number of levels is m, so nm trials to be tested.

Taguchi's orthogonal method is a statistical and highly fractional design of experiment, consists of array used to investigate the main effects with run of a few number of trials. This method can estimate the main and interaction effects when factors have more than two levels or in the case of mixed level experiments where factors have not the same number of levels.

Table 3.3 shows an optimized L9 orthogonal array designed by Taguchi's method which avoids running the experiments combine all levels of all factors. All trials have been carried out on the factors run at the specific levels. The results of each run were inserted into software and analyzed them in two ways, graphical and statistical. The main effect plot and interaction plot are useful and simple representation for the influence of the factors on the results visually.

TABLE 3.3: Experimental design parameters and results using an L9 (3^3) orthogonal array

Trial	A: Volume Fraction $\%$	B: Speed of Sliding $cm.s-1$	C: Load N
W1	0	5	5
W2	0	10	10
W3	0	20	20
W4	4	5	10
W5	4	10	20
W6	4	20	5
W7	8	5	20
W8	8	10	5
W9	8	20	10

The results of coefficient of friction and the specific wear rate of samples were determined and imported to software for further analysis. All experimental runs must be

conducted and repeated twice times to remove any errors or mistakes, using the combination of levels for each control factor. Analysis of variance and determination of interaction effects and of each erosion parameters (weight loss and coefficient of friction) were performed by using MINI TAB v.16. The worn surfaces and wear debris were characterized using scanning electron microscopy (Jeol JSM-5600) with energy dispersive X-ray (EDAX) analysis.

3.12.1.1 Analysis of Variance (ANOVA)

The analysis of variance is the statistical method helps us to find the optimum values of response by changing the values of parameters or testing the significance of regression. This analysis is also used to test hypotheses concerning when we have several populations, when two or more groups are equal under same assumption and the sampled populations are normally distributed [Whitt et al., 2006]. In statistical studies, regression analysis includes any techniques for analyzing several variables, focusing on the relationship between dependent variables (main effects) and one or more independent variables (interaction effects or errors). An interaction is the relationship among two or more variables, when the effect of one variable differs depending on the level of a second variable [Giles et al., 2005].

The components of an ANOVA table are:

- Source - refers of the type of variation, which can be the factor, interaction, or the error. The total indicates a sum of all the sources
- DF - degrees of freedom for each source, If you have a total of 30 observations, the degrees of freedom total is 29 (n - 1)
- SS - sum of squares can be estimated using observed data if it is between the groups (factor) or within groups (error)
- MS - mean square can be calculated by dividing the total variance by respective degree of freedom
- F-value -by dividing the MS by the error MS

- P-value – is used to determine whether a factor is significant. If the p-value is lower than 0.05(α-value), then the factor is significant.

3.13 Corrosion Study on Aluminum Silicon/C_{sf} Composites Fabricated by Thixomixing

Metal composite which is made by aluminum silicon alloy and carbon fiber can be utilized in various applications, so the corrosion behavior of matrix, matrix/fiber interface and the reaction of intermetallics are interesting [Wielage and Dorner, 1999*b*]. It has been reported, the crevice corrosion was occurred at the interface of C_{sf} and aluminum matrix. The C_{sf} plays as conductive and more noble element and aluminum as active metal are composed a galvanic cell. On the other hand, the presence of C_{sf} in MMC decreases the integrity of oxide film on the aluminum surface that leads to pitting without any polarization [Wang et al., 2003]. Potentially, the intermetallic compounds may act as cathodic sites.

The electrochemical reaction and galvanic corrosion between carbon fiber and matrix were investigated. In order to evaluate the corrosion properties of this composite, the effect of current modes and the electrochemical mechanism both potentiodynamic polarization and electrochemical impedance spectroscopy (EIS) were conducted on matrix alloy, aluminum/C_{sf} composite and T6 heat treated aluminum/C_{sf} composite.

3.13.1 Sample preparation for Electrochemical Testing

Three aluminum matrix A356, A357 and 4017 (3 samples) and their thixomixed composites reinforced with 4.1 vol.% of C_{sf} (3 samples) with the T6 heat treated samples (3 samples) were chosen for electrochemical investigations based on ASTM G13. All samples were cut by cutting wheel machine (Struers) and the faces were polished with the series of emery papers 500, 800, 1200 according to the method specified in Section 3.10. The fibers axis which embedded into the matrix is perpendicular to the exposure

surface of samples into the electrolyte solution. Then, the working electrode surfaces washed with the ethanol and distilled water to degrease and remove any impurities onto the surface. Finally, the thin samples were adjusted at the bottom of an electrolyte cell (shown in Figure 3.22a) with the arrangements of three electrodes for electrochemical test.

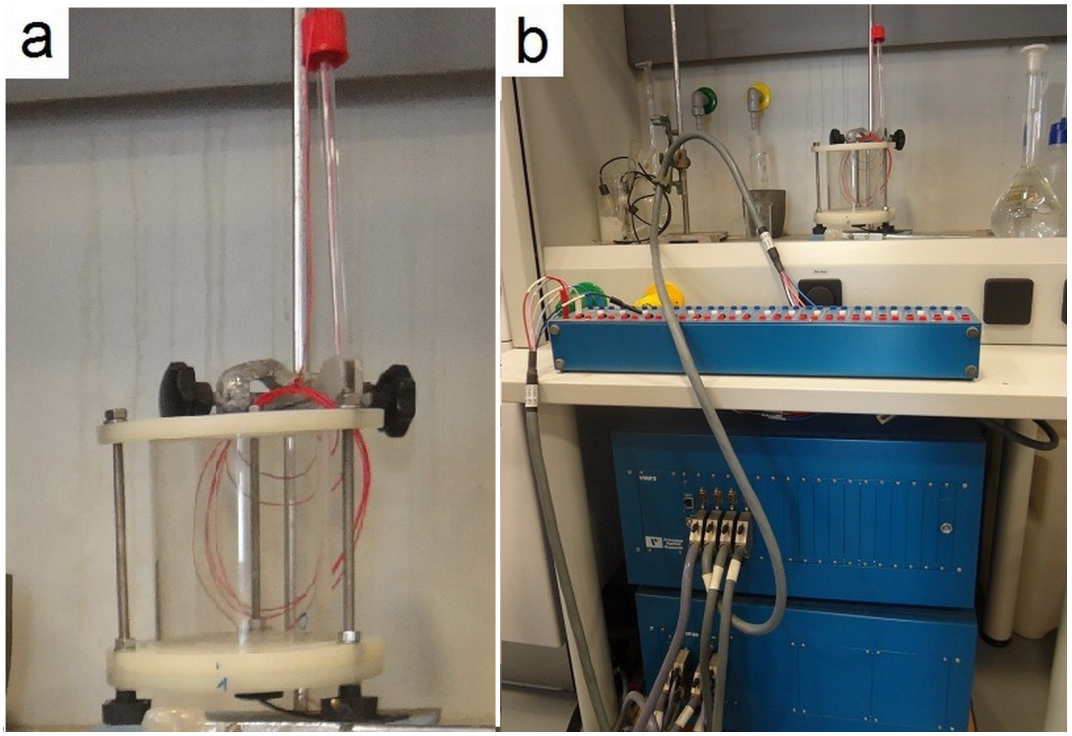

FIGURE 3.22: (a) electrolyte cell (b) potentiostat EG&G PARC model 273A

3.13.2 Test Conditions and Parameters

All electrochemical examinations were carried out by exposure the sample surfaces to the 3.5% NaCl solution at pH 6 and the room temperature according to ASTM G5. The glass cell used which has a circular hole at the bottom with 1 cm^2 area. The reference electrode used in all tests is a saturated calomel electrode (SCE), which has a potential of +0.241 V relative to hydrogen reference electrode at 37 °C. In this work all potentials are referred to the potential of SCE. A platinum wire was utilized as counter electrode and the samples adjusted as working electrode. The same machine as shown in Figure 3.22b was utilized to carry out the both potentiodynamic and EIS test at the above

conditions. In the case of composite materials which either matrix or fiber is more noble than another, a galvanic corrosion may occur. If the aluminum alloy exposure to the alkaline media, a pitting corrosion is more possible by digging a hole under limited diffusion ions and due to the high amount of oxygen and acidic fluids around.

3.13.3 Potentiodynamic Test

Potentiodynamic polarization method are often used for laboratory corrosion testing. The polarization curve or Tafel plot were obtained by running potentiodynamic test and the current represents the rate of anodic or cathodic reactions on working electrode.

A Tafel Plot as shown in Figure 3.23 is log i (logarithmic values of current) versus E (potential), which can be performed on a sample by polarizing it anodically (positive potential direction) and cathodically (negative potential direction) from the corrosion potential E_{corr}. The corrosion current, i_{corr} can be measured by the intersection of the extrapolated Tafel lines to the E_{corr} of the working electrode. In this test variable electric potential between the sample and the reference electrode is imposed and an electrical current between the sample and the counter electrode is generated which is done both by potentiostat machine.

The open circuit potential (OCP) is necessary to be held after specific time (in this case 60 min) for stabilization of the electrolyte with the electrodes. The OCP is the potential of working electrode relative to reference electrode when no potential or current is being applied to the cell.

The scanning process begins in potentiodynamic polarization from cathodic to anodic region instantly after OCP measurement. It performed by applying a potential sweep from -1.2 mV to -0.6 mV compared to the OCP, with a scan rate of 0.166 $mV.s^{-1}$. After test running, the corrosion potential, corrosion rate and Tafel's slopes can be determined, by interpreting and calculating Tafel plot. It is possible to determine the pitting potential $(E_{pitt.})$.

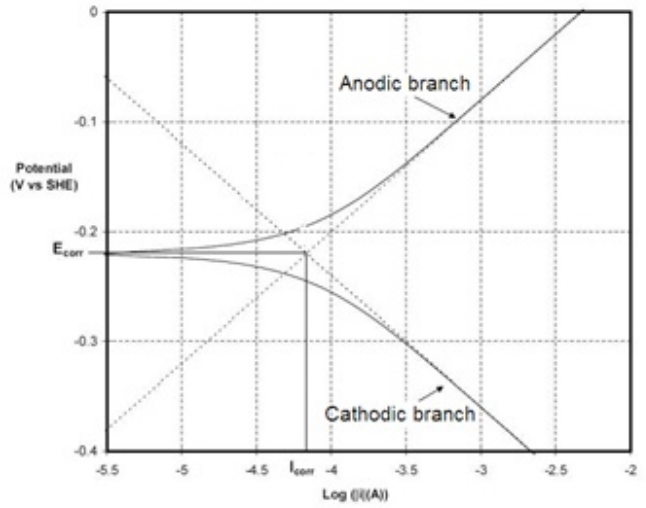

FIGURE 3.23: An example of Tafel plot

3.13.4 Electrochemical Impedance Spectroscopy (EIS)

In this technique, a very small amplitude signals applied on the working electrode and it is big advantage of this technique over others without significant destructive effect on the surface. A small amplitude sinusoidal signal is applied to a specimen usually in the range of 5 to 50 mV as potential and the frequencies of 1 mHz to 1 MHz, and the response to this AC signal can be detected and finally the electrochemical impedance is measured. The impedance is a measure of the circuit ability to resist the flow of electrical current. The impedance Z is then represented as a complex number is composed of a real and an imaginary part,

$$Z(\omega) = E/I = Z_0 exp(j\omega) = Z_0(cos\varphi + jsin\varphi) \tag{3.5}$$

where, Z is the impedance and ω is radial frequency. The Nyquist plot obtains when the real part of impedance is plotted on the X-axis and the imaginary part is plotted on the Y-axis and each point represented the impedance at the specific frequency (Figure 3.24). In this plot the high frequencies are pointed at left side and the low frequencies are at the right side. The semicircle shape of Nyquist plot characterized as a constant phase element (CPE) that modeled as a parallel combination of a capacitor and a resistor in reverse of the angular frequency. The impedance of the CPE is shown as:

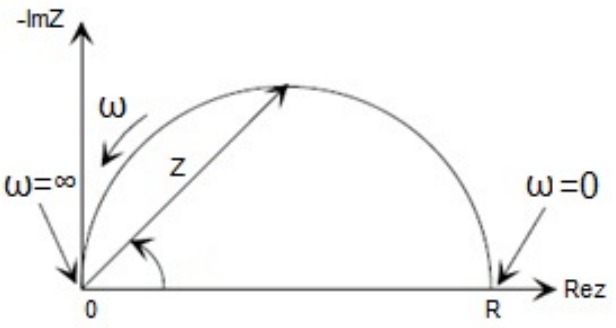

FIGURE 3.24: An example of Nyquist Plot with Impedance Vector

$$Z_{CPE} = \frac{1}{Y_0(j\omega)^n} \tag{3.6}$$

where Y_0 is the admittance or magnitude of the CPE, j is a complex number equal , ω is radial frequency, n is the phase shift value = $\alpha/(\pi/2)$; α is the phase angle ($-1 \leq n \leq 1$) . Z_{CPE} represents different functions in a circuit, for n = 0 it can be modeled as a resistance with R = Y^{-1}, for n = 1 a capacitance with C = Y, for n = 0.5 a Warburg element and for n = -1 is an inductive with L = Y^{-1} (L is inductive capacity) [Lopez et al., (2005].

EIS data is commonly analyzed by fitting it to an equivalent electrical circuit model. Most of the circuit elements in a model are common electrical elements such as resistors (E = IR and Z = R), capacitors (I = C(dE/dt) and Z = $1/j\omega$C) and inductors (E = L(di/dt) and $Z = j\omega$L) where R is resistance, C is a capacitor capacitance and L is inductive capacitance. The electrical elements follow the electrical laws, and components in an electrochemical cell can be related to these electrical elements for further analyzing.

The impedance at high frequency is related to the ohmic resistances of the corrosion product films and the solution enclosed between the working electrode and the reference electrode (SCE). This ohmic resistive behavior is valued by a zero degree phase angle between current and potential at high frequency like the constant current (Z = R = E/I).

The EIS analyses were carried out by alternative current amplitude of 10 mV as peak-to-peak at an open circuit potential applied to the working electrode with the varied frequency ranging from 100 kHz to 10 mHz. The equivalent circuit for all trials was

proposed and measured from Nyquist plots. The analyzing and the calculation of elements values were carried out from the equivalent circuits and results were compared.

3.14 X-ray Diffraction on Fabricated and Heat Treated Composite Samples

The non-destructive X-ray diffraction (XRD) technique was utilized to understand the material's crystallography and in this study to determine the crystallography of intermetallic that was formed under fabricating process. When the X-ray beam take contact to a crystaline material, the beam diffraction takes place. Take into the account of Bragg's Law (nλ=2dsen θ), the wave length of X-ray diffraction and the interplanar distance can be related to the angle of diffracted beam. In order to analysis of XRD, it is necessary to prepare the samples previously. The sample was first polished for one side with 800 and 1200 grit paper then cut into a sheet with parallel sides and 1 mm of thickness. After that the specimen was stacked by silicon-paste on a glass plates of 2mm of thickness and mounted in standard sample holders (PW1812/00) by means of plasticine.

The prepared sample was analyzed using a PANalytical X'Pert PRO MPD Alphal powder diffractometer equipment. A Cu Kα (λ =1.5406 $\AA$) radiation was applied because the wave length is similar to the distance between planes in the crystalline net. Measurements were taken with $\theta/2\theta$ scan from 4 to 100^o 2θ with step size of 0.017^o and measuring time of 400 seconds per step. The power diffraction file (PDF) data base were used for identification and to index the phases which are presence in the sample. The detection of the phases was performed by direct comparison between the PDFs spectra and the ones which obtained by experiment.

Chapter 4

RESULTS & DISCUSSION

4.1 Feasibility of Thixomixing Process

In this part first the dispersion and distribution were examined on the fabricated composite by the innovated method as called ”Thixomixing” and the effects of fabricating parameters such temperature or speed of mixing were analyzed on them. The microstructure and the intermetallic compounds formation were also investigated which can be used for further discussions on physical and mechanical properties.

4.1.1 Dispersion and Distribution of C_{sf} into the Matrix after Thixomixing

The main aim of this study was to develop a new method for fabrication of the Al/C_{sf} composite without damaging the fibers to have better dispersion and distribution in the matrix along with good adherence at the interface. The convectional mixers with impeller may damage the fibers undesirably, which due to its sharp edges of conventional impeller. As it was described theoretically (in Chapter II), thixomixing provides high shearing force as result of the viscosity of a thixotropic fluid (semi-solid slurry of aluminum). Thixotropic state supposed as a gel, when sheared becomes liquid and reverts back when static.

When a pair of parallel plates with a distance is moving against each other creates the shear rate. The shear rate depends on velocity and distance of two rotating plates. It can be expressed as formulated in Equation 4.1

$$\gamma = \frac{4\pi n}{(1-k^2)} \tag{4.1}$$

where, the stirrer frequency is n and geometric parameter k is a ratio between stirrer diameter (d) and crucible diameter (D) ($k = d/D$). Values of shear stress τ (Pa) during mixing of SSMs were calculated as a dependence on total solid fraction according to Equation 4.2:

$$\tau = \eta \times \dot{\gamma} \tag{4.2}$$

where, η is apparent viscosity and $\dot{\gamma}$ is shear rate. The amount of apparent viscosity depends on solid fraction in the slurry and also the temperature determines the solid fraction of slurry and various amount of viscosity.

Short fiber bundles were dispersed under intensive shear stress as shown in Figure 4.1. Thixomixing process with no blade protects the carbon fiber from damaging even though this method is simple. Specimens were cut from different samples and positions for study the microstructural evolution and distribution of fibers. In all successful composite samples, the C_{sf} well distributed with randomized orientation. The successful samples refer to the samples which the C_{sf} were well distributed and dispersed completely in the matrix and reveal a relatively good adherence. The successful and unsuccessful samples have been recognized by the images from optical microscopy or SEM. Shearing may alter the microstructure of primary α-phase in the eutectic in aluminum slurry which can be useful to have better mechanical properties. Silicon concentration increases in the liquid metal caused of concentration gradient of silicon as result of the alpha particles is formed and grown in the molten.

The Thixomixing also have been tried on the alumina fibers (Nextel 610) but the short fibers were cracked and became to the small particles. The short fiber of alumina can

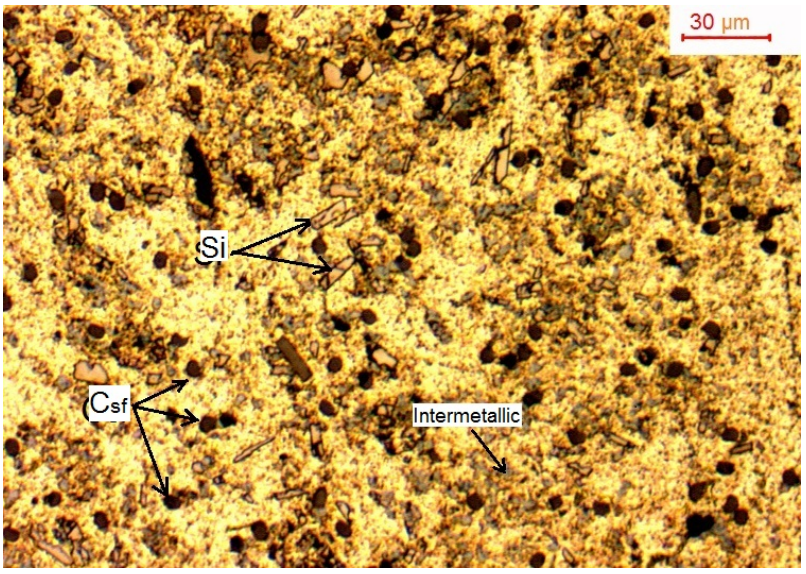

FIGURE 4.1: Optical microscopy shows good dispersion and homogenous distribution of C_{sf} into A356 matrix composite (A356/C_{sf}) reinforced by thixomixing method

not bear the high shearing load was provided in this mixer. For more information, refer to Appendix B.

4.1.2 The Effect of Solid fraction and Speed of Mixing on Thixomixing Process

Three different levels of solid fraction 10%, 48% and 90% were selected to study the relationship between the solid fraction and speed of mixing at 100 rpm and 300 rpm for A356 and A357 aluminum alloys. The effects of the solid fraction and rotational speed of mixing on the success of dispersion, distribution and infiltration ratio was examined and shown in Figure 4.2 for A356 as matrix. In this thesis, the term distribution means distributing of C_{sf} into the matrix and the term dispersion is used for segregation of fibers from each other. The infiltration ratio was calculated based on the amount of dispersed fibers to un-dispersed fibers in the composite. The C_{sf} segregate from liquidus by the centrifugal force at high speed that reduces the viscosity and infiltration. The marks provided in Figure 4.2 indicate the successful ($\circ$) and unsuccessful ($\times$) thixomixed samples with the values of infiltration ratio attached to them. The infiltration ratio was calculated by the ratio of dispersed fibers to the total area of C_{sf} in the matrix for different samples.

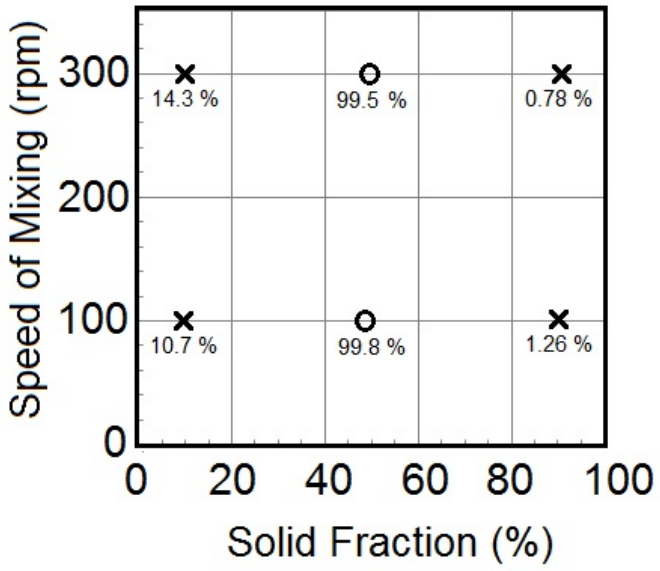

FIGURE 4.2: Influence of solid fraction and speed of mixing on success of mixing and infiltration on A356 (the infiltration percentages were illustrated in the figure)

It shows that the composite samples which the reinforcement have been distributed homogeneously in the matrix were fabricated under a specific fraction of solids in semi-solid slurry and at the appropriate rotational speed of mixer.

Both 10% and 90% solid fraction regardless of mixing speed were unsuccessful, and C_{sf} did not infiltrated effectively into the matrix due to very low and too high shear stress, respectively (Figure 4.3). The slurry with 90% solid fraction was too stiff and just surrounds the cluster of fibers with no infiltration then fibers were agglomerated and cracked by solid particles. In the other point of view, semisolid slurry with 10% solid fraction does not provide sufficient viscosity and shear rate as required for dispersion of short fibers, so a few infiltration with more agglomeration was occurred.

Both high and low solid fractions in slurry cannot be suggested for thixomixing process for dispersion and distribution of fibers or other type of reinforcement. The mushy state of slurry is necessary to provide shearing stress on fiber clusters and dispersion of them to being well distributed in the eutectic. Semi-solid thixomixing method can be assumed for alloys which have a long interval of solidus-liquids. Homogeneous distribution and well dispersion are highly recommended to get the superior strength with suitable ductility. Fiber to fiber contacts and agglomeration leads to a non-homogeneity and caused the lower mechanical properties. It has been found that, the best dispersion

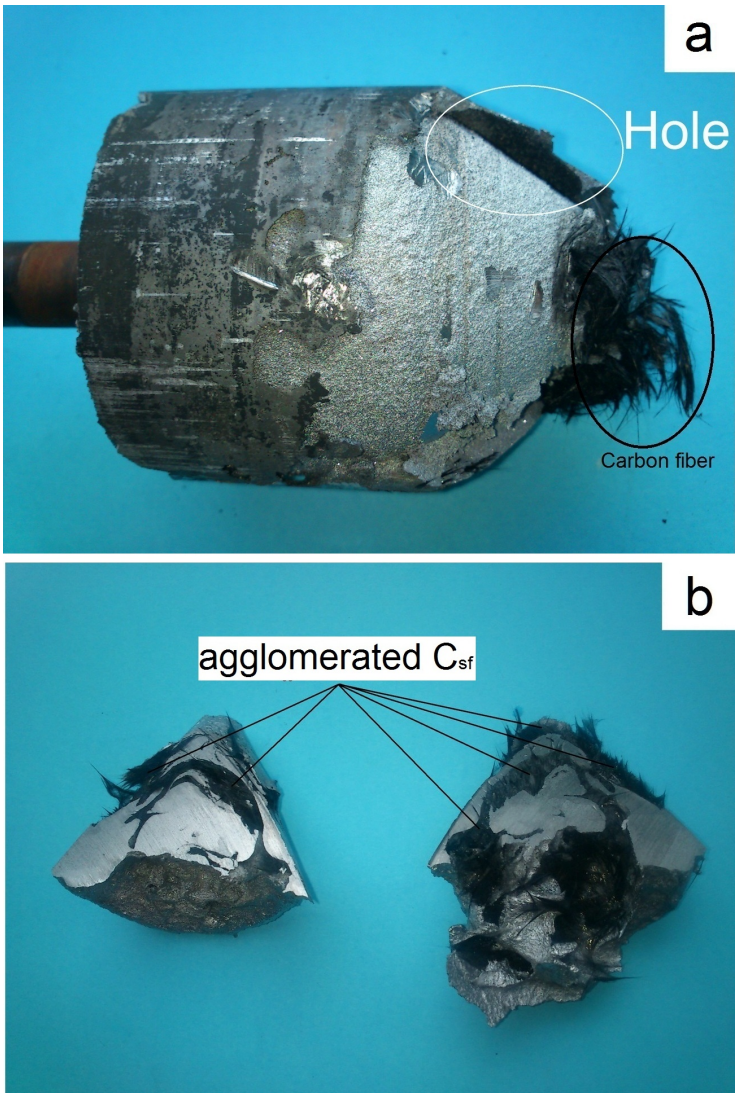

FIGURE 4.3: Unsuccessful thixomixed composite at high solid fraction with agglomerated fibers (a) at 90 % solid fraction and 100 rpm of mixing speed (b) at 10 % solid fraction and 300 rpm of mixing speed

and distribution of C_{sf} achieved at 48% solid fraction at 100 rpm as fabricating speed for both alloys. The mushy flow of slurry sheared and overcome to the agglomeration between carbon filaments, so it can entrap through the fibers and surrounds over fibers. All of the further process and characterization were carried out on based on 48 % of solid fraction and 100 rpm of mixing speed as optimized conditions achieved for successful thixomixing. At high speed of mixing (300 rpm) the possibility of segregation between solid particles and liquids in the slurry and fibers cracking is higher than 100 rpm.

4.1.3 Microstructure of A356/C_{sf} and A357/C_{sf} Composite

Figure 4.4 shows the distribution and dispersion of C_{sf} in the composite at same resolution for both alloys with different volume fraction of C_{sf} under optimum condition of thixomixing. As it was mentioned the optimum condition for composite fabrication via thixomixng was determined as temperature (576-580 °C) set for achieving 48 % solid fraction for each alloy and mixing speed of 100 rpm, with 4.2 and 8.1 vol.% C_{sf} and quenching in water after finishing. The values of volume fraction of C_{sf} were calculated related to conversion of fibers mass to the volume and the density of alloy and carbon fiber as described in the section 2.5.

The microstructure of as-mixed aluminum/C_{sf} composite was evaluated on two aluminum silicon alloys (A356 and A357). Figure 4.4 were taken at perpendicular plane to the bar length and short fibers were aligned to it. Both images exhibited a good distribution of short fibers in the aluminum matrix which are well dispersed with few agglomerations, but contain some porosity. Figure 4.4b shows a slightly non-homogeneity of C_{sf} distribution may due to the temperature tolerance during mixing process or post-process.

The α-size in the reinforced samples was shown smaller than which was non-reinforced because of good distribution and dispersion of fibers in the matrix and provides a lot of heterogonous nucleation site as can be seen in Figure 4.4b and Figure 4.4c. It has been reported by previous authors [Wu and Kim, 2011].

4.1.4 Investigation and Characterization of the Intermetallic Compounds in the Fabricated Composite

The iron intermetallic compounds have been detected as main intermetallic compounds in all samples due to the Fe, an average atomic concentration which exits from matrix alloy or slightly dissolving from the steel body of die. As substantiated by Taghiabadi et al. with the concentration of Al, Fe and Si formed the needle-like $\beta - Al_5FeSi$ and

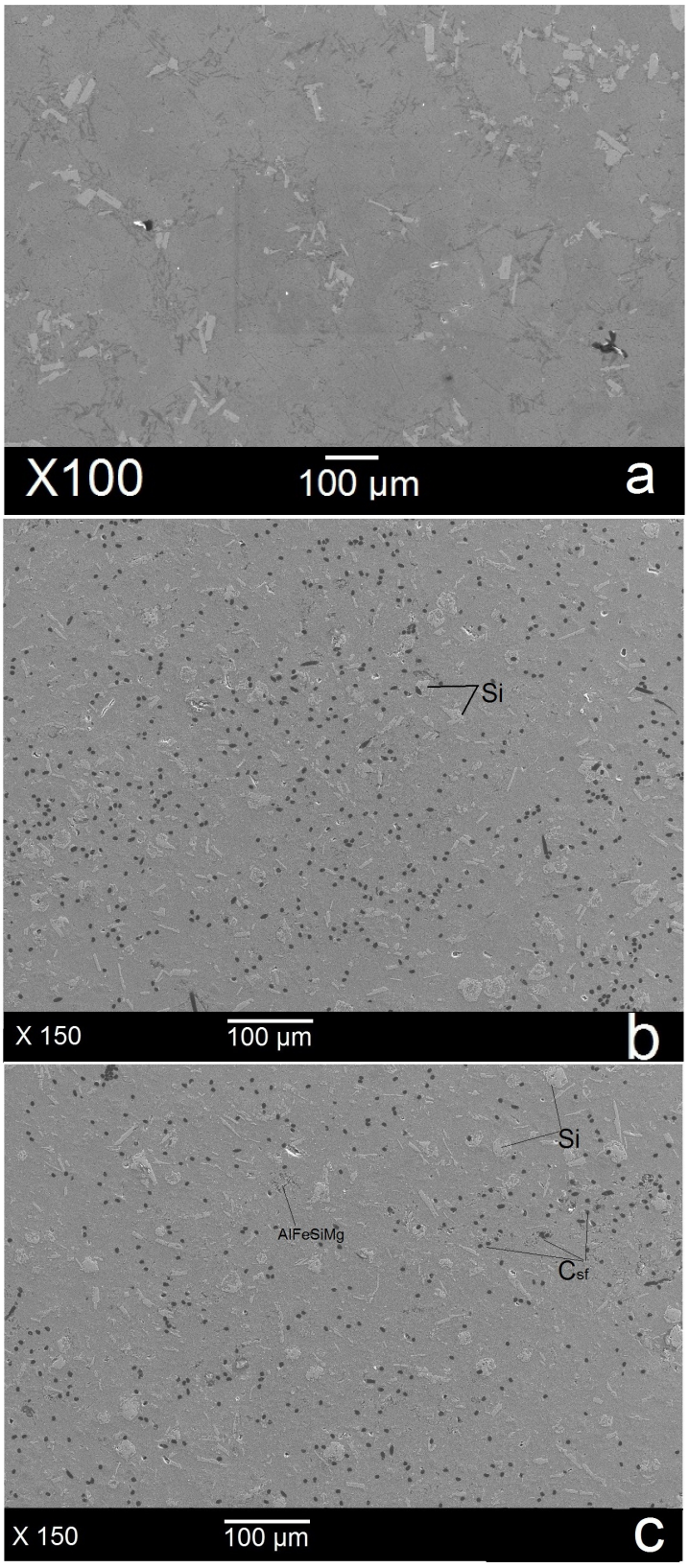

FIGURE 4.4: SEM microstructure of successful fabricated (a) as-thixomixed sample without reinforcement of A357 which shows bigger α-size than same composite samples (b) A356/8.1 vol.% C_{sf} and (c) A357/4.2 vol.% C_{sf}

$Al_9Si_2Fe_2$ [Taghiabadi et al., 2008]. These type of intermetallic compounds were shown in the images inset in the Figures 4.4 and 4.5.

As illustrated in Figure 4.5a, the fibers has been embedded in the eutectic with higher concentration of silicon; whereas the primary spherical α-phase was nucleated initially prior of stirring. The dendritic structures of primary α-phase were broken under high shear stress and converted to a globular shape as it can be seen in Figure 4.5a, and surrounded by the eutectic. During the process, the mixture contains the eutectic, short fibers and globular α-phase is being sheared continuously to get a homogeneous mixture. The α-phase has been solidified initially in the semisolid slurry in the shape of globular and participates with short fibers in the mixing process under high shearing load in the molten eutectic. As silicon and the iron intermetallics in the eutectic were solidified after primary α-phase in the process, so they have been deposited at the fiber/-matrix interface (Figure 4.6).

It seems that the lower temperature and short time involved in thixomixing process under intensive shearing prohibited or delayed the undesirable chemical reactions such as fragile aluminum carbide (Al_4C_3) at the interface of fibers and matrix [Yamaguchi et al., 2009]. In additions, the high cooling rate such as quenching in water decreased the interfacial reactant and formation of Al_4C_3, remarkably. As mentioned previously in the introduction, aluminum carbide which formed locally at the interfacial surface of matrix/fiber as needle-like affected the surface quality of C_{sf}, thermal conductivity and mechanical properties are due to the low capability of load transferring from matrix to fibers.

Silicon content in aluminum alloy (having at least 7 wt.%) is a dual action element which improves the adherence and prevents the formation of aluminum carbide especially at temperatures up to 750 °C [Lee et al., 1998]. In this method with the lower temperature and the high concentration of silicon in the eutectic might be helpful to overcome the problem in order to the lack of wettability between the carbon fiber and aluminum and will be discussed later.

It can be expressed that, the silicon was deposited in form of layer or as intermetallic compounds composed of Fe and Al over C_{sf}, which could be improve the wettability

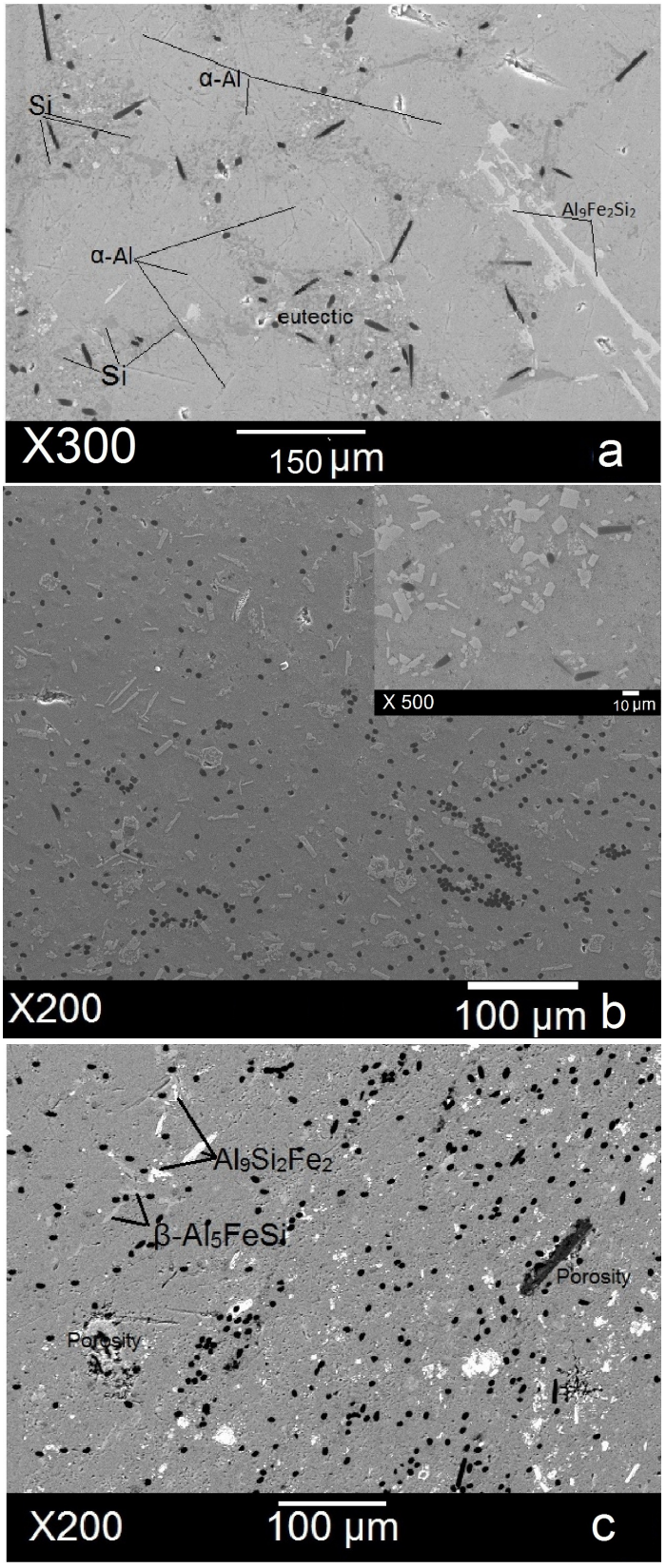

FIGURE 4.5: SEM microstructure of successful fabricated (a) A356/4.2 vol.% C_{sf} composite as-mixed samples showing random orientation of fibers distributed in eutectic and surrounded by globular Al-α (b) A356/8.1 vol.% C_{sf} after extrusion (c) A357/8.1 vol.% C_{sf} after extrusion

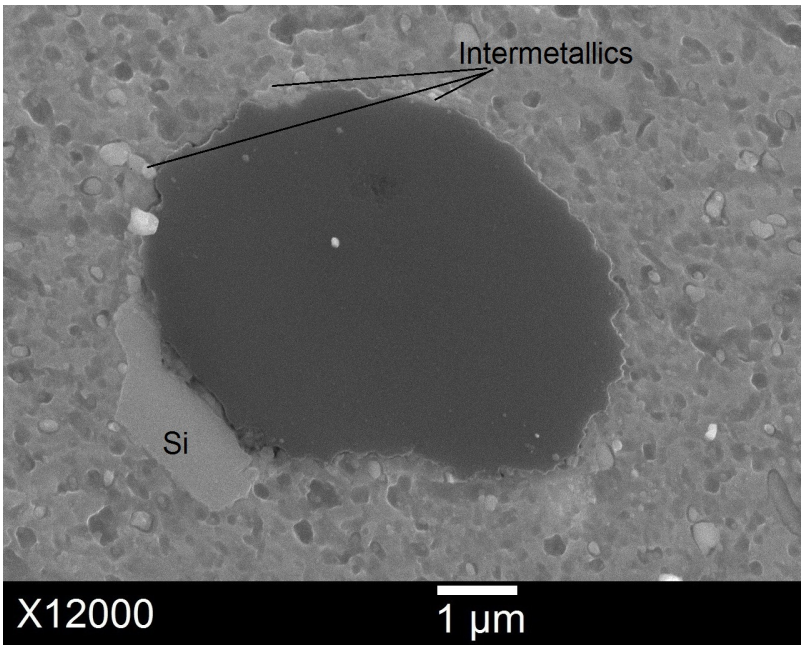

FIGURE 4.6: SEM microstructure of Si and intermetallic compounds deposition on a single fiber

and inhibiting undesirable reactions, thus the extra coatings mentioned [Urena et al., 2007] such as copper or nickel are not needed. The size of Si particles in this method was very fine with an average size around 1 μm (Figure 4.5b). During solidification the formation of such fine Si particles has been observed by the other authors in rheo-process due to uniform dispersion of particles in the matrix which provides a lot of heterogeneous nucleation sites (in this case, C_{sf} as nucleation sites) [Hari Babu et al., 2008].

The fine and homogeneous microstructure achieved by this method is expected to improve simultaneously the tensile strength and ductility, since that the agglomeration of particulates and non-dispersed reinforcement induces unwanted brittle nature in composite by predominant crack initiation sites [Wang, Chen and Wu, 2009].

The globular α-phase (shown in Figure 4.5a) has been changed to small α-size with different morphology after the extrusion. In the Figure 4.5a, it has been tried to keep the original morphology of as-mixed composite in semi-solid condition to demonstrate the globular α-phase and presence of reinforcement in the eutectic. Any post-process such as remelting or extrusion may alter the original microstructure of as-mixed composite

of thixomixing which is illustrated in Figure 4.5b and c. The globular form of α-phase has been changed and the specific properties of them might be lost.

The aluminum matrix composite developed by thixomixing have a homogeneous and uniform microstructure throughout the whole area and in different cross-sections. The initial morphology represented in as-mixed, was globular and made up of fragments of dendritic structure of primary α-phase with carbon fibers embedded in eutectic region around them.

It is notable that the majority of C_{sf} are at the eutectic regions and in the boundaries of α-phase, as reason of initial formation of α-phase and embedding of C_{sf} in eutectic as liquid phase of semi-solid slurry. The process of thixomixing is so sensitive to temperature, chemical composition and the speed of mixing.

The EDAX results which are illustrated in Figure 4.7 can prove the presence of iron in the alloys by dissolving from the die or alloying element in the raw material. Most of aluminum silicon alloys are sensitive to the presence of iron, because of its low solubility in α-phase at solid solution and form Fe-intermetallic compounds which is harmful for mechanical properties and ductility.

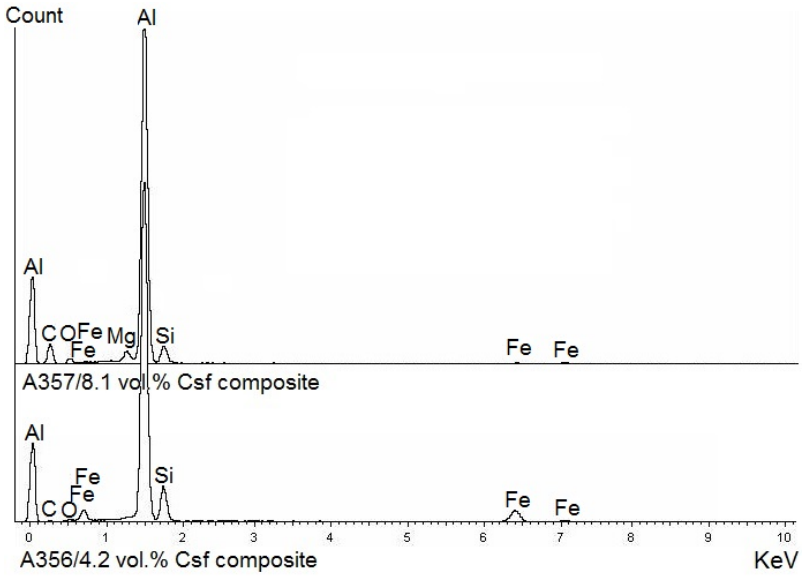

FIGURE 4.7: EDAX spectra of two composites with different matrix alloy

4.1.5 Density and Hardness Values of the A357 and A356/C_{sf} Composites Fabricated by Thixomixing

The values of C_{sf} fraction and porosity was tabulated in Table 4.1 for both matrix alloys after extrusion and also T6 heat treatment under different test conditions. The amount of porosity was increased by increasing of volume fraction and slightly increasing with implementing of heat treatment. It is clearly demonstrated that the pores quantity increased tangibly by increasing of rotating speed of rotor due to high agitation of slurry and sucking air into the matrix. For the samples which are not contain C_{sf} but just thixomixing was performed, the porosity is considerable which is related to the stirring effect of semi-solid slurry.

TABLE 4.1: Experiment condition of thixomixing method with hardness and porosity values

Alloy	Solid fraction %	Speed of mixer rpm	C_{sf} fraction %	Hardness HBW	Porosity %
A356	48	100	0	73±2.1	2.8±0.7
A356	48	300	8.1	64±1.8	5.7±0.6
A356	48	100	4.2	72±2.2	3.6±0.5
A356	48	100	8.1	75±1.7	4.4±0.7
A356-T6	48	100	4.2	87±1.8	3.8±0.4
A356-T6	48	100	8.1	84±1.8	4.1±0.6
A357	48	100	0	76±1.5	2.7±0.4
A357	48	300	8.1	66±1.7	6.1±0.6
A357	48	100	4.2	73±1.6	3.1±0.5
A357	48	100	8.1	71±1.8	4.7±0.4
A357-T6	48	100	4.2	88±2.0	4.2±0.4
A357-T6	48	100	8.1	91±1.9	4.8±0.6

Theoretically, most of the physical properties such as density are being depended to volume fraction of C_{sf} in composite. The main challenge remained unsolved in thixomixing process is the porosity which caused by entrapment of air between the bundles and release during mixing. The content of the porosity in composite increased with increasing volume fraction. In some cases, the turbulence and agitation of slurry by stirring process of mixer may introduce a quantity of air bubbles and pores into the semi-solid slurry.

The porosity has the significant negative effect on the tensile properties of composites which tangibly decreased when the content of pores increased. Any impurities or pores can be act as crack initiation site. The heat treatment can intensified this bad effect by increasing the size of pores in the composite. It must be mentioned, the porosity increased with increasing of stirring temperature due to the level of gas entrapment increased with increasing of casting temperature [Karbalaei Akbari et al., 2015].

Therefore, the porosity content in thixomixing is much lower than other methods which using stirring process at fully liquid condition [Sanchez et al., 2010]. It seems that the low temperature of matrix slurry in thixomixing provides the beneficial impact on reinforcement distribution beside of lower destructive effect of porosity content. The amount of pores in composite can be reduced by promoted designing on the mixer and the process sequence in further studies.

4.1.6 Extrusion and T6 Heat Treatment on A357 and A356/C_{sf} Composites Fabricated by Thixomixing

It was inevitable to carried out hot extrusion on fabricated composite samples, to perform further characterization such as tensile test. At first, it was expected to reduce porosity and improvement of mechanical properties of metal matrix by extrusion. The T6 heat treatment also was chosen to study the effect of heat treatment on microstructure of metal matrix in composite, intermetallic compounds reformation and mechanical improvements. In the following sections, the effect of each process of extrusion and heat treatment will be discussed.

4.1.7 Porosity and Air Entrapment in Composite Samples After Thixomixing and Extrusion

As it is shown in Figure 4.8 the pores in the thixomixed samples were attributed from the air entrapment and were not occurred by the contraction causes of solidification, so after T6 heat treatment were grown and are bigger in size.

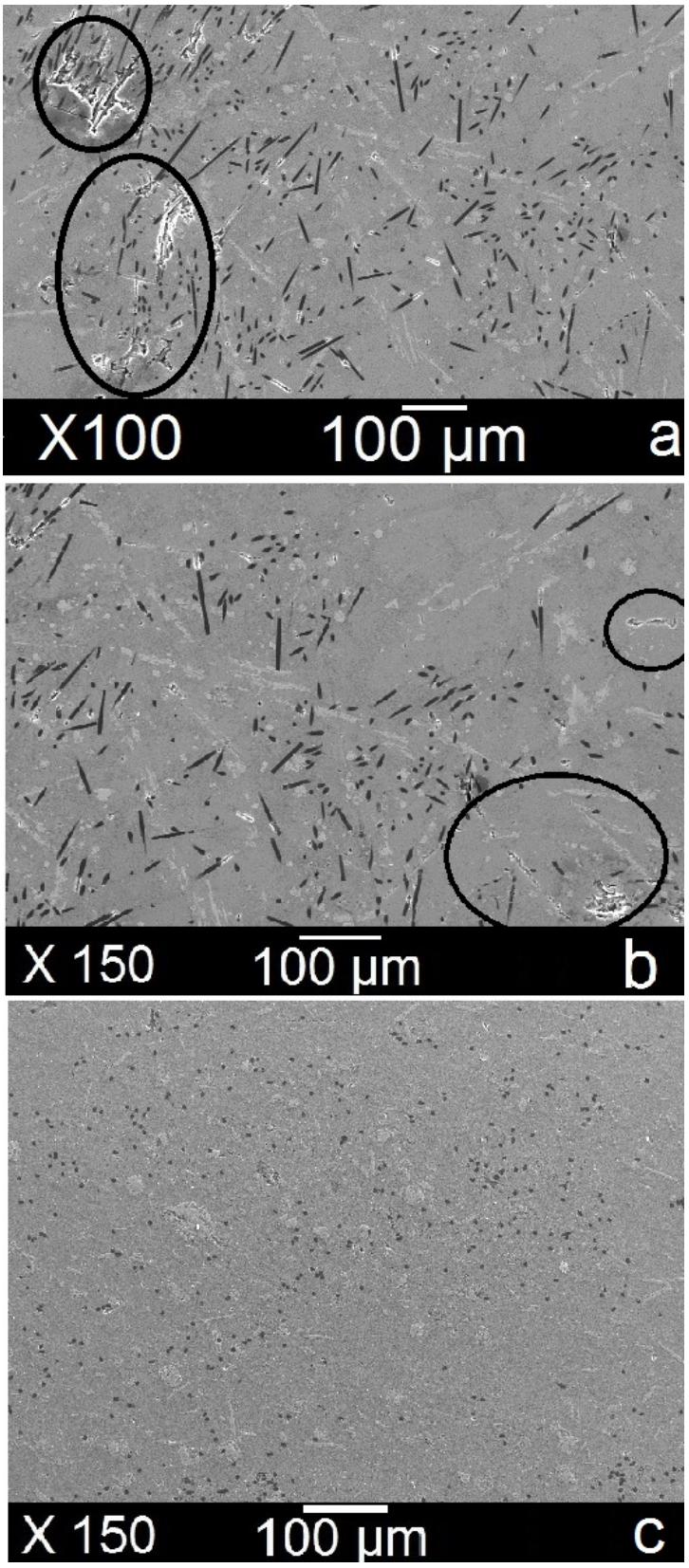

FIGURE 4.8: The pores existed in as-mixed composite samples (a) A356/8.1 vol.% C_{sf}, (b) A357/8.1 vol.% C_{sf} (c) A357/8.1 vol.% C_{sf} after extrusion

The chopped bundles of fibers contain air which was arrested throughout the fibers so when added to the semisolid slurry of aluminum while mixing, the gases were released into matrix and the porosity formed. For instance, some pores (sometimes are big or even micro-size) were indicated in Figure 4.8 for two different composite at the same conditions. Some of the pores may come from the air which was drawn in during the thixomixing process.

The porosities can be reduced or removed by further processes such as extrusion or forging especially at semi-solid state. Further modification on the die (proposed for future studies) or thixomixing process can be useful as solutions for reduce the porosity content as a main problem of this method of compo-casting. These gases or porosities strongly effect on final mechanical properties of composite especially when heat treated. The heat treatment expands the pores and forms the blisters which will be discussed in further parts.

Figure 4.8c shows the morphology of A357 composite reinforced with 8.1 vol.% C_{sf} after extrusion with no pores and minimum porosity for instance. The pores size was reduced to micro size by high strain rate of extrusion as well as its quantity. A few amount of porosity and air entrapment could be harmful for the mechanical properties of composite during heat treatment or under loading.

4.1.8 Microstructure Evolution on Extruded Composite Samples After T6 Heat Treatment

To evaluate the effect of heat treatment on mechanical properties and morphology of microstructure, T6 heat treatment was conducted on the extruded samples that were done as described in section 3.5. Heat treatment was applied to obtain an expanded primary α-phase which contains C_{sf}.

Figures 4.9 and 4.10 shows the optical microscopy images of ax-extruded sample before and after T6 heat treatment which were etched by hydrofluoric acid 5 vol.%. The effect of T6 heat treatment on the morphology and size of eutectic silicon to change from a smaller to coarser and bigger shape. The needle-like iron intermetallic ($\beta - Al_5FeSi$)

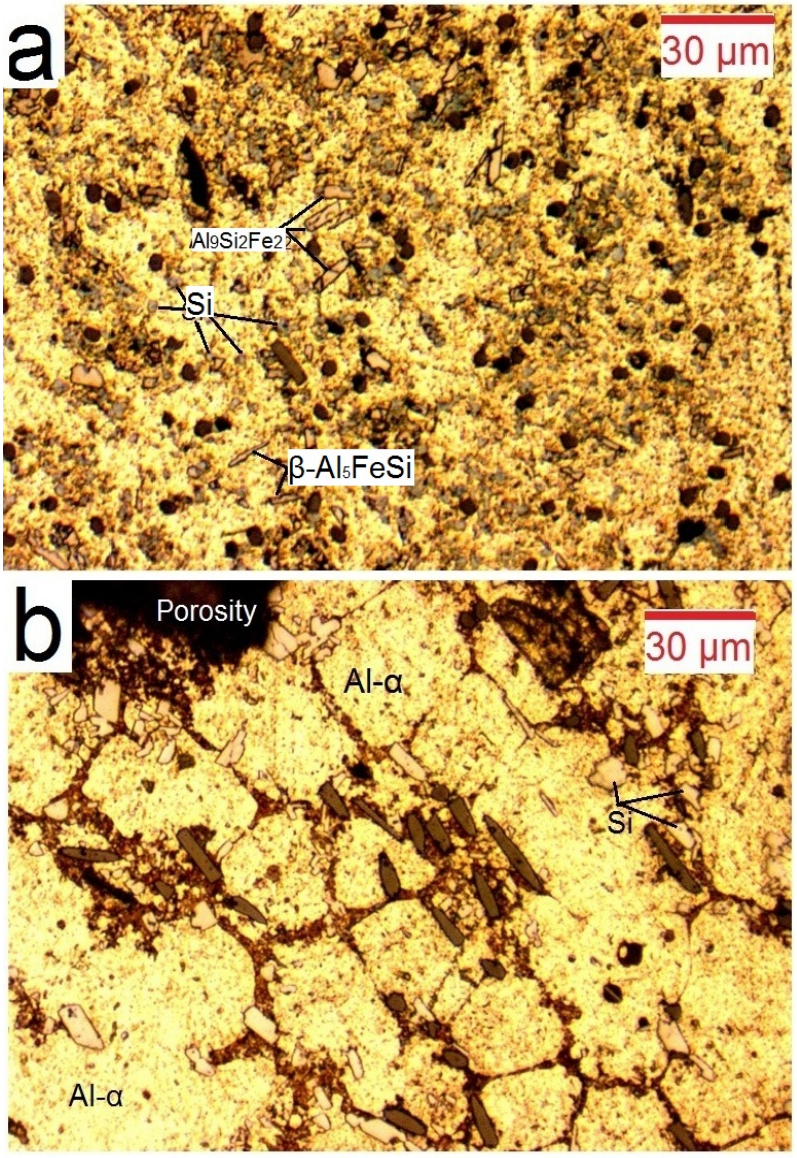

FIGURE 4.9: Optical microscopy images showing the etching with diluted HF acid: (a) A356/C_{sf} as-extruded sample before T6 heat treatment with intermetallic compounds and (b) A356/C_{sf} composite after T6 shows bigger globular alpha size

was identified easily in the eutectic region and appeared as small size and gray color under optical microscopy in the composite sample before heat treatment (Figure 4.9). The microstructure has been totally changed after T6 heat treatment and the micro-porosity was changed and converted to macro-porosity as shown in Figure 4.10.

The globular α-phase was grown and its size increased; this encompassed the carbon fibers and formed the homogeneous structure, so the C_{sf} were no longer located solely in the eutectic region, even in the spherical α-phase. It can be mentioned, the fibers were relocated in a uniform matrix especially in α-phase in contrast with microstructure

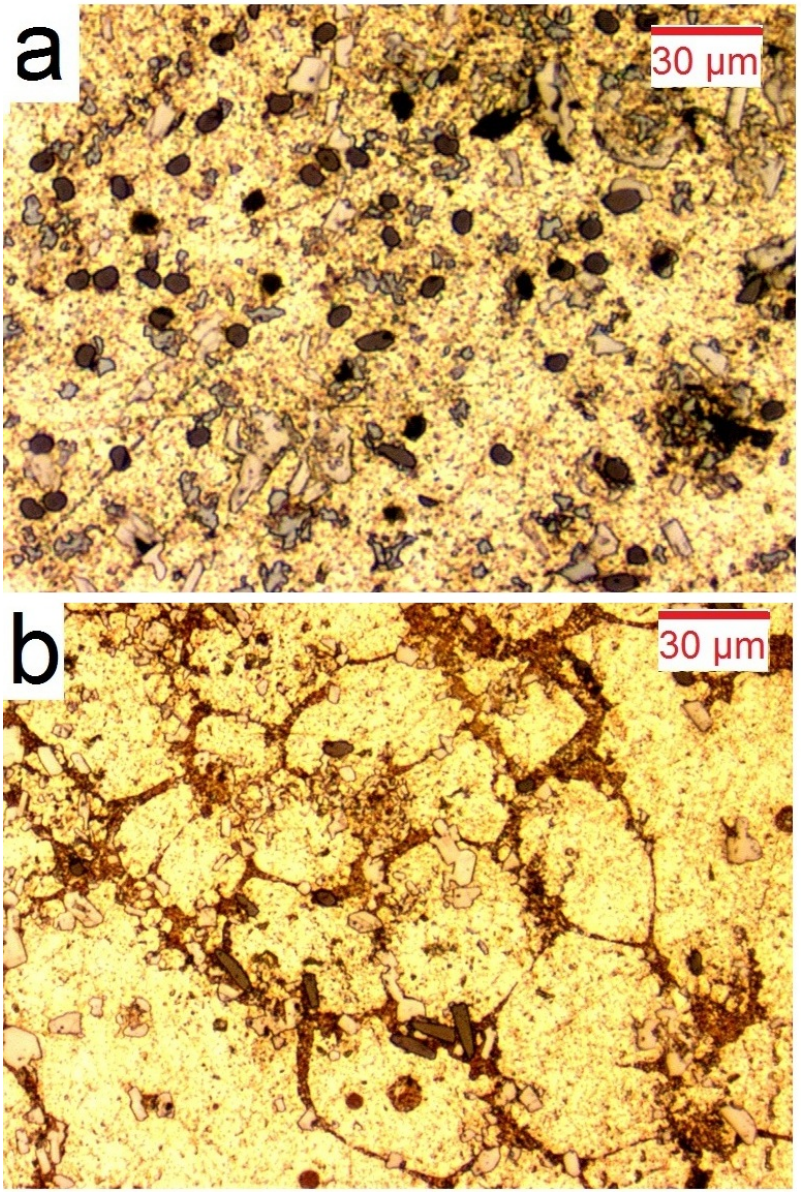

FIGURE 4.10: Optical microscopy images showing the etching with diluted HF acid: (a) A357/C_{sf} as-extruded sample before T6 heat treatment and (b) A357/C_{sf} composite after T6 shows globular alpha size

of as-mixed composite due to growing of primary α-phase which illustrated in Figure 4.10.

The silicon particle size was increased and became very regular in shape but the size of iron intermetallic compounds decreased during solutionizing. The silicon growth and re-shaping to a regular shape was illustrated after heat treatment (Figure 4.11).The T6 heat treatment changes the acicular silicon to more separated and rounded silicon. The size of pores increased while the micro-pores fused; a further weakening of mechanical

properties. Generally the wettability of carbon fiber with molten aluminum is poor but high local concentration of silicon in eutectic facilitated an early nucleation and precipitation over the carbon fibers [Li and Chao, 2004]. The T6 heat treatment changed the morphology when the matrix hardening took place and led to higher hardness and strength and reduced the ductility.

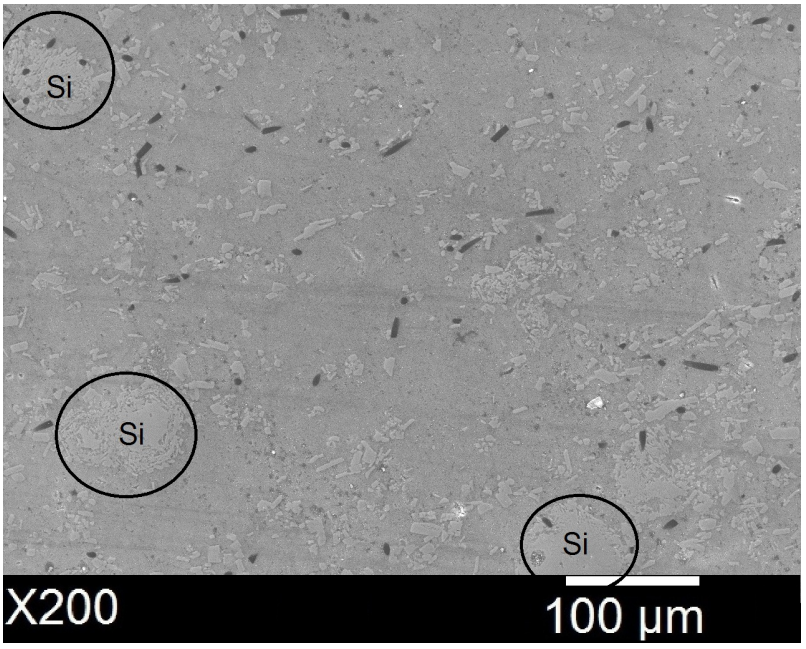

FIGURE 4.11: SEM images of A357/C_{sf} composite extruded T6 heat treated sample shows the growing of Si particles

Figure 4.12 shows SEM micrographs of a heat treated composite and some details of identified intermetallic phases at higher resolutions. Both images inset in Figure 4.12 were captured when focusing on single fiber at high resolution for samples heat treated and un-treated, respectively. The interfacial adherence seems promising in the case of heat treated composite with well distributed intermetallic compounds particularly around or in contact with the fiber (Figure 4.12b).

Heat treatment expanded primary α-phase and provides a uniform structure which the carbon fibers, silicon particles and intermetallic compounds were surrounded by expanded α-phase as matrix. The heat treatment was indicated as good effective method to improve the adherence in this case. As suggested by other authors, in aluminum alloys with Mg content (0.5–2%) improve the wettability of aluminum on carbon fiber [Hashim et al., 2002, Matsunaga, Matsuda, Hatayama, Shinozaki and Yoshida, 2007]. A portion of magnesium content in the alloy may crystallize as Al–Fe–Si–Mg compounds in the form of Chinese scripts. Therefore, the localized high content of silicon and magnesium in the molten eutectic which was being sheared at semi-solid provides relatively strong adherence.

The advantages of thixomixing compare to other conventional liquid compo-casting are high shearing load for dispersion and distribution of fibers and relatively good adherence, even though the weaker adherence can be indicated in Figure 4.12a at the fiber/-matrix interface even with silicon deposition around the fiber. This miss-bonding might be occurred in some cases for extruded composites under intensive extrusion loads.

As it shown in Figure 4.12, both silicon and iron intermetallics have not attached to carbon fiber perfectly and a tiny gap can be observed that leads to a weak interfacial bonding. It was understood that, thixomixing altered the dendritic form to a globular shape of primary alpha under high shearing stress and also could provide extra heterogeneous nucleation sites caused by rotation of the mixer. The eutectic contains acicular and tiny particles of Si and irregular shape of iron intermetallic.

It has been assumed that, the heat treatment can be done to growing of globular alpha size which encompassed C_{sf} with good interfacial bonding and improve the mechanical properties. But it had some deleterious impact on mechanical properties as consequence

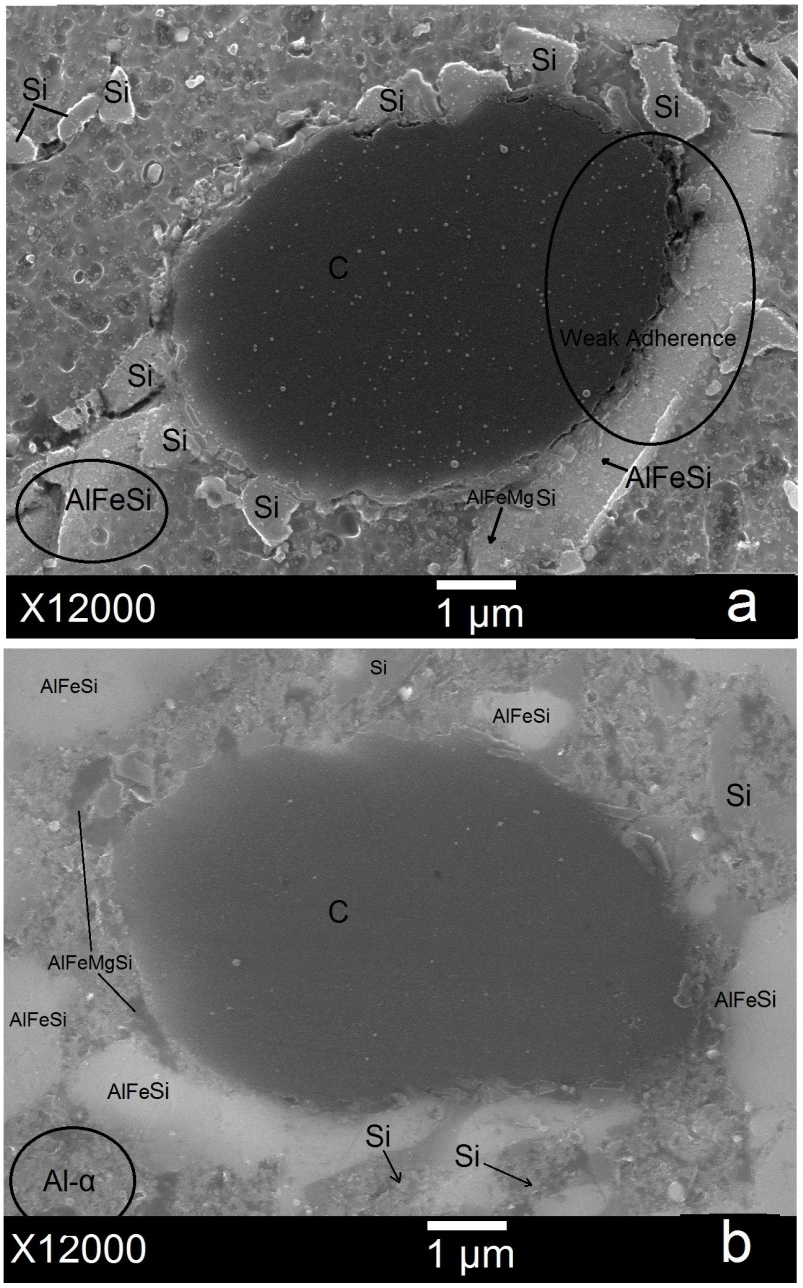

FIGURE 4.12: SEM images of A357/C_{sf} composite showing the T6 heat treatment effect on extruded aluminum/C_{sf} composite (a) before T6 heat treatment X12000 and (b) after T6 heat treatment X12000

increasing of pores size (macro-porosity) on aluminum composite reinforced with C_{sf} by thixomixing. However, it can be suggested that the amount of micro-porosity contents was reduced by T6 heat treatment on thixomixed composite samples. The small pores joined to each other and form larger pores which were reduced the mechanical properties in all samples.

Figure 4.13 and 4.14 shows the EDAX mapping of A357/C_{sf} composite fabricated by thixomixing before and after heat treatment. Thermal conductivity of C_{sf} is lower than aluminum so it leads to heat transferring from the aluminum to carbon fibers. It could be say, the temperature of molten becomes lower and it causes to the solidification of silicon or intermetallic compounds onto the fibers. The surface of C_{sf} could be heterogeneous nucleation sites for Si, when it nucleates in the eutectic compared to Al. The chemical compositions of the intermetallic were detected using EDAX.

The presence of silicon and in some cases iron have been illustrated in the images and reinforced the hypothesis which described above. Silicon was solidified on the outer surface of C_{sf} in the eutectic area and the wettability of the molten aluminum on carbon was improved remarkably, which is proposed in this study. The magnesium was distributed as shown in EDAX mapping analysis homogenously in the composite. This predominate disposition provides better adherence than fully liquid infiltration and prohibits deleterious formation of aluminum carbide. Poor wettability and weak adherence in other conventional methods such vacuum pressure infiltration, liquid casting or squeeze casting can be improved by thixomixing at semi-solid state with relatively good adherence respect to the other methods.

The morphology of needle-like β-Al_5FeSi before T6 was changed, and reduced the deleterious effect of Fe on mechanical properties [Mohamed and Samuel, 2012]. However, the brittle intermetallic causes a reduction of tensile properties of Al/C composite because of the crack which might be propagate into an intermetallic and then propagates into matrix or adhering compounds on fibers and causes a premature fracture. Consequently, the formation and quantity of intermetallic formation must be controlled during fabrication of high strength Al/C_f composite.

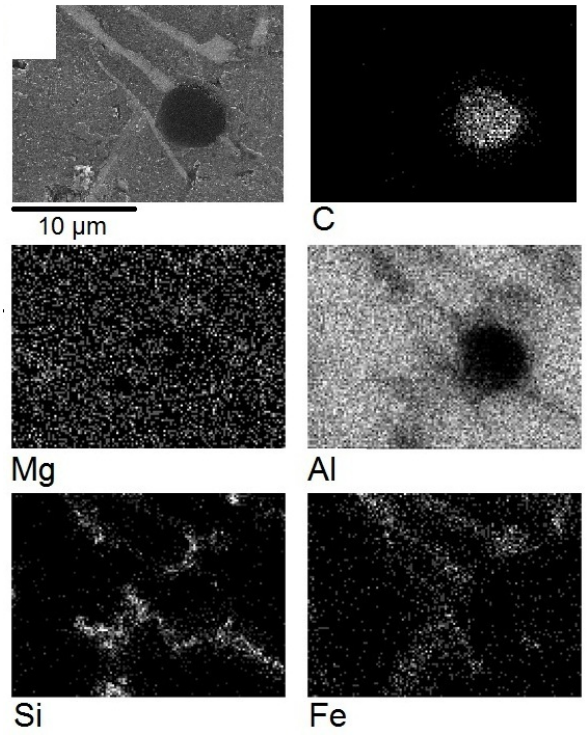

FIGURE 4.13: EDAX mapping of single carbon fiber in A357 before T6 heat treatment

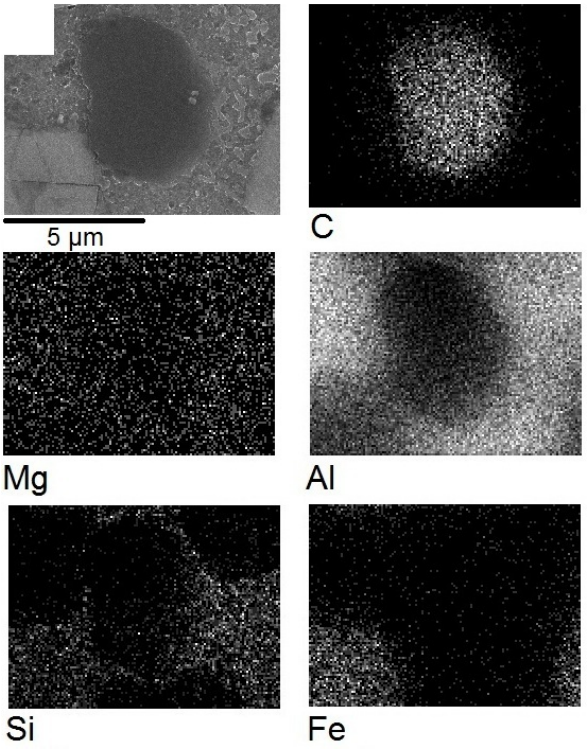

FIGURE 4.14: EDAX mapping of single carbon fiber in A357 with T6 heat treatment

4.1.9 X-ray Diffraction on Composite and Heat Treated Samples

The XRD pattern of fabricated composite of A356 and A357 reinforced with C_{sf} by thixomixing was shown in Figure 4.15. It was revealed that, the iron intermetallic ($Al_9Fe_2Si_2$) is present. The presence of Al_4C_3 and $\beta - Al_5FeSi$ compounds cannot be detected by X-ray due to very few amounts of concentration and the similarity and lower intensity of peaks related to them. The iron intermetallic might be a result of the reaction of aluminum with thus steel body of the die, and with the iron content in the initial alloy.

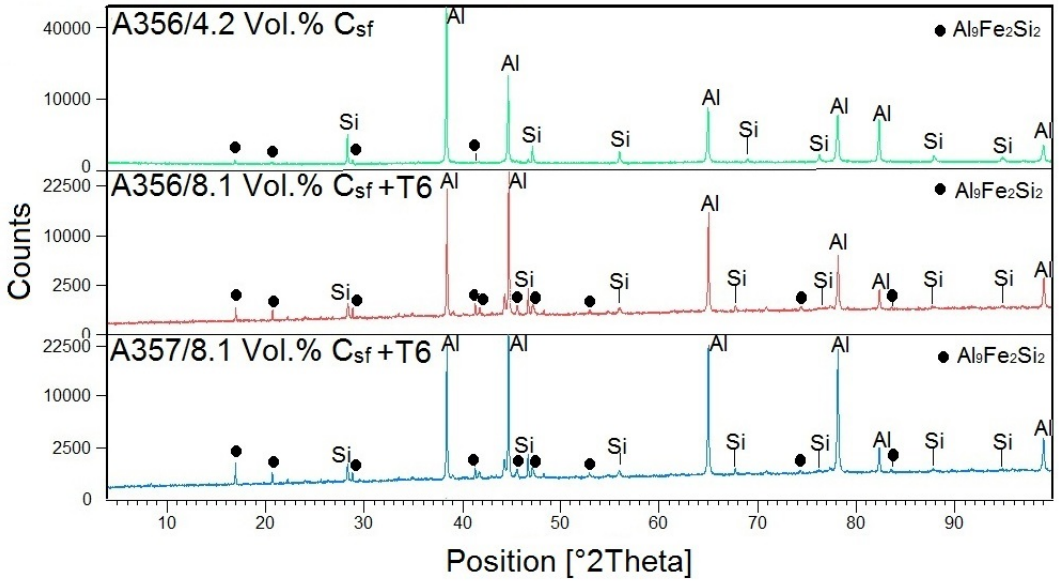

FIGURE 4.15: XRD pattern of aluminum silicon alloy/C_{sf} composite with and without heat treatment

It is possible to control the intermetallic formation by coating or selecting with sustainable and suitable material for the die in further experiments. The ternary Al–Fe–Si phases, such as monoclinic $\beta - Al_5FeSi$, are very common intermetallic compound in Al–Si based alloys. The Manganese in the alloy consumes iron and stabilizes by form an equilibrium quaternary phase (AlSiMnFe) which can be helpful to improve the ductility [Tzamtzis et al., 2009].

4.2 Mechanical Properties of Thixomixed Aluminum/C_{sf} Composite

4.2.1 Tensile Properties of Composite Samples before and after Heat Treatment

The tensile flow curves of A356 and A357 aluminum/C_{sf} reinforced metal matrix composites fabricated by thixomixing at 48% solid fraction which were remelted and extruded, especially before and after T6 heat treatment as shown in Figure 4.16. The values of tensile properties such as yield stress, UTS and elastic modulus of the composite and matrix alloy samples along the direction of extrusion were tabulated in Table 4.2.

Both matrix alloys were processed by the thixomixing without C_{sf} at the same parameters as the reference for comparison. At high speed of mixing (300 rpm), the strength of samples was decreased due to increasing of volume of porosity or more agglomeration of fibers which segregated at high rotating speed.

The tensile properties have differences between theoretical and practical values due to the high volume of pores which were entrapped in the composite and reduce the tensile strength especially when heat treated. The values of tensile tests were improved by increasing the volume fraction of fibers in the composite through the same fabrication process. It can be seen that the significant improvement in tensile strength was achieved and UTS marginally increased when the samples were T6 heat treated.

The differences in the thermal expansion coefficient between aluminum and carbon fiber can produce residual stresses during post-fabrication treatment. The quenching process to the heat treatment can build-up residual stresses and high dislocation density strengthening by accumulation of dislocation next to the reinforcement particles or at the interface. Dislocation density was increased by the cooling rate and related to the size and the volume fraction of reinforcement particles [Arsenault et al., 1991].

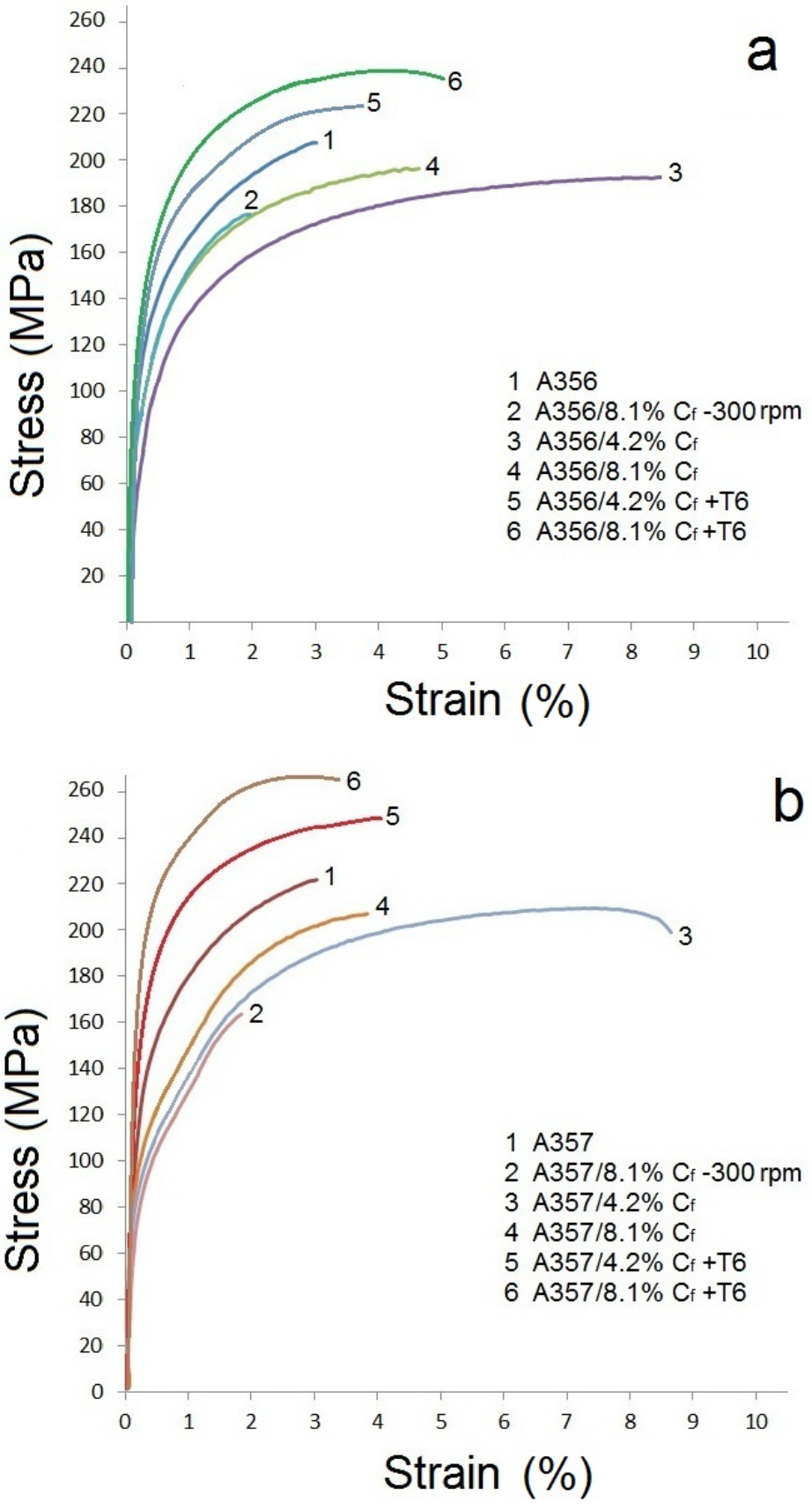

FIGURE 4.16: The tensile flow curves of aluminum silicon/C_{sf} metal composite with the matrix (a) A356 and (b) A357

TABLE 4.2: Tensile properties of composites and aluminum alloys

Alloy	Yield stress MPa	UTS MPa	Elastic modulus GPa	Strain %
A356	178	223	71	3.1
A356/8.1% C_{sf}-300	164	176	69	1.9
A356/4.2% C_{sf}	147	183	66	8.3
A356/8.1% C_{sf}	158	191	69	4.5
A356/4.2% C_{sf} +T6	176	220	81	3.8
A356/8.1% C_{sf} +T6	188	238	83	4.9
A357	182	219	72	3.0
A357/8.1% C_{sf}-300	124	160	65	1.9
A357/4.2% C_{sf}	158	208	66	8.5
A357/8.1% C_{sf}	167	222	72	3.8
A357/4.2% C_{sf} +T6	198	240	85	4.1
A357/8.1% C_{sf} +T6	224	261	86	3.2

The strengthening mechanism in reinforced composite materials pertained to the load transferring from matrix to fiber which provided a load bearing effect. The subsequent load transferring from the matrix to the carbon fiber pertained to the interfacial mechanical quality or adherence which improved by silicon deposition onto the fiber in thixomixing. The results of mechanical properties obtained in this study showed further increase in C_{sf} content. The values corresponded to ultimate tensile strength was improved slightly better for T6 heat treated reinforced composite samples than other samples made of A356 alloy (without T6).

The UTS for A357/8.1% C_{sf} was increased more than matrix alloy (A357) but it was higher than UTS for A357/4.2% C_{sf}. The UTS of A356 and A357 obtained by conventional die casting, are more than 255 MPa and 310 MPa, respectively [Aluminum, 2008] whereas the UTS of A356 and A357 processed by thixomixing method were achieved 223 MPa and 219 MPa, respectively and this can be related to presence of pores and porosity which was made in this method. The mechanical properties tabulated in Table 4.2 also indicated the better values such as yield strength or UTS of A357 than A356.

The T6 heat treated A357/C_{sf} at both volume fraction shows better mechanical properties than un-treated A357/C_{sf} composite may attributed to improvement of strength caused by heat treatment but their ductility was reduced. Heat treatment seems promote the interfacial bonding and strengthening of matrix alloy generally by aging hardening

but not as much as expected because it increases the pores size formed through the heat treatment can reduce the mechanical strength and decline the effect of T6 heat treatment on final values of mechanical properties.

The Mg improve the mechanical properties through the T6 heat treatment and also promote the adherence by formation the suitable intermetallic compound over fiber surface in composite even though the air pores' size increased by T6. It was shown the better mechanical properties of T6 heat treated A357/C_{sf} than A356/C_{sf}. For instance, the values of UTS belong to T6 heat treated sample of A357/8.1% C_{sf} are much higher than A356/8.1% C_{sf} and may due to higher amount of Mg in A357 alloy and it can provide the better adherence.

The values of strain for both heat treated and un-treated of A356/C_{sf} and A357/C_{sf} were improved markedly than matrix alloys. The maximum amounts of ductility were achieved from A356/4.2% C_{sf} and A357/4.2% C_{sf} due to good interfacial bonding and adherence between matrix and fibers.

The decrease in strength for both composites without heat treatment pertain to the matrix alloys might be related to the agglomeration of fibers and porosity content. It can be detected that, the mechanical strength of aluminum alloys/C_{sf} fabricated by the thixomixing were controlled by three main parameters as, quality of interfacial adherence, porosity content and agglomeration. This is especially so when the samples were heat treated but this resulted in large difference between the measured and theoretical values. The strength values and elongation decreased for both A356 and A357 composite samples which fabricated at 300 rpm of rotational speed compare with other samples at lower speed of mixing.

In the present study, the heat treated samples have shown higher tensile properties compared with those of composites which were not done. The T6 heat treatment increases the globular α-size of matrix and increases elongation of composite. The strength, elongation and toughness might be improved by grain refinement in the metallic matrix. The A357/C_{sf} composite exhibited better tensile properties than A356/C_{sf} in most of the samples, especially when T6 heat treated, when A357 contains higher content of

magnesium and so improves the wettability and provides stronger adherence by formation of desirable intermetallic compounds due to the quality of the interfacial region.

Some previous attempts have been conducted to improve the interfacial adherence by additional coating such as Cu, Ni or alumina onto the carbon fiber surface in aluminum matrix composites, whereas the properties of coated Al/C_{sf} composites were lower than the un-coated composite, although the extra coatings may possess lower mechanical properties [Tang et al., 2008, 2009, Urena et al., 2009, Zhang et al., 2009]. In the stress-stain flow curve shown in Figure 4.16 both alloy composites demonstrated high fracture toughness with increasing volume fraction of C_{sf}, particularly when increased from 0 to 4.2 vol.%, which caused the composite to be ductile.

The heat treatment declined the fracture toughness relative to the samples without heat treatment. In fact, shear banding debonding, fiber pull-out or fiber breakage consumed the fracture energy during matrix deformation, on the other hand C_{sf} functioned as a barrier which increased the fracture energy [Jiang and Gao, 2001, Lee et al., 2000].

4.2.2 Fracture Behavior of the Thixomixed Composite Sample

The morphology of the fractured surface of fabricated composites which were conducted under standard tensile test show in Figure 4.17. The quasi-plastic deformation is indicated in the matrix of both samples in Figure 4.17a and 4.18 with dimple and no flat fracture. The fracture mechanism predominates for all of the samples in this study revealed as non-flat or ductile fractures with few fiber pull-outs.

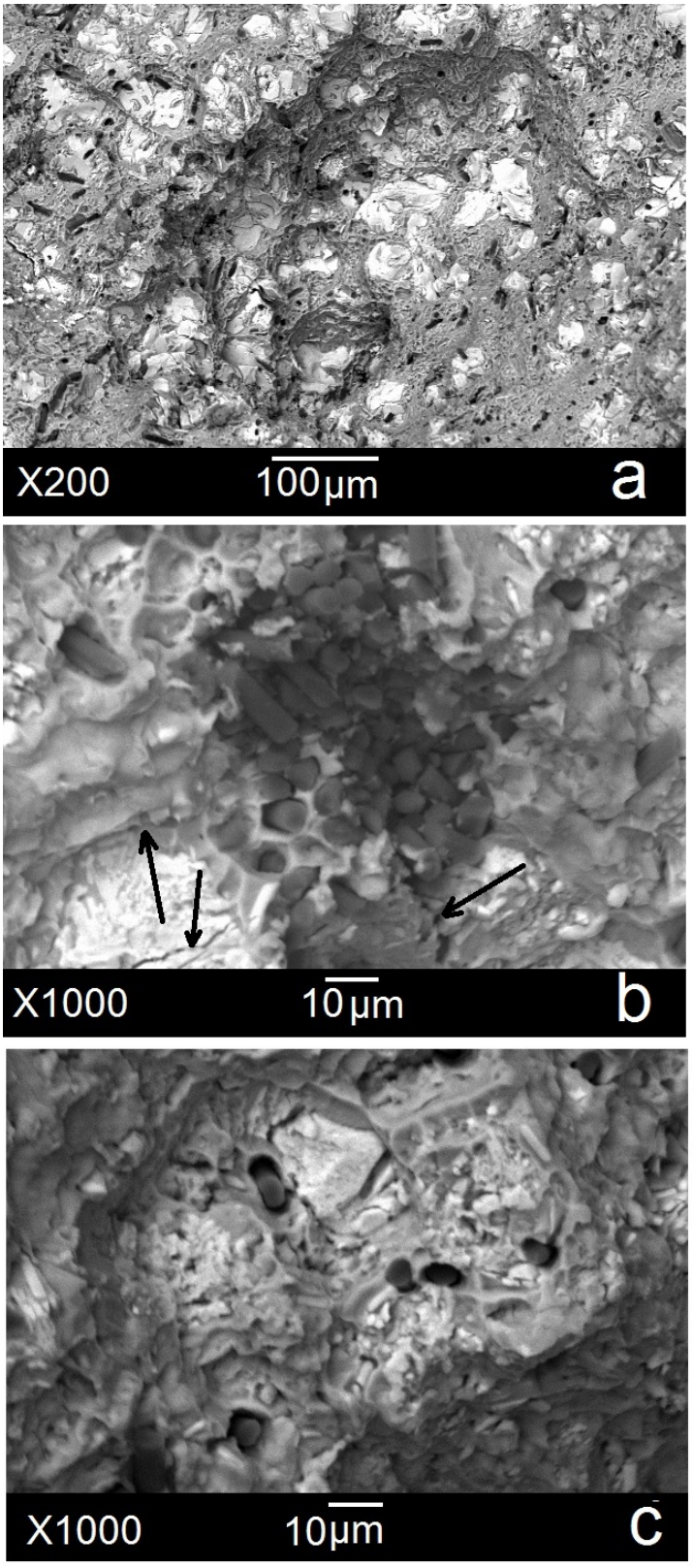

FIGURE 4.17: Fracture morphologies of the different aluminum silicon alloy/C_{sf} composites: (a) A356/8.1 vol.% C_{sf}; (b) A356/4.2 vol.% C_{sf} fabricated under speed of mixing 300 rpm and agglomerated fibers and (c) A356/4.2 vol.% C_{sf}

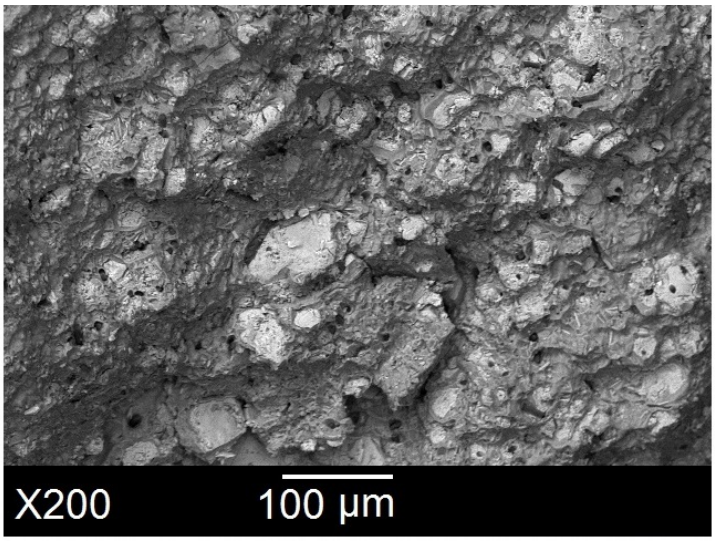

FIGURE 4.18: Fracture morphologies of the aluminum silicon alloy/C_{sf} composites A357/8.1 vol.% C_{sf}

Conversely, a brittle structure might be produced, if the carbon fibers were not dispersed or distributed effectively. The agglomeration can be seen, in Figure 4.17b due to the higher speed of mixing, cracks (indicated by pointer in the figure) initiated locally from the agglomeration of fibers and grow through the matrix and phases until the composite is broken. This phenomenon will happen also for porosities and may be the presence of brittle phases such as Al_4C_3 which function as crack initiation sites. The good adherence of aluminum with carbon fibers caused plastic deformation. Thus, a few C_{sf} de-boned and pulled-out were illustrated (Figure 4.17c) due to better adherence and wettability by silicon. Some plastic deformation occurred around the fibers.

Figure 4.19 and 4.20 illustrates the fracture morphology of thixomixed composites, heat treated and un-treated at different magnifications. Neither alloy before heat treatment showed macro-pores. The big holes in the composite samples were formed during heat treatment; this is due to the amount of trapped gas in the matrix. The micro-pores and air bubbles likely formed due to the volume fraction of carbon fiber and the high rotation speed of the slurry [Ozdin, 2012]. The hot extrusion process was carried in current study have a little impact on the porosity contents. Short carbon fiber might be cracked undesirably under intensive shearing load in the thixomixing process. The optimum length for short carbon fiber must be kept throughout the whole process of manufacturing [Naji et al., 2008].

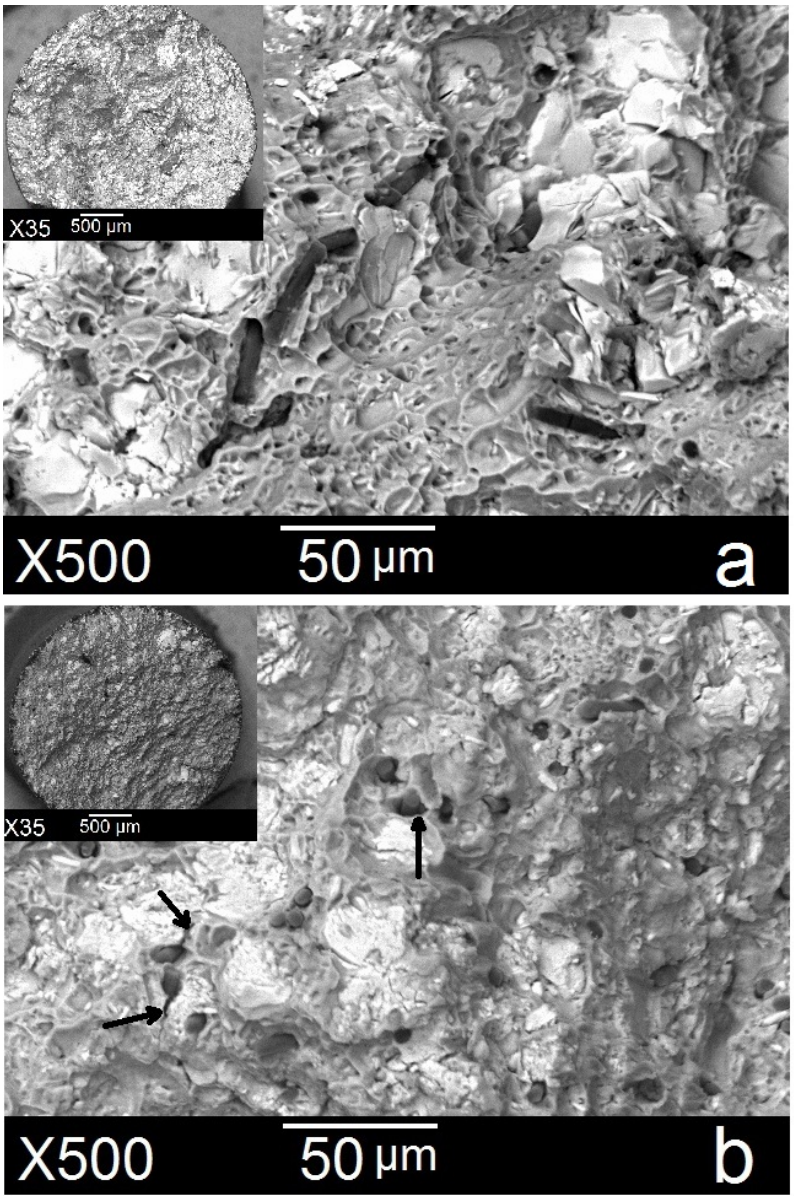

FIGURE 4.19: Fracture morphologies of the different aluminum silicon alloy/C_{sf} composite samples: (a) A356/4.2 vol.% C_{sf}; (b) A357/4.2 vol.% C_{sf}

Figure 4.19a reveals the fracture surface with some fiber pull-out whilst some amount of fibers did not orient along the extrusion direction and cracked. The probability of composite failure is a function of filament length when loaded under specific stress [Rossoll et al., 2012]. As demonstrated by the illustration in Figure 4.19b, the micro-cracks were initiated from the interface of matrix/reinforcement and the matrix deforms near the fibers and fibers are pulled-out relatively. Therefore it demonstrates when the load transmits from matrix to C_{sf} by interfacial bonding [Tang et al., 2009].

Silicon and intermetallic compounds' precipitation on the fiber leads to concentration

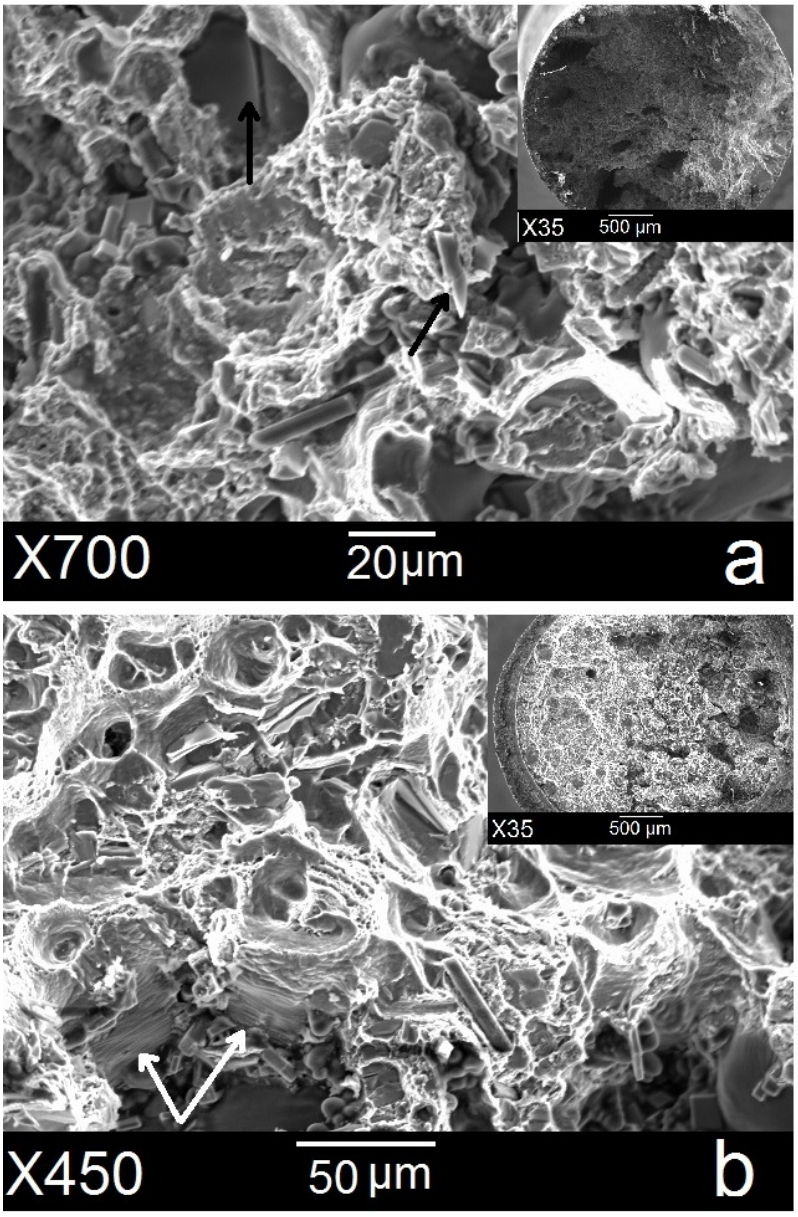

FIGURE 4.20: Fracture morphologies of the different aluminum silicon alloy/C_{sf} composite samples: (a) T6 heat treated A356/4.2 vol.% C_{sf}; and (b) T6 heat treated A357/4.2 vol.% C_{sf}

of the stress, and micro-cracks form predominately near to fibers. These compounds strengthen the bonding, favoring plastic deformation. Many dimples and tearing ribs appeared for T6 heat treated A356/C_{sf} and A357/C_{sf} composite, as Figure 4.20a and b show, with some short pull-out fibers. Big holes can be detected easily in both alloy composites after heat treatment which reduced the mechanical properties and tensile strength. The good interfacial bonding could be a barrier to passing the crack across the fiber, so some pullout occurred in the fractured surface. The micro-cracks and cracked

fibers can be seen in Figure 4.19a due to high applied load during fabrication process and this might be repeated across all tested samples. The mixed ductile fragile fracture occurred in T6 heat treated A357/4.2 vol.% C_{sf} caused the dimples around fibers and tearing ribs, marked by pointers in the Figure 4.20b.

4.2.3 Ultra Micro-Hardness Analysis to Investigate the Interfacial Adherence

Ultra micro-hardness was utilized across the line passing through the carbon fiber in different points (with an equal distance between them) in order to study the interface of matrix/fiber and to measure the hardness of matrix close to short carbon fiber. The hardness represents the materials resistance against deformation, particularly at the interface. The values for the above characterization were illustrated in Figure 4.21 for the composite samples with and without heat treatment.

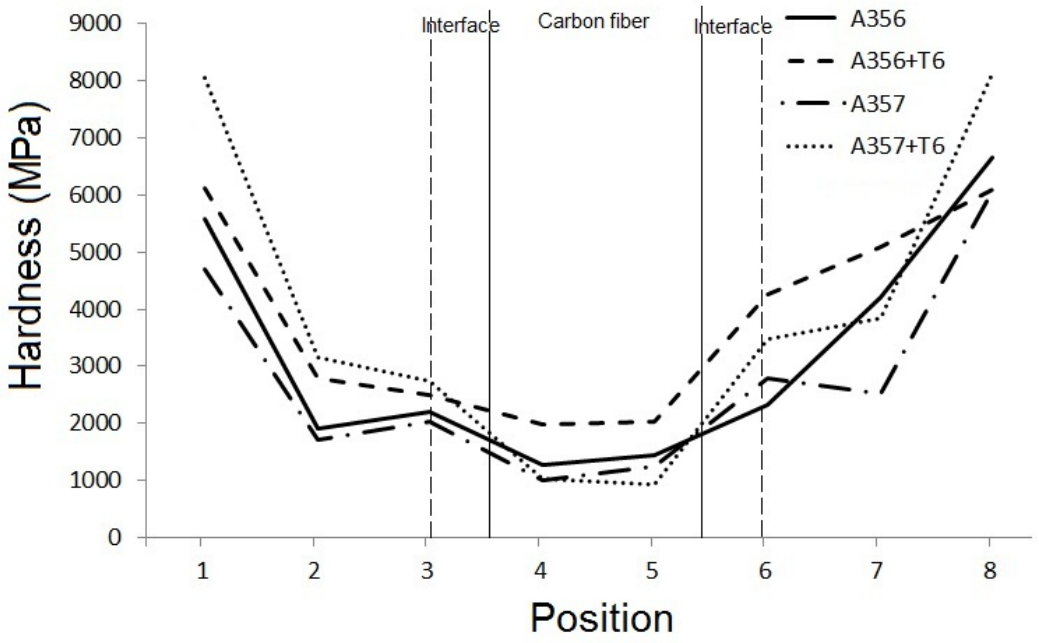

FIGURE 4.21: Hardness profiles obtained across the fiber/matrix interface in A356/4.2 vol.%C_{sf} and A357/4.2 vol.% C_{sf} with and without heat treatment samples

It is clearly shown that the heat treated samples are stronger against deformation and the interfacial bonding adherence increased marginally. In the case of A357, when the C_{sf} embedded in matrix, such as intermetallic compounds and Si can improved the

hardness, so the silicon and the intermetallic compounds precipitation improved the hardness of interface. The measured values of hardness at the distances far from C_{sf} increased markedly. Composite samples which are not treated have a small impact on the hardness at the matrix/fiber interface; values in the range of 1800-2100 MPa as indicated in Figure 4.21.

This hardening effect at zones close to the fibers could be related to the favored deposition of alloying elements in the matrix during thixomixing or improvement of interfacial adherence associated with the thermal evolution of compounds after heat treatment. The interfacial bonding seems was improved by thixomixing due to the solidification mechanism caused by segregation of alloying elements between primary α-phase and eutectic. This predominate deposition was modified for further heat treatment as shown in hardness values of ultra micro-hardness.

4.3 Wear and Tribological Characterization on Hypereutectic Aluminum/C_{sf} Composite by Thixomixing

The wear and friction properties are interesting for characterization of metal composite which made of soft matrix especially when reinforced with good self-lubricant material such as carbon fiber. The significance of tribological properties of aluminum/carbon fiber composite materials can be remarkable when the rubbing parts are made on them. There is no previously published information available, regarding the influence of wear parameters and their interactions on the tribological behavior of metal matrix composites reinforced with C_{sf}. There are few reports available on the investigations of C_{sf} in the aluminum composite whereas the interfacial improvement and the process were focused mostly. In this part of study, the high silicon content aluminum alloy (hypereutectic, 4047) was chosen to study the wear and tribological properties of the composite reinforced with C_{sf}. The hypereutectic aluminum alloys are the suitable choices for the applications which is impressed by wearing.

A Taguchi model was applied on the effective parameters in wearing and C_{sf} in the composite to specify the main effect and the possible interaction effect on tribological parameters. The C_{sf} were located at wearing area on the surface ground and squeezed, then mixed to form a tribo-film on the worn surface, which improved the wear greatly. The low friction coefficient of C_{sf}/Al composite caused little change in the temperature and further ensured the stable state of sliding [Liu et al., 2009].

4.3.1 Influence of Testing Parameters on the Main Effect Plots

Physical properties such as density and hardness values of successful sample after thixomixing were illustrated in Table 4.3. Differences between theoretical and experimental density refer back to the porosity which exists in the samples. Taguchi method is used in experimental design and provides a simple, powerful tool to determine optimal and effective parameters. In this study, a loss of function was used to determine

the quality of a characteristic that was converted into a signal-to-noise ratio (S/N) to reduce the number of interactions. Table 4.4 shows each test parameters and arrangement

TABLE 4.3: Physical and Hardness properties of the samples

Sample	Theoretical Density $g.cm^{-3}$	Experimental Density $g.cm^{-3}$	Hardness HB	Micro-hardness HV0.1
4047	2.60	2.59	70±2.1	51±2.4
4047+4.2% C_{sf}	2.57±0.3	2.55±0.1	74±2.3	56±2.4
4047+8.1% C_{sf}	2.53±0.2	2.51±0.3	85±1.8	59±2.2

based on Taguchi method for design of experiment. Three different quality characteristics can be calculated based on S/N ratios, namely "Nominal is the best", "Larger is better" and "Smaller is better". Our objective is to minimize the values for specific wear rate and coefficient of friction to the possible minimum limit so; the S/N ratios for three factors at three levels are calculated by equation 4.3 for quality characteristic selected as smaller-is-better:

$$\frac{S}{N} = -10\log\frac{1}{n}(\sum y^2) \tag{4.3}$$

where, n is number of observations and y is the response value.

TABLE 4.4: Experimental design parameters and results using an L9 (3^3) orthogonal array

Run	Volume Fraction %	Speed of Sliding $cm.s^{-1}$	Load N	Specific Wear Rate $m^3.(N.m)^{-1}$	Coefficient of Friction	S/N Ratio for Wear Rate db	S/N Ratio for Coefficient of Friction db
W1	0	5	5	5.4/ 5.2	0.39/ 0.38	65.30	8.48
W2	0	10	10	5.5/ 5.5	0.44/ 0.44	65.18	8.51
W3	0	20	20	5.8/ 5.8	0.47/ 0.41	64.71	8.74
W4	4	5	10	4.9/ 4.7	0.37/ 0.37	66.14	9.06
W5	4	10	20	5.1/ 5.2	0.36/ 0.33	65.61	9.17
W6	4	20	5	5.0/ 4.9	0.33/ 0.37	66.04	9.18
W7	8	5	20	3.3/ 3.2	0.32/ 0.34	69.84	9.25
W8	8	10	5	3.3/ 3.1	0.34/ 0.33	70.08	9.16
W9	8	20	10	3.7/ 3.2	0.37/ 0.33	69.88	8.95

The main effect plots on both specific wear rate and coefficient of friction were plotted for the mean values of S/N ratio, is shown in Figure 4.22. The impact of the three factors

at three levels can be studied by using an L9 orthogonal array and reducing the number of interactions evolved to nine.

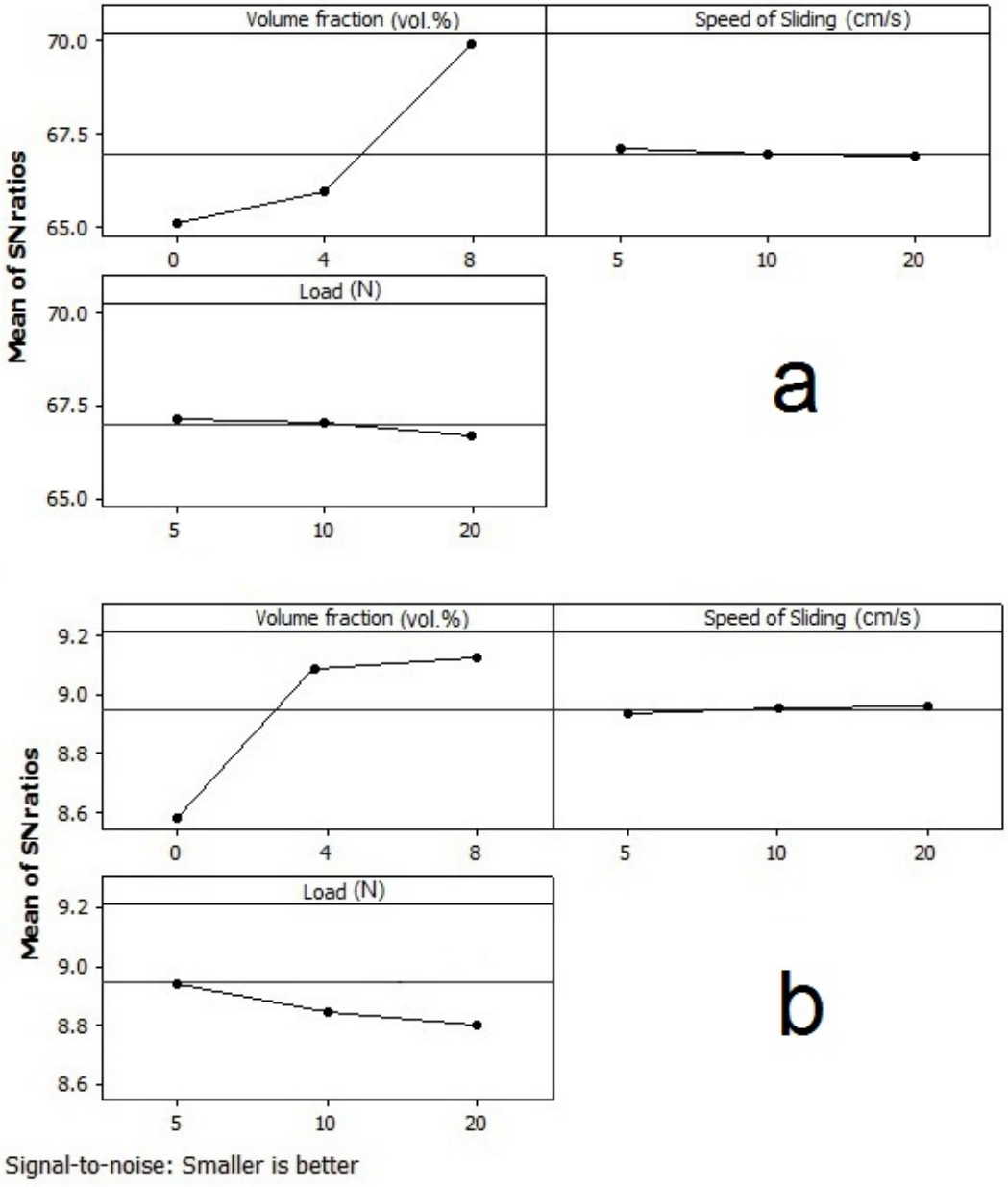

FIGURE 4.22: The main effect plots for (a) specific wear rate and (b) coefficient of friction

The significant of the factors can be assessed by viewing the main effect plot. A steep line segment in this plot indicates a strong effect of factor on the response and if the line segment is flat the factor is insignificant [Hunter, 1996]. In general, the best value

for each study parameter is the higher S/N values on the main effect graph, which is an easy way to determine optimal testing conditions [Ravindran et al., 2013].

Increasing the volume fraction of carbon fibers in aluminum composites and increase the S/N ratio in the main effect plot result in a lower specific wear rate (Figure 4.22a). But increasing the load and sliding speed does not significantly affect the wear rate in the main effect plot as indicated in Figure 4.22a due to the near-horizontal line for both mentioned parameters in this type of plot. Wear loss for this composite did not increase with increases in the applied load and sliding speed, which pertain to the wear debris retained on the worn surface that covers a greater area of contact.

The increase in load causes more erosion and the formation of wear debris, which in turn leads to the enhancement of forces that impact the wear debris to form a resistant layer. The detached material during the wear process cannot be eliminated but can be reduced at appropriate chemical composition and/or a harder microstructure. The increasing of volume fraction of carbon fiber leads to decrease of wear loss by covering more area of contact, but the applied load and speed, which indicated twofold action, first remove more materials from the surface in consequence decreases wear rate by forming debris as a layer on the surface [Ramesh and Prasad, 2008].

The wear mechanism is classified as abrasive wear, erosive wear, adhesive wear, fatigue wear [Davis, 2001]. The adhesive wear mechanism was proposed in this study for Al/C_{sf} composite due to some interaction through the process. The main plot of coefficient of friction was exhibited in Figure 4.22b and the influence of testing parameters demonstrated. The S/N ratio corresponding to the coefficient of friction increased with increasing of volume fraction. The developed composites revealed lower values of coefficient of friction when compared to the matrix alloy, which indicated the self-lubrication effect of grinding fibers on the surface and formed the graphite-rich layer. When the counterpart slides over the sample with carbon fibers in the composite get sheared and ground continuously, at higher load levels which get squeezed between two counting surfaces.

The very fine particles of carbon were squeezed out and formed an antifriction layer with appropriate properties mainly on the coefficient of friction. The adherent tribo-film reduces the coefficient of friction at different sliding speeds, but the film may be broken at very high sliding speeds which are not interested in his study. The coefficient of friction is detected lower when the load of sliding increased in the most studied materials, for instance Ureña et al. [Urena et al., 2009] have been reported, the lower values of coefficient of friction for carbon fiber-6061 aluminum composite, whereas the fiber was coated with copper and nickel by electrolysis. The high inclination from 0 % to 4 % in Figure 4.22b shows high influence of carbon content in the composite on the coefficient of friction. In addition, increasing of sliding speed and load cannot change the frictional coefficient remarkably in this composite. Consequently, the superior improvement of wear parameters of Al/C_{sf} composite versus the matrix alloy can be attributed to:

- Enhancement of hardness as plastic deformation resistance and toughness caused to increase of wear resistance.
- No pull out of carbon fibers even at high sliding speeds, shown a good adherence between carbon fiber and matrix alloy which plays a key role in composite materials.
- Instead of, the most of individual fibers is fragmented and ground onto the surface during wear process and formed a graphite tribo-film, which has high load carrying capacity and high lubricity [Chen and Alpas, 1996]. The high load capacity of carbon fiber will result in reduced plastic deformation and the size of worn particles while sliding at high loads. The larger worn particles indicated high plastic deformation and high wear rate. The improvement of wear resistance with the presence of good bonding at the interface of matrix and fiber has been reported [Ramesh et al., 2013, Wilson and Alpas, 1997].
- In addition, some authors reported the formation of mechanical mixed layer by comprising of possible metallic or non-metallic oxides with fine carbon particles [Wei et al., 2013].

- This sticky fine mixture formed a layer and reduces the direct contact between a pair of sliding interfaces and decrease results to lower coefficient of friction. The mechanical mixed layer formation increased with the increasing of volume fraction of carbon fiber in developed composite.
- Good thermal conductivity of carbon fibers (500 W.m^{-1}.K^{-1}, longitudinal) [Korab et al., 2002] helps to more heat dissipation, and the softening effects will be retarded despite of high velocity of sliding or loads.

1. S = 0.284089 R-Sq = 99.45 % R-Sq(adj) = 97.82 %
2. S = 0.387826 R-Sq = 95.53 % R-Sq(adj) = 82.12 %

4.3.2 Interaction Plots

Figure 4.23 shows the interaction plots which belongs to the parameters in wear process that effectively impress each other as determining roles. The failure of one factor in the response to the same effect on various levels of another factor is called an interaction. An interaction plot is a graphical tool for displaying the interaction effect between two factors. In interaction plot, if the line segments which are connected the mean values of each level are parallel, indicate no interaction exists between two factors; otherwise an interaction is existent. As a general, when the interaction lines of a parameter are parallel with other parameter lines, indicated no interaction in against point of view when they have different inclinations, can be detected with interaction.

In Figure 4.23a shows that the wear rate was increased with increasing of sliding speed and load while the carbon fiber does not exist in sample, whereas the presence of carbon fiber does not change the wear rate with increasing of speed and load. The wear rate followed the same trend when the volume fraction increased regarding the different levels of sliding speed and load.

Figure 4.23b shows the interaction between parameters on the responses of coefficient of friction. At sliding speed of 10 and 20 cm.s^{-1} of and high values of load, the coefficient of friction has shown different values due to strong interaction effect between

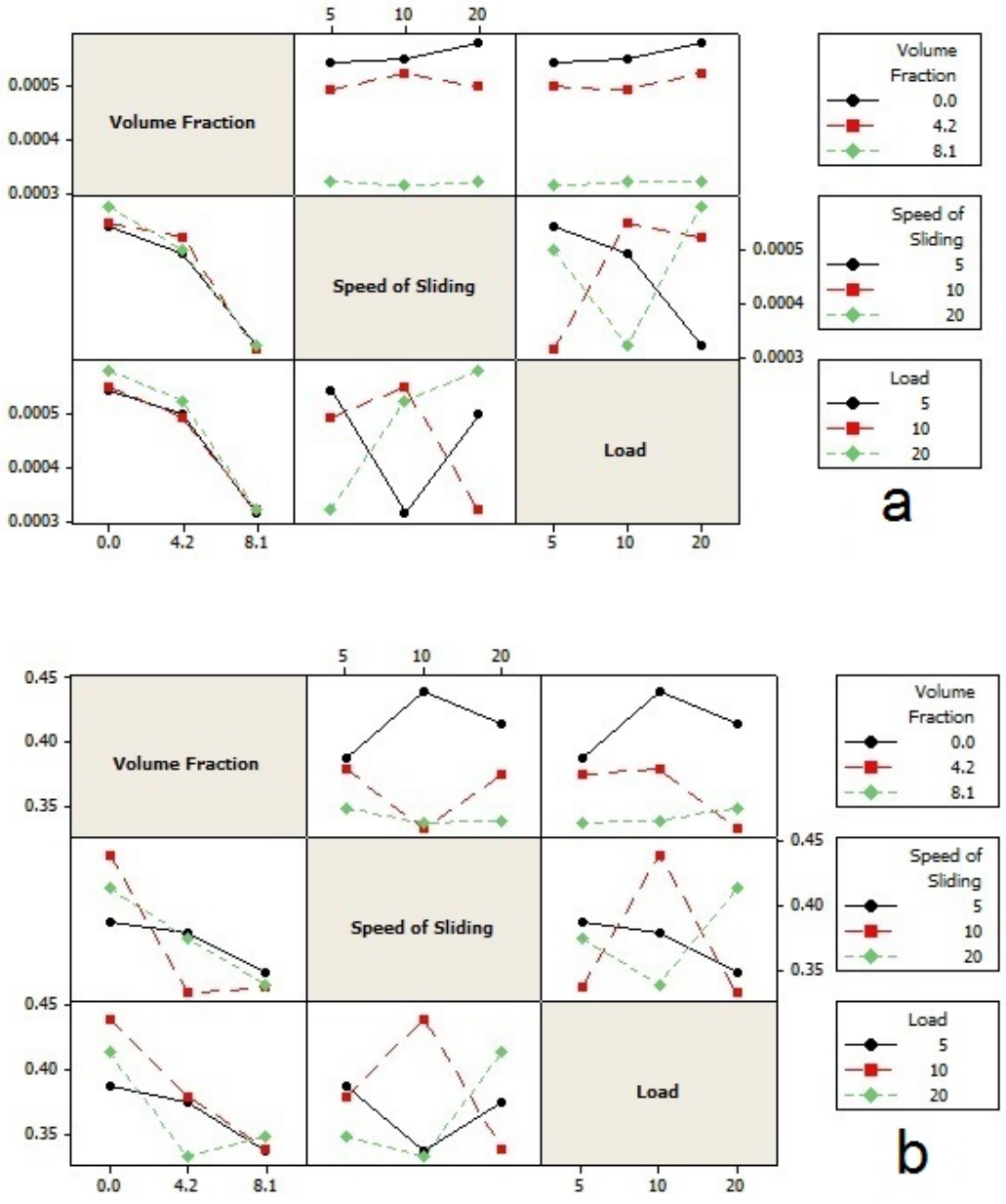

FIGURE 4.23: Interaction plots for (a) specific wear rate and (b) Coefficient of friction

two sliding parameters. The interaction of load and sliding speed on the wear rate and coefficient of friction was determined clearly. The differences in value of responses can be seen clearly in the samples contains carbon fiber and the samples without them. The highest inclination of volume fraction of carbon fiber was appeared as the most significant factor on both wear rate and the coefficient of friction of the composite but has no interactions with the other parameters in wear rate.

However, the friction was influenced by variations of sliding distance and load, because the increasing of applied load leads to stabilization of tribo-film, especially at high load, and it was destroyed at high sliding speed. The trend of interaction plot was conformed to the information achieved from main effect plot. In composite of Al/C_{sf} produced by thixomixing, the presence of carbon content has an individual effect on specific wear rate and also on friction coefficient, which improved the wear resistance of composite when the speed of sliding and load of wear increased.

4.3.3 Analysis of Variance

The values of ANOVA for the prepared thixomixed aluminum/carbon fiber composites were tabulated in Table 4.5, based on the degree of freedom (D), the sum of the square (SS), the percentage of the contribution (P), and F statistics (F) to evaluate the source of variation during the wear process. The analysis of variance (ANOVA) table was desirable to understand and determine the order and the impact of various factors such as volume fraction, load, sliding speed and their interactions.

The p-value use to detect the significance of a factor to compare with alpha value of 0.05, so the factor is significant when the p-value is lower than 0.05. The F-value means that parameters in experiment show a significant effect on optimal characteristic when the F bigger than 4. The statistical calculation was accomplished by determining the total variability of the S/N ratios. The effect of order of parameters on wear rate and coefficient of friction is relatively easy to identify.

The Contributions of each design parameters and the errors calculated by sum of the squared deviations (SS) from total mean values of signal to noise ratio. A very high

TABLE 4.5: Analysis of variance (ANOVA) for S/N ratios

Responses	Source	DF	Seq. SS	Adj. SS	Adj.MS	F	P	Contribution (%)
Wear $Rate^1$	Volume of Fraction	2	28.63	28.63	14.31	177.42	0.006	96.72
	Speed of Sliding	2	0.64	0.64	0.32	3.99	0.20	2.17
	Load	2	0.16	0.16	0.08	1.02	0.49	0.55
	Error	2	0.16	0.16	0.08			0.005
	Total	8	29.60					100
Coefficient of $Friction^2$	Volume of Fraction	2	5.55	5.55	2.77	18.45	0.04	82.46
	Speed of Sliding	2	0.24	0.24	0.12	0.83	0.54	3.69
	Load	2	0.63	0.63	0.31	2.10	0.32	9.36
	Error	2	0.30	0.30	0.15			4.46
	Total	8	6.73					100

1) S = 0.284089 R-Sq = 99.45% R-Sq(adj) = 97.82%
2) S = 0.387826 R-Sq = 95.53% R-Sq(adj) = 82.12%

impact of volume fraction of carbon fiber on the wear rate (96.72 %) and friction coefficient (82.46) and relatively low influence of load (0.55 %) on wear rate were measured (Table 4.5). It might be observed also the influence of sliding speed and load on coefficient of friction for this composite.

The average of each response for each level of the factors has been shown in the response table (Table 4.6) which includes a ranking of important factors. The ranking assigned to the important factors and have been detected by comparison to the relative Delta statistics, which is the difference between averages (=highest average - lowest average) for each factor. The optimum testing conditions were investigated as the volume fraction of carbon at 8.1 %, load of 5 N and sliding velocity 5 cm.s^{-1} for the best wear resistance and the best friction values for the thixomixed Al/C_{sf} composite.

4.3.3.1 Confirmation Test

The final step was to verify the improvement of the quality characteristic using the optimal levels of the design parameters (A3B1C1). The estimated S/N ratio η using the

TABLE 4.6: Response table for S/N ratios

Responses	Level	Volume fraction %	Speed of Sliding $cm.s^{-1}$	Load N
Specific Wear Rate	1	65.07	67.10	67.15
	2	65.94	66.96	67.07
	3	69.94	66.88	66.72
	Delta	4.87	0.22	0.42
	Rank	1	3	2
Coefficient of Friction	1	8.580	8.933	8.944
	2	9.142	8.953	8.846
	3	9.125	8.961	9.057
	Delta	0.562	0.028	0.211
	Rank	1	3	2

optimal level of the wear process can be calculated by equation 4.4 as;

$$\eta = \eta_m + \sum_{i=0}^{q} (\eta_i - \eta_m) \tag{4.4}$$

where η_m is the total mean of the S/N ratio, η_i is the mean S/N ratio at the optimal level and q is the number of the main design parameters that significantly affect the performance characteristic. Statistical analysis can predict the S/N ratio based on the optimal testing parameters which achieved from the last section. The S/N ratio was found for specific wear rate and coefficient of friction to be 70.21 dB and 9.77 dB, respectively. According to the experimental results obtained from the new practical test, the corresponding values for the same responses are 3.12 dB and 0.32 dB (Table 4.7).

This table shows a comparison of values of specific wear rate and coefficient of friction of the predicted and experimented using the optimal parameters. The experimented wear parameters have shown shown an improvement on minimum wear parameters at the initial trial (A3B2C1), which meant that the wear process modified for better application. This powerful method of analyzing can be developed for optimizing the other parameters which influence on the wear process. The key role of carbon fiber in reducing of wear parameters was proved in conformation tests of thixomixed Al/C_{sf} composite.

TABLE 4.7: Results of the confirmation tests

	Minimum Initial Responses	Optimal Wear Parameters	
		Experiment	Prediction
Level	A3B2C1	A3B1C1	A3B1C1
Wear Rate $(m^3.(m.N)^{-1} * 10^{-7})$	3.13	3.12	3.00
S/N Ratio	70.08	70.09	70.21
Coefficient of Friction	0.33	0.32	0.32
S/N Ratio	9.16	9.79	9.77

4.3.4 Microstructural Analysis and Wear Mechanism

The initial microstructure of hypereutectic Al/Si alloy was prepared by thixomixing method which is shown in Figure 4.24. The fiber has been dispersed and distributed homogenously in the matrix which shows relatively good adherence at the interface.

During this novel process of compo-casting, some porosities and air holes were arrested in composite which are indicated clearly, but it can be removed by further metal shaping such as extrusion or forging. Hypereutectic Al/Si alloys have shown the good tribological properties, due to containing wear resistance elements such as silicon [Mahato et al., 2010]. It has been reported that thixoforming methods can increase the wear resistance Saklakoglu et al. [2014].

But, the presence of iron in the matrix alloy is not negligible in current thixomixing process due to the dissolution of Fe from the die to the composite during compo-casting process (Figure 4.24b). The $\beta - Al_5FeSi$ intermetallic precipitated and forms a needle-like structure which is hard and brittle and good site for micro cracks initiated, at end increases the wear rate [Mbuyaa et al., 2003]. The modification elements such manganese (0.6 wt.%) has been reported to change the flake like β-intermetallic into star-like π-intermetallic, and reduce the deleterious effect of Fe and reduce the wear rate [Abouei, Saghafian, Shabestari and Zargham, 2010, Abouei, Shabestari and Saghafian, 2010]. However, the presence of iron in the Al/Si alloy improves the high temperature properties and the thermal stability of the alloy [Ye, 2003].

Figure 4.25a shows SEM micrographs of the worn surface of the 4047/4.2 % C_{sf} composite exhibited the deep, permanent grooves related to high speed of sliding and also

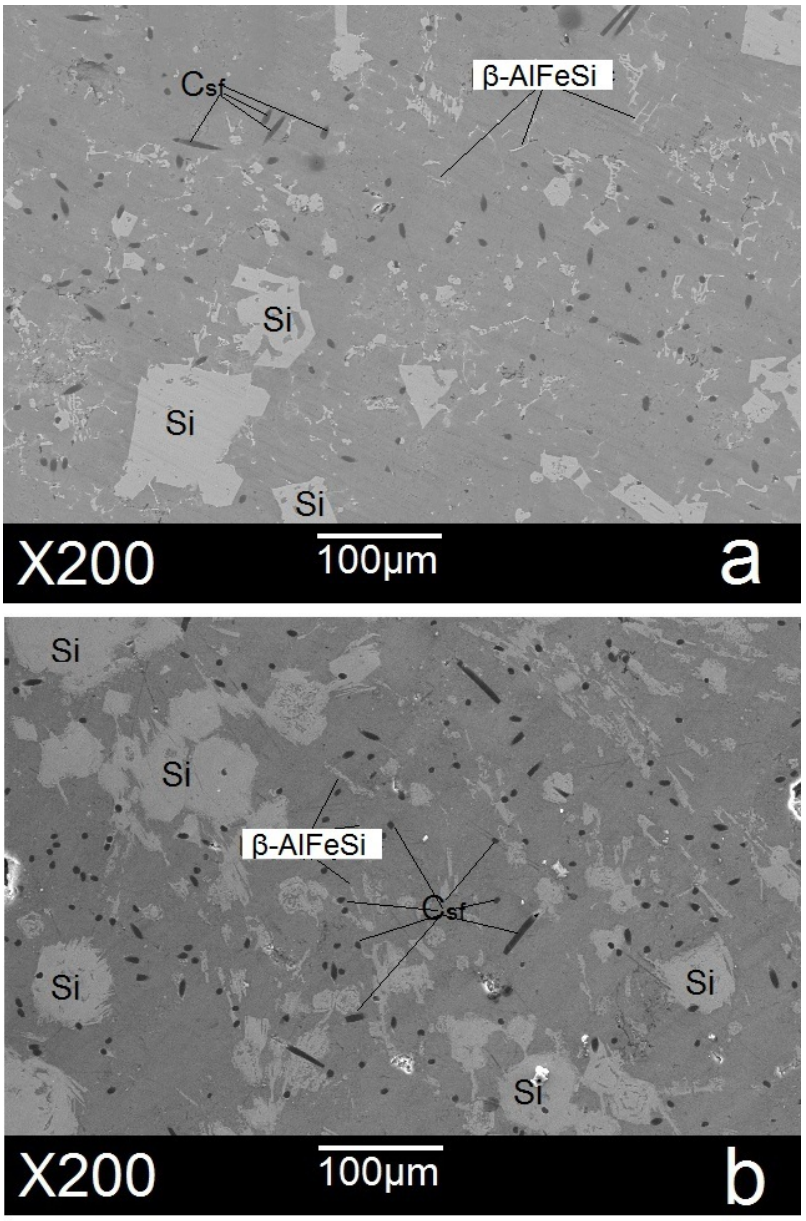

FIGURE 4.24: SEM images of samples before wearing (a) 4047/4.2 % C_{sf} composite (b) 4047/8.1 % C_{sf} composite

the tribo-film formed on the surface. The coefficient of friction was reduced probably by the formation graphite rich-layer from carbon fiber in the composite samples as result of solid lubricant effect. These wear mechanisms were produced by the ploughing and formed the relatively deep grooves made by two asperities as counter pin and the hardened worn debris such as silicon or metal oxides.

During the wear sliding, the loose small particles were packed tightly layer over layer

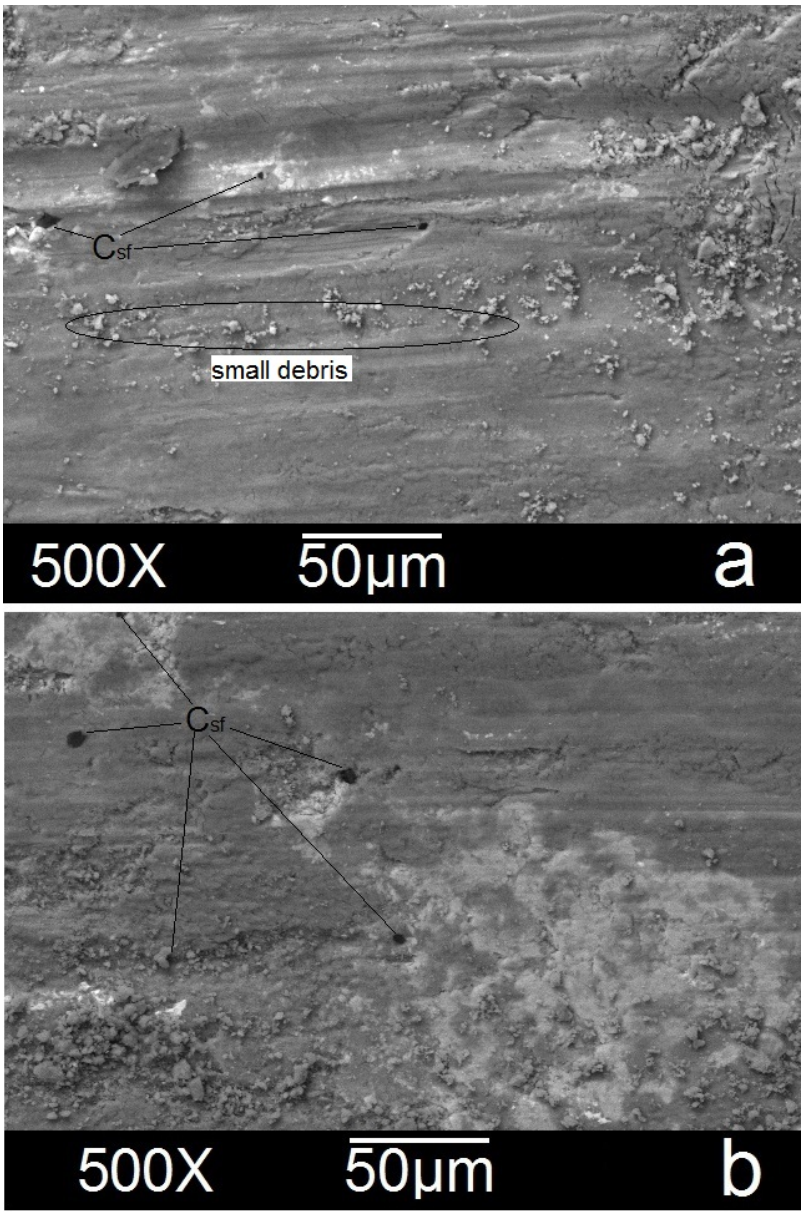

FIGURE 4.25: SEM images of (a) 4047/4.2% C_{sf} composite at sliding speed 20 cm/s and load 5 N (b) 4047/8.1% C_{sf} composite at sliding speed 10 cm/s and load 5 N

and an adherent smooth graphite-rich film formed over the track area. The micro-hardness values increased from 56 HV for un-tracked area of composite to 67 HV for track area which enhanced 20 %, on the other hand the hardness was increased just 6 % of the matrix samples when the micro-hardness increased from 51 to 54 for untracked and tracked area, respectively. The hardness values of track area was carried out after the testing so the values measured separately and not included in Table 4.3. Some of the residual worn debris which remained unpacked contains smaller amounts of oxide particles and small size microcrystals of graphite were at the surface eventually leads to

exhibit the slight plastic deformation.

The smooth surface at tracking area and the smaller size of debris are cause of the carbon content and the lower coefficient of friction. It has been reported that the temperature in contact area is an important influential parameter on the wear mechanism during the wear test [Ravindran et al., 2013]. When the coefficient of friction decreased the temperature will be decreased so the adherence between two interfaces, reduced. However, the worn particle sizes become smaller at a lower temperature because of the high thermal conductivity of composite and solid lubrication of carbon content in the composite. In Figure 4.25b the lighter region at the micrograph is belonging to silicon particles (as result of EDX spectrum taken from this region can be seen in Figure 4.28) with some carbon fibers remained in the wear track.

A severe plastic deformation undergone in Figure 4.26a and big detachments revealed the softening effect due to the enhancement of temperature. While the wear is processed, the dislocations were accumulated under the track area and formed the cracks at a certain depth which is parallel to the surface, so they become stretched and expand to the critical length [Liu et al., 2009]. Finally the wear surface between expanded cracks and surface is being peeled like wear debris and the fresh layer under it oxidized as shown in Figure 4.26a. The morphology of the worn surface revealed that some materials were removed due to abrasive wear.

The wear track areas at lower resolution have been shown in Figure 4.26 while the difference in the wear mechanism is illustrated. Wear process produces heat and has been dissipated much more when carbon fiber presented in composite samples and slightly plastic deformation will occur. The coherent surface in track area without any detachments exhibited in Figure 4.26b and 4.26c.

Figure 4.27 shows the cross sectional area of 4047/8.1 % C_{sf} composite worn surface under sliding speed 20 cm/s and load 10 N. This microscopy illustration proves the presence of carbon fiber at wear track and good adherence to the matrix which were not pulled out. In spite of, the absence of any coating on the carbon fiber, the good adherence to matrix and no pull out of the fiber was shown in the microscopy illustrations.

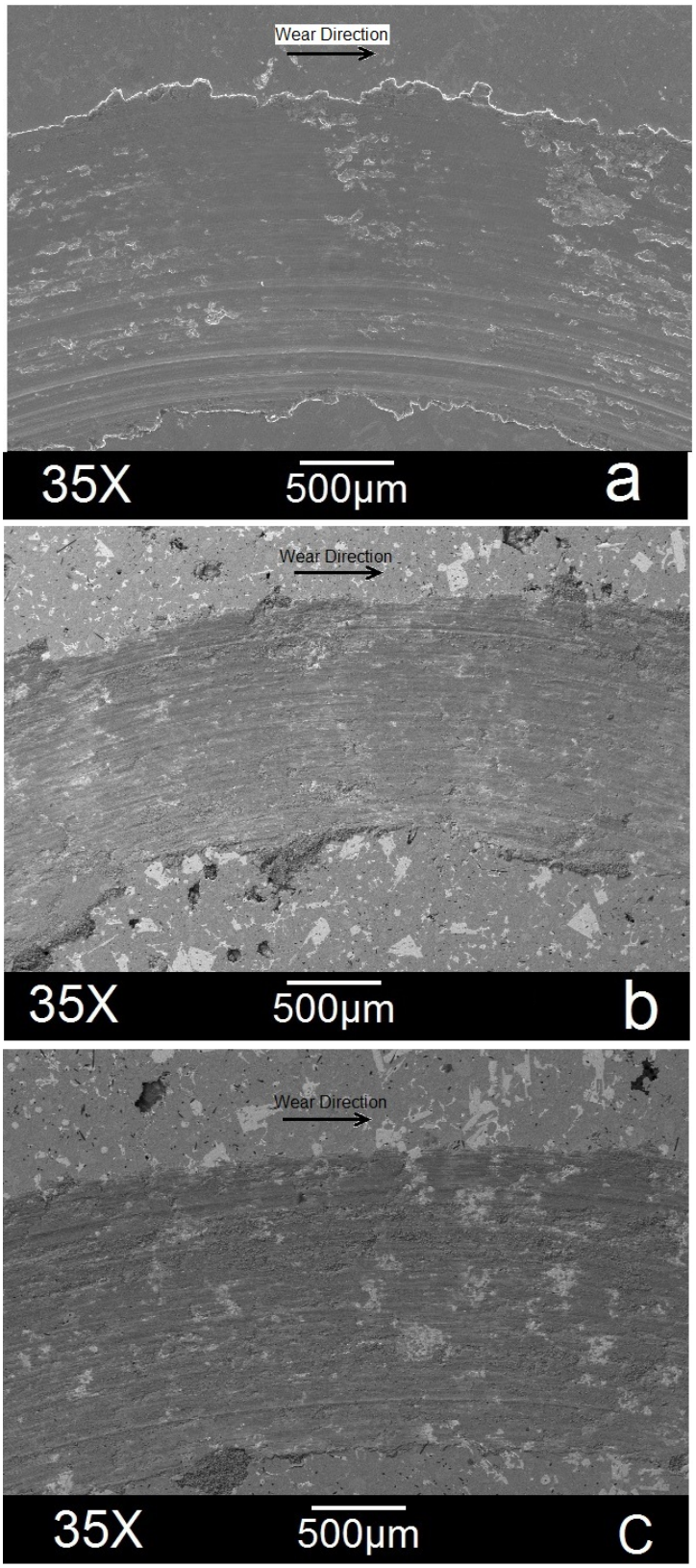

FIGURE 4.26: SEM image of worn track surface for (a) matrix alloy (4047) without carbon fiber at sliding speed 5 $cm.s^{-1}$ and load 5 N (b) 4047/4.2%C_{sf} composite at sliding speed 20 $cm.s^{-1}$ and load 5 N (c) 4047/8.1% C_{sf} composite at sliding speed 20 $cm.s^{-1}$ and load 10 N

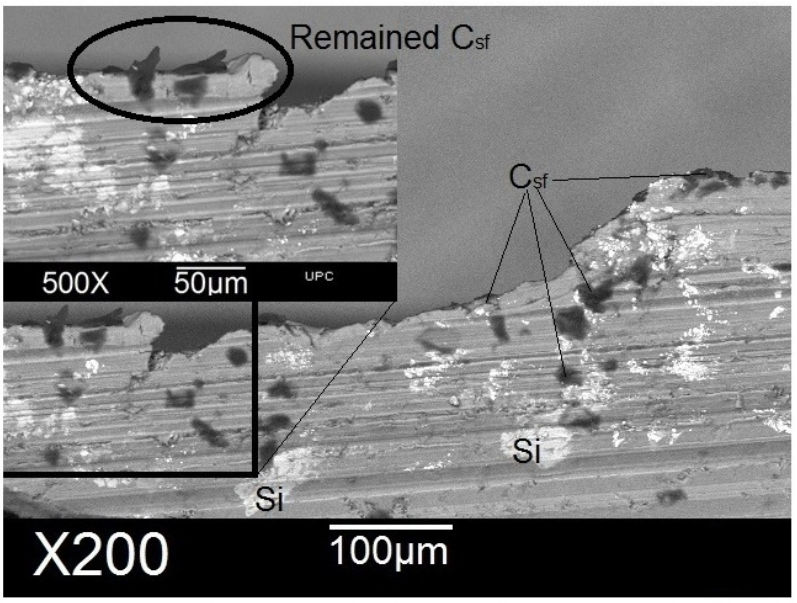

FIGURE 4.27: SEM image of worn track surface for cross section of worn track of 4047/8.1% C_{sf} composite

Additionally, the fibers have been ground and the very small size graphite particles were tightly packed with small loose oxide particles and formed an adherent film over the worn surface. The asperities of the hard worn debris and counter pin caused the formation of grooves like ploughing and can be seen in the cross sectional view.

Figure 4.28 shows the EDAX pattern of the worn surface of matrix alloy and composite sample contains 4.1 vol.% of C_{sf}. The EDAX of the track area of composite sample shows that C and O are present, as Figure 4.28b represents. In the EDAX spectrum of the C_{sf}/Al (Figure 4.28b), the peak belongs to O appeared lower than that of the matrix alloy (Figure 4.28a), because of the low temperature caused by the C_{sf}.

Figure 4.29 shows the mapping EDAX of a worn track area of hypereutectic silicon aluminum alloy/C_{sf} composite. The mapping EDAX analysis contains bright and dark spots which reveal them to be rich of the individual elements in that point. The carbon in worn surface came from the carbon fiber which ground on tracking area, and oxygen is cause of the oxidized debris which was composed of materials from composite and oxidation of aluminum by air.

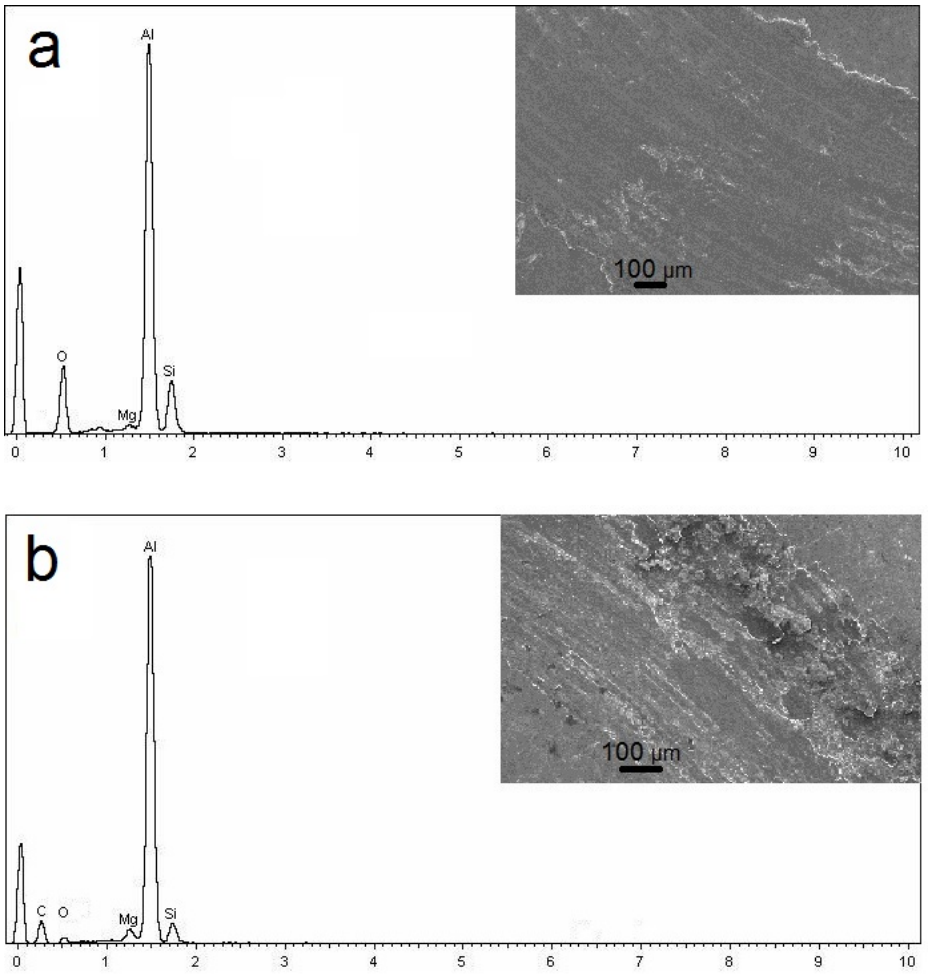

FIGURE 4.28: EDAX with SEM pattern of worn surfaces area of (a) hypereutectic silicon aluminum as matrix alloy and (b) hypereutectic silicon aluminum/C_{sf} 4.1 vol.% composite

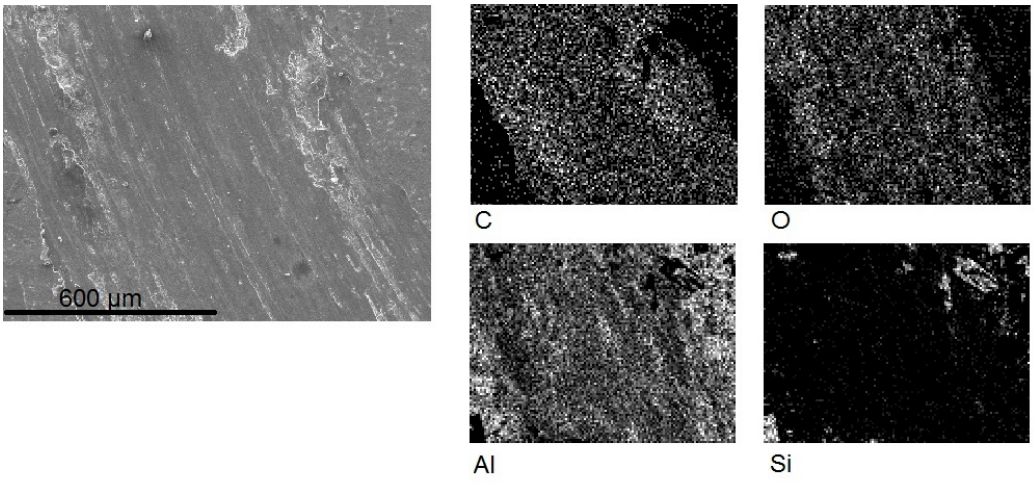

FIGURE 4.29: Element distribution from mapping EDAX of worn surface of aluminum/4.1 vol.% C_{sf} composite

4.4 Corrosion and Electrochemical Investigation on Aluminum/C_{sf} Composites

Aluminum silicon/carbon fiber composite has wide applications and one of the challenge regarding its application are the corrosion resistance and the durability. In this study, the corrosion characteristics such as potentiodynamic (PD) and electrochemical impedance spectroscopy (EIS) were conducted on the three types of aluminum silicon alloy (A356, A357 and 4047 (hypereutectic)), the composites made of those alloys and C_{sf} fabricated by thixomixing and the heat treated samples of composites, then the corrosion potential and other electrochemical parameters were figured out in 3.5% NaCl solution.

From the electrochemical point of view, both silicon and carbon fiber play a cathodic role resulting in galvanic couples with aluminum as anode in electrolyte solution. The carbon fiber is a good electrical conductor and more noble than aluminum where join to the aluminum and lead to a localized destructive galvanic corrosion at aluminum/carbon fiber interface. The iron intermetallic compounds were formed in the composite during mixing may act as additional cathodic sites. Arrabal et al. have been reported a cathodic behaviour of Si and iron-intermetallics relative to aluminum matrix by scanning Kelvin probe force microscopy [Arrabal et al., 2013].

The SSM process generally improve the critical disadvantages of conventional casting by producing a homogenous globular microstructure where both mechanical and electrochemical properties have been promoted [Bastidas et al., 2001, Tahamtan and Boostani, 2009]. SSM process can provide globular primary α-phase, lower amount of gas entrapped in work piece and lower anodic to cathodic surface ratio which can reduce corrosion susceptibility of components made of this technique. However, the corrosion behaviour of thixomixed aluminum/C_{sf} composites remains poorly explored, just few studies have been reported on pitting attacks in chloride solutions at eutectic regions along the silicon interface and α-phase in the eutectic area [Arrabal et al., 2013, Park et al., 2005, Tahamtan and Boostani, 2009, Yu et al., 2002].

The corrosion resistance of aluminum silicon alloy composites (alloys 7075-T6 and 2024-T6) processed by SSM routs such as rheo- or thixo-casting is strongly attributed to volume fraction of reinforcement and initial solid particles in slurry, size and shape of eutectic silicon particles and the morphology and chemical composition of intermetallics. Masuku et al. have been expressed that surface liquid segregation (SLS) phenomenon at high pressure die casting leads to susceptible to corrosion pitting because of high eutectic excited on the surface as a main problem of SSM casting [Masuku et al., 2010].

Generally, the anode to cathode area ratio is associated to corrosion susceptibility of metal samples. The small size of silicon particles facilitate the formation of stable passive film and acts as noble silicon in contrast of less-noble eutectic area. The role of intermetallics in semi-solid casting routs was not elucidated in none of the previous studies clearly, although it should be similarly to as-cast or wrought alloys. In this study, the effect of thixomixng as semi-solid compo-casting method was evaluated on corrosion behavior, the role of silicon and intermetallics in metal matrix composite as C_{sf} reinforced aluminum silicon alloys. The corrosion potential and morphological properties of corroded samples were discussed.

4.4.1 Potentiodynamic Polarization

The potentiodynamic polarization were conducted on the samples and the curves were figured out in Figure 4.30 and the values of the electrochemical parameters were tabulated in Table 4.8. Polarization curve belongs to A356/C_{sf} composite was shifted to anodic region with higher current density than un-reinforced alloy. This phenomenon can be seen in the other type of aluminum alloys in compare with the corresponded aluminum/C_{sf} composite. The C_{sf} plays as micro-cathode in galvanic couple with matrix alloy. For the T6 heat treated composite samples a few improvement were detected due to the morphological refinement after heat treatment. The corrosion potential for A356 was reduced by refining of Si and intermetallic particles (such as β-AlFeSi as secondary phases) due to SSM casting routs or heat treatment process, as reported previously [Arrabal et al., 2013, Forn et al., 2006].

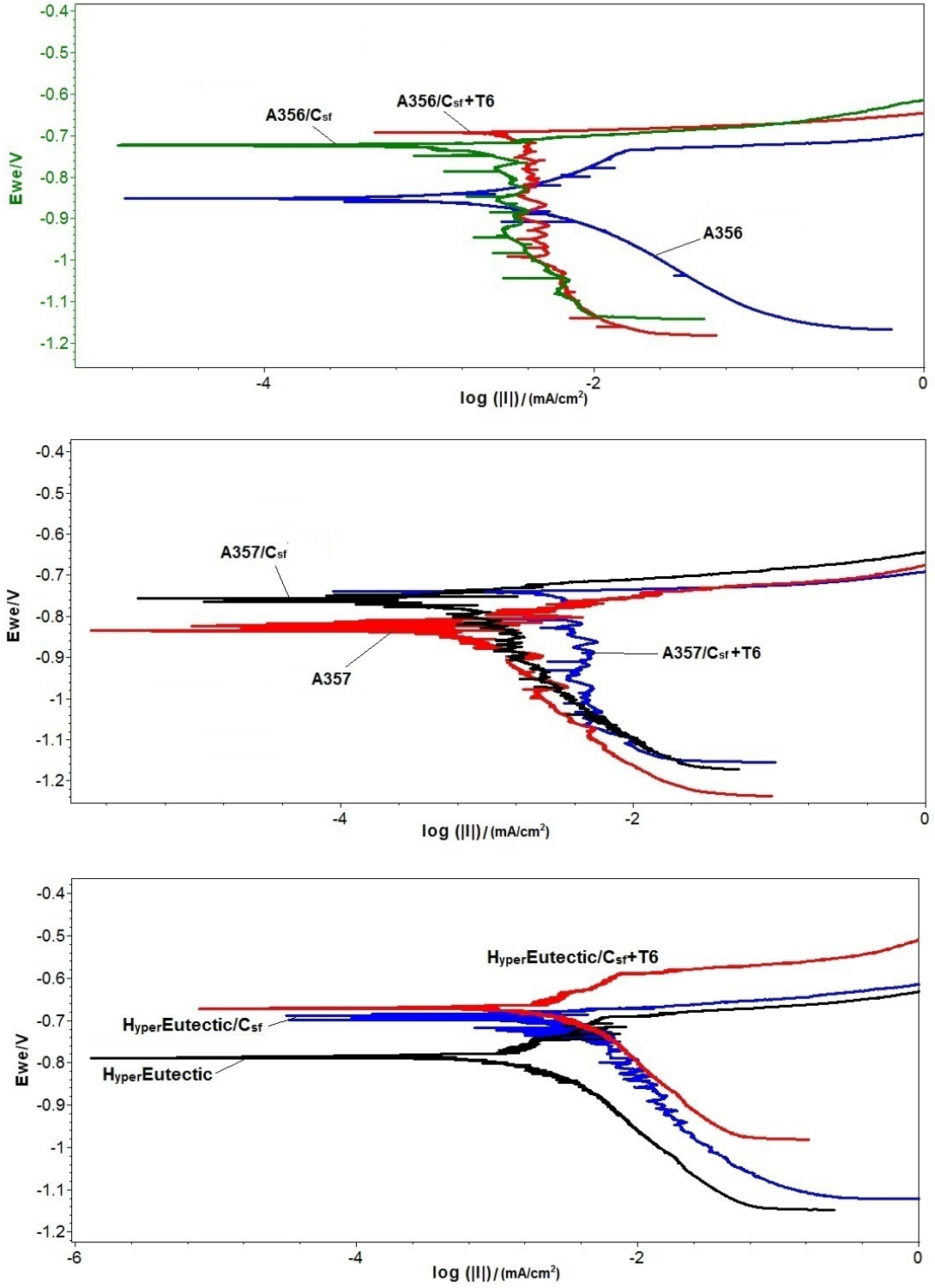

FIGURE 4.30: Potentiodynamic polarization curves for A356, A357 and Hypereutectic 4017 alloys and their composites reinforced with C_{sf} and T6 heat treated composites

TABLE 4.8: Electrochemical parameters achieved from potentiodynamic polarization curves

	I_{corr} mA.cm^{-2}	E_{corr} mV	β_a $mV.decade^{-1}$	β_c $mV.decade^{-1}$
A356	6.71	-860	80.2	96.1
A356/C_{sf}	8.78	-721	34.7	132.5
A356/C_{sf}+T6	9.07	-683	36.1	143.2
A357	6.35	-844	66.3	104.5
A357/C_{sf}	8.91	-763	26.7	136.9
A357/C_{sf}+T6	9.17	-741	29.8	143.3
4047	5.31	-797	78.3	87.1
4047/C_{sf}	6.31	-693	133.8	88.5
4047/C_{sf}+T6	6.98	-678	71.6	80.8

Silicon as a very low soluble element in aluminum, precipitates purely in the coarse flake shape which provides inhomogeneous properties in alloy, whereas the current density is low as a result of high polarization of silicon. When the Si makes compounds with iron as impurity in the alloy, the intermetallic compounds can form depend on the amount of silicon or iron in alloy, so AlFeSi can be detected in different forms. The β-AlFeSi is fragile looks like a thin plates particles, and the amount of iron impact on needles shape. In the case of A356, Si and partly π-AlSiFeMg intermetallic compound play as cathode when coupled as galvanic cell [Arrabal et al., 2013].

The T6 heat treatment increase the matrix grain size in order to reduce crevice corrosion from part to part along the matrix/fiber interface or Si interface in alloy. Most of the sample after T6 heat treatment procedure exhibited corrosion resistance by the solutionizing. T6 heat treatment increase the current corrosion in order to A356 and A357 composite reinforced with C_{sf} because heat treatment change the microstructure thus modifying the corrosion behavior. In this case, the T6 redistributes and grows the eutectic silicon and β-AlFeSi. T6 heat treatment has effect on solutionizing and disappearance of Mg_2Si in alloy and the disconnect the crevice corrosion. It the case of aluminum silicon reinforced with C_{sf} the fibers play acs cathodic site and increase the corrosion rate for T6 heat treated samples. As result, the T6 heat treatment increase the corrosion rate and reduce pitting evolution.

From Table 4.8, the A356 and A357 had the highest corrosion current density than 4047. The composite samples made of these alloys showed higher I_{corr} when the C_{sf} embedded into the alloys. In general as a corrosion concept, the surface ratio of anodic to cathodic may cause to increase corrosion rate when it is low. The corrosion potential also shifted to anodic region for the aluminum/C_{sf} composite and the heat treated samples.

In the heat treated composite samples made of A356 and A357, the cathodic branch shows a plateau that controls the corrosion reaction and can be associated with a reduction reaction of oxygen. The alloy A357 revealed better corrosion resistance than A356 due to higher content of Mg in the chemical compositions. Both changes in corrosion current and corrosion potential in composite samples than un-reinforced samples were attributed to galvanic corrosion with a tendency to form galvanic cell between aluminum and C_{sf}. The crevice corrosion at the aluminum/fiber interface changed the protective oxide layer on the aluminum.

The heat treatment increases the grain size of Si, then for the aluminum alloy such as 4047 which has high content of silicon leads to higher ratio of cathode to anode and increase the current corrosion and accelerate corroding. In contrast, the thixomixing process reduces the both grain size of silicon and alpha phase as it was discussed in the previous parts (section 4.1.3).

The aluminum oxide layer is an outstanding barrier again corrosion to protect aluminum in different media. The integrity of protective film on the aluminum was reduced by embedding of C_{sf} into the aluminum matrix during composite fabrication, which leads to higher susceptibility of pitting. The presence of carbon fiber (4.1 vol.% of C_{sf}) was affecting both I_{corr} and E_{corr} parameters.

It has been reported that the increasing of volume fraction of carbon fibers in composite causes the higher corrosion current density [Pardo et al., 2009]. The external coatings such nickel on the carbon fibers may increase the I_{corr} [Wielage and Dorner, 1999*b*]. The intermetallic compounds also act as additional cathodic sites beside Si particles which decrease corrosion current density and lower degradation on the surface. Low corrosion current densities are due to highly polarization of silicon particles in media.

4.4.2 Electrochemical Impedance Spectroscopy (EIS)

Figure 4.31 shows the impedance spectra of the samples as described previously, by the immersion in 3.5 wt.% NaCl solution. The electrochemical parameters achieved by EIS corresponded to equivalent circuit have been tabulated in Table 4.9. The form of Nyquist plots belong to different testing samples is similar to each other so the equivalent circuit like Figure 4.32 was proposed to calculate the different electrochemical elements in this circuit.

The capacitance loop was shown at high frequencies when goes to lower frequencies reveled a Warburg element. In the equivalent circuit, the R_1 is the solution resistance between the working and reference electrode. The CPE and R_2 corresponded to capacitance and resistance of C_{sf}, silicon and intermetallics, which are strongly cathodic in against of aluminum surrounding them. The W_2 is the Warburg element with open circuit transmission line corresponds to pitting, as illustrated in Figure 4.32 The end part of capacitive arc at low frequencies is belong to localised corrosion such as pitting. CPE is a non-ideal capacitive behaviour of heterogeneous interface and its impedance is described as (equation 4.5):

$$Z_{CPE} = \frac{1}{Q(i\omega)^p} \tag{4.5}$$

where, Q is the CPE constant, which nominally equals to admittance of the system at 1 rad/s; i = $\sqrt{}$-1, ω is the angular frequency (rad/s) and the value of P ranges between 0 to 1 and if P = 1 becomes the impedance of a pure capacitor and for P = 0, CPE acts as a pure resistor. The Warburg impedance as described in equation 4.6

$$Z_W = \frac{R\cosh(iQ\omega)^P}{(iQ\omega)^P} \tag{4.6}$$

where R is the limiting diffusion resistance, Q is a time constant and P is the capacitive character of the diffusion as described above. On a Nyquist Plot the Warburg impedance appears as a diagonal line with an slope of 45°. The cathodic resistance was reduced for all un-reinforced matrix samples compared to the composites, which indicated the

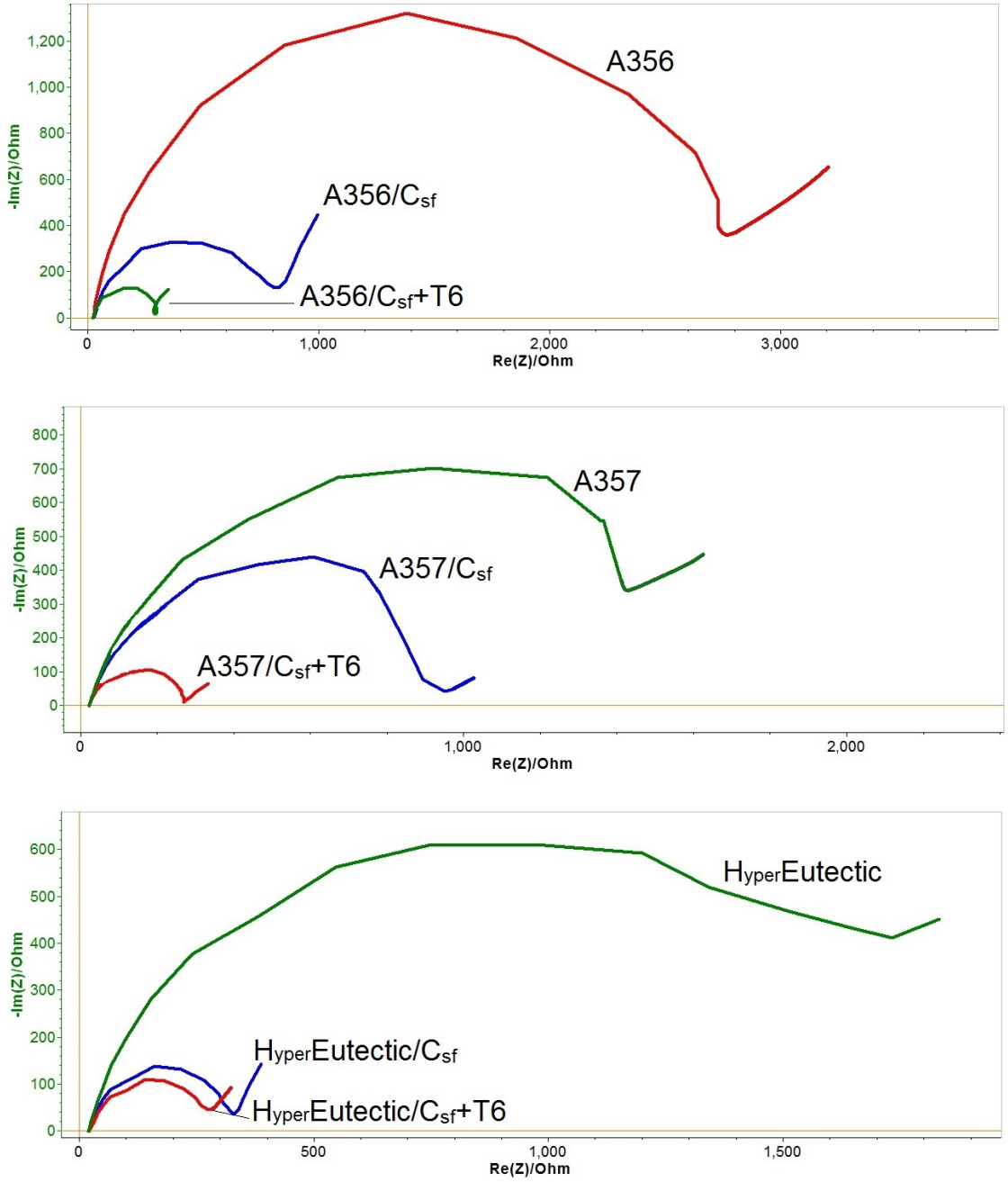

FIGURE 4.31: Electrochemical Impedance Spectroscopy (EIS) Nyquist' plots for A356, A357 and Hypereutectic 4017 alloys and their composites reinforced with 4.1% C_{sf} and T6 heat treated composites

galvanic formation. This reduction was also repeated slightly when the composites were heat treated. The inductive character of CPE was attributed to the nucleation of pits near or around the intermetallics. The new pitting is active area on the exposure surface provides the noise which can be detected by EIS measurements. The cathodic sites play as desirable location for hydrogen reduction and releasing bubbles in the close

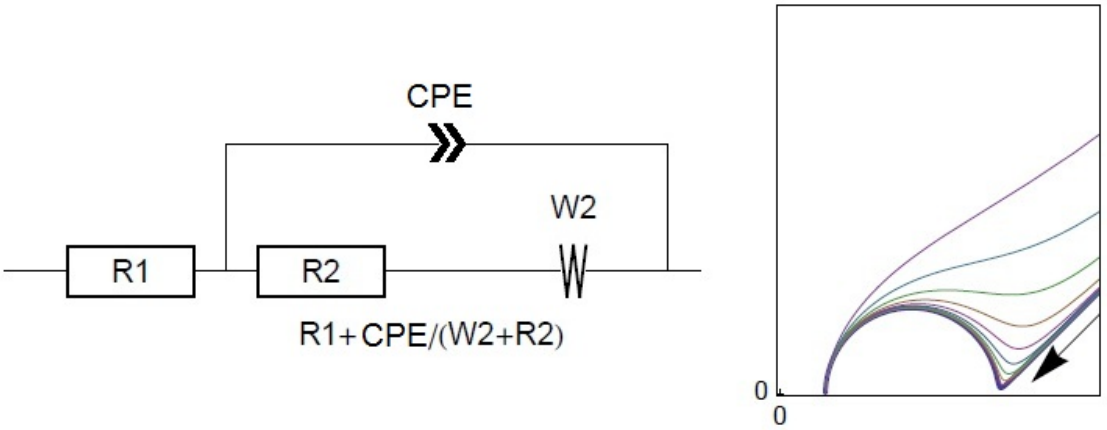

FIGURE 4.32: Equivalent Circuit of Nyquist Plot corresponded to the examined samples

TABLE 4.9: Electrochemical parameters of EIS results simulation by equivalent circuit

	R_1	R_2	CPE	W_2
	Ω	Ω	$\mu S s^p.cm^{-2}$	$\Omega.s^{-1/2}$
A356	22.6	2398	45.8	27.8
A356/C_{sf}	24.4	640	114.1	94.5
A356/C_{sf}+T6	22.8	219	209.7	123.4
A357	26	1438	18.3	12.8
A357/C_{sf}	34	812	37.6	36.3
A357/C_{sf}+T6	30	221	65.2	76.9
4047	21.4	1113	12	11.4
4047/C_{sf}	22.6	244.4	190	45.9
4047/C_{sf}+T6	21.7	178	221	49.3

distance of pitting sites. A crevice corrosion also occurred at the matrix/fiber interface as discussed before. T6 heat treatment caused to growth of Si or the intermetallic particles as cathode so the ratio of anode to cathode will be reduced in order to accelerate the corrosion rate and progress of pit depth or the scale of crevice around C_{sf}.

It can be say that the T6 heat treatment modify the morphology of the Si and intermetallic compounds and resulted to intensify corrosion rate in this study. Warburg diffusion values are higher for heat treated composite samples than those un-treated and un-reinforced samples.

4.4.3 Micrographs of Corroded surface of Aluminum/C_{sf} Composites

The microstructural morphology of corroded samples after the electrochemical analyses were examined by SEM as illustrated in Figures 4.33 for different samples and the heat treated ones. A356 without reinforcement (4.33a) seems a uniform corrosion with less critical localised corrosion compared to the similar matrix alloy which reinforced with C_{sf} as shown in Figure 4.33b. The high amount of corrosion products and protective film which covered surface in hypereutectic alloy was compared to A356.

The localised corrosion near to fibers or around them were shown in Figures 4.33b-d for the composite samples made of A356 and A357 as matrix and C_{sf}. In contrast, the interfacial bonding and adherence between C_{sf} and matrix in hypereutectic alloy was remained unchanged when they were located in Si (Figure 4.33f). The interfacial adherence of other fibers were not located in Si have been degraded. The corrosion products were precipitated over surface apparently than the other alloys.

The interesting point is the localised corrosion exactly at silicon/fiber or intermetallic/-fiber interface that reduce the adherence, but the silicon particle or iron intermetallic were un-attacked. It has been expressed that the silicon and iron intermetallics can be deposited predominately to improve the wettability and adherence onto the fiber surface for good load transferring from matrix to alloy, therefore any factor that deteriorates interfacial bonding such as crevice corrosion, decrease mechanical strength certainly.

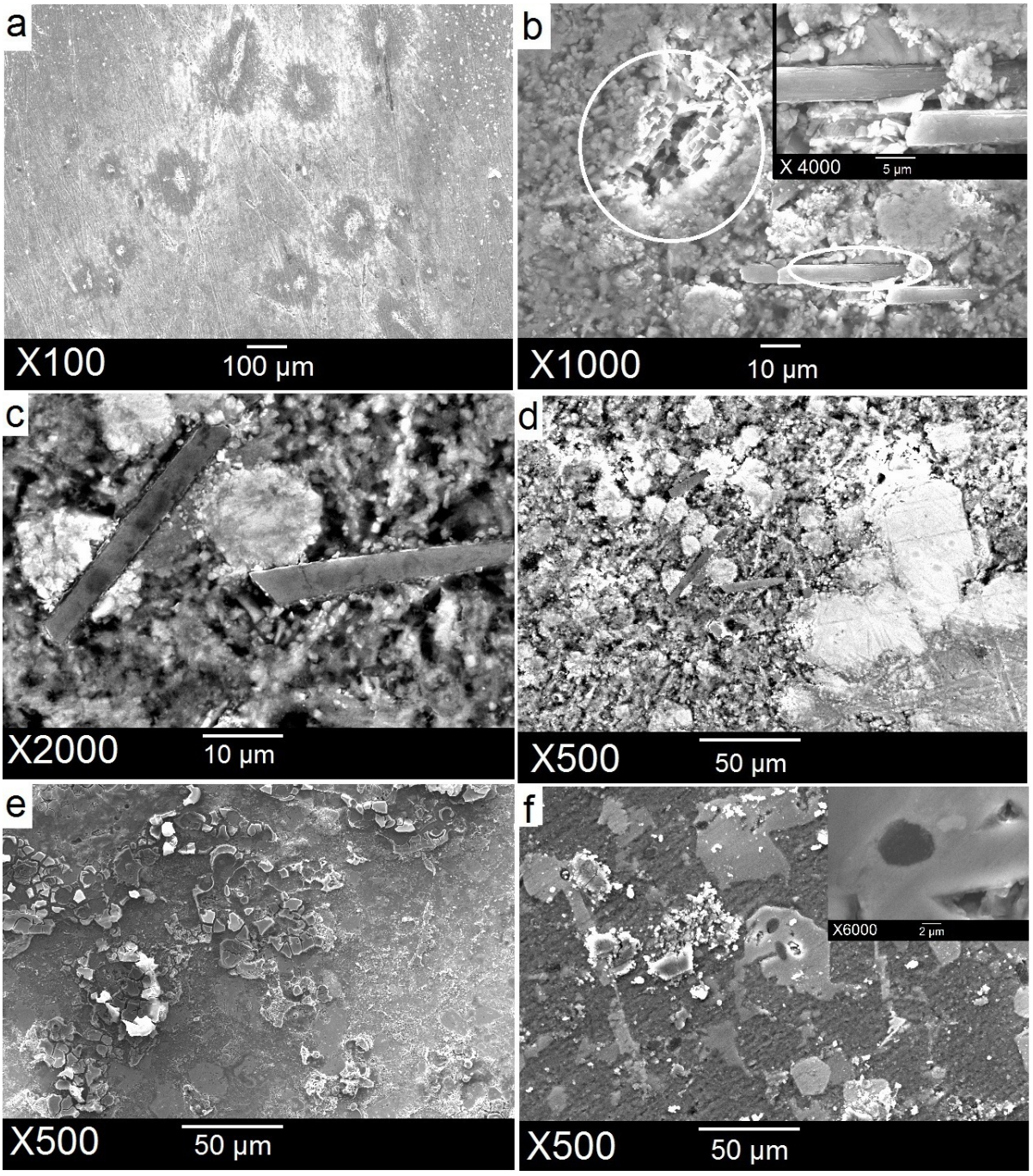

FIGURE 4.33: SEM micrographs of corroded surface after electrochemical testing (a) A356 alloy (b) A356/C_{sf} composite (c) high resolution of A357/C_{sf} composite shows interfacial degradation around fiber and (d) A357/C_{sf} composite (e) 4047/C_{sf} composite with the corrosion products presence onto the surface (f) 4047/C_{sf} composite

Some factors are influence in the absence and presence of corrosion products such as dissolved aluminum ions in media, the fluid convection that carried away dissolved ions and the pH is either too high or too low for precipitation [Hughes et al., 2011]. As it was distinguished, the pitting corrosion progresses under condition where the protective surface film was not covered uniformly. The protective film was degraded completely in the case of A356 and A357 alloy and composite samples.

Figure 4.34a was shown the localised corrosion (crevice) caused by galvanic cell made of C_{sf} as cathode (noble) and matrix alloy as anode leads to loosing the interfacial bonding. This is a main phenomenon occurs in the case of MMC reinforced with noble reinforcement such as carbon fiber, CNT or alumina [Bakshi et al., 2010]. Regardless of casting rout the eutectic α-phase revels localised corrosion at the interface of iron-intermetallics.

In the samples of this study, no corrosion attacked was observed on the primary globular α-phase, but the eutectic area was attacked as shown in Figure 4.34b, it was also reported by [Bastidas et al., 2001, Tahamtan and Boostani, 2009] with the pits may created at the vicinity of them. The oxygen reduction by cathodic reaction (equation 4.7) near to primary α-phase produce alkaline media locally which occurs localised corrosion. The globular α-phase reveals better corrosion resistance than eutectic area which surrounded them as can be seen in Figure 4.34b.

$$O_2 + 2H_2O + 2e^- \rightarrow 2OH^- \tag{4.7}$$

In this study was proposed that, the eutectic areas around the primary globular α-phase were corroded by progressing of pitting or other localised corrosion. Although the interface of Si particles and α-phase was remain unchanged as detected in Figure 4.34c. Although the primary α-phase was shown good corrosion resistance than, the α-phases in the eutectic areas which were attacked and degraded at longer immersion time.

The formation of different intermetallics may alter corrosion behavior and resistance, by playing as cathode or anode over surface. For example based on electrochemical point of view, the β-AlFeSi is more noble than the matrix or even Si particles that plays as cathode to increase the alloy susceptibility to localised corrosion. Some of the alloying

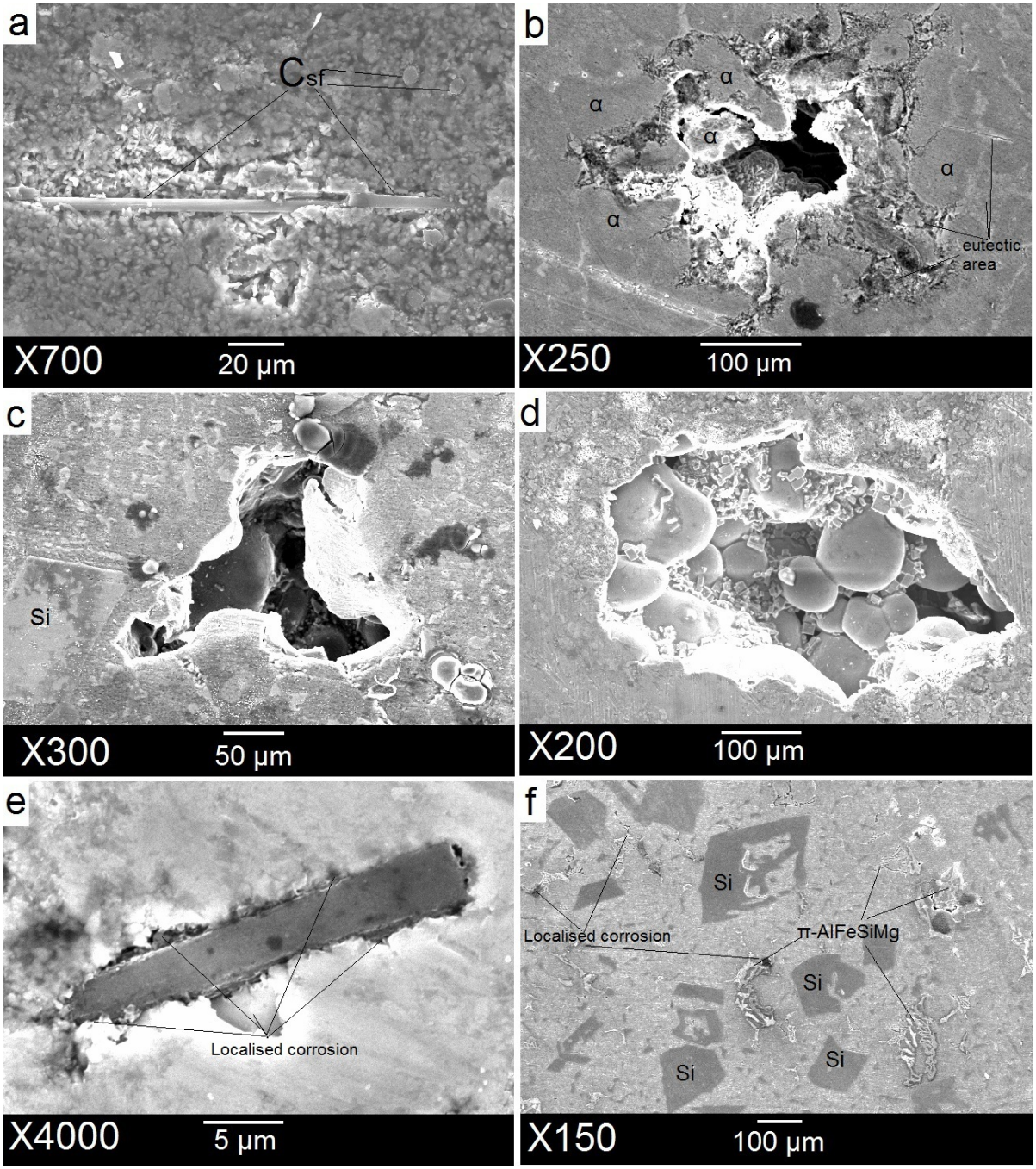

FIGURE 4.34: SEM micrographs after corrosion illustrated pits at (a) A356/C_{sf} composite (b) A357 alloy (c) 4047/C_{sf} composite (d) A356/C_{sf}+T6 composite (e) crevice corrosion around a C_{sf} belong to A357/C_{sf}+T6 composite and (f) 4047 alloy

element as it was discussed previously, such as Manganese can modify the morphology of AlFeSi compounds to the AlFeSiMn compounds to improve mechanical properties, also reduce cathodic effect of iron and less intensity of galvanic corrosion. In fact, Mn reduces the cathodic effect of Fe to less intense galvanic couples compared with AlFeSi intermetallic compounds [Nisancioglu, 1990].

The primary α-phase can be extended by T6 heat treatment, so the clear boundary and interface between different phases cannot be distinguished. Figure 4.34d shows a pit was occurred in heat treated A356/C_{sf} composite and small particles as corrosion products or the Si particles remain after corrosion. There is differences between heat treated and un-treated composite samples in crevice corrosion along the fiber/matrix interface as indicated in Figure 4.34e. In the case of base metal A356 and A356/C_{sf} composite, the progress of corrosion surrounding Si and intermetallic compounds and semicircular pits in the aluminum matrix.

The tiny localised corrosion were indicated in hypereutectic aluminum alloy (4047) in Figure 4.34f with the presence of Si particles and the iron-intermetallics acting as cathodic sites. Although the localised corrosion mostly occurred in the eutectic area respect to the other location, the localised corrosion resistance was increased with reducing the surface ratio of eutectic silicon to eutectic aluminum.

A crevice corrosion and/or pitting may occur at the interface due to changes in protective oxide layer on the aluminum surface [Wielage and Dorner, 1999*b*]. Although, the protective film provides outstanding corrosion resistance of aluminum, any reasons to decrease its integrity lead to localized corrosion attack such as pitting [Liu et al., 2014]. The pitting is an accelerated corrosion type without polarization which is occurred specifically in the contact with carbon fibers [Tahamtan and Boostani, 2009]. The fibers axis is perpendicular to the exposure surface in electrolyte solution. The corrosion reduce the mechanical strength by pitting and interfacial failure at matrix/fiber [Wielage and Dorner, 1999*b*].

The semi-solid casting aluminum samples show higher corrosion resistance and less susceptibility to pitting than gravity casting or fully liquid process. The previous examination revealed lower potential differences between Si and iron-intermetallics and the

eutectic aluminium phase at initial stages of corrosion process may be attributed to the formation of primary globular α-phase and refinement of iron-intermetallics (β-AlFeSi and π-AlFeSiMg) and Si particles and creation of homogenous passive film or rapid re-passivation [Arrabal et al., 2013, Park et al., 2005].

Chapter 5

CONCLUSIONS

Aluminum matrix composite reinforced with carbon fibers are promising advanced materials due to its high strength to weight ratio but the interfacial adherence and homogenous distribution in the matrix are the main problems with their production. Although many attempts have been carried out to improve the interfacial and mechanical properties of the composite, the effective method for fabrication was not achieved yet. A novel thixomixing method was developed based on semi-solid state and the thixotropic. The mechanical, morphological and electrochemical characterizations have been carried out on fabricated composite samples in this study. According to the research objectives, results and discussions, the following conclusions can be expressed:

5.1 Feasibility of Fabrication Aluminum/C_{sf} by Thixomixing

The innovative thixomixing process to fabricate aluminum silicon/short carbon fiber composites, under intensive shearing of semi-solid slurry maintained at the specific temperature for appropriate solid fraction, was developed. For good dispersion and distribution of fibers into the matrix, the amount of shearing load and viscosity must be optimized and controlled within the thixomixing process depend on each kind of alloy and reinforcement. The temperature affect on solid fraction and then on viscosity and

shearing load. High shearing at semi-solid state provided globular microstructure in the as-mixed samples. In thixomixing process, the C_{sf} first dispersed under intensive shear load and then distributed in the slurry made of globular primary α-phase and the eutectic.

Microstructural evidences were clearly indicated that C_{sf} dispersed and distributed homogeneously in the matrix with acceptable interfacial bonding as consequence of predominant precipitation of alloying elements (Si and Mg). Mixing under optimum conditions (for A356, A357, the solid fraction 48% and mixing speed 100 rpm) produced relatively good wettability, homogeneity, few damages on the fibers and probably inhibition of aluminum carbide formation and improvement on microstructure of the matrix. The silicon and desirable intermetallics (AlSiFeMg) have been observed as probably bonding mechanism and to promote the wettability on the carbon fibers.

Although the XRD and SEM analysis are not the strong technique to demonstrate the presence of aluminum carbide, they were carried out to demonstrate the intermetallic which can be formed during the process for further specifications, but no evidence was found for the presence of aluminum carbide formed by thixomixing. The gas entrapment and porosity were produced alongside of thixomixing, whereas the post-fabrication processes such as semi solid extrusion can be reasonable solutions. The hot extrusion applied in this study and it had no effective impact on random distributed C_{sf} to be aligned across the extrusion direction as represented in microstructure of composite samples and fractured surfaces.

5.2 Effect of Heat Treatment on Mechanical Properties and Interfacial Adherence

The T6 Heat treatment on both A356 and A357 thixomixed composites modified the microstructure and improved the interfacial bonding between fiber and matrix. The intermetallic compounds were also modified to achieve better mechanical properties. The SEM images show good dispersion and distribution of fibers into the matrix with

good wettability and adherence. The EDAX mapping results demonstrate the deposition of Si or intermetallic compounds onto the surface of C_{sf}.

Tensile strength and mechanical properties marginally improved through the increase of volume fraction of reinforcement and T6 heat treatment. The ultimate tensile strength of T6 heat treated samples was improved about 20-25% rather than those not heat treated. Furthermore, the fiber increased the ductility of the composite made of A356 and A357 by 50-170% and Young modulus for both composite by 5-10%. The porosity and pores contents in the tensile samples decreased mechanical strength. The pores size were shown bigger in SEM images after T6 heat treatment.

5.3 Wear and Tribological Characterization

The tribological properties were studied for hypereutectic silicon (4047)/C_{sf} composite produced by thixomixing method. The wear properties was optimized by Taguchi method. Three factors, volume fraction of fiber, sliding speed and load have been chosen and tested at three levels.

According to ANOVA, the carbon fiber volume fraction has the most significant effect on the wear parameters. The contribution percentage for each parameter was determined by the analysis of variance. The contribution percentages are 96.72 % and 82.46 % for specific wear rate and coefficient of friction, respectively. The statistical evaluation shows the improvement of wear parameters compare to the initial values, and these impacts are related to first volume fraction of fibers and second to the load and sliding speed as third place over ranking by software analyzing.

In order to find out the wear mechanism, the surface deformations of the worn surfaces were analyzed by SEM. The SEM images of the worn surface indicated the smooth and graphite layer in the track area with the small debris particles causing low plastic deformation.

The thixomixing provided relatively good adherence at the interface of C_{sf} and matrix alloy. The presence of carbon fiber was produced for reduction of specific wear rate

and coefficient of friction due to formation of rich graphite layer in the wear track and increase the thermal conductivity. No pull out of carbon fiber was detected and it was ground onto the sample surface which works as solid-lubricant. The coefficient of friction decreased by increasing the volume fraction of C_{sf} in the composite sample. Moreover, the thixomixed composite represented a lower coefficient of friction and wear rates for comparing the matrix alloy at all levels of loads and sliding speeds.

In summary: the following conclusions can be drawn:

- The incorporation of C_{sf} in Al hypereutectic alloy improved the wear resistance greatly.
- As the C_{sf} content increased, the friction coefficient and wear mass loss decreased.
- As the load and rotating speed increased, the wear rate did not change markedly. The wear displayed a linear evolution in all the range of load.
- C_{sf} reinforced the aluminum matrix and reduced direct contact between the matrix and counterpart.
- No fiber pull out were detected in wear track area and it proves the good interfacial adherence between matrix and fibers.

This composite reveals a good material choice for wear as required in light weight parts.

5.4 Electrochemical and Corrosion Evaluations

The composite samples either heat treated or without heat treatment reveled high corrosion current density compare to the un-reinforced matrix alloy. The corrosion potential also shifted to the anodic region for composite and heat treated samples. Because, the C_{sf} in the composites play as cathode to form a galvanic couples when joint to the Si particles and iron-intermetallics to increase pitting susceptibility and localised corrosion at the fiber/matrix interface and weaken the bonding. The protective film over

aluminum surface is outstanding resistive against corrosion so any reason decrease its integrity such as C_{sf} may increased corrosion rate.

The results of electrochemical tests expressed that the presence of C_{sf} and the heat treatment on the fabricated composite increased the corrosion current density and reduced the corrosion resistance. The presence and increasing the amount of C_{sf}, Si and iron-intermetallics increased the cathode to anode ratio which lead to accelerated pitting or crevice corrosion. Although the lower corrosion resistance of composite sample made of C_{sf}, the semi-solid casted samples were demonstrated lower corrosion susceptibility.

T6 heat treated composite samples for A356 and A357 demonstrated higher corrosion current than un-treated composite, and the 4047/C_{sf} T6 heat treated was shown a higher corrosion current respect to the un-treated composite, because the heat treatment dissolved the intermetallic compounds and the crevice corrosion was disconnected. The potentiodynamic polarization curves show the higher corrosion current density of both composite and heat treated composite samples compared to matrix alloy where the corrosion potential increased respectively.

The EIS results show the cathodic resistance of matrix alloy was decreased versus of composite samples which indicated galvanic couples formation. Warburg diffusion values are higher for heat treated composite samples than those un-treated and un-reinforced samples, which is a good reason to demonstrate high susceptibility to pitting of un-reinforce and composite samples than heat treated. The pitting corrosion progresses under condition where the protective surface film was not covered uniformly.

The primary globular α-phase in the thixomixed composite sample reveals better corrosion resistance as obtained by electrochemical analysis. The localised corrosion exactly occurred at silicon/fiber or intermetallic/fiber interface that reduce the adherence, but the silicon particle or intermetallic were unattacked. In another word, the crevice corrosion just attacked on the tiny area as matrix/C_{sf} interface which caused to lower mechanical strength and adherence.

5.5 Recommendations of Future Research

In spite of the benefits, this technique has some problems that could be limited the industrial application of carbon fiber reinforced aluminum composites. The formation of porosity and fragile intermetallic compounds were distinguished as main deleterious effect on mechanical strength of final composite by this technique. It is necessary to control and remove the harmful effects in this fabrication process. The recommendation for future studies can be divided in the following categories:

- The thixotropic mixer can be useful for fabrication of various metal composites, but the new version and development are essential. The new design in the shape of thixomixer must be implemented with focusing on low iron contamination during mixing, low porosity content and continuous production. The big problem regarding all mechanical mixing is air entrapment and pores formation in the matrix. The air can be arrested between fiber filaments and released by dispersion into the matrix, so it must be noted in designing of new mixer.

- Thixomixing can be proposed to fabricate aluminum metal composite reinforced by SiC, SiO_2 and alumina powder. As it was demonstrated, the soft and more fragile reinforcement such as alumina fiber (Appendix B) needs more attention against of cracking, such as controlled shearing force or slurry with low solid fraction or lower viscosity.

- This process can be proposed to fabricate the other type of metal matrix such as magnesium or even the slurries of ceramics or polymeer based materials. The potential ability of thixomixing can be utilized for effective dispersion of reinforcement in the form of particles, whiskers or mono-filaments.

- The global mechanical properties includes, tensile strength, fatigue and impact resistance requires the improvement to reach theoretical levels for aluminum/C_{sf} composite. Obviously, prior this promoting the new version of thixomixing process that overcame on the present problems is necessary.

Appendix A

Appendix A. Dies of Extrusion and Thixomixer

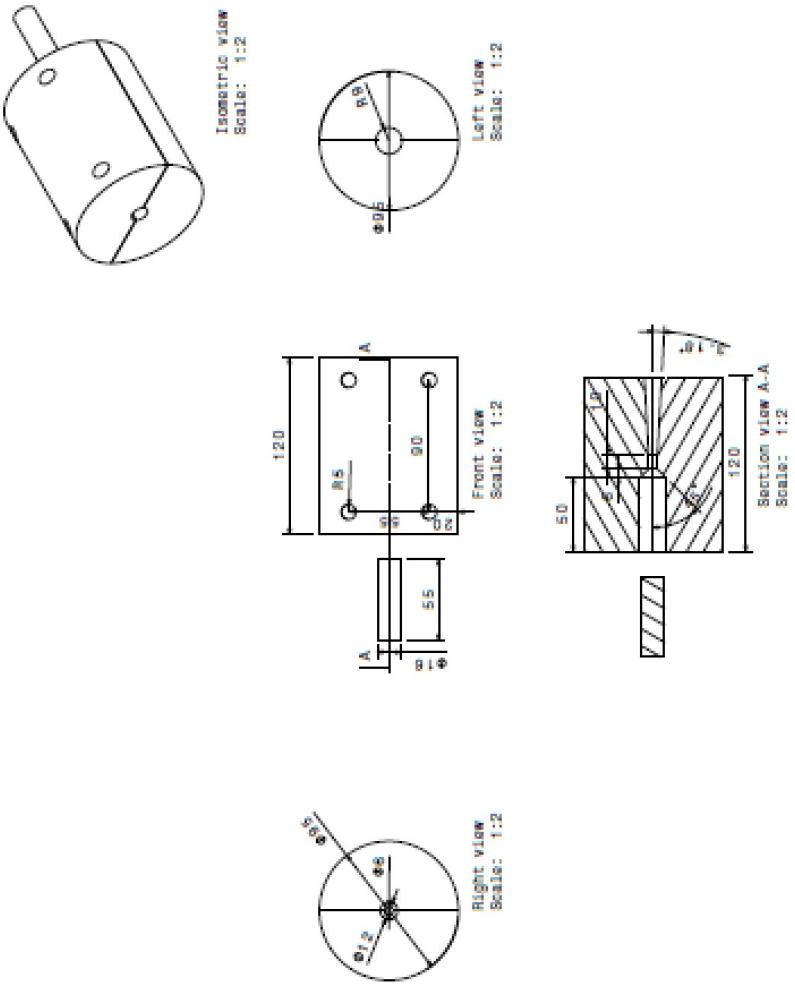

FIGURE A.1: Extrusion die

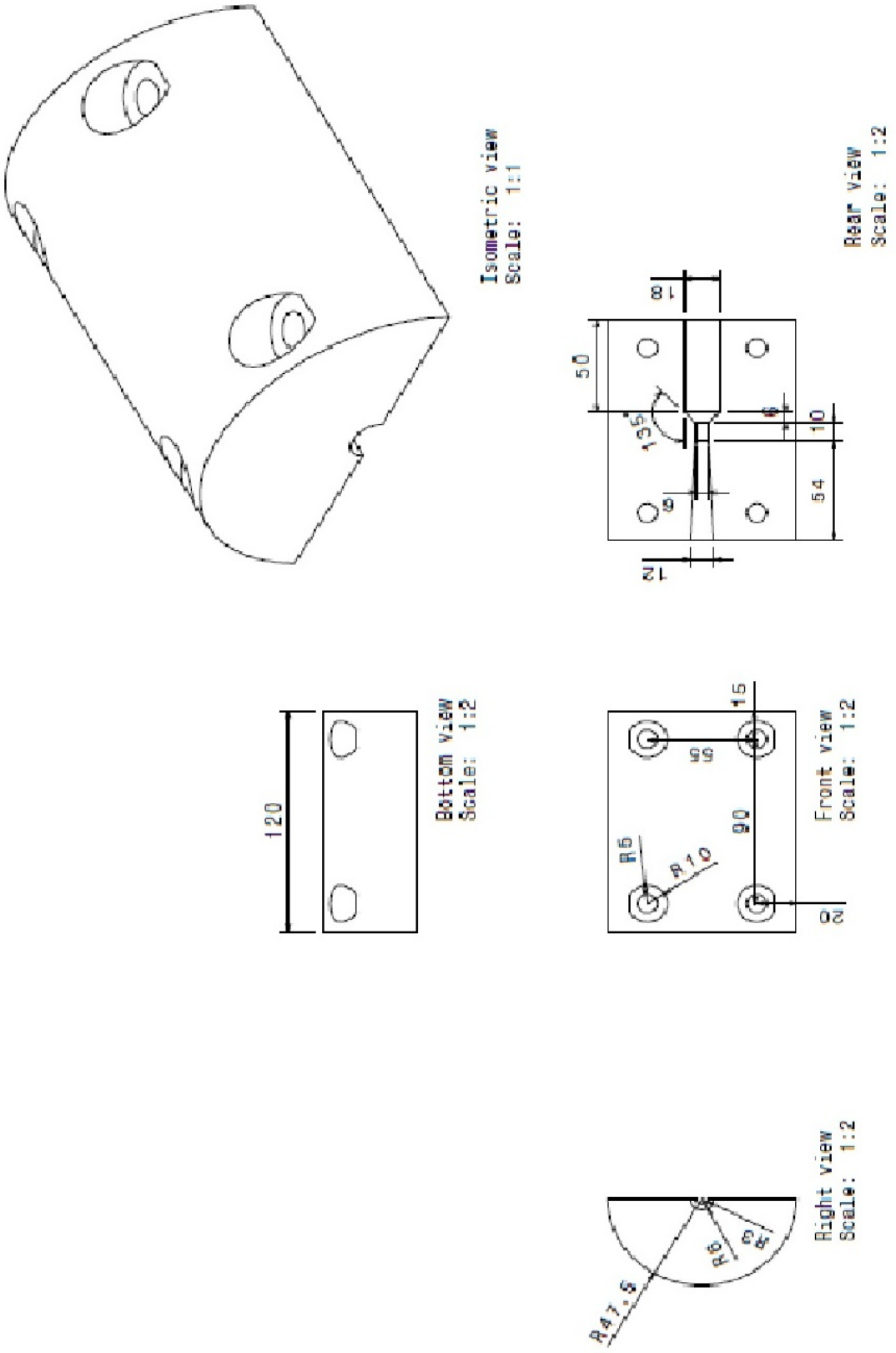

FIGURE A.2: Extrusion die

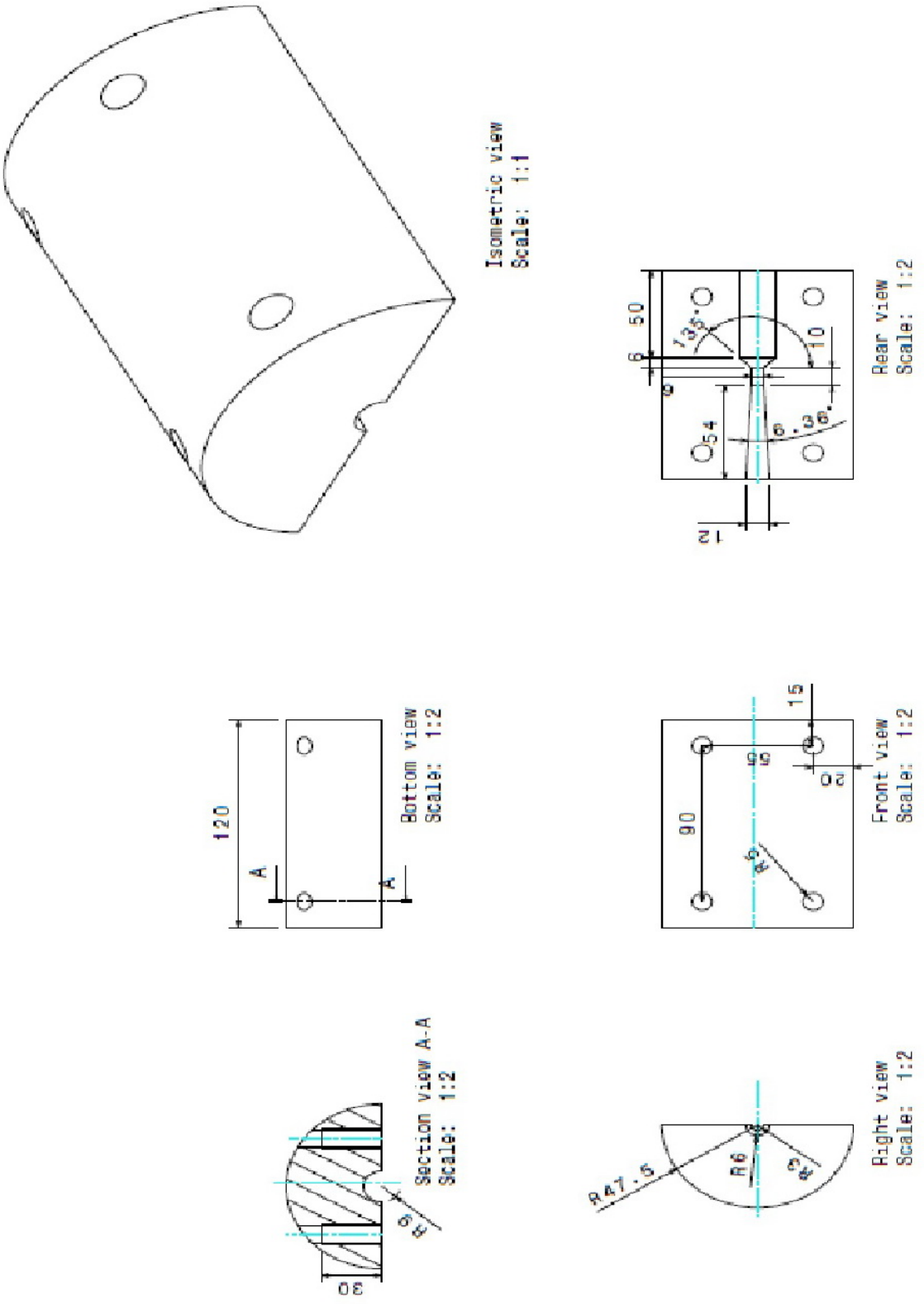

FIGURE A.3: Extrusion die

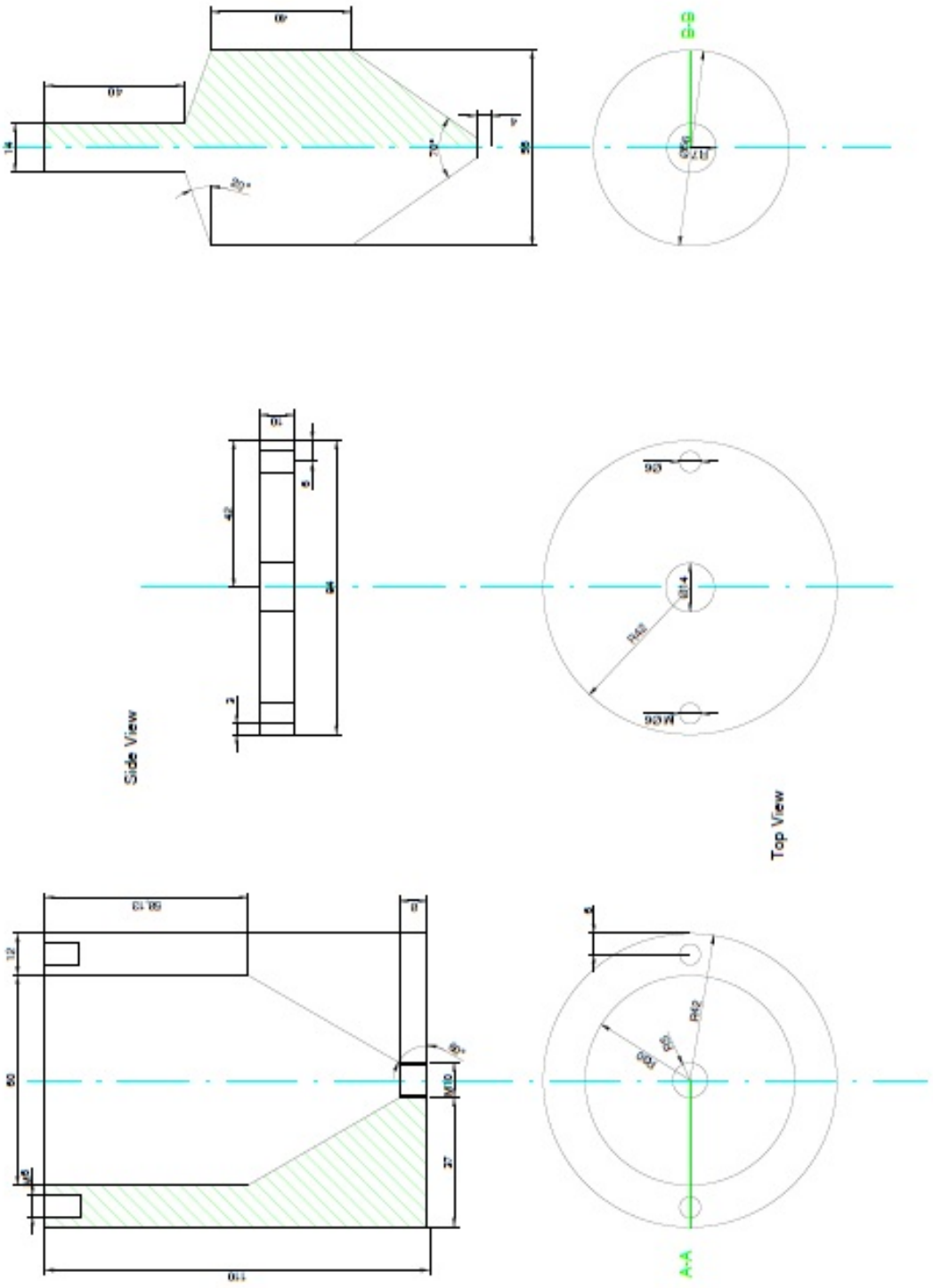

FIGURE A.4: Thixomixer Die

Appendix B

Appendix B. Thixomixing on Alumina short Fibers

The alumina fiber is more fragile than carbon fiber and it was shown in Figure B.1 that the filaments of alumina fibers have been broken by high intensive shearing loads and were converted to the small particles of alumina distributed in the matrix. The fragility

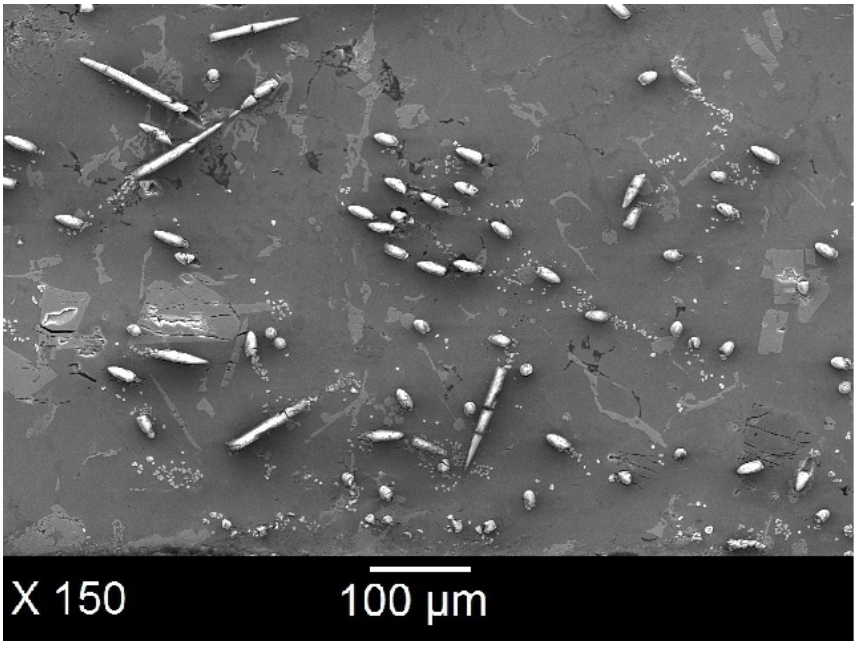

FIGURE B.1: SEM micrograph of A357/alumina short fiber composite by thixomixing

of alumina fiber was observed in Figure B.2 clearly and shows that the thixomixing with high shearing is not sufficient for distribution of fragile fibers or particles and it needs

to maintain for each type of reinforcement. Actually, the thixomixer have been used in this study was specifically designed for the carbon fibers.

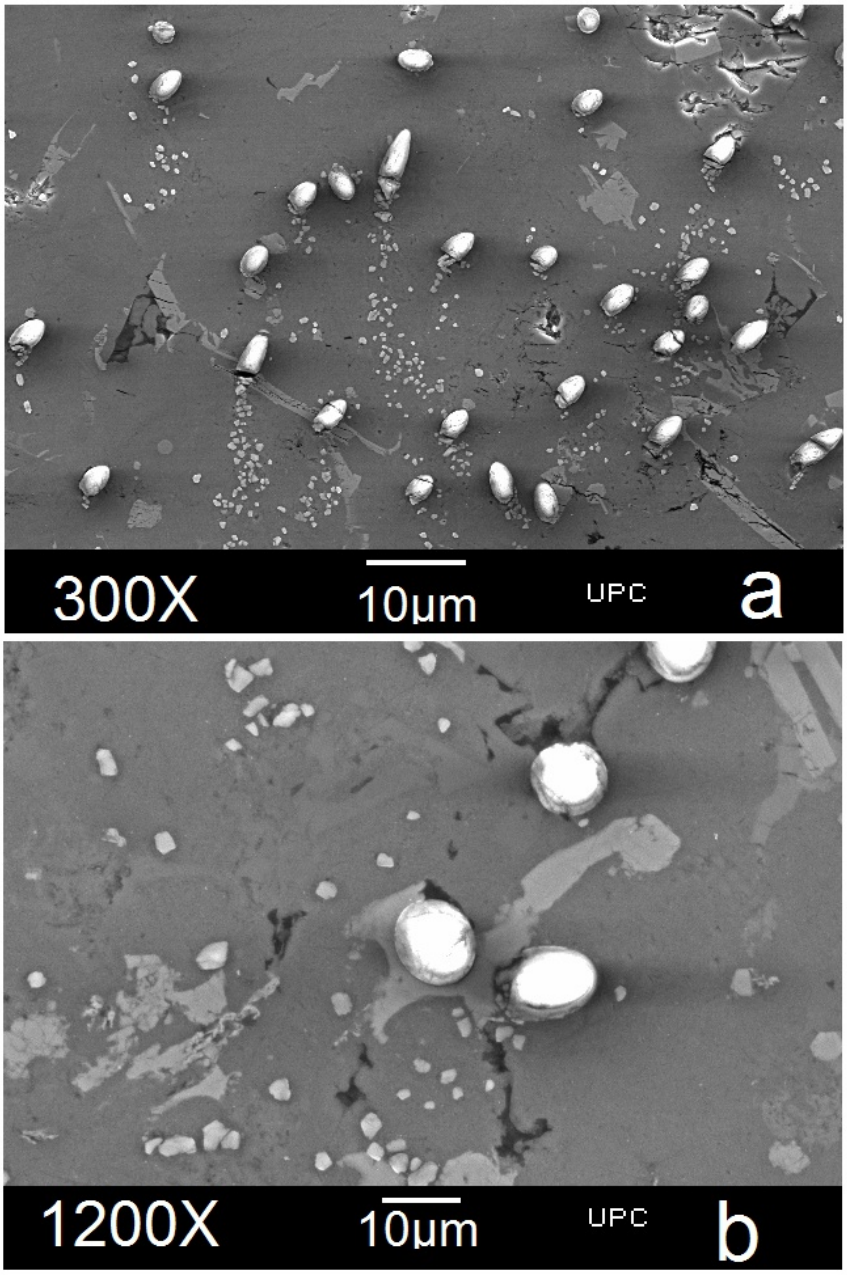

FIGURE B.2: Microstructure of successful A357/alumina short fiber composite showing breakage of alumina fiber in aluminum matrix (a) ×300 (b) ×1200

Appendix C

Appendix C. Equal Channel Angular Pressing (ECAP) on A357/C_{sf} Composite

C.1 Sever Plastic Deformation (SPD) & ECAP Processing

Sever plastic deformation (SPD) processes referred to a group of metalworking techniques in which a very large plastic strain or deformation by high shearing or complex stress mechanisms are imposed on a bulk material. As results, a refined structure is reformed by high density of defects and ultrafine equiaxed grains of metal are created which have grain size $d < 500$ nm or nano-crystalline. The refined grain size materials show high mechanical strength [Meyers et al., 2006].

The traditional forming processes such as rolling, forging or extrusion a plastic deformation rate is less than 2 but if the plastic deformation is repeated the rate can be more than 2. The SPD are referred to the processes those impose a much greater strain on a metal without causing dimensional changes. Currently, there are a number of processes described in the literatures:

- Pressure / channel angular extrusion with constant section (ECAP / ECAE)
- High pressure torsion (HPT)
- Mechanical milling (MM)
- Rebar and wire drawing repetitive (RCS)
- Deformation by severe twist (STS)
- Cyclic extrusion compression (CEC)
- Forging closed cyclic matrix (CCDF)

One of the main processes of severe plastic deformation is ECAP which has been widely studied for the production of metals generally ultrafine structure with an average grain size less than 500 nm. The severe plastic deformation methods must meet a series of requirements that must be taken into consideration to develop materials with nanocrystalline structures. These requirements are as follows:

- To change a significant impact on materials properties, it is necessary to obtain ultrafine grain structures with a predominance of grain boundaries with high angle of disorientation.
- The uniform ultrafine structure in the entire processed sample is required to provide stable properties.
- The samples shall show no mechanical damage or cracks even though intense plastic deformation.

C.1.1 Equal Channel Angular Pressing (ECAP)

Equal channel angular pressing, ECAP was first innovated in the 1970s, to press a metal billet through an angled channel as shown schematically in Figure C.1 and deforming of the material by simple shear. An intensive plastic deformation is subjected to the material without any change in the cross-sectional dimension of the sample while the

angle in the channel effects on the strain level. The ECAP process can be involved several times of passing on a sample of material to obtain high total strain. The lower angle causes increasing the strain and the homogeneity of strain distribution. The repetitive pressings on the same sample can be performed since the cross-sectional dimensions unchanged to achieve high total strain and grain refinement caused of the strain hardening. The most important role of ECAP is that it refines the grain size of a polycrystalline material to a sub-micrometer or nano-meter scale [Chen et al., 2005].

The ECAP processed materials show a very fine microstructure with unique mechanical properties such as high yield stresses, low strain hardening and good ductility or high super-plasticity at high temperatures. To perform the ECAP process, the sample must

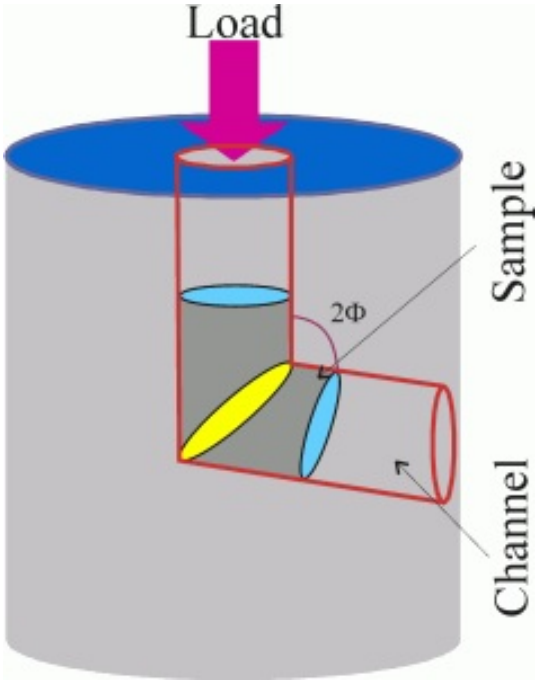

FIGURE C.1: Schematic illustration of ECAP process

be lubricated and placed into the first channel then pressed by a punch forced by high pressure hydraulic piston and extrude the sample to the second channel as illustrated in Figure C.1. When the sample pass through the first channel up to the intersection plane of the channels acts as a rigid material but it deformed plastically by simple shear where passing through the second channel. The deformation is concentrated at the intersection of the channels in a plane coincident or layer by layer extrusion and all the material is subjected to a uniform plastic deformation except at the ends. To achieve high levels

of deformation or high total strain, the ECAP process can be carried out repeatedly by different routs as schematically shown in Figure C.2. There are the possibility to rotate the according to its symmetry axis in order to alter the final structure obtained after each pass. Each pass rout gives different microstructure or even final mechanical properties to the processed sample by activate different slip systems.

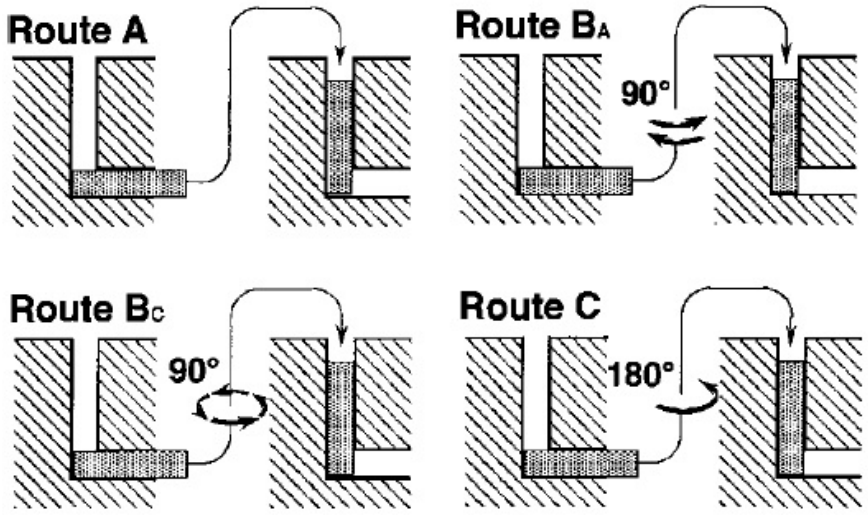

FIGURE C.2: The four main routs which utilized for ECAP processing [Segal, 2002]

This process may repeat several times to achieve optimum results with changing the orientation of billet after each pass for a uniform shear stress. Increasing of strain level needs higher press pressure. There are four fundamental routs for repetitive pressing steps of ECAP namely as A, B_A, B_C and C. Rout Bc is common and most effective for microstructural refinement when the die has channel's angle = 90° [Stolyarov et al., 2001] but is less effective for redistribution of particles [Garcia-Infanta et al., 2008]. The ECAP has been investigated as significant impact on microstructural refinement and the fragmentation and distribution of reinforcement particles [Bian et al., 2011].

The main goal of this part of study is to find out the effect of ECAP processing on refining of grain size of polycrystalline of aluminum matrix, the porosity and the interfacial carbon/aluminum adherence. As described in the literatures, the ECAP change the grain size to sub-micrometer or even to nano scale and homogenous distribution of particles in metal composite fabricated by casting methods [Sabirov et al., 2005].

In general, the materials processed by ECAP have high yield stresses and super plasticity over very small grain size at high temperatures [Cabrera and Barcaldo, 2008]. This process helps a sample gains high total strain on the same cross-section throughout the all pressing passes which repeated sequentially through the ECAP channel. There are few study have been carried out to investigate the ECAP routs on reinforced metal composite. The significant impact of ECAP on microstructural refinement and the fragment and redistribution of reinforced particles have been conducted [Bian et al., 2011].

In this study, the route BC was employed to process thixo-mixed A357/4.1 vol.% C_{sf} composite to refine the microstructure and remove the pores and modifies the distribution of C_{sf}, in order to improve the tensile mechanical properties of the composites and investigate both the benefits and drawbacks of ECAP processing for this material. Four passes, as a complete processing cycle for route BC were performed.

C.2 Experimental Method

The ECAP is a processing technique provides very fine grain size in order to have unique mechanical properties such as high yield stress [Langdon, 2007, Ramu and Ranjit, 2009]. Although interesting and considerable emphasis on these mechanical properties, just a limited number of studies have been performed by ECAP on composite materials to having ultrafine-grained metal matrix. This process was selected to evaluate the effect of severe plastic deformation techniques such as ECAP on the carbon fiber, the matrix/fiber interface and the matrix morphology.

Thixomixed A357/C_{sf} composite and thixomixed A357 (without reinforcement) samples were casted to form billets with appropriate diameter for ECAP processing. The samples were subjected to study the effect of sever plastic deformation on strength, microstructural characterization and the interfacial adherence. All ECAP samples had diameters of 60 mm and the lengths of 10 mm and their surfaces were polished before the ECAP processing. The pressing process was carried out for a series of five passes using a MoS_2 lubricant to reduce friction between internal die wall and sample with a pressing speed of 2 $mm.s^{-1}$. The temperature of process was chosen at 400 °C as high

as possible to reduce the deleterious impacts on C_{sf}. The experimental parameters of ECAP process have been extracted from the previous attempts and the conditions of fabricated composite.

For all samples route BC were used which means that the rods rotated in one direction either clockwise or anti clockwise around their longitudinal axes by 90° after each successive consecutive pass. The different samples were taken after 1, 2, 3, 4 and 5 passes to evaluate the mechanical and microstructural characterization. A pressing machine with variable speed traveling equipped with an oven as shown in Figure C.3. The die for ECAP processing was designed as channel with 10 mm diameter and the angle between the ECAP channels is 90° and the outer are of curvature where the two channels intersect was 20°.

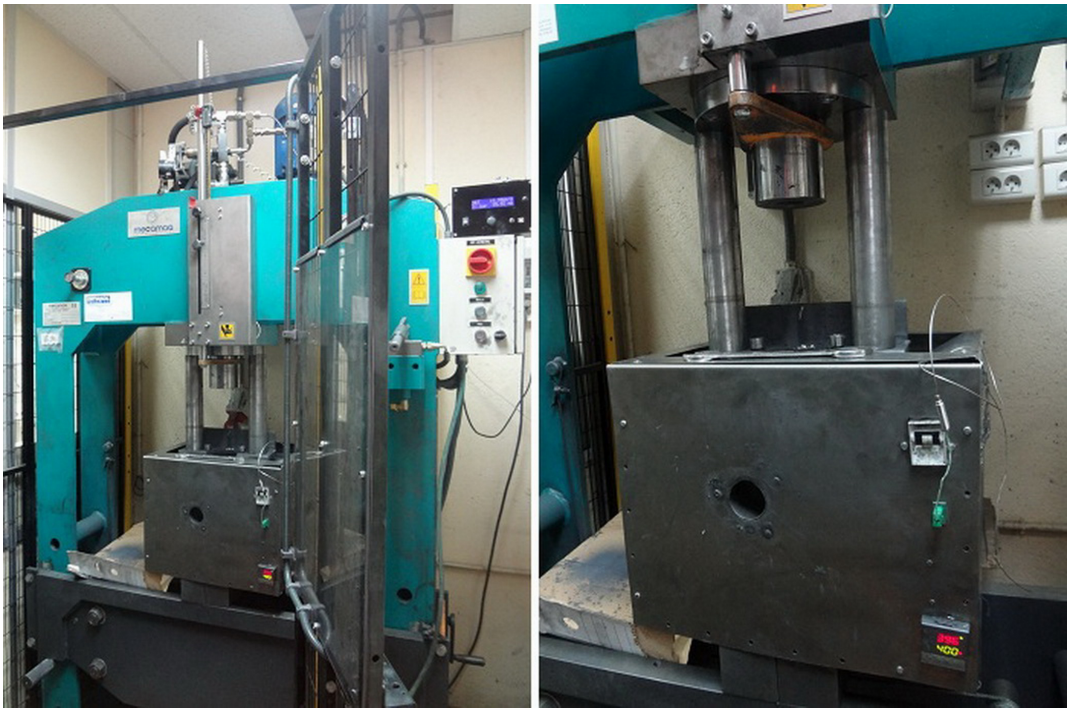

FIGURE C.3: A pressing machine with an ECAP die

C.2.1 Micro-Tensile Test

The micro-tensile test was carried out for un-reinforced A357 matrix alloy (without C_{sf} and after thixomixing) before ECAP pressing and A357/C_{sf} composite alloy before and

after ECAP processing at consecutive passes. The specimens for this type of tensile test examination must be cut by cutting technique electrical wire with a gauge length design 3 mm per 1 mm thick. The shape and dimensional values (thickness, width and gauge length) as illustrated in Figure C.4.

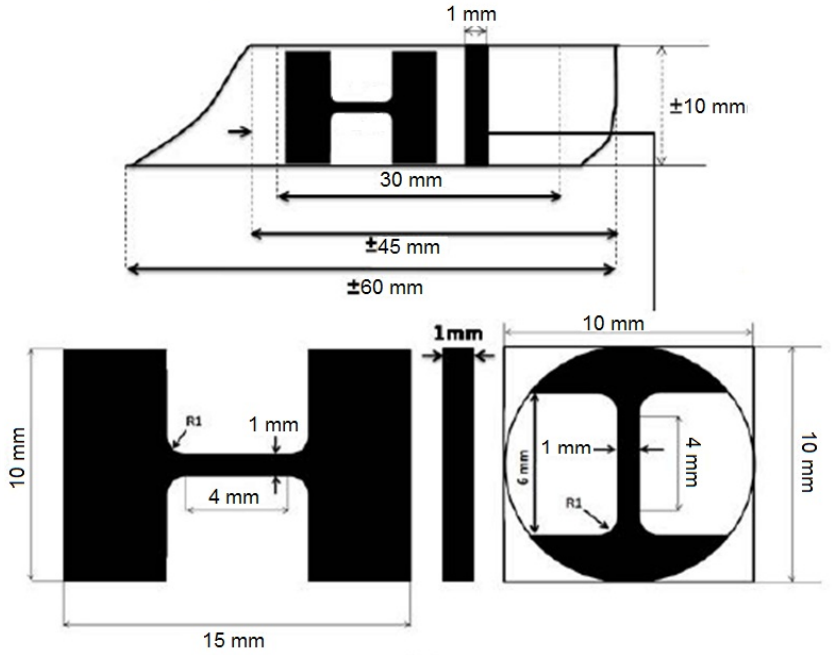

FIGURE C.4: Schematic of specimens for micro-tensile test with its dimensions

In this study, the samples for micro-tensile test evaluation were prepared from the post-ECAP billets which were parallel to the pressing axis according to ASTM D1708. This testing process were conducted at room temperature by using a servo hydraulic MTS machine (Microtest 5 kN), equipped with a TestStar IIs controller. All of the tensile tests were examined under an axial displacement control with a control shift jaws 0.2 mm.min^{-1} an initial strain rate of 5×10^{-3} s^{-1}. The machine also equipped with anchoring system such as jaws to ensure the correct positioning and prevents the sliding problems while the test is running.

Before starting the machine, it is necessary to set the force and displacement parameters of machine at 0 and be sure the specimen was adjusted correctly. After start running the two jaws will take distance to each other at controlled speed as mentioned above and the extensometer records the displacements. The data of force and displacement provided in the software of machine can be extracted to a Excel spreadsheet file with

the values of initial section dimensions and the length to calculate the engineering stress and strain to plot them for visual illustration. The correct stress-strain flow curves has been ensured for the accuracy and examined by mathematical analysis.

C.2.2 Analysis of Physical Properties of Samples after ECAP Processing

C.2.2.1 Evaluation of Porosity

Archimedes' principle was conducted to measure density and porosity of ECAP processed on A357/C_{sf} composite with 4.1 vol.% of reinforcement and A357 alloy thixomixed without fiber. The percentage of porosity is comparison between the measured value of density and the theoretical density which was calculated by the rule of mixture.

One of the objects to perform ECAP process is to study the porosity contents before and after plastic deformation during thixomixing a lot of micro-pores and air bubbles arrested in the matrix, as it mentioned and discussed previously (section 4.1.5). Long time of stirring, increasing of reinforcement content in composite and temperature are as the potential factors to increase porosity in all compo-casting methods which employ stirring.

The results of density and porosity were shown in Table C.1 measured before ECAP and after each pass. The values of the porosity for un-reinforced alloy were lower than those achieved from composite samples. But the same trend was followed as a reduction of porosity through the consecutive passes. Around 100% densification was obtained when the matrix alloy processed by ECAP which was occurred relatively for the A357/C_{sf} composite. The reduction of porosity content was attributed to the ECAP process and its severe plastic deformation mechanism that is created.

Densification could be due to intensive shear stress in the sample that replace the bulk layers over each other and move the pores to outer surfaces. The cracked surface as shown in Figure C.5 could be attributed to the surface tension and releasing the pores by ECAP which reduced by progressing in the steps. For the samples which contain

TABLE C.1: The results of density measurement for A357 and A357/C_{sf} composite processed by ECAP

Sample	Pass number	Measured density $g.cm^{-3}$	Theoretical density $g.cm^{-3}$	Porosity %
A357	0	2.63±0.17	2.67	1.31±1.1
	1	2.64±0.18	2.67	1.08±1.1
	2	2.65±0.20	2.67	0.60±1.2
	3	2.64±0.19	2.67	0.78±0.9
	4	2.66±0.18	2.67	0.37±1.0
	5	2.66±0.18	2.67	0.07±0.9
A357/C_{sf}	0	2.51±0.21	2.63	3.87±0.7
	1	2.56±0.19	2.63	2.66±0.8
	2	2.58±0.20	2.63	1.63±1.1
	3	2.60±0.19	2.63	0.87±1.1
	4	2.60±0.18	2.63	1.06±0.9
	5	2.62±0.19	2.63	0.27±0.9

few amount of porosity the outer cracks on the surface was lower than the samples have high amount of porosity. The surface tension caused by thermal differences between core and surface of composite samples was mentioned for the cracks on the surface of

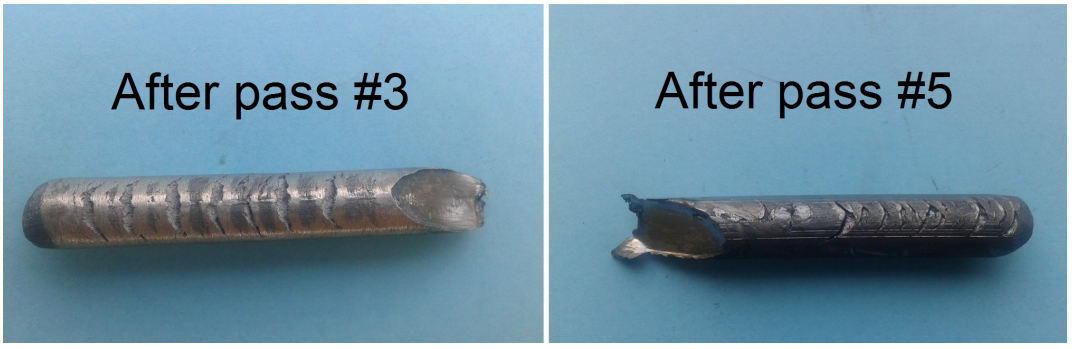

FIGURE C.5: The A357/C_{sf} composite samples after different steps of ECAP process

metal samples after ECAP [Goto et al., 2011]. Semiatin et al. have been investigated on the surface cracks formation on AISI 4340 steel during the ECAP deformation and the relationship between values of strain rate sensitivity (m) and cracks [Semiatin et al., 2000].

The metal matrix composites (MMCs) are potentially talented to surface cracking due to higher strain rate sensitivity than the base metal and deformation for the strain-hardenable materials is non-uniform. The MMCs are strain-hardenable with high value

of strain rate sensitivity (m).

Generally, the plastic deformation for most metal and metal composite is non-uniform. Non-uniform stress distribution can be main reason for this kind of crack, where the compressive stress created in the low radius curvature of two channel intersect while the front surface experiences in the high radius curvature of two channel intersect is under tensile stress. Finally, the vertical cracks from the top surface to the center of the billet were formed. The SiC-particulate reinforced Al (2024-O) metal matrix composite shows higher strain rate sensitivity than base metal that increases with increasing reinforcement contents [Tirtom et al., 2008].

C.2.2.2 Microstructural Characterization on Refined globular α-size

Microstructural characterization have been conducted for all different samples which un-processed and processed by ECAP at the sequences that mentioned previously. All morphology were analyzed from different aspects: fiber orientation and distribution, fiber situation and cracks, porosity content and interfacial condition have been investigated by scanning electron microscope (SEM) and optical microscope. For these objects, all samples belong to each set of passes of two materials were cut by cut-off wheel machine at unidirectional or perpendicular of cross section and polished gently as described in part 2-7-1.

The distribution of C_{sf} in SEM micrographs of processed composite samples in Figure C.6 is fairly uniform with good dispersion as shown for as-mixed samples with no segregation or clustering of short fibers. The random orientations of C_{sf} was changed, and re-orientated to the pressing rout like the extrusion process. The amount of porosity and the number of pores were decreased based on the comparison between the figures throughout the progressive sequences. The macro-size pores were distributed in the ax-mixed samples or that at the initial steps, but their size decrease to macro pores or removed by continuing the ECAP passes on them (Figure C.6). The micro cracks which were created at the first steps, were removed in the next passes, or in the other words the sample strengthen by ECAP process.

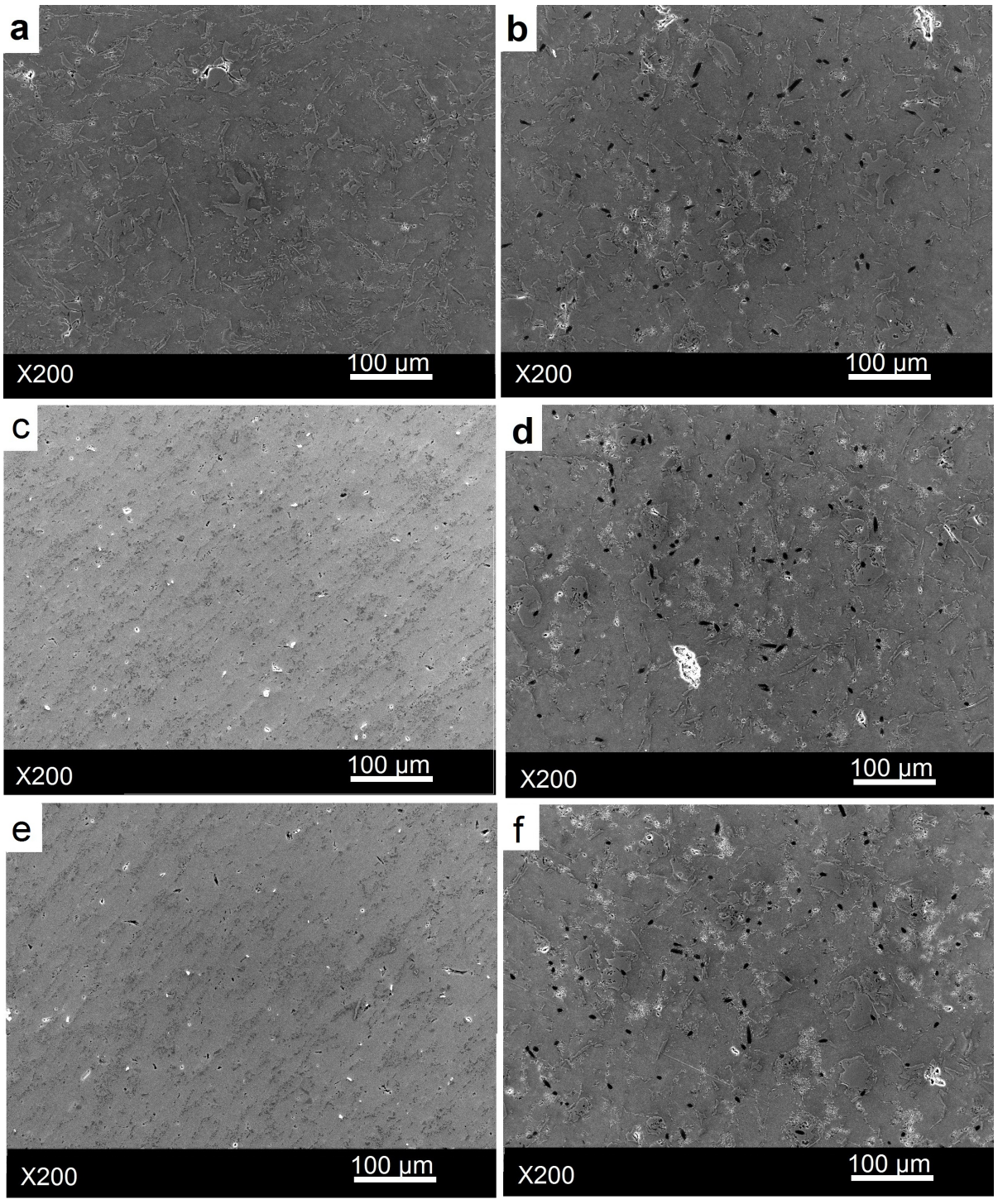

FIGURE C.6: SEM micrographs on different matrix alloy and metal composite samples unidirectional to the cross section belong to (a) A357 after 3 passes (b) A357/C_{sf} after 3 passes (c) A357 after 4 passes (d) A357/C_{sf} after 4 passes (e) A357 after 5 passes (f) A357/C_{sf} after 5 passes of ECAP processing

The interfacial bonding between the reinforcement particles and the matrix in all composite materials is a key factor to obtain good mechanical properties, whatever the matrix globular α-size refinement or mechanical strength. Figure C.7 shows the interfacial

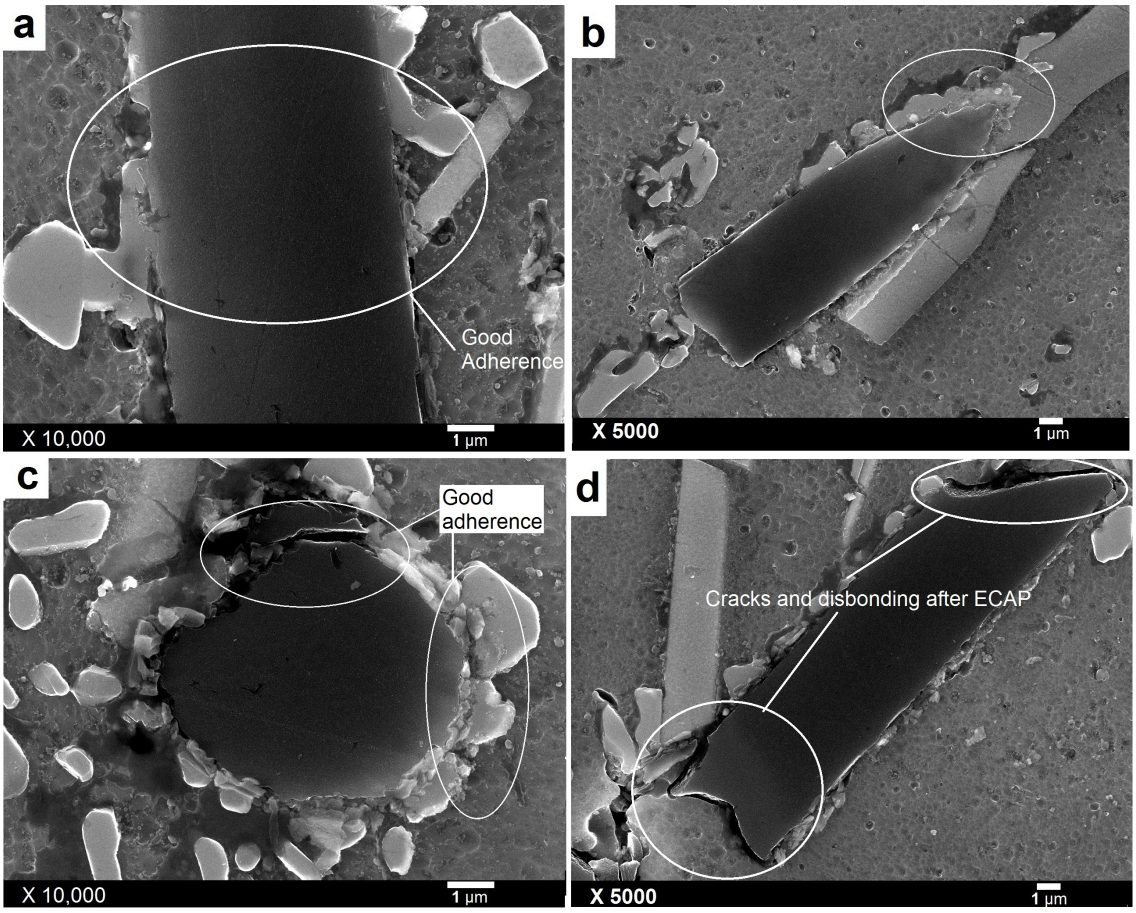

FIGURE C.7: SEM micrographs at high resolution of fiber/matrix interfacial of A357/C_{sf} composite (a) bonding remained after 1 pass of ECAP processing (b) bonding with cracks after 3 passes (c) disbonding and fiber crack after 5 passes (d) disbonding after 5 passes

bonding for different samples that the short fibers in the matrix are unidirectional or perpendicular to the ECAP direction. Fibers are so sensitive to shearing and deformation even at high temperature because most of them cracked at more steps. The bonding and adherence were lost especially after 5^{th} pass with cracks on the fibers whereas the adherence remained after the initial passes of ECAP process. Bonding and adherence are much stronger when the fibers were at the contact of Si or the intermetallics (Figure C.7a-c). The indication of suitable physical or chemical interfacial bonding to achieve a better adherence is attended.

To avoid any damaging or crack on the fibers, the processing temperature has been chosen high (400 °C) to achieve soft plastic deformation, but the majority numbers of fibers were cracked. By the increasing of ECAP temperature, dislocation density decreases significantly and mechanisms on strengthening may reduce [Shaeria et al., 2016]. Cracking may cause disbonding from matrix or produce sharp edges on the carbon fiber as crack initiation site. Figure C.7d is a good example to demonstrate high tension zone in the matrix created by sharp edges of carbon fiber which mounted in the matrix. The shorter length of C_{sf} than the critical length which discussed in the literatures [Karl, 2003]. The reduction of strength was first occurred when the fibers are shorter.

In A357/C_{sf}, the morphology of globular α-size and silicon was changed when the ECAP passes applied on the samples. The morphology of silicon particles in matrix have been reshaped and refined. In case of the composite, the internal micro-cracks starts appearing after the first ECAP pass (inset in Figure C.8), but they were removed

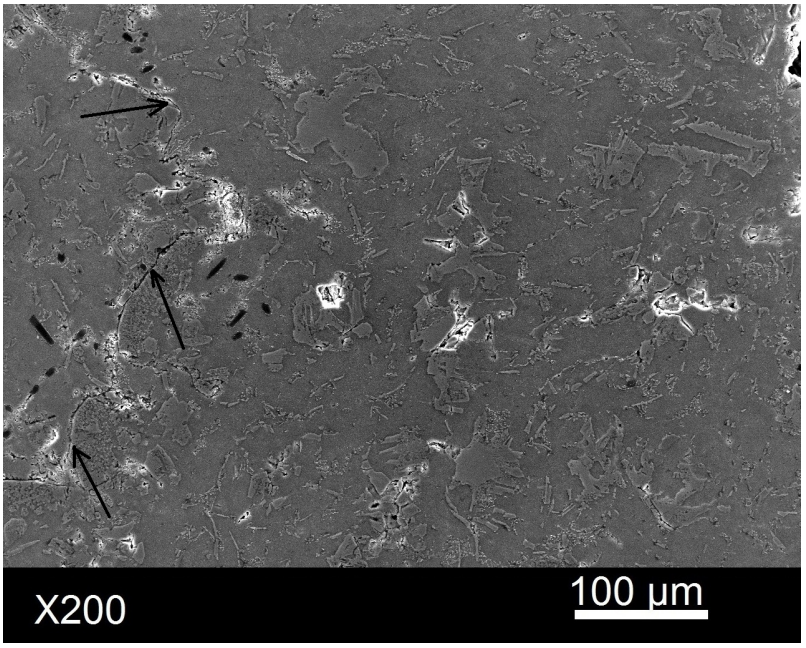

FIGURE C.8: SEM micrographs of A357/C_{sf} composite after 1 pass which showing the micro-cracks in matrix

with increasing of pass numbers. The micro-cracks develop along the boundaries α-phases also dislocation slip probably occurs in the metal crystalline structure.

The former study on composite materials have investigated and reported that intermetallic compounds and the pores plays an important role to initiate and propagate the micro-cracks in the composite samples [Ramu and Ranjit, 2009]. In the composite material, the load is transferred from matrix via the reinforcement/matrix interface to the reinforcement particles, so a appropriate bonding at the interface make it possible [Ibrahim et al., 1991].

Optical micro-graphs of the etched samples before ECAP (as-mixed) and 5^{th} pass of ECAP are shown in Fig. C.9. The α-size of matrix alloy in all samples was reduced with increasing the number of passes of each set as shown in image inset in Figure C.9. A considerable change in the size of matrix α-size after ECAP refinement was

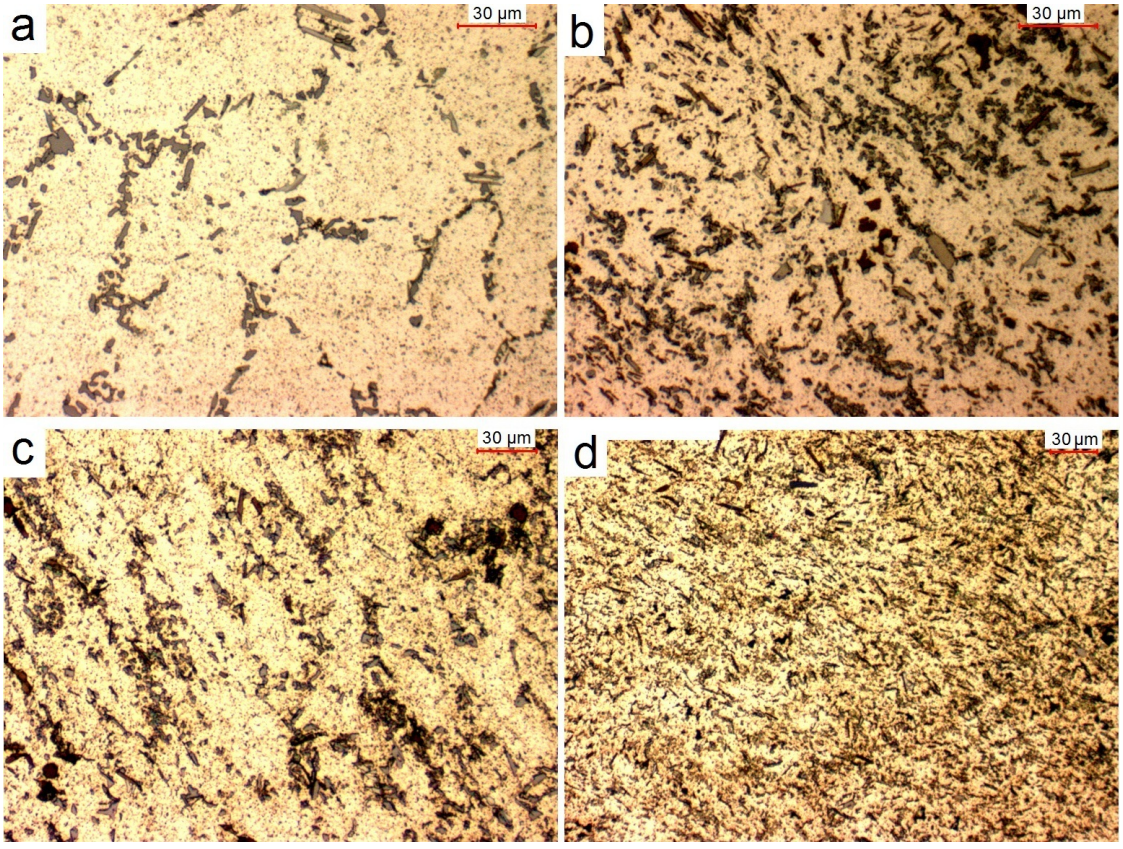

FIGURE C.9: Optical micrographs of (a) as-mixed A357 (b) A357 after 5 passes (c) as-mixed A357/C_{sf} (d) A357/C_{sf} after 5 passes after ECAP processing

observed in this figure for both matrix and the composite samples. The interesting point here is the smaller α-sizes which are refined and probably recrystallized in the case of composite [Tirtom et al., 2008]. The average α-size was determined by image analysis for as-mixed sample before ECAP was around 68 μm and 34 μm respectively for A357

and A357/C_{sf}. The grain size of both the matrix alloy and composite in 5^{th} pass was observed to be around 25 μm and 8 μm, respectively. Then, the long range of gradual hardening has been occurred when the ECAP processing was applied.

C.2.2.3 Micro-Tensile Results of ECAP Processed on Thixomixed Samples

Microtensile tests were performed on specimens machined from thixomixed samples with and without C_{sf} as reinforcement particles. The stress-strain flow curves of this test are shown in Figure C.10 for matrix alloy and composite samples after ECAP. The mechanical values such as yield stress, elongation percentage and UTS were detailed in Table C.2 for all samples. It is apparent that the composite samples were hardened and

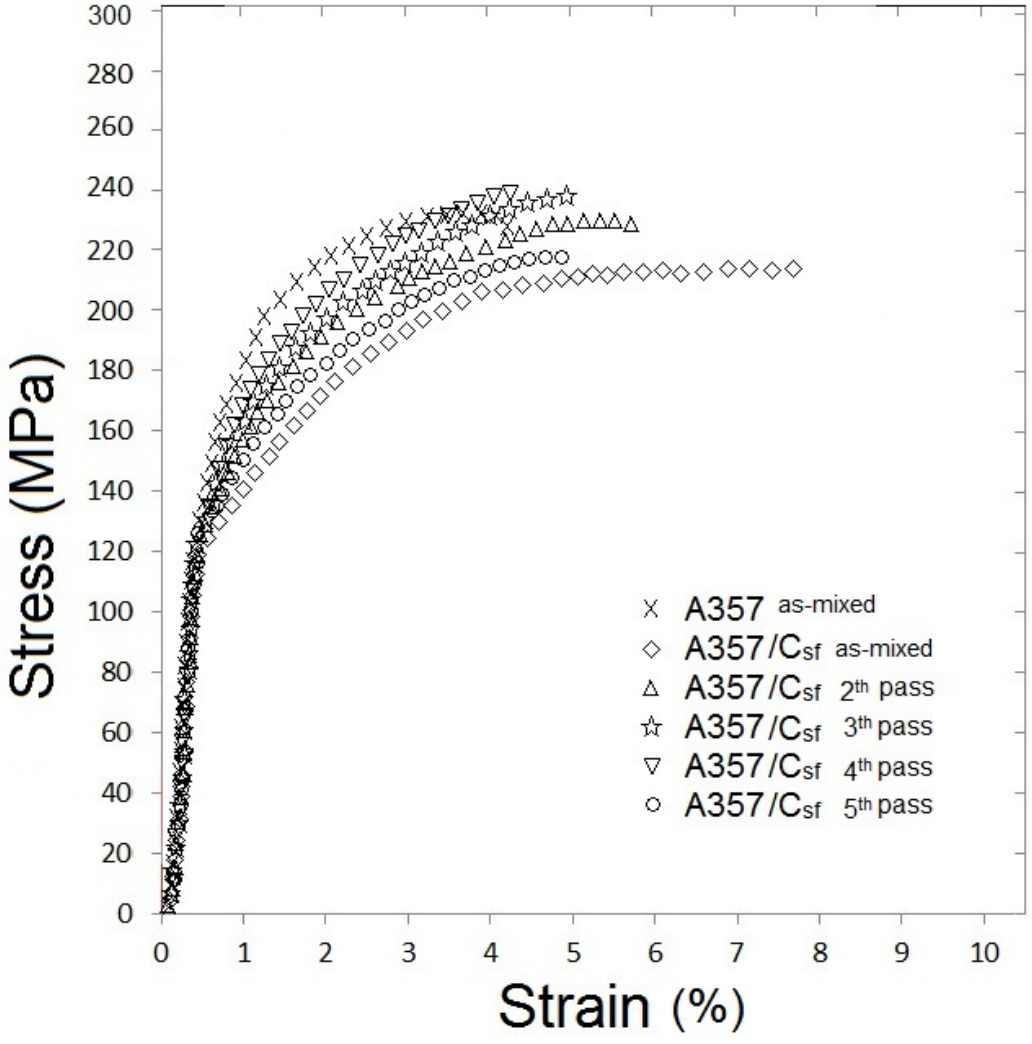

FIGURE C.10: Stress-strain flow curve of as-mixed A357 alloy and A357/C_{sf} composite after different passes of ECAP

strengthen than un-pressed sample. All samples reach to the ultimate tensile strength after relatively long rang of hardening as exhibited in flow stress curve. This implies these materials possess quasi-ductility, as reveled by the stress–strain curves in Figure C.10. Early failure of composite after 5^{th} pass may attributed to the C_{sf} fragment and disbonding from matrix under intensive plastic deformation (Figure C.7). The composite samples reinforced with fibers reveal lower mechanical improvement after ECAP process, and the sample after 5^{th} pass made of the composite material was the worst in against of others. The better mechanical properties can be detected from 4^{th} pass composite sample.

UTS increasing from 204 MPa for as-mixed to 238 for composite sample after 4^{th} corresponded to 17% can be attributed to the α-size refinement of the matrix alloy and the fragmentation and redistribution of coarse Si or intermetallic particles in the eutectic. The reduction of UTS for A357/C_{sf} related to its matrix alloy can be due to the cracks of fibers and reducing of interfacial bonding to the matrix. The yield stress was increased with increasing the number of ECAP pass, and demonstrate significant strain hardening and higher yield strength due to the high density of dislocations accumulated during pressing.

TABLE C.2: Tensile properties ofA357 alloy and A357/C_{sf} composite after different passes of ECAP

Sample	Yield stress MPa	UTS MPa	Elastic modulus GPa	Strain %
A357-as mixed	174	228	71	4.1
A357-1^{st} pass	178	233	68	3.7
A357-2^{nd} pass	171	239	66	3.3
A357-3^{rd} pass	182	244	69	3.1
A357-4^{th} pass	187	251	67	2.8
A357-5^{th} pass	195	263	69	3.2
A357/C_{sf} -as mixed	126	204	68	7.8
A357/C_{sf} -1^{st} pass	134	212	66	6.4
A357/C_{sf} -2^{nd} pass	146	221	65	5.7
A357/C_{sf} -3^{rd} pass	145	236	67	5.1
A357/C_{sf} -4^{th} pass	157	238	68	4.3
A357/C_{sf} -5^{th} pass	137	216	70	4.8

But ductility of un-processed samples was decreased when ECAP processing have been applied on the composite sample. This reduction in ductility is typical for the materials processed using ECAP due to increasing of the strain hardening [Bian et al., 2011]. This was pertained to the fragment of C_{sf} into the matrix. When the fibers are cracked, It is possible to see more crack initiation sites formed in the composite and also the load transferring due to lower critical fiber length was declined.

In this case and with the obtained results, the plastic deformation cannot be an effective rout to increase global mechanical properties of composite aluminum reinforced with C_{sf} because the undesirable fragment of fragile fibers and losing interfacial bonding at the matrix/fiber interface. The improvement which achieved by ECAP process was related to the reduction of porosity and grain refinement of matrix. The porosity content that arrested in the matrix as potential sites for crack initiation and weakening. The ECAP process was not effective in the case of Aluminum/C_{sf}, mainly due to the undesirable fiber cracking.

C.2.3 Conclusion

As a conclusion, the ECAP process has not great impact to improve tensile strength of composite even though the strain hardening has been effected. ECAP processing has been carried out on the A357/C_{sf} composite and it was revealed a considerable impact on the porosity content after thixomixing. The plastic deformation can remove markedly the pores that arrested into the matrix during mixing in semi-solid state. The severe plastic deformation such as ECAP shown a bad effect on the fragile fiber reinforcements and reduce their interfacial bonding especially on high total strain or more consecutive steps. The silicon or other desirable intermetallics which lead to good bonding between aluminum matrix and the surface of carbon fiber in the thixomixing process, which has been fragmented and redistributed into the matrix. So, the ECAP was demonstrated as low efficient process on aluminum composite reinforced with C_{sf} due to its deleterious impacts on fibers and the interfacial bonding. Weak bonding or cracked fibers could be crack initiation sites and of course cannot play as load transferring element in the composite.

The analysis of fracture surface expressed a quasi-ductile deformation for composite samples. The big dimples with no fiber pull out were demonstrated for most of samples at initial steps of pressing but the dimple size was decreased by more plastic deformation. The ECAP process was affected on matrix alloy but as overall impact on composite was not more effective to reveal better mechanical properties. The effects of ECAP process by BC rout were investigated on structural refinement and the tensile strength of global mechanical properties of aluminum/C_{sf} composite. The UTS of composite samples was increasing for the samples after different consecutive passes, but it was decreased at 5^{th} pass of ECAP processing due to the fragment of fibers.

The hardness values were achieved for composite sample higher than the matrix alloy after different implemented ECAP passes. Although the hardness of matrix alloy was lower than composite, then a considerable enhancement was detected by increasing the number of steps as shown in the results. The adherence evaluation by nano-indentation as a semi-qualitative was shown a weak bonding at matrix/fiber interface for composite samples processed with high strain level by ECAP (at 5^{th}). The severe plastic deformation such as ECAP cannot promote the mechanical properties of aluminum/C_{sf} composite especially at high total strain level, although it can be proposed to reduce the porosity with few steps or lower total strain.

Bibliography

Abbasipour, B., Niroumand, B. and Monir Vaghefi, S. M. [2010], 'Compocasting of a356-cnt composite', *Transactions of Nonferrous Metals Society of China* **20**(9), 1561–1566.

Abouei, V., Saghafian, H., Shabestari, S. G. and Zargham, M. [2010], 'Effect of fe-rich intermetallics on the wear behavior of eutectic al–si piston alloy (lm13)', *Materials & Design* **31**(7), 3518–3524.

Abouei, V., Shabestari, S. G. and Saghafian, H. [2010], 'Dry sliding wear behaviour of hypereutectic al-si piston alloys containing iron-rich intermetallics', *Materials Characterization* **61**(11), 1089–1096.

Adamiak, M. [2008], 'Mechanical alloying for fabrication of aluminium matrix composite powders with ti-al intermetallics reinforcemen', *Journal of Achievements in Materials and Manufacturing Engineering* **31**(2), 191–196.

Agarwal, B. D., Broutman, L. J. and Chandrashekhara, K. [2006], *Analysis and Performance of Fiber Composites,*, 3rd edition edn, John Wiley & Sons, New York, NY.

Akbarzadeh, E., Picas, J. A. and Baile, M. T. [2015*a*], 'Microstructure and properties of aluminum silicon/short fibre carbon composites fabricated by semi-solid thixomixing', *Materials and Design* **88**, 683–692.

Akbarzadeh, E., Picas, J. A. and Baile, M. T. [2015*b*], 'Orthogonal experimental design applied for wear characterization of aluminum/csf metal composite fabricated by the thixomixing method', *International Journal of Material Forming* pp. 1–12.

Alexandrou, A. N. [2008], On the modeling of semisolid suspensions, *in* '10th International Conference on Semi-Solid Processing of Alloy and Composites, S2P 2008', Vol. 141-143 of *Semi-Solid Processing of Alloys and Composites 10 - Selected, peer reviewed papers from the 10th International Conference on Semi-Solid Processing of Alloy and Composites, S2P 2008*, pp. 17–23.

Aluminum, A. [2008], 'Standards for aluminum sand and permanent mold castings', Washington D.C. : Aluminum Association, 15th Edition.

Amateau, M. F. [1976], 'Progress in the development of graphite- aluminum composites using liquid infiltration technology', *Journal of Composite Materials* **10**(4), 279–296.

Anon [1969], 'Carbon fibre composite materials', *Plast Aust* **20**(7), 15–18.

Arrabal, R., Mingo, B., Pardo, A., Mohedano, M., Matykina, E. and Rodríguez, I. [2013], 'Pitting corrosion of rheocast a356 aluminium alloy in 3.5wt.% nacl solution', *Corrosion Science* **73**(0), 342–355.

Arsenault, R. J., Wang, L. and Feng, C. R. [1991], 'Strengthening of composites due to microstructural changes in the matrix', *Acta Metallurgica et Materialia* **39**(1), 47–57.

Atkinson, H. V. [2005], 'Modelling the semisolid processing of metallic alloys', *Progress in Materials Science* **50**(3), 341–412.

Aykut, Y., Pourdeyhimi, B. and Khan, S. A. [2013], 'Catalytic graphitization and formation of macroporous-activated carbon nanofibers from salt-induced and h2s-treated polyacrylonitrile', *Journal of Materials Science* **48**(22), 7783–7790.

Baker, A. A. [1975], 'Carbon fibre reinforced metals - a review of the current technology', *Materials Science and Engineering* **17**(2), 177–208.

Baker, A. A., Braddick, D. M. and Jackson, P. W. [1972], 'Fatigue of boron-aluminium and carbon-aluminium fibre composites', *Journal of Materials Science* **7**(7), 747–762.

Baker, A. A., Shipman, M. C., Cripwell, P. A. and Jackson, P. W. [1972], 'Oxidation of aluminium-coated carbon fibres and carbon-aluminium composites', *Fibre Science and Technology* **5**(4), 285–302.

Bakshi, S. R., Lahiri, D. and Agarwal, A. [2010], 'Carbon nanotube reinforced metal matrix composites - a review', *International Materials Reviews* **55**(1), 41–64.

Barman, N. and Dutta, P. [2008], Rheological behavior of semi-solid slurry of a356 alloy at high shear and cooling rates, Vol. 141-143 of *Semi-Solid Processing of Alloys and Composites 10 - Selected, peer reviewed papers from the 10th International Conference on Semi-Solid Processing of Alloy and Composites, S2P 2008*, Aachen, pp. 409–414.

Bastidas, J., Forn, A., Torres, C., Baile, M. and Polo, J. [2001], 'Pitting corrosion of a357 aluminium alloy obtained by semisolid processing', *Materials Corrosion* **52**, 691–696.

Baumli, P., Sychev, J., Budai, I., Szabo, J. T. and Kaptay, G. [2013], 'Fabrication of carbon fiber reinforced aluminum matrix composites via a titanium-ion containing flux', *Composites Part A: Applied Science and Manufacturing* **44**(1), 47–50.

Bhav Singh, B. and Balasubramanian, M. [2009], 'Processing and properties of copper-coated carbon fibre reinforced aluminium alloy composites', *Journal of Materials Processing Technology* **209**(4), 2104–2110.

Bian, L., Liang, W., Xie, G., Zhang, W. and Xue, J. [2011], 'Enhanced ductility in an al-mg2si in situ composite processed by ecap using a modified bc route', *Materials Science and Engineering A* **528**(9), 3463–3467.

Blucher, J. T., Narusawa, U., Katsumata, M. and Nemeth, A. [2001], 'Continuous manufacturing of fiber-reinforced metal matrix composite wires — technology and product characteristics', *Composites Part A: Applied Science and Manufacturing* **32**(12), 1759–1766.

Botelho, E. C., Silva, R. A., Pardini, L. C. and Rezende, M. C. [2006], 'A review on the development and properties of continuous fiber/epoxy/aluminum hybrid composites for aircraft structures', *Materials Research* **9**(3), 247–256.

Brown, M., Hayes, P. and Prangnell, P. [2002], 'Characterisation of thin silica films deposited on carbon fibre by an atmospheric pressure non-equilibrium plasma (apnep)', *Composites Part A: Applied Science and Manufacturing* **33**(10), 1403–1408.

Burgos, G. R., Alexandrou, A. N. and Entov, V. [2001], 'Thixotropic rheology of semisolid metal suspensions', *Journal of Materials Processing Technology* **110**(2), 164–176.

Burkanudeen, A., Krishnan, G. S. and Murali, N. [2013], 'Thermal behavior of carbon fiber precursor polymers with different stereoregularities', *Journal of Thermal Analysis and Calorimetry* **112**(3), 1261–1268.

Cabrera, J. M. and Barcaldo, R. R. [2008], Obtencion de materiales metalicos de tamano de grano ultrafino, *in* 'Scientia et Technica Ano XIV', Vol. 38.

Calcom, S. A. [1997], 'Implementation of a new non-newtonian model for thixocasting in procast', *Lausanne: CTI Report Project n.2942.1* .

Chawla, K. [2012], *Metal Matrix Composites*, Springer New York, chapter 6, pp. 197–248.

Che, D. H., Yao, G. C., Hua, Z. S. and Zhang, X. [2011], 'Improvement of dispersibility of short carbon fibers by hydroxyethl cellulose(hec)', *Dongbei Daxue Xuebao/Journal of Northeastern University* **32**(9), 1286–1290.

Chen, H. and Alpas, A. T. [1996], 'Wear of aluminium matrix composites reinforced with nickel-coated carbon fibres', *Wear* **192**(1–2), 186–198.

Chen, L. J., Ma, C. Y., Stoica, G. M., Liaw, P. K., Xu, C. L. and Langdon, T. G. [2005], 'Mechanical behavior of a 6061 al alloy and an al2o3/6061 al composite after equal-channel angular processing', *Materials Science and Engineering A* **410-411**, 472–475.

Cheng, H. M., Lin, Z. H., Zhou, B. L., Zhen, Z. G., Kobayashi, K. and Uchiyama, Y. [1993], 'Preparation of carbon fibre reinforced aluminium via ultrasonic liquid infiltration technique', *Materials Science and Technology* **9**(7), 609–614.

Clyne, T. W. and Withers, P. J. [1993], *An Introduction to Metal Matrix Composites*, Cambridge University Press, Cambridge.

Daoud, A. [2004], 'Wear performance of 2014 al alloy reinforced with continuous carbon fibers manufactured by gas pressure infiltration', *Materials Letters* **58**(25), 3206–3213.

Davis, J. R. [2001], *Surface Engineering for Corrosion and Wear Resistance*, ASM International, Materials Park, OH.

Diefendorf, R. J. [1987], *Engineered Materials Handbook*, Vol. 1 of *Composites*, ASM International, Metals Park.

Du, J., Liu, Y., Yu, S. and Dai, H. [2003], 'Effect of fibre-orientation on friction andwear properties of al2o3 and carbon short fibres reinforced alsi12cumgni hybrid composites', *Wear* **254**, 164–172.

Es-Said, O., Lee, D., Pfost, W., Thompson, D., Patterson, M., Foyos, J. and Marloth, R. [2002], 'Alternative heat treatments for a357-t6 aluminum alloy', *Engineering Failure Analysis* **9**(1), 99–107.

Esawi, A. and Morsi, K. [2007], 'Dispersion of carbon nanotubes (cnts) in aluminum powder', *Composites Part A: Applied Science and Manufacturing* **38**(2), 646–650.

Even, C., Arvieu, C., Coutand, B. and Quenisset, J. M. [2010], 'Validity of powder metallurgy-based method for processing carbon fibres reinforced titanium matrix composites', *Journal of Composite Materials* .

Fan, Z. [2002], 'Semisolid metal processing', *International Materials Reviews* **47**(2), 49–85.

Feng, Y., Yuan, H. L. and Zhang, M. [2005], 'Fabrication and properties of silver-matrix composites reinforced by carbon nanotubes', *Materials Characterization* **55**(3), 211–218.

Flemings, M. [1991], 'Behaviour of metal alloys in the semisolid state', *Metallurgical Transactions* **22A**, 957–981.

Flemings, M. C. [1974], 'Solidification processing', *Metallurgical Transactions* **5**(10), 2121–2134.

Forn, A., Picas, J. A., Baile, M. T., Martin, E. and García, V. G. [2007], 'Microstructure and tribological properties of anodic oxide layer formed on al-si alloy produced by semisolid processing', *Surface and Coatings Technology* **202**(4-7), 1139–1143.

Forn, A., Picas, J. A., Baile, M. T., Menargues, S. and García, V. G. [2006], Anodic oxide layer formation on a357 aluminium alloy produced by thixocasting, Vol. 116-117 of *9th International Conference on Semi-Solid Processing of Alloys and Composites, S2P 2006*, Busan, pp. 80–83.

Forn, A., Vaneetveld, G., Pierret, J. C., Menargues, S., Baile, M. T., Campillo, M. and Rassili, A. [2010], 'Thixoextrusion of a357 aluminium alloy', *Transactions of Nonferrous Metals Society of China (English Edition)* **20**(SUPPL. 3), s1005–s1009.

Galasso, F. S. and Pinto, J. [1970], 'Oxidation of carbon and metal coated carbon fibers', *Fibre Science and Technology* **2**(4), 303–315.

Garcia-Infanta, J. M., Zhilyaev, A. P., Cepeda-Jiménez, C. M., Ruano, O. A. and Carreño, F. [2008], 'Effect of the deformation path on the ductility of a hypoeutectic al-si casting alloy subjected to equal-channel angular pressing by routes a, ba, bc and c', *Scripta Materialia* **58**(2), 138–141.

Giles, J. H. F., Wagner, J. J. R. and Mount Iii, E. M. [2005], *Design of Experiments*, William Andrew Publishing: Norwich, New York.

Girot, F. A., Albingre, L., Quenisset, J. M. and Naslain, R. [1987], 'ha', *Journal of Metals* **39**(11), 18–21.

Goto, M., Han, S. Z., Euh, K., Kang, J.-H., Kamil, K., Kawagoishi, N. and Kim, S. S. [2011], 'Evaluation of crack growth rate and growth model of ultrafine grained copper', *WIT Transactions on Modelling and Simulation* **51**, 327–338.

Guigon, M. and Klinklin, E. [1994], 'The interface and interphase in carbon fibre-reinforced composites', *Composites* **25**(7), 534–539.

Hajjari, E. and Divandari, M. [2008], 'An investigation on the microstructure and tensile properties of direct squeeze cast and gravity die cast 2024 wrought al alloy', *Materials & Design* **29**(9), 1685–1689.

Hajjari, E., Divandari, M. and Mirhabibi, A. R. [2010], 'The effect of applied pressure on fracture surface and tensile properties of nickel coated continuous carbon fiber reinforced aluminum composites fabricated by squeeze casting', *Materials & Design* **31**(5), 2381–2386.

Hammel, E., Tang, X., Trampert, M., Schmitt, T., Mauthner, K., Eder, A. and Pötschke, P. [2004], 'Carbon nanofibers for composite applications', *Carbon* **42**(5–6), 1153–1158.

Hao, S., Tang, H. and Zhang, J. [n.d.], Research of dispersion uniformity of carbon fiber in short carbon fiber reinforced silicon carbide composites, *in* 'Strategic Technology (IFOST), 2012 7th International Forum on', pp. 1–4.

Hari Babu, N., Tzamtzis, S., Barekar, N., Patel, J. and Fan, Z. [2008], 'Fabrication of metal matrix composites under intensive shearing', *Solid State Phenomena* **141-143**, 373–378.

Hashim, J., Looney, L. and Hashmi, M. S. J. [2002], 'Particle distribution in cast metal matrix composites—part i', *Journal of Materials Processing Technology* **123**(2), 251–257.

Himbeault, D. D., Varin, R. A. and Piekarski, K. [1989], 'Tensile properties of titanium carbide coated carbon fibre — aluminum alloy composites', *Composites* **20**(5), 471–477.

Hiramatsu, T. and Nishimura, T. [1989], 'Recent technological progress of pan-based carbon fibre', *Materials and Design* **10**(2), 93–100.

Huang, X. [2009], 'Fabrication and properties of carbon fibers', *Materials* **2**(4), 2369.

Hughes, A., Boag, A., Glenn, A., McCulloch, D., Muster, T., Ryan, C., Luo, C., Zhou, X. and Thompson, G. [2011], 'Corrosion of aa2024-t3 part ii: co-operative corrosion', *Corrosion Science* **53**, 27–39.

Hunter, E. [1996], *Experimental design. In: Data Handling in Science & Technology*, Elsevier, Amsterdam, chapter 16: Multivariate Analysis of Data in Sensory Science, pp. 37–69.

Ibrahim, I. A., Mohamed, F. A. and Lavernia, E. J. [1991], 'Particulate reinforced metal matrix composites - a review', *Journal of Materials Science* **26**(5), 1137–1156.

Islam, M. U. and Wallace, W. [1988], 'Carbon fiber reinforced aluminium matrix composites. a crtitical review', *Adv Mater Manuf Processes* **3**(1), 1–35.

Ivanchev, L., Wilkins, D., Govender, G., Du Preez, W. and Bean, R. [2008], 'Rheoprocessing of semi-solid metal alloys: a new technology for manufacturing automotive and aerospace components', *South African Journal of Science* **104**, 257–259.

Ivens, J., Wevers, M. and Verpoest, I. [1994], 'Influence of carbon fibre surface treatment on composite ud strength', *Composites* **25**(7), 722–728.

Jahedi, M., Mani, B., Shakoorian, S., Pourkhorshid, E. and Hossein Paydar, M. [2012], 'Deformation rate effect on the microstructure and mechanical properties of al-sic p composites consolidated by hot extrusion', *Materials Science and Engineering A* **556**, 23–30.

Jiang, X. and Gao, Q. [2001], 'Stress-transfer analysis for fibre/matrix interfaces in short-fibre-reinforced composites', *Composites Science and Technology* **61**(10), 1359–1366.

Johnson, J. W. [1969], 'Factors affecting the tensile strength of carbon-graphite fibers', (9), 229–243.

Juhasz, K. L., Baumli, P. and Kaptay, G. [2012], 'Fabrication of carbon fibre reinforced, aluminium matrix composite by potassium iodide (ki) - potassium hexafluoro-titanate (k2tif6) flux', *Materialwissenschaft und Werkstofftechnik* **43**(4), 310–314.

Juhasz, K. L., Baumli, P., Sytchev, J. and Kaptay, G. [2013], 'Wettability of graphite by liquid aluminum under molten potassium halide fluxes', *Journal of Materials Science* **48**(21), 7679–7685.

Jung, H. K. [2000], 'The induction heating process of semi-solid aluminium alloys for thixoforming and their microstructure evaluation', *Journal of Materials Processing Technology* **105**(1–2), 176–190.

Karbalaei Akbari, M., Baharvandi, H. R. and Shirvanimoghaddam, K. [2015], 'Tensile and fracture behavior of nano/micro tib2 particle reinforced casting a356 aluminum alloy composites', *Materials & Design* **66, Part A**(0), 150–161.

Karl, U. K. [2003], *Metal Matrix Composites. Custom-made Materials for Automotive and Aerospace Engineering*, Metallische Verbundwerkstoffe Wiley-VCH.

Khan, I. H. [1976], 'The effect of thermal exposure on the mechanical properties of aluminum-graphite composites', *Metallurgical Transactions A* **7**(8), 1281–1289.

Khoddamzadeh, A., Liu, R., Liang, M. and Yang, Q. [2012], 'Novel wear-resistant materials/carbon fiber reinforced low-carbon stellite alloy composites', *Composites Part A: Applied Science and Manufacturing* **43**(3), 344–352.

Kirkwood, D. H., Suary, M., Kapranos, P., Atkinson, H. V. and Young, K. P. [2010*a*], 'Introduction to industrial applications of semisolid processing semi-solid processing of alloys', *Springer Series in Materials Science, Springer Berlin Heidelberg* **124**, 109–111.

Kirkwood, D. H., Suary, M., Kapranos, P., Atkinson, H. V. and Young, K. P. [2010*b*], 'Raw material semi-solid processing of alloys', *Springer Series in Materials Science, Springer Berlin Heidelberg* **124**, 113–128.

Kohara, S. and Muto, N. [1988], 'Degradation behavior of carbon fibers by molten aluminum', *Nippon Kinzoku Gakkai-si* **52**(11), 1063–1069.

Kokcharov, I. and Burov, A. [2013], *Structural Integrity Analysis*, Amazon Digital Services LLC.

Korab, J., Stefanik, P., S, K., Sebo, P. and Korb, G. [2002], 'Thermal conductivity of unidirectional copper matrix carbon fibre composites', *Composites Part A: Applied Science and Manufacturing* **33**(4), 577–581.

Kozera, R., Bieliński, J., Broda, A., Boczkowska, A. and Kurzydłowski, K. J. [2011], Preparation of carbon fibres for aluminium composites, Vol. 264-265 of *International Conference on Advances in Materials and Processing Technologies, AMPT 2009*, pp. 1487–1493.

Kwon, H., Estili, M., Takagi, K., Miyazaki, T. and Kawasaki, A. [2009], 'Combination of hot extrusion and spark plasma sintering for producing carbon nanotube reinforced aluminum matrix composites', *Carbon* **47**(3), 570–577.

Lancin, M. and Marhic, C. [2000], 'Tem study of carbon fibre reinforced aluminium matrix composites: influence of brittle phases and interface on mechanical properties', *Journal of the European Ceramic Society* **20**(10), 1493–1503.

Landry, K., Kalogeropoulou, S. and Eustathopoulos, N. [1998], 'Wettability of carbon by aluminum and aluminum alloys', *Materials Science and Engineering: A* **254**(1–2), 99–111.

Langdon, T. G. [2007], 'The principles of grain refinement in equal-channel angular pressing', *Materials Science and Engineering: A* **462**(1-2), 3–11.

Lashkari, O. and Ghomashchi, R. [2007], 'The implication of rheology in semi-solid metal processes: An overview', *Journal of Materials Processing Technology* **182**(1–3), 229–240.

Lee, J.-C., Byun, J.-Y., Park, S.-B. and Lee, H.-I. [1998], 'Prediction of si contents to suppress the formation of al4c3 in the sicp/al composite', *Acta Materialia* **46**(5), 1771–1780.

Lee, W.-S., Sue, W.-C. and Lin, C.-F. [2000], 'The effects of temperature and strain rate on the properties of carbon-fiber-reinforced 7075 aluminum alloy metal-matrix composite', *Composites Science and Technology* **60**(10), 1975–1983.

Li, S.-H. and Chao, C.-G. [2004], 'Effects of carbon fiber/al interface on mechanical properties of carbon-fiber-reinforced aluminum-matrix composites', *Metallurgical and Materials Transactions A* **35**(7), 2153–2160.

Lin, C. B., Chang, R. J. and Weng, W. P. [1998], 'A study on process and tribological behavior of al alloy/gr. (p) composite', *Wear* **217**(2), 167–174.

Liu, L., Li, W., Tang, Y., Shen, B. and Hu, W. [2009], 'Friction and wear properties of short carbon fiber reinforced aluminum matrix composites', *Wear* **266**(7–8), 733–738.

Liu, Z., Curioni, M., Jamshidi, P., Walker, A., Prengnell, P., Thompson, G. E. and Skeldon, P. [2014], 'Electrochemical characteristics of a carbon fibre composite and the associated galvanic effects with aluminium alloys', *Applied Surface Science* **314**(0), 233–240.

Liu, Z., Zu, G., Luo, H., Liu, Y. and Yao, G. [2010], 'Influence of mg addition on graphite particle distribution in the al alloy matrix composites', *Journal of Materials Science and Technology* **26**(3), 244–250.

Lopez, D. A., Simison, S. N. and Sanchez, S. R. [(2005], 'Inhibitors performance in co2 corrosion: Eis studies on the interaction between their molecular structure and steel microstructure', *Corrosion Science* **47**(3), 735–755.

Lu, F., Zhang, X., Tang, Z. and Liu, M. [2005], 'Galvanic corrosion behavior between carbon fiber reinforced plastic materials and aluminum alloys', *Journal of the Chinese Society of Corrosion and Protection* **25**(1), 39–43.

Mahato, A., Xia, S., Perry, T., Sachdev, A. and Biswas, S. K. [2010], 'Role of silicon in resisting subsurface plastic deformation in tribology of aluminium–silicon alloys', *Tribology International* **43**(1–2), 381–387.

Mallick, P. . K. . [2007*a*], *Materials*, Dekker Mechanical Engineering, CRC Press, New York. doi:10.1201/9781420005981.ch2.

Mallick, P. . K. . [2007*b*], *Mechanics*, Dekker Mechanical Engineering, CRC Press, New York. doi:10.1201/9781420005981.ch3.

Masuku, E., Moller, H., Curle, U., Pistorius, P. and Li, W. [2010], 'Influence of surface liquid segregation on corrosion behavior of semi-solid metal high pressure die cast

aluminium alloys', *Transactions of Nonferrous Metals Society of China* **20**, s837–s841.

Matsunaga, T., Matsuda, K., Hatayama, T., Shinozaki, K. and Yoshida, M. [2007], 'Fabrication of continuous carbon fiber-reinforced aluminum-magnesium alloy composite wires using ultrasonic infiltration method', *Composites Part A: Applied Science and Manufacturing* **38**(8), 1902–1911.

Matsunaga, T., Ogata, K., Hatayama, T., Shinozaki, K. and Yoshida, M. [2007], 'Effect of acoustic cavitation on ease of infiltration of molten aluminum alloys into carbon fiber bundles using ultrasonic infiltration method', *Composites Part A: Applied Science and Manufacturing* **38**(3), 771–778.

Mbuyaa, T. O., Oderaa, B. O. and Ng'ang'a, S. P. [2003], 'Influence of iron on castability and properties of aluminium silicon alloys: literature review', *International Journal of CastMetals Research* **15**(5), 451–4665.

Mehrabian, R., Riek, R. G. and Flemings, M. [1974*a*], 'Preparation and casting of metal-particulate non-metal composites', *Metallurgical Transactions* **5**(8), 1899–1905.

Mehrabian, R., Riek, R. G. and Flemings, M. C. [1974*b*], 'Preparation and casting or metal-particulate non-metal composites', *Metall Trans* **5**(8), 1899–1905.

Menargues, S., Martin, E., Baile, M. and Picas, J. [2015], 'New short t6 heat treatments for aluminium silicon alloys obtained by semisolid forming', *Materials Science and Engineering: A* **621**, 236–242.

Meyers, M., Mishra, A. and Benson, D. [2006], 'Mechanical properties of nanocrystalline materials', *Progress in Materials Science* **51**(4), 427–556.

Mohamed, A. and Samuel, F. [2012], 'A review on the heat treatment of al-si-cu/mg casting alloys', *INTECH* .

Moller, H., Govender, G. and Stumpf, W. [2008], 'The t6 heat treatment of semi-solid metal processed alloy a356', *The Open Materials Science Journal* **2**, 6–10.

Mondolfo, L. F. [2013], *Aluminum Alloys: Structure and Properties*, Elsevier.

Mortensen, A. and Cornie, J. A. [1987], 'On the infiltration of metal matrix composites', *Metallurgical transactions. A, Physical metallurgy and materials science* **18 A**(6), 1160–1163.

Murray, J. L. and McAlister, A. J. [n.d.], 'The al-si (aluminum-silicon) system', *Bulletin of Alloy Phase Diagrams* **5**(1), 74–84.
URL: *http://dx.doi.org/10.1007/BF02868729*

Naji, H., Zebarjad, S. M. and Sajjadi, S. A. [2008], 'The effects of volume percent and aspect ratio of carbon fiber on fracture toughness of reinforced aluminum matrix composites', *Materials Science and Engineering: A* **486**(1–2), 413–420.

Nayeb-Hashemi, H. and Seyyedi, J. [1989], 'Study of the interface and its effect on mechanical properties of continuous graphite fiber-reinforced 201 aluminum', *Metallurgical Transactions A* **20**(4), 727–739.

Nie, X. W. [2012], 'Recent progress in preparation of nanometer aluminium composites by powder metallurgy', *Micro and Nanosystems* **4**(2), 157–164.

Niedermainer, F., Langgatner, J., Hirt, G. and Niedick, I. [1998], Horizontal continuous casting of ssm billets,, *in* '5th International Conference on Semi-solid Processing of Alloys and Composites, Golden (USA)', pp. 407–414.

Nisancioglu, K. [1990], 'Electrochemical behavior of aluminum-base intermetallics containing iron', *Journal of The Electrochemical Society* **137**, 69–77.

Ogawa, F., Hirakawa, T., Oda, M., Masuda, C. and Nishimura, T. [2010], 'Fabrication of carbon nano-fiber (cnf) reinforced aluminum matrix composites by pressureless infiltration: Effect of aluminum coatings on infiltration behavior'.

Otani, S. and Yokoyama, A. [1969], 'Characteristic chemical constitution of pitch materials suitable for the mp carbon fiber', *Chem Soc Japan-VBul* **42**(5), 1417–1424.

Ozdin, K. [2012], 'Production of metal matrix composites by the vortex method and investigation of the effect of changing casting temperature on particles ratio of product-composite', *Experimental Techniques* pp. no–no.

Padilla, F., Harrigan, W. C. and Jr. ; Amateau, M. F. [1975], *Determination of aluminum carbide and the volume percent fiber content in aluminum-graphite composites*, el segundo edn, chapter 9-15.

Pai, B. C., Pillai, R. M., Kelukutty, V. S., Srinivasa Rao, H., Soman, T., Pillai, S. G. K., Sukumaran, K., Satyanarayana, K. G., Ravikumar, K. K., Gupta, A. K. and Sikand, R. [1994], 'Semi-solid slurry process for making short carbon fibre dispersed aluminium alloy matrix composites', *Journal of Materials Science Letters* **13**(17), 1278–1280.

Pai, D., Acharya, Y., Yarmolenko, S., Sankar, J., Lua, J. and Zawada, L. [2008], Exploration of reliable oxide fiber testing procedures and development of a multicontinuum based creep analysis module, *in* M. Singh and T. Jessen, eds, '25th Annual Conference on Composites, Advanced Ceramics, Materials and Structures: A', Vol. 22, pp. 429–438.

Panton, R. L. [2013], *Incompressible Flow*, Vol. 5, John Wiley & Sons, Inc.

Pardo, A., Merino, M. C., Mohedano, M., Casajús, P., Coy, A. E. and Arrabal, R. [2009], 'Corrosion behaviour of mg/al alloys with composite coatings', *Surface and Coatings Technology* **203**(9), 1252–1263.

Park, C., Kim, S., Kwon, Y., Lee, Y. and Lee, J. [2005], 'Mechanical and corrosion properties of rheocast and low-pressure cast a356-t6 alloy', *Materials Science & Engineering, A* **391**, 86–94.

Patankar, S. N., Gopinathan, V. and Ramakrishnan, P. [1990], 'Chemical interactions at the carbon fiber aluminium interface', *Scripta Metallurgica et Materialia* **24**(11), 2197–2202.

Payan, S., Le Petitcorps, Y., Olive, J. M. and Saadaoui, H. [2001], 'Experimental procedure to analyse the corrosion mechanisms at the carbon/aluminium interface in composite materials', *Composites Part A: Applied Science and Manufacturing* **32**(3–4), 585–589.

Pearce, D. G. [1969], 'Designing in carbon-fibre reinforced metals', *Composites* **1**(1), 13–18.

Pelleg, J., Ashkenazi, D. and Ganor, M. [2000], 'The influence of a third element on the interface reactions in metal-matrix composites (mmc): Al-graphite system', *Materials Science and Engineering A* **281**(1-2), 239–247.

Peng, T. and Chang, I. [2014], 'Mechanical alloying of multi-walled carbon nanotubes reinforced aluminum composite powder', *Powder Technology* **266**, 7–15.

Peng, Z. and Nie, X. [2013], 'Galvanic corrosion property of contacts between carbon fiber cloth materials and typical metal alloys in an aggressive environment', *Surface and Coatings Technology* **215**(0), 85–89.

Picas, J. A. [2000], 'Optimizacion y caracterizacion de la aleacion 2ti- 0'2pd para aplicaciones clinicas', Thesis Doctoral, 2.73-2.91.

Pio, L. [2011], 'Effect of t6 heat treatment on the mechanical properties of gravity die cast a356 aluminium alloy', *Journal of Applied Sciences* **11**, 2048–2052.

Pippel, E., Woltersdorf, J., Doktor, M., Blucher, J. and Degischer, H. P. [2000], 'Interlayer structure of carbon fibre reinforced aluminium wires', *Journal of Materials Science* **35**(9), 2279–2289.

Qin, X., Jiang, D. and Dong, S. [2004], 'Investigation of the semisolid mechanical stirring method to deposit an aluminum particle coating on the surface of sic short fibers', *Surface Review and Letters* **11**(2), 205–210.

Rafaja, D., Wustefeld, C., Motylenko, M., Schimpf, C., Barsukova, T., Schwarz, M. R. and Kroke, E. [2012], 'Interface phenomena in (super)hard nitride nanocomposites: from coatings to bulk materials', *Chem. Soc. Rev.* **41**(15), 5081–5101.
URL: *http://dx.doi.org/10.1039/C2CS15351C*

Ramesh, C. S., Adarsha, H., Pramod, S. and Khan, Z. [2013], 'Tribological characteristics of innovative al6061-carbon fiber rod metal matrix composites', *Materials & Design* **50**, 597–605.

Ramesh, C. S. and Prasad, T. B. [2008], 'Friction and wear behavior of graphite-carbon short fiber reinforced al-17%si alloy hybrid composites', *Journal of Tribology* **131**(1), 014501–014501.

Rams, J., Ureña, A., Escalera, M. D. and Sánchez, M. [2007], 'Electroless nickel coated short carbon fibres in aluminium matrix composites', *Composites Part A: Applied Science and Manufacturing* **38**(2), 566–575.

Ramu, G. and Ranjit, B. [2009], 'Effect of equal channel angular pressing (ecap) on microstructure and properties of al-sicp composites', *Materials and Design* **30**(9), 3554–3559.

Ravindran, P., Manisekar, K., Narayanasamy, R. and Narayanasamy, P. [2013], 'Tribological behaviour of powder metallurgy-processed aluminium hybrid composites with the addition of graphite solid lubricant', *Ceramics International* **39**(2), 1169–1182.

Rosso, M. and Actis Grande, M. [2006], 'Optimization of heat treatment cycles for automotive parts produced by rheocasting process', *Solid State Phenom.* **116, 117**, 505–508.

Rossoll, A., Moser, B. and Mortensen, A. [2012], 'Tensile strength of axially loaded unidirectional nextel 610^{TM} reinforced aluminium: A case study in local load sharing between randomly distributed fibres', *Composites Part A: Applied Science and Manufacturing* **43**(1), 129–137.

Roy, A. K., Schulze, S., Hietschold, M. and Goedel, W. A. [2012], 'Oxidation protection of carbon fibers by coating with alumina and/or titania using atomic layer deposition', *Carbon* **50**(3), 761–770.

Ruiz-Navasa, E., Fogagnoloa, J., Velascoa, F., Ruiz-Prietob, J. and Froyenc, L. [2006], 'One step production of aluminium matrix composite powders by mechanical alloying', *Composites Part A: Applied Science and Manufacturing* **37**(11), 2114–2120.

Sabirov, I., Kolednik, O., Valiev, R. Z. and Pippan, R. [2005], 'Equal channel angular pressing of metal matrix composites: Effect on particle distribution and fracture toughness', *Acta Materialia* **53**(18), 4919–4930.

Saklakoglu, N., Irizalp, S. G., Ercayhan, Y. and Birol, Y. [2014], 'Investigation of wear behaviour of thixoformed and conventional gravity cast alsi8cu3fe alloys', *Industrial Lubrication and Tribology* **66**(1), 46–50.

Sanchez, M., Rams, J. and Urena, A. [2010], 'Fabrication of aluminium composites reinforced with carbon fibres by a centrifugal infiltration process', *Composites Part A: Applied Science and Manufacturing* **41**(11), 1605–1611.

Scharhoff, J., Yawny, A., Skrotzki, B. and Eggeler, G. [2004], 'Fibre breakage in short fibre reinforced metal matrix composites during creep and constant strain rate compression testing', *Materials Science and Engineering: A* **387-389**, 896–899.

Segal, V. M. [2002], 'Severe plastic deformation: simple shear versus pure shear', *Materials Science and Engineering* **A338**, 331–344.

Semiatin, S., Delo, D. and Shell, E. [2000], 'The effect of material properties and tooling design on deformation and fracture during equal channel angular extrusion', *Acta Materials* **48**(8), 1841–1851.

Seong, H. G., Lopez, H. F., Robertson, D. P. and Rohatgi, P. K. [2008], 'Interface structure in carbon and graphite fiber reinforced 2014 aluminum alloy processed with active fiber cooling', *Materials Science and Engineering: A* **487**(1–2), 201–209.

Shaeria, M., Shaerib, M., Ebrahimic, M., Salehid, M. and Seyyedeind, S. H. [2016], 'Effect of ecap temperature on microstructure and mechanical properties of al-zn-mg-cu alloy', *Progress in Natural Science: Materials International* .

Shalu, T., Abhilash, E. and Joseph, M. A. [2009], 'Development and characterization of liquid carbon fibre reinforced aluminium matrix composite', *Journal of Materials Processing Technology* **209**(10), 4809–4813.

Shi, J., Liu, Y., Yao, G., Yan, P. and Liu, H. [2012], Effect of mg on microstructure and mechanical properties of copper-coated short carbon fiber reinforced al alloy matrix composite, Vol. 457-458 of *2011 International Conference on Advanced Materials and Engineering Materials, ICAMEM2011*, Shenyang, Liaoning, pp. 348–353.

Siegert, K., Unseld, P., Baur, J., Kauffmann, F., Arzt, E. and Niessen, K. v. [2006], 'Thixoforging of continuous fiber-reinforced alsi/almg-alloys', *International Journal of Machine Tools and Manufacture* **46**(11), 1227–1232.

Simancik, F. and Jangg, G. [1994], 'Influence of processing parameters on fiber damage and mechanical properties of extruded composite with aluminum matrix and short carbon fibers', *Theoretical and Applied Fracture Mechanics* **20**(1), 11–20.

Song, J. I. and Han, K. S. [1997], 'Effect of volume fraction of carbon fibers on wear behavior of al/al2o3/c hybrid metal matrix composites', *Composite Structures* **39**(3–4), 309–318.

Stolyarov, V. V., Zhu, Y. T., Alexandrov, I. V., Lowe, T. C. and Valiev, R. Z. [2001], 'Influence of ecap routes on the microstructure and properties of pure ti', *Materials Science and Engineering: A* **299**(1–2), 59–67.

Suresha, S. and Sridhara, B. K. [2010], 'Wear characteristics of hybrid aluminium matrix composites reinforced with graphite and silicon carbide particulates', *Composites Science and Technology* **70**(11), 1652–1659.

Taghiabadi, R., Ghasemi, H. M. and Shabestari, S. G. [2008], 'Effect of iron-rich intermetallics on the sliding wear behavior of al–si alloys', *Materials Science and Engineering: A* **490**(1–2), 162–170.

Tahamtan, S. and Boostani, A. F. [2009], 'Quantitative analysis of pitting corrosion behavior of thixoformed a356 alloy in chloride medium using electrochemical techniques', *Materials & Design* **30**, 2483–2489.

Tahamtan, S. and Fadavi Boostani, A. [2010], 'Evaluation of pitting corrosion of thixoformed a356 alloy using a simulation model', *Transactions of Nonferrous Metals Society of China* **20**(9), 1702–1706.

Tanaka, H., Nakamura, H., Yanagi, H., Kita, T., Yokoyama, K., Magario, A. and Noguchi, T. [2009], 'Side electron emission device using a composite of carbon nanofibers and aluminum', *Thin Solid Films* **518**(2), 530–533.

Tang, Y., Deng, Y., Zhang, K., Liu, L., Wu, Y. and Hu, W. [2008], 'Improvement of interface between al and short carbon fibers by a-al2o3 coatings deposited by sol-gel technology', *Ceramics International* **34**(7), 1787–1790.

Tang, Y., Liu, L., Li, W., Shen, B. and Hu, W. [2009], 'Interface characteristics and mechanical properties of short carbon fibers/al composites with different coatings', *Applied Surface Science* **255**(8), 4393–4400.

Tirtom, I., Mustafa, G. and Hasan, Y. [2008], 'Simulation of the strain rate sensitive flow behavior of sic-particulate reinforced aluminum metal matrix composites', *Computational Materials Science* **42**, 570–578.

Totten, G. E. and MacKenz, D. S. [2003], *Handbook of Aluminum: Vol. 1: Physical Metallurgy and Processes*, CRC Press, pp. 278–279.

Towata, S., Yamada, S. and Ohwaki*, T. [1985], 'Strength and interfacial reaction of high modulus carbon fiber-reinforced aluminum alloys', *Transactions of the Japan Institute of Metals* **26**(8), 563–570.

Tzamtzis, S., Barekar, N. S., Hari Babu, N., Patel, J., Dhindaw, B. K. and Fan, Z. [2009], 'Processing of advanced al/sic particulate metal matrix composites under intensive shearing - a novel rheo-process', *Composites Part A: Applied Science and Manufacturing* **40**(2), 144–151.

Urena, A., Rams, J., Campo, M. and Sanchez, M. [2009], 'Effect of reinforcement coatings on the dry sliding wear behaviour of aluminium/sic particles/carbon fibres hybrid composites', *Wear* **266**(11-12), 1128–1136.

Urena, A., Rams, J., Escalera, M. D. and Sanchez, M. [2005], 'Characterization of interfacial mechanical properties in carbon fiber/aluminium matrix composites by the nanoindentation technique', *Composites Science and Technology* **65**(13), 2025–2038.

Urena, A., Rams, J., Escalera, M. D. and Sanchez, M. [2007], 'Effect of copper electroless coatings on the interaction between a molten al-si-mg alloy and coated short carbon fibres', *Composites Part A: Applied Science and Manufacturing* **38**(8), 1947–1956.

Ustinov, L. M. and Verkhovsky, L. A. [1992], 'Effect of fibre/matrix interface structure on strength and plasticity of boron aluminium reinforced with discontinuous fibres', *Journal of Materials Science* **27**(2), 335–342.

Varshavskij, V. Y. [1995], 'Realization of properties of carbon fibres (cf) in composite materials. part 2. carbon-fibrous composites with metallic matrix (review)', *Khimicheskie Volokna* **1**(3), 37–42.

Vencl, A., Bobić, I. and Mišković, Z. [2008], 'Effect of thixocasting and heat treatment on the tribological properties of hypoeutectic al–si alloy', *Wear* **264**(7–8), 616–623.

Venkata Siva, S., Sahoo, K., Ganguly, R. and Dash, R. [2011], 'Effect of hot working on structure and tribological properties of aluminium reinforced with aluminium oxide particulates', *Journal of Materials Engineering and Performance* pp. 1–6.

Vidal-Setif, M. H., Lancin, M., Marhic, C., Valle, R., Raviart, J. L., Daux, J. C. and Rabinovitch, M. [1999], 'On the role of brittle interfacial phases on the mechanical properties of carbon fibre reinforced al-based matrix composites', *Materials Science and Engineering: A* **272**(2), 321–333.

Wang, C., Chen, G., Wang, X., Zhang, Y., Yang, W. and Wu, G. [2012], 'Effect of mg content on the thermodynamics of interface reaction in cf/al composite', *Metallurgical and Materials Transactions A: Physical Metallurgy and Materials Science* **43**(7), 2514–2519.

Wang, C., Chen, G. and Wu, G. [2009], 'Surface treatment of cf/al composites with immersion in aqueous solution containing ce ions for corrosion barrier', *Materials and Corrosion* **60**(11), 859–864.

Wang, C., Wu, G., Kang, P., Zhang, Y., Xiu, Z. and Chen, G. [2003], 'The improvement of corrosion resistant for the cf/al composites by ni-p coatings', *Key Engineering Materials* **353-358**(3), 1675–1678.

Wang, J., Hong, T., Li, G. and Li, P. [1997], 'A combined process of coating and hybridizing for the fabrication of carbon fiber reinforced aluminum matrix composites', *Composites Part A: Applied Science and Manufacturing* **28**(11), 943–948.

Wang, X., Chen, G., Li, B., Wu, G. and Jiang, D. [2009], 'Microstructure and mechanical properties of graphite fiber-reinforced high-purity aluminum matrix composite', *Journal of Materials Science* **44**(16), 4303–4307.

Watt, W. and Johnson, W. [1969], 'Effect of length changes during the oxidation of polyacrylonitrile fibers on the young's modulus of carbon fibers', (9), 215–227.

Wei, T. Z., Shamsuri, S. R. B., Yee, C. S., Rashid, M. W. A. and Ahsan, Q. [2013], 'Effect of sliding velocity on wear behavior of magnesium composite reinforced with sic and mwcnt', *Procedia Engineering* **68**(0), 703–709.

Whitt, W., Shane, G. H. and Barry, L. N. [2006], *Handbooks in Operations Research and Management Science*, North-Holland: Elsevier, chapter Chapter 13: Analysis for Design.

Wielage, B. and Dorner, A. [1999*a*], 'Corrosion studies on aluminium reinforced with uncoated and coated carbon fibres', *Composites Science and Technology* **59**(8), 1239–1245.

Wielage, B. and Dorner, A. [1999*b*], 'Corrosion studies on aluminium reinforced with uncoated and coated carbon fibres', *Composites Science and Technology* **59**(8), 1239–1245.

Wilson, S. and Alpas, A. T. [1997], 'Wear mechanism maps for metal matrix composites', *Wear* **212**(1), 41–49.

Wu, Y. and Kim, G.-Y. [2011], 'Carbon nanotube reinforced aluminum composite fabricated by semi-solid powder processing', *Journal of Materials Processing Technology* **211**(8), 1341–1347.

Yamaguchi, S., Mikuni, J., Mizoguchi, I., Matsunaga, T., Shinozaki, K. and Yoshida, M. [2009], 'Influence of high temperature holding on tensile strength of pan-based carbon fiber reinforced aluminum-magnesium alloy composites fabricated by ultrasonic infiltration method', *Keikinzoku/Journal of Japan Institute of Light Metals* **59**(5), 241–247.

Yan, M. and Fan, Z. [2001], 'Review durability of materials in molten aluminum alloys', *Journal of Materials Science* **36**(2), 285–295.

Yang, M. and Scott, V. D. [1991], 'Carbide formation in a carbon fibre reinforced aluminium composite', *Carbon* **29**(7), 877–879.

Ye, H. [2003], 'An overview of the development of al-si-alloy based material for engine applications', *Journal of Materials Engineering and Performance* **12**(3), 288–297.

Yu, W. and Yao, J. [2006], 'Tensile strength and its variation of pan-based carbon fibers. i. statistical distribution and volume dependence', *Journal of Applied Polymer Science* **101**(5), 3175–3182.

Yu, Y., Kim, S., Lee, Y. and Lee, J. [2002], 'Phenomenological observations on mechanical and corrosion properties of thixoformed 357 alloys: a comparison with permanent mold cast 357 alloys', *Metallic Materials Transaction A* **33**, 1399–1412.

Yumitori, S., Wang, D. and Jones, F. R. [1994], 'The role of sizing resins in carbon fibre-reinforced polyethersulfone (pes)', *Composites* **25**(7), 698–705.

Zambon, A., Badan, B. and Maddalena, A. [2004], 'Production, microstructural and mechanical characterization of spray formed al-6 wt.fe/sicp composite', *Materials Science and Engineering A* **375-377**(1-2 SPEC. ISS.), 645–650.

Zhang, H., Loukus, J. and Loukus, A. [2009], 'Improvement of the bonding interface in hybrid fiber/particle preform reinforced al matrix composite', *Materials Letters* **63**(2), 310–312.

zoltek.com [has been surfed in May, 2016], *http://zoltek.com/carbonfiber/how-is-it-made*.